Functional specialization of *Arabidopsis* poly(A) polymerases in relation to flowering time and stress

Dissertation

zur Erlangung des akademischen Grades

doctor rerum naturalium (Dr. rer. nat.)

eingereicht an der

Mathematisch-Naturwissenschaftlichen Fakultät der Universität Potsdam

Institut für Biochemie und Biologie

von

Hjördis Czesnick

geboren am 22.04.1985 in Berlin

Published online at the
Institutional Repository of the University of Potsdam:
URN urn:nbn:de:kobv:517-opus4-78015
http://nbn-resolving.de/urn:nbn:de:kobv:517-opus4-78015

Contents

Abbreviations

35S	promoter of the *35S* gene from cauliflower mosaic virus
A's	adenosine monophosphates
Agrobacterium	*Agrobacterium tumefaciens*
ahg2	*ABA-hypersensitive germination 2*
APA	alternative polyadenylation
APS	ammonium persulfate
AS	antisense
AT	3-amino-1, 2, 4-triazole
At	*Arabidopsis thaliana*
Arabidopsis	*Arabidopsis thaliana*
bp	base pairs
BH	Benjamini-Hochberg
BSO	buthionine-S, R-sulfoximide
CAPS	cleaved amplified polymorphic sequences
CTD	carboxy-terminal domain
cDNA	complementary DNA
CF	Cleavage Factor
Co-IP	co-immunoprecipitation
Col-0	Columbia-0
cPAP	canonical poly(A) polymerase
CPSF	Cleavage and Polyadenylation Specificity Factor
CstF	Cleavage-stimulating Factor
Ct	cycle threshold
Δ	delta; difference in
ΔTLN	total leaf number difference
D	day
DAG	days after germination
ddH2O	double distilled water; in this work: ultrapure, autoclaved water
DMSO	dimethylsulfoxide
DNA	deoxyribonucleic acid
DNase	deoxyribonuclease
dNTPs	deoxynucleoside triphosphates
DTT	dithiothreitol
DW	dry weight
E. coli	*Escherichia coli*
EDTA	ethylendiaminetetraacetic acetate
EMS	ethyl-methanesulfonate
esp	*enhanced silencing phenotype*
Fig.	figure
Fip1	Factor interacting with Pap1p
FLC	*FLOWERING LOCUS C*
FLD	*FLOWERING LOCUS D*
FLK	*FLOWERING LOCUS K*
FLM	*FLOWERING LOCUS M*
FPI	floral pathway integrators
FRI	*FRIGIDA*
FT	*FLOWERING LOCUS T*

FTA	flowering time analysis
FW	fresh weight
GA	gibberellic acid
GUS	ß-glucuronidase
GSH	glutathione
H_2O_2	hydrogen peroxide
HCl	hydrochloric acid
His	histidine
KASP	KBiosciences Competitive Allele-Specific PCR
kb	kilo base pairs
LC480	Light Cycler 480 I (Roche)
LD	long day
LED	light-emitting diode
L*er*	Landsberg *erecta*
LFY	*LEAFY*
M	molar; mol/l
MAF	*MADS AFFECTING FLOWERING*
mRNA	messenger RNA
MS	Murashige and Skoog basal salt mixture
MV	methyl viologen
N	night
NTD	amino-terminal domain
NaCl	sodium chloride
NADP(H)	nicotinamide adenine dinucleotide phosphate (reduced form)
NaOH	sodium hydroxide
NASC	Nottingham *Arabidopsis* stock centre
NCBI	National Center for Biotechnology Information
ncPAP	noncanonical poly(A) polymerase
NLS	nuclear localisation sequence
NO	nitric oxide
nt	nucleotide(s)
NTC	non-treated control
OE	overexpression
O/N	overnight
oxt6	*oxidative stress resistant 6*
PAGE	polyacrylamide gel electrophoresis
PAP	poly(A) polymerase
PAPS	*Arabidopsis* poly(A) polymerase
PAPS2/4	*PAPS2/PAPS4*
PAR	photosynthetically active radiation
PAS	poly(A) site
PAT	poly(A) tail
PCR	polymerase chain reaction
PolII	RNA Polymerase II
PPT	phosphinotricin (Basta)
PRC	Polycomb repressive complex
pre-mRNA	precursor messenger ribonucleic acid
qPCR	quantitative real-time PCR
REF6	*RELATIVE OF EARLY FLOWERING 6*

RIP	RNA immunoprecipitation
RNA	ribonucleic acid
RNase	RNA nuclease
RNA-seq	RNA sequencing
ROS	reactive oxygen species
RT	room temperature (20–23 °C)
RT-PCR	reverse transcriptase PCR
SA	salicylic acid
SD	short day
SDS	sodium dodecyl sulfate
SEM	standard error of the mean
seq	sequencing
Sf-2	San Feliu-2
SOC	Super optimal broth with catabolite repression
SOC1	*SUPPRESSOR OF OVEREXPRESSION OF CONSTANS1*
SOD	superoxide dismutase
sof	*suppressor of overexpressed FCA*
SPL	*SQUAMOSA PROMOTER BINDING PROTEIN-LIKE*
SSC	standard saline citrate
SVP	*SHORT VEGETATIVE PHASE*
TAIR	The *Arabidopsis* Information Resource
TAE	Tris-acetate EDTA
T-DNA	transfer-DNA
Taq	*Thermus aquaticus*
TE	Tris EDTA
TEMED	tetramethylethylenediamine
TLN	total leaf number
Tm	melting temperature
UTR	untranslated region
var	variant
v/v	volume per volume
v/w	weight per volume
vol	volume
vYFP	venus yellow fluorescent protein
WT	wild type
YFP	yellow fluorescent protein

List of Figures

List of Tables

Summary

Polyadenylation is a decisive 3' end processing step during the maturation of pre-mRNAs. The length of the poly(A) tail has an impact on mRNA stability, localization and translatability. Accordingly, many eukaryotic organisms encode several copies of canonical poly(A) polymerases (cPAPs). The disruption of cPAPs in mammals results in lethality. In plants, reduced cPAP activity is non-lethal. *Arabidopsis* encodes three nuclear cPAPs, PAPS1, PAPS2 and PAPS4, which are constitutively expressed throughout the plant. Recently, the detailed analysis of *Arabidopsis paps1* mutants revealed a subset of genes that is preferentially polyadenylated by the cPAP isoform PAPS1 (Vi et al. 2013). Thus, the specialization of cPAPs might allow the regulation of different sets of genes in order to optimally face developmental or environmental challenges.

To gain insights into the cPAP-based gene regulation in plants, the phenotypes of *Arabidopsis* cPAPs mutants under different conditions are characterized in detail in the following work. An involvement of all three cPAPs in flowering time regulation and stress response regulation is shown. While *paps1* knockdown mutants flower early, *paps4* and *paps2 paps4* knockout mutants exhibit a moderate late-flowering phenotype. *PAPS1* promotes the expression of the major flowering inhibitor *FLC*, supposedly by specific polyadenylation of an *FLC* activator. *PAPS2* and *PAPS4* exhibit partially overlapping functions and ensure timely flowering by repressing *FLC* and at least one other unidentified flowering inhibitor. The latter two cPAPs act in a novel regulatory pathway downstream of the autonomous pathway component *FCA* and act independently from the polyadenylation factors and flowering time regulators *CstF64* and *FY*. Moreover, *PAPS1* and *PAPS2/PAPS4* are implicated in different stress response pathways in *Arabidopsis*. Reduced activity of the poly(A) polymerase *PAPS1* results in enhanced resistance to osmotic and oxidative stress. Simultaneously, *paps1* mutants are cold-sensitive. In contrast, *PAPS2/PAPS4* are not involved in the regulation of osmotic or cold stress, but *paps2 paps4* loss-of-function mutants exhibit enhanced sensitivity to oxidative stress provoked in the chloroplast. Thus, both *PAPS1* and *PAPS2/PAPS4* are required to maintain a balanced redox state in plants. *PAPS1* seems to fulfil this function in concert with *CPSF30*, a polyadenylation factor that regulates alternative polyadenylation and tolerance to oxidative stress.

The individual *paps* mutant phenotypes and the cPAP-specific genetic interactions support the model of cPAP-dependent polyadenylation of selected mRNAs. The high similarity of the polyadenylation machineries in yeast, mammals and plants suggests that similar regulatory mechanisms might be present in other organism groups. The cPAP-dependent developmental and physiological pathways identified in this work allow the design of targeted experiments to better understand the ecological and molecular context underlying cPAP-specialization.

Zusammenfassung

Polyadenylierung ist ein entscheidender Schritt der 3‘-End-Prozessierung und somit der Reifung von prä-mRNAs. Die Länge des Poly(A)-Schwanzes entscheidet unter anderem über die Stabilität und Lokalisierung von mRNAs. Viele Eukaryoten besitzen mehrere Kopien der kanonischen Poly(A)-Polymerasen (PAP). In Säugetieren ist das Ausknocken dieser Enzyme letal. Pflanzen mit reduzierter PAP-Aktivität sind hingegen überlebensfähig. *Arabidopsis* exprimiert drei im Zellkern lokalisierte PAPs namens PAPS1, PAPS2 und PAPS4. Kürzlich ergab die Analyse von *Arabidopsis paps1*-Mutanten, dass eine Gen-Untergruppe vorzugsweise von PAPS1 polyadenyliert wird (Vi et al. 2013). Die Spezialisierung der PAPs könnte der Regulierung verschiedener Gengruppen in Anpassung an die Pflanzenentwicklung und an bestimmte Umweltbedingungen dienen.

In der vorliegenden Arbeit werden die Phänotypen von *Arabidopsis* PAP-Mutanten unter verschiedenen Bedingungen im Detail charakterisiert, um die PAP-basierte Genregulation besser zu verstehen. Es wird gezeigt, dass alle drei PAPs an der Regulation der Blühzeit und an der Regulation von Stressantworten beteiligt sind. Während *paps1*-Mutanten früh blühen, zeigen *paps4*- und *paps2 paps4*-Mutanten einen spät blühenden Phänotypen. *PAPS1* fördert die Expression des Blühzeitinhibitors *FLC* vermutlich über die Polyadenylierung eines *FLC*-Aktivators. *PAPS2* und *PAPS4* haben teilweise überlappende Funktionen und unterdrücken die Expression von *FLC* und mindestens einem weiteren, bisher unbekannten Blühzeitinhibitor. Die beiden PAPs agieren in einem neu entdeckten, genetischen Pfad gemeinsam mit dem Blühzeitregulator *FCA*, jedoch unabhängig von den Polyadenylierungsfaktoren und Blühzeitregulatoren *CstF64* und *FY*. Des Weiteren regulieren *PAPS1* und *PAPS2*/*PAPS4* verschiedene Stressantworten. Das Reduzieren der *PAPS1*-Aktivität führt zu verstärkter Resistenz gegen osmotischen und oxidativen Stress, bei gleichzeitig erhöhter Kältesensitivität der Pflanzen. *PAPS2*/*PAPS4* sind im Gegensatz dazu nicht an der Regulation von Kälte- oder osmotischem Stress beteiligt. Die *paps2 paps4*-Mutanten besitzen jedoch reduzierte Toleranz gegen oxidativen Stress in Chloroplasten. Das heißt, sowohl *PAPS1* als auch *PAPS2*/*PAPS4* sind nötig, um einen ausgeglichenen Redoxstatus der Pflanzenzellen zu gewährleisten. *PAPS1* arbeitet bei dieser Regulation scheinbar mit dem Polyadenylierungsfaktor *CPSF30* zusammen.

Die individuellen Phänotypen der *paps*-Mutanten und die spezifischen genetischen Interaktionen der Poly(A)-Polymerasen in *Arabidopsis* unterstützen das Modell der PAP-abhängigen Polyadenylierung von selektierten mRNAs. Da die Polyadenylierungskomplexe in Hefen, Säugetieren und Pflanzen starke Ähnlichkeiten aufweisen, ist es denkbar, dass dieser Regulierungsmechanismus auch in anderen Organismengruppen präsent ist. Basierend auf den Ergebnissen dieser Arbeit können gezielt weitere Experimente entwickelt werden, um die ökologischen und molekularen Grundlagen der PAP-Spezialisierung zu untersuchen.

1. Introduction

1.1 Poly(A) polymerases: functions and implications in gene expression regulation

1.1.1 The 3' end processing complex regulates transcriptional termination

One of the most basic and essential processes to form living cells is gene expression, the process of transcribing and translating information encoded by DNA into RNAs and proteins. Genes encoding proteins are first transcribed into messenger RNAs (mRNAs) by RNA polymerase II (Pol II). To generate mature templates for the subsequent translation by ribosomes, eukaryotic precursor mRNAs (pre-mRNAs) undergo several processing steps, including 5' capping, splicing, editing and polyadenylation. These modifications occur simultaneously with transcription (Proudfoot 2004; Bentley 2014). Polyadenylation is catalysed by a poly(A) polymerase (PAP in yeast/mammals; PAPS in plants) which is embedded in a large protein complex that detects poly(A) sites and cleaves the RNA substrate. Since mRNA 3' end processing is critical for the final structure and the exonic content of the mature mRNA, it is elaborately regulated. The processing machinery decides between alternative polyadenylation (APA) sites which can be found in up to 79% of mammalian genes and in up to 82% of plant genes (Shen et al. 2011; Hunt 2011; Tian and Manley 2013). Around 60% of the *Arabidopsis thaliana* (from here on *Arabidopsis*) mRNAs were found to be alternatively polyadenylated (Shen et al. 2011). In addition, splicing and polyadenylation have to be coordinated, since polyadenylation sites might be located in alternatively spliced regions of the mRNA (Xing and Li 2011).

Polyadenylation sites are defined by regulatory *cis*-elements in the mRNA. These elements have been discovered by mutation and sequencing analysis. In contrast to the highly conserved polyadenylation signals known from animals, such as the AAUAAA element or the downstream element, plants exhibit several sequence stretches enriched in certain nucleotides upstream of the cleavage site known as far upstream element and near upstream element (Hunt 1994; Rothnie 1996; **Fig. 2**). Both the base composition and the relative distances between the elements seem to be important for correct 3' end processing in plants (Rothnie et al. 1994; Loke et al. 2005). The so-called cleavage element harbours the actual cleavage and polyadenylation site (PAS) which is defined by a conserved YA dinucleotide surrounded by a U-rich region (Loke et al. 2005). Notably, secondary structure formation of the 3' untranslated region (UTR) of mRNAs has been suggested to be required for PAS recognition by protein complexes (Loke et al. 2005; Ding et al. 2014b). Functional aspects of mRNA secondary structures have been reviewed recently (Silverman et al. 2013).

The respective *trans*-acting factors have been studied largely in yeast and mammals. Tremendous progress in understanding the composition and function of the eukaryotic 3' end processing machinery was made during the 1990s (Wahle and Rüegsegger 1999). In animals three major protein complexes act together and constitute the large processing machinery in which the poly(A)

polymerase (PAP) is embedded: the Cleavage Factor (CF), the Cleavage-stimulating Factor (CstF) and the Cleavage and Polyadenylation Specificity Factor (CPSF) (**Fig. 1**). In yeast, most of these factors have conserved counterparts, albeit certain factor subunits may take over different functions (reviewed by Mandel et al. 2008; Millevoi and Vagner 2010; Proudfoot 2011).

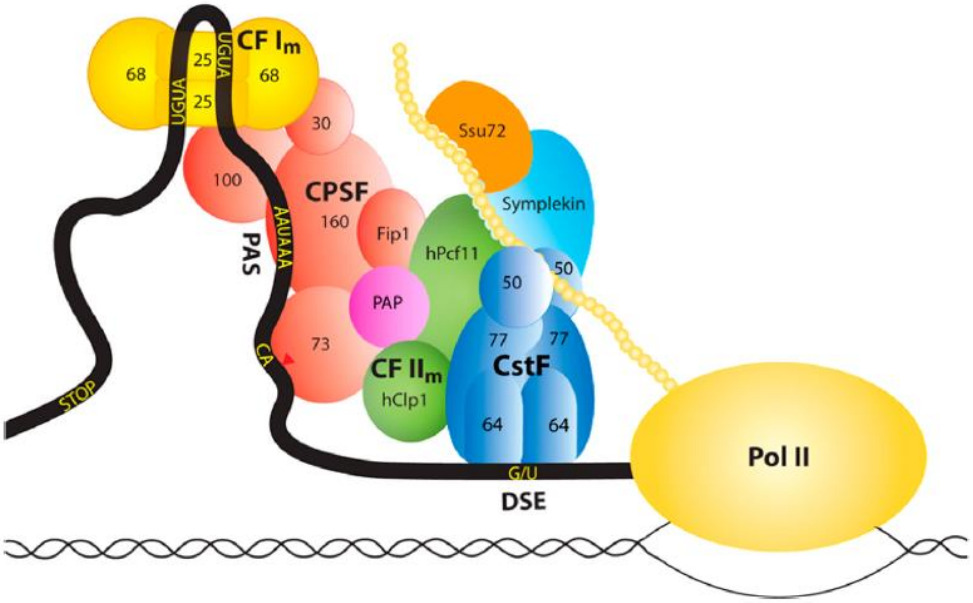

Fig. 1 The mammalian 3' end processing machinery (from Jurado et al. 2014).
Several conserved protein complexes consisting of various subunits constitute the polyadenylation and cleavage machinery. The CPSF complex binds the AAUAAA signal surrounding the polyadenylation site (PAS). The CPSF73 subunit performs the cleavage at the CA dinucleotide (red arrowhead). The CstF complex binds the downstream element (DSE), but also the C-terminal domain of RNA polymerase II (Pol II), which is illustrated by yellow circles. The CFI complex binds auxiliary RNA signals.

The CstF complex consists of three subunits, named 50, 64 and 77, after their molecular mass in kilo Dalton (kDa). CstF binds the downstream polyadenylation element and is involved in both cleavage and polyadenylation (Takagaki and Manley 1997; Millevoi and Vagner 2010). It recognizes RNA elements via its 64 kDa subunit and binds the CPSF complex with its 77 kDa subunit, which helps defining the PAS (Mandel et al. 2008). In mammals, loss of *CstF64* function leads to diverse APA events and cellular deregulations (Millevoi and Vagner 2010).

The Cleavage Factor subunits CFI and CFII aid in positioning the complex (Mandel et al. 2008). Specifically CFI, a factor unique to mammals, exhibits high positional specificity relative to the PAS and thus determines proper PAS selection and correct 3' UTR length (Gruber et al. 2012; Martinson 2011).

A crucial role for cleavage and polyadenylation is fulfilled by the CPSF complex which is composed of five subunits: CPSF30, CPSF73, CPSF100, CPSF160 and Fip1. The CPSF subunits may be referred to as CPSF1 to CPSF4 in the literature. In this work, subunits will be named after their weight in kDa. In

mammals, CPSF160, the largest subunit, strongly binds the AAUAAA signal, associates with CstF77 and recruits the PAP to the mRNA (Murthy and Manley 1995; Zhao et al. 1999). In yeast, Fip1 (*F*actor *i*nteracting with *P*ap1p) binds PAP and other polyadenylation factors and seems to serve as a molecular bridge (Preker et al. 1995; Meinke et al. 2008). The actual cleavage, i.e. the hydrolysis of a phosphodiester bond in the pre-mRNA, is most likely performed by the CPSF73 subunit, which possesses metal-dependent endonuclease activity (Ryan et al. 2004; **Fig. 1**, **Fig. 2**).

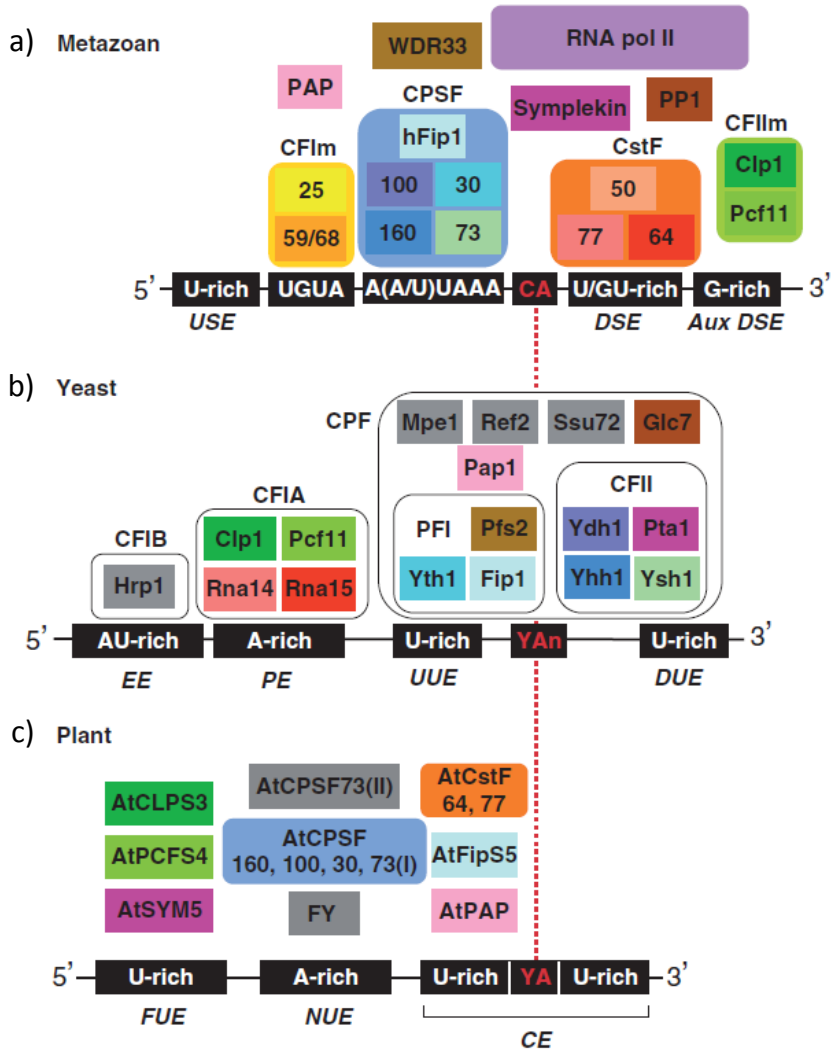

Fig. 2 Comparison of 3' end processing complexes (from Millevoi and Vagner 2010, modified).
The polyadenylation complexes from a) metazoans, b) yeast and c) plants are shown. Homologous factors are colour-matched while organism-group specific factors are depicted in grey. RNA-binding and protein interactions are considered. A dotted red line represents the cleavage and polyadenylation site. Legend of *cis*-elements in black rectangles: USE – upstream element; DSE – downstream element; Aux DSE – auxiliary downstream element; EE – efficiency element; PE – positioning element; UUE – upstream U-rich element; DUE – downstream U-rich element; FUE – far upstream element; NUE – near upstream element; CE – cleavage element.

Table 1 Comparison of core polyadenylation factors from mammals, yeast and plants.
The table is based on Hunt 2008; Mandel et al. 2008 and Millevoi and Vagner 2010. Listed are gene names in humans and yeast and the respective protein functions in the 3' end processing complex. *Arabidopsis* counterparts are designated. Amino acid sequences of the *Arabidopsis* factors were compared to the human proteins with regard to length (amino acid number) and identity (extent to which two sequences have the same residues at the same positions in an alignment, expressed in percentage). References to protein or mutant studies in *Arabidopsis* are listed.

Subunit terminology (mammal/ yeast)	Protein function (mammal and/ or yeast)	*Arabidopsis* counterpart	*Arabidopsis* gene	% identity	% length	References to *Arabidopsis* studies
PAPα/ PAP1p	polyadenylates mRNAs	PAPS1 PAPS2 PAPS3 PAPS4	*At1g17980* *At2g25850* *At3g06560* *At4g32850*	44 44 33 45	96 106 68 100	Addepalli et al. 2004; Meeks et al. 2009; Vi et al. 2013; Trost et al. 2014
CPSF160/ Yhh1	binds AAUAAA	CPSF160	*At5g51660*	50	100	Xu et al. 2006
CPSF100/ Ydh1	unknown	CPSF100/ ESP5	*At5g23880*	37	94	Elliott et al. 2003; Tzafrir et al. 2004; Herr et al. 2006
CPSF73/ Ysh1	endonuclease	CPSF73-I CPSF73-II	*At1g61010* *At2g01730*	54 36	101 90	Xu et al. 2004, 2006
CPSF30/ Yth1	RNA-binding, endonuclease	CPSF30/ OXT6	*At1g30460*	35	213	Reviewed by Hunt 2014
CstF77/ Rna14	RNA-binding, itself alternatively processed	CstF77	*At1g17760*	37	102	Yao et al. 2002; Bell and Hunt 2010; Liu et al. 2010
CstF64/ Rna15	RNA-binding, controls APA	CstF64	*At1g71800*	47	80	Yao et al. 2002; Liu et al. 2010
CstF50/ -	binds PolII and splicing factors	CstF50	*At5g60940*	57	100	Yao et al. 2002
CFIm25/ -	cleavage factor, RNA-binding	CFIm-25	*At4g29820* *At4g25550*	40 59	97 88	-
CFIm68/59/ -	cleavage factor	-	-	-	-	-
Clp1/ Clp	RNA kinase	CLPS3 CLPS5	*At3g04680* *At5g39930*	42 26	104 100	Xing et al. 2008a
PCF11/ Pcf11	interacts with CstF	PCFS1 PCFS4 PCFS5	*At1g66500* *At4g04885* *At5g43620*	28 36 29	26 52 26	Xing et al. 2008b, 2013
FIP1L1/ Fip1	interacts with PAPα, regulates CPSF30 activity	Fip1 [V]/ FIPS5 FIPS3	*At5g58040* *At3g66652*	44	213	Forbes et al. 2006; Hunt et al. 2008
WDR33/ Pfs2	connects 3' end complex factors	FY	*At5g13480*	48	198	Simpson et al. 2003
Symplekin/ Pta1	part of CPSF	SYM1 SYM2 SYM5/ESP4	*At1g27590* *At1g27595* *At5g01400*	25 29 31	20 75 115	Herr et al. 2006
PAPB/ Pab1p	poly(A) extension, length control	PABN1	*At5g51120*	64	42	-

Plants exhibit orthologues to all 3' end processing factors described above and several factors are encoded by more than one gene (**Table 1**; **Fig. 2**; Hunt 2008; Hunt et al. 2012). Most of these factors are essential. However, weak and hypomorphic alleles of several complex components have been identified in *Arabidopsis*. Interestingly, these mutants display quite specific and sometimes common phenotypes.

In a screen for mutants showing enhanced silencing of a reporter gene, several polyadenylation factor mutants were discovered as so called *e*nhanced *s*ilencing *p*henotype (*esp*) mutants (Herr et al. 2006). The *esp1* mutant exhibits a mutation in a protein related to CstF64 that is lacking an RNA recognition motif. *Esp5* mutants are defective in *AtCPSF100* function and additionally exhibit an early flowering phenotype. *AtCPSF100* interacts with *AtPAPS* and is essential for embryonic development (Elliott et al. 2003; Tzafrir et al. 2004). It was moreover found to physically interact with FY, another highly conserved polyadenylation factor (Herr et al. 2006). Hypomorphic *fy*, *cstf64* and *cstf77* mutants exhibit a late flowering phenotype (Henderson et al. 2005; Liu et al. 2010). Knockout mutations of FY are lethal and stronger c*stf64* and c*stf77* mutant alleles exhibit sterility or female gametophytic lethality, respectively, underlining the significance of proper PAS choice for plant development (see chapter 1.2.2). CPSF30, another core polyadenylation factor, was identified in a completely different approach that sought to unravel elements regulating the response to oxidative stress in *Arabidopsis* (Zhang et al. 2008; see chapter 1.3.3).

1.1.2 The regulation of alternative polyadenylation

Several findings demonstrate the tight coupling of transcription and 3' end processing. With its large carboxy-terminal domain (CTD), RNA PolII binds CstF77 and CstF50, which in turn have been shown to interact with a splicing factor (**Fig. 2**; McCracken et al. 1997, 2003). A functional PAS is required to terminate transcription, and PolII is involved in the cleavage reaction (Proudfoot 1989; Ryan et al. 2002).In yeast, PAP and CF1 have been found to interact with transcription factor IIB (TFIIB). This interaction supports gene looping and transcription re-initiation (Medler et al. 2011; Al Husini et al. 2013).

A tremendous amount of genes in diverse organisms was found to contain more than one PAS, raising the question how the processing machinery decides on one specific PAS. In recent years, several mechanisms contributing to PAS selection have been unravelled (reviewed by Tian and Manley 2013). PASs can possess different strengths depending on their signal composition, and polyadenylation core complex factors exhibit preferences for proximal (i.e. upstream) or distal PASs (Takagaki et al. 1996). Thus, abundance changes of certain factors can have wide effects on PAS choice and mRNA fate. Additional miRNA-target sites or RNA-binding protein target sites influence mRNA stability. Accessory factors like RNA-binding proteins can block *cis*-elements in a tissue-specific

manner (Wang et al. 2008a). In addition, also chromatin accessibility influences PAS selection, although it is a matter of debate whether APA is a cause or effect of variations in nucleosome density (Tian and Manley 2013; Huang et al. 2013). Polyadenylation and splicing are particularly coupled in a competing relationship when PASs are located in introns (Martinson 2011). In *Drosophila melanogaster* (fruit fly) it was discovered that 17% of all genes are arranged in nested patterns and that intronic poly(A) signals are mostly silenced (Tikhonov et al. 2013). The splicing factor U1 has been shown to simultaneously bind RNA 3' ends and PAP, thereby inhibiting the polyadenylation of mRNAs, including its own pre-mRNA (Gunderson et al. 1994, 1998).

Recently, a unified polyadenylation code has been suggested (Davis and Shi 2014). The model integrates PAS positions, strength of *cis*-elements, concentrations of *trans*-factors as well as transcription elongation rates and aims to enable predictions of preferential PASs.

Since deregulated APA can cause human diseases and APA manipulations bear therapeutic potential, a lot of attention has been paid to the mechanism of PAS selection in mammals (Hollerer et al. 2014). Regulatory aspects of 3' end processing in animals have been currently reviewed by Tian and Manley 2013; Elkon et al. 2013; Davis and Shi 2014 and Gruber et al. 2013. In recent years, the meaning of APA in plants has also been unravelled in more detail and several mechanistic principals have been found to be transferable from mammals to plants (Xing and Li 2011; Wu et al. 2011; Sherstnev et al. 2012; Tsuchiya and Eulgem 2013; Hunt 2014). The plant-specific autonomous pathway that influences flowering time is an example for a regulatory network in which deregulations in PAS usage can result in strong phenotypes (see chapter 1.2.2).

1.1.3 Canonical poly(A) polymerases

Eukaryotic cells express several kinds of nuclear and cytoplasmic poly(A) polymerases with diverse functions (Schmidt and Norbury 2010; Laishram 2014). Canonical PAPs (cPAPs) are defined as proteins that share a high amino acid sequence identity with the human PAPα or the yeast PAP1p (Lingner et al. 1991; Thuresson et al. 1994). These enzymes polyadenylate mRNAs and are mostly localized in the nucleus, but can also be found in the cytoplasm (Lee et al. 2000; Meeks et al. 2009). Remarkably, the number of cPAPs encoded by different eukaryotic organisms can vary. *Drosophila melanogaster*, *Saccharomyces cerevisiae* (budding yeast) or the green unicellular algae *Chlamydomonas reinhardtii* encode only one cPAP, but in the genomes of a large variety of organisms several cPAPs can be identified.

In humans, three cPAPs named PAPα (also PAPOLA), PAPβ (also PAPOLB, testis-PAP or TPAP), and PAPγ (also PAPOLG or neo-PAP) are expressed (Thuresson et al. 1994; Martin and Keller 2007; **Fig. 3**). PAPα and PAPγ perform the bulk mRNA polyadenylation in animal cells, and while PAPα can be detected in nucleus and cytosol, PAPγ is located exclusively in the nucleus (reviewed by Martin and

Keller 2007). Different splice forms have been detected for both enzymes, but only the larger proteins with molecular masses of around 80 kDa are catalytically active (Wahle and Rüegsegger 1999). The actual polyadenylation is performed by a catalytical centre in the highly conserved N-terminal domain (NTD), which resembles other nucleotidyl transferases (Martin and Keller 1996).

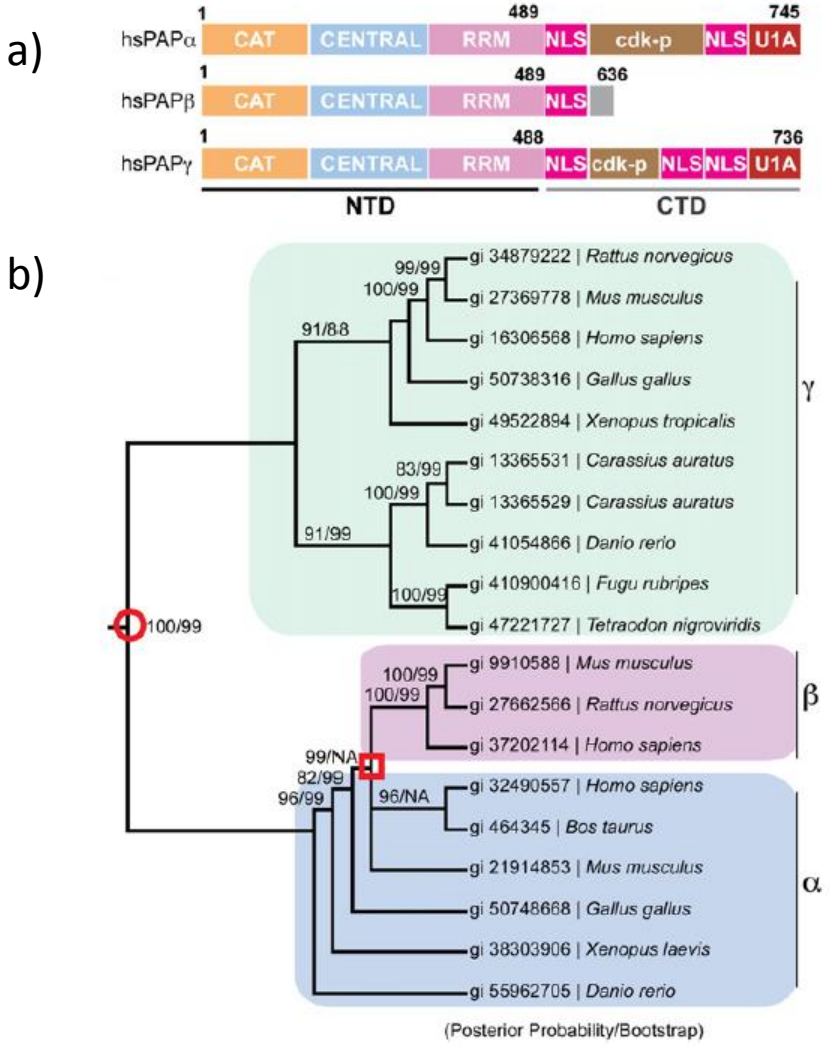

Fig. 3 Structure and alignment of mammalian cPAPs (from Yang et al. 2014).
a) Schematic image of the protein structures of human cPAPs. The N-terminal domain (NTD) comprises a catalytic domain (CAT), a central domain and an RNA recognition motif (RRM), followed by a nuclear localization sequence (NLS). *HsPAPα, hsPAPβ* and *hsPAPγ* exhibit similar modular protein structures. However, the cytosolic *hsPAPβ* does not contain the C-terminal domain, comprising cyclin-dependent kinase phosphorylation sites (cdk-p) and a U1A interaction motif (U1A). The domain sizes are not proportional to the length of the amino acid sequences. b) Phylogenetic tree of vertebrate cPAPs. Animal cPAPs group into the three clades α, β, and γ named after the human cPAPs. For the alignment, cPAP sequences from rat (*Rattus norvegicus*), mouse (*Mus musculus*), human (*Homo sapiens*), chicken (*Gallus gallus*), cattle (*Bos taurus*), frog (*Xenopus tropicalis*), goldfish (*Carassius auratus*), zebrafish (*Danio rerio*) and pufferfish (*Fugu rubripes* and *Tetraodon nigroviridis*) were used.

Via an RNA-binding domain, the mammal PAP-NTD is connected with a less conserved regulatory carboxy-terminal domain (CTD) (Raabe et al. 1994; **Fig. 3**). The CTD contains two nuclear localization signals followed by a serine/threonine-rich region, which has been shown to undergo

phosphorylation, sumoylation or acetylation (Colgan et al. 1996, 1998; Shimazu et al. 2007; Vethantham et al. 2008). These modifications can alter the catalytic activity of cPAPs during a cell cycle, the localization or protein interactions of the cPAP. In contrast, the third mammalian PAP, PAPβ, lacks the CTD and functional nuclear localization domains and is found exclusively in the cytoplasm of testis cells (Kashiwabara et al. 2000; Lee et al. 2000), where it polyadenylates mRNAs required for spermatogenesis (Kashiwabara et al. 2002). Accordingly, the lack of PAPβ leads to male sterility in mice.

While animals have been shown to express one (chicken), two (zebrafish) or three cPAPs (e.g. cow, mouse, human), plants encode between two (moss fern *Selagenilla*, moss *Physcomitrella*) and up to six PAPSs (*Oryza sativa*) (Meeks et al. 2009; **Fig. 4**).

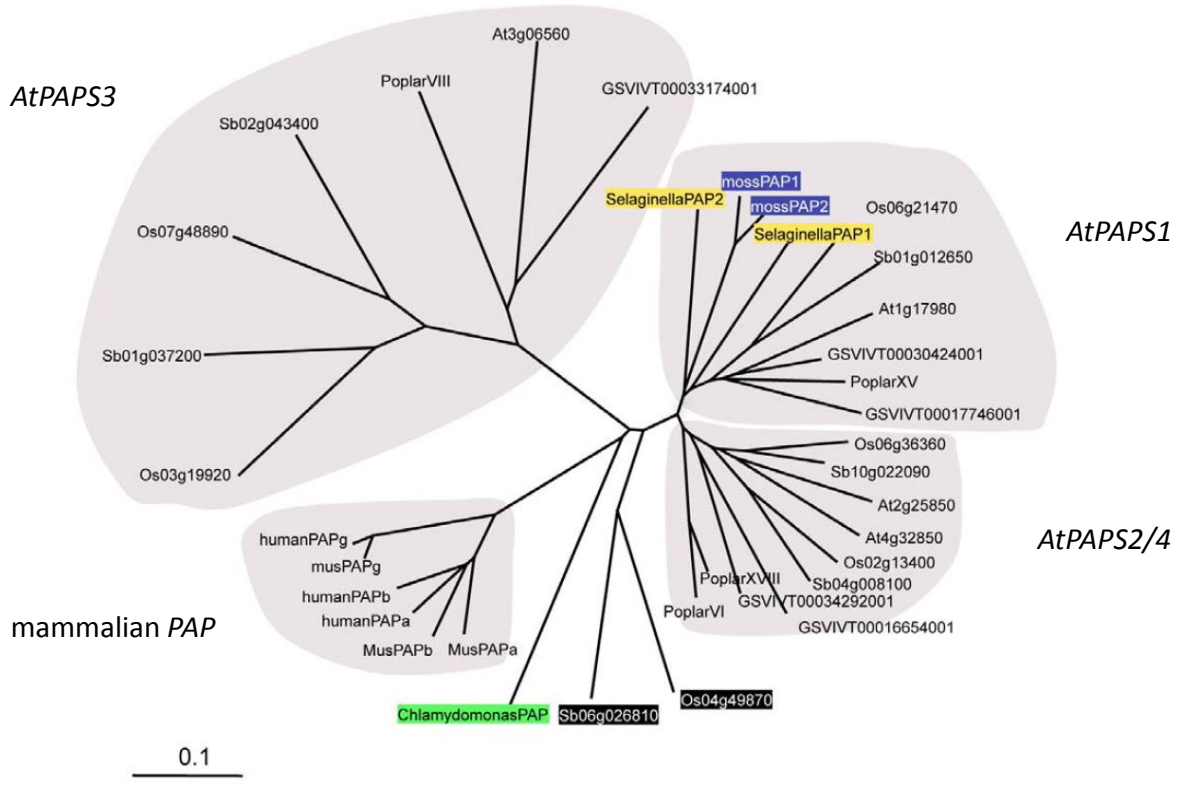

Fig. 4 Alignment of cPAPs from plants and animals (from Meeks et al. 2009, modified).
Plant cPAPs group in clusters around the *Arabidopsis* cPAPs *PAPS1, PAPS2/4* and *PAPS3*, indicated by gray areas. The PAPs from mouse and human group in a separate mammalian clade. Indicated by colors are PAPs from *Chlamydomonas reinhardtii* (green), *Selaginella moellendorfii* (yellow), *Physcomitrella patens* (blue) and two putative pseudogenes from monocots (black). Other plant PAP sequences were taken from *Arabidopsis*, rice (*Oryza sativa*), sorghum (*Sorghum bicolor*), poplar (*Populus trichocarpa*) and grapevine (*Vitis vinifera*).

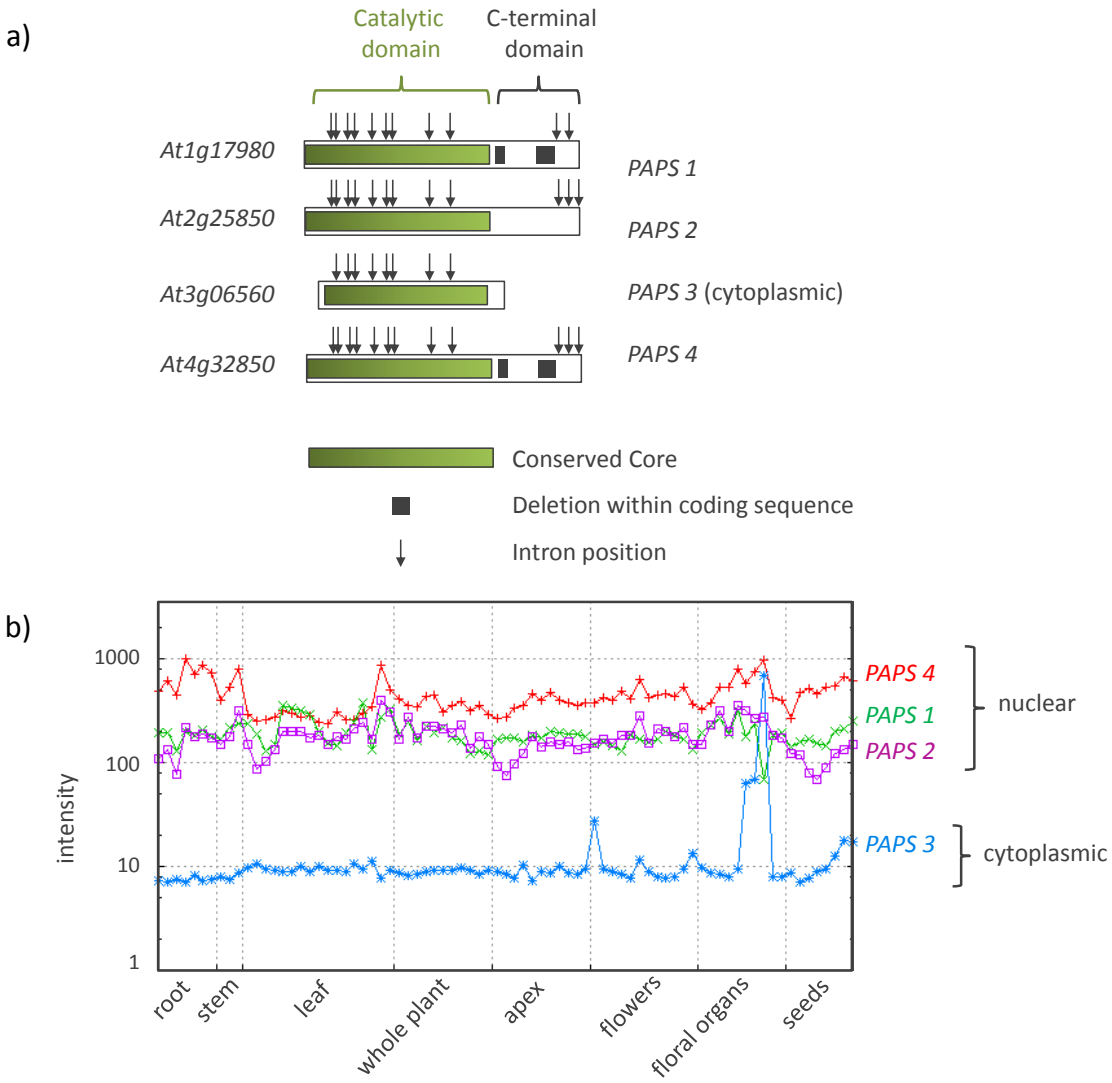

Fig. 5 Protein structure and expression pattern of *Arabidopsis* poly(A) polymerases.
a) Schematic presentation of the four AtPAPS proteins (after Addepalli et al. 2004, graphics modified). The conserved core that performs the catalysis, deletions and intron positions are indicated. The nuclear PAPSs contain a regulatory C-terminal domain, while the cytoplasmic PAPS3 consists entirely of the catalytic core domain. b) Expression level of the four *AtPAPS* genes in different plant tissues. While the nuclear *PAPSs* are expressed throughout the plant at high levels (with *PAPS4* showing the strongest expression), the cytoplasmic *PAPS3* is mainly expressed in floral organs. The strong peak reflects the expression of *PAPS3* in pollen samples. The image was generated using the AtGenExpress Visualization Tool AVT (Schmid et al. 2005).

Arabidopsis encodes four cPAPs, named *PAPS1* to *PAPS4*. The gene names correspond to the chromosome localization of the four *AtPAPS* loci (Addepalli et al. 2004). So far, no crystal structure is available for plant PAPs. However, with regard to the protein sequences, the domain arrangement of the three nuclear enzymes PAPS1, PAPS2 and PAPS4 is similar to that of the mammalian nuclear cPAPs. A highly conserved NTD performs the catalytic reaction, while the CTD sequences are less conserved. With regard to their protein sequences, PAPS2 and PAPS4 exhibit a high overall similarity, suggesting functional redundancy (**Fig. 5**). In contrast to PAPS1 and PAPS2/PAPS4, the PAPS3 protein lacks the CTD and is located solely in the cytoplasm (Meeks et al. 2009). In an alignment with other plant and animal c*PAP* sequences, the four *AtPAPSs* group in three clusters along with the other plant

PAPs, while the animal cPAPs form a fourth clade (**Fig. 4**). Moreover, *PAPS3* is mainly expressed in the pollen, while the three nuclear PAPSs are expressed throughout the plant (**Fig. 5 b**). These structural and localization features resemble the characteristics of the three human PAPs described before (Hunt 2008).

All AtPAPS proteins have been shown to exhibit unspecific polyadenylation activity *in vitro* (Hunt et al. 2000; Meeks et al. 2009). Meeks et al. (2009) could not detect homozygous *paps* transfer-DNA (T-DNA) insertion mutants among plant populations segregating for seven different mutant alleles of the four different *AtPAPSs*. The group suggested that mutations in either *AtPAPS* gene are gametophytic lethal and thus all cPAPs are essential for plant development. Later, Vi et al. (2013) showed that homozygous T-DNA insertion and point mutants can be obtained for all four AtPAPSs. The function of the three nuclear PAPSs was analysed more in detail. It was shown that homozygous *paps2* and *paps4* knockout mutants as well as *paps2 paps4* double mutants are viable and show a wild-type like phenotype. However, knockout mutations of *PAPS1* are indeed gametophytic lethal and homozygous mutants could be obtained for hypomorphic alleles only. The loss-of-function *paps1-1* mutant, which was identified in an ethyl-methanesulfonate (EMS) mutagenesis screen, carries a point mutation in the essential N-terminal domain between the catalytic core and the RNA-binding domain. *paps1-1* mutants exhibit smaller serrated leaves and larger floral organs than the *Arabidopsis* wild type, a surprisingly specific phenotype for a ubiquitously expressed enzyme (Vi et al. 2013; Vi 2013, PhD thesis). The leaf phenotype is at least partly caused by the deregulated polyadenylation of SMALL AUXIN UP RNA (SAUR) mRNAs. This was the first example of an mRNA sub-group being polyadenylated specifically by one canonical PAP. Substrate specificity had so far only been shown for noncanonical PAPs (ncPAPs) like the Star-PAP or GLD2 in animals (Mellman et al. 2008; Wang et al. 2002).

1.1.4 Poly(A) tail length control and its implications for gene expression regulation

Polyadenylation is an integral part of pre-mRNA maturation of almost all eukaryotic mRNAs. The only exceptions are certain metazoan histone mRNAs which form a stem loop at their 3’ end instead of being polyadenylated (Dávila López and Samuelsson 2008). Subsequent to the cleavage in the 3’ UTR, a PAP adds adenosine monophosphates (A’s) to the released 3’ OH group. The poly(A) tail (PAT) is elongated to an organism-specific length reaching from around 80 nucleotides (nt) in yeast up to 250 A’s in mammals (Wahle 1995; Amrani et al. 1997). In *Arabidopsis*, the tail was found to start with an average length of around 150 nt (Vi 2013, PhD thesis).

The PAT serves several functions in the cell. It was shown to be required for mRNAs to pass the nuclear envelope and to enter the cytoplasm (Dower et al. 2004; Fuke and Ohno 2008). In the cytoplasm, the PAT is progressively degraded at a transcript-specific deadenylation rate and the

remaining short tails ultimately trigger decapping and exosomal decay of the mRNA (Decker and Parker 1993; Beelman and Parker 1995). A higher stability of mRNAs is supported by cytoplasmic poly(A) binding proteins which prevent deadenylation (Bernstein et al. 1989; Ford et al. 1997). Interestingly, with more advanced techniques determining the 3' terminome (the entity of mRNA 3' ends), a high proportion of stable oligo(A)-containing transcripts has been discovered in recent years (e.g. Choi and Hagedorn 2003; Meijer et al. 2007; Chang et al. 2014).

Longer PATs have been found to correlate with higher protein expression levels by stimulating mRNA translation (e.g. Preiss et al. 1998; Novoa et al. 2010). In mammals and yeast, the cytoplasmic poly(A) binding protein PABP interacts with the cap-binding translation initiation factor subunit eIF4, which results in pseudo-circularization of the mRNA and an enhancement of translation efficiency (Tarun and Sachs 1996; Weill et al. 2012).

1.2 Control of flowering time and the role of 3' end processing

1.2.1 The flowering time network: Key regulators and pathways in *Arabidopsis*

During the plant life cycle, the transition to flowering is a decisive step. To ensure reproductive success, the change of the developmental program has to occur under favourable environmental conditions. Optimal climate or nutrient requirements for flowering might differ from species to species and a tight regulatory network is a prerequisite for the plant to survive seasonal fluctuations. Some plants flower annually or even have several reproductive cycles per year; others flower in a perennial mode. The life cycle of biennial plants lasts for two years. Biennials often need a prolonged period of cold in winter as a trigger to leave the vegetative growth phase and to enter the reproductive cycle. This process is known as vernalization and has been studied intensely in the last two decades. *Arabidopsis* serves as a good model plant since both vernalization-dependent and -independent accessions are available.

Before the competence to flower is gained, plants undergo a change from the juvenile to the adult phase, which is often accompanied by morphological changes regarding leaf size and shape or plant architecture (Poethig 2003). Mainly internal factors, like the sugar status, hormonal changes and epigenetic mechanisms are involved in the process of plant maturation (reviewed e.g. by Poethig 2013 and Thomas 2013). Two antagonistic miRNA families named *miR156* and *miR172* play a major role in age-dependent flowering time control (extensively reviewed by Yamaguchi and Abe 2012; Wang 2014; Spanudakis and Jackson 2014).

While the promotive role of the plant hormone gibberellic acid (GA) for flowering has been observed long ago, its molecular mode of action has only been revealed in recent years (Langridge 1957; Wilson and Somerville 1995). GA acts through so-called DELLAs, nuclear proteins that contain a

DELLA domain and are degraded by the proteasome upon GA perception (Sun and Gubler 2004; Gao et al. 2011).

Plants react to environmental factors, like the amount of available light or the external temperature, with intricate and interconnected molecular networks. Environmental signals are perceived and integrated, leading to specific growth responses adapted to the surrounding conditions. Day length is measured by the photoperiod pathway which is tightly connected with the plant internal circadian clock (reviewed by Srikanth and Schmid 2011; Kinmonth-Schultz et al. 2013). The complex internal clock system is daily entrained by light and aids to adjust the photosynthetic metabolism in advance to the rhythmic environmental changes. Furthermore, blue and red light receptors located in the leaf sense light quality and quantity.

In addition to light, elevated ambient temperatures promote flowering. Plants react very sensitively to thermal changes. Under low temperatures, the flowering inhibitor *FLOWERING LOCUS M* (*FLM*) represses gene expression of floral pathway integrators (FPIs) in concert with the flowering time regulator *SHORT VEGETATIVE PHASE* (*SVP*). In response to increased temperatures, *FLM* mRNA is spliced alternatively. The FLM-SVP protein complex induced by warm temperatures has a reduced DNA binding activity. Consequently, FPI promoters are released (Lee et al. 2013; Posé et al. 2013). Moreover, the nucleosome composition and DNA accessibility of flowering key regulators, like *FLOWERING LOCUS T* (*FT*), are modified in response to ambient temperature (Kumar and Wigge 2010; Kumar et al. 2012).

A major inhibitor of flowering is the MADS box-type transcription factor *FLOWERING LOCUS C* (*FLC*) (Michaels and Amasino 2001). FLC typically binds genes containing a CarG-box in their promoter region and can act as transcriptional activator or repressor in diverse developmental processes (Deng et al. 2011; Willmann and Poethig 2011). It represses flowering by inhibiting the expression of FPIs like *FT*, *LEAFY* (*LFY*) or *SUPPRESSOR OF OVEREXPRESSION OF CONSTANS1* (*SOC1/ AGL20*) (Michaels and Amasino 2001; Simpson and Dean 2002; Helliwell et al. 2006; **Fig. 6**). Several chromatin modifiers and RNA-processing factors are required for the upregulation of *FLC* (summarized by Quesada et al. 2005). High expression levels of *FLC* cause the late flowering phenotype of vernalization-dependent *Arabidopsis* accessions (Michaels and Amasino 1999). The *FLC*-promoting component in these ecotypes is *FRIGIDA* (*FRI*) (Koornneef et al. 1994; Johanson et al. 2000). FRI is a scaffold protein acting in a complex that recruits chromatin modifiers to the *FLC* promoter (Choi et al. 2011). Long periods of cold cause epigenetic changes at the *FLC* locus, resulting in a stringent and persistent downregulation (see chapter 1.2.3).

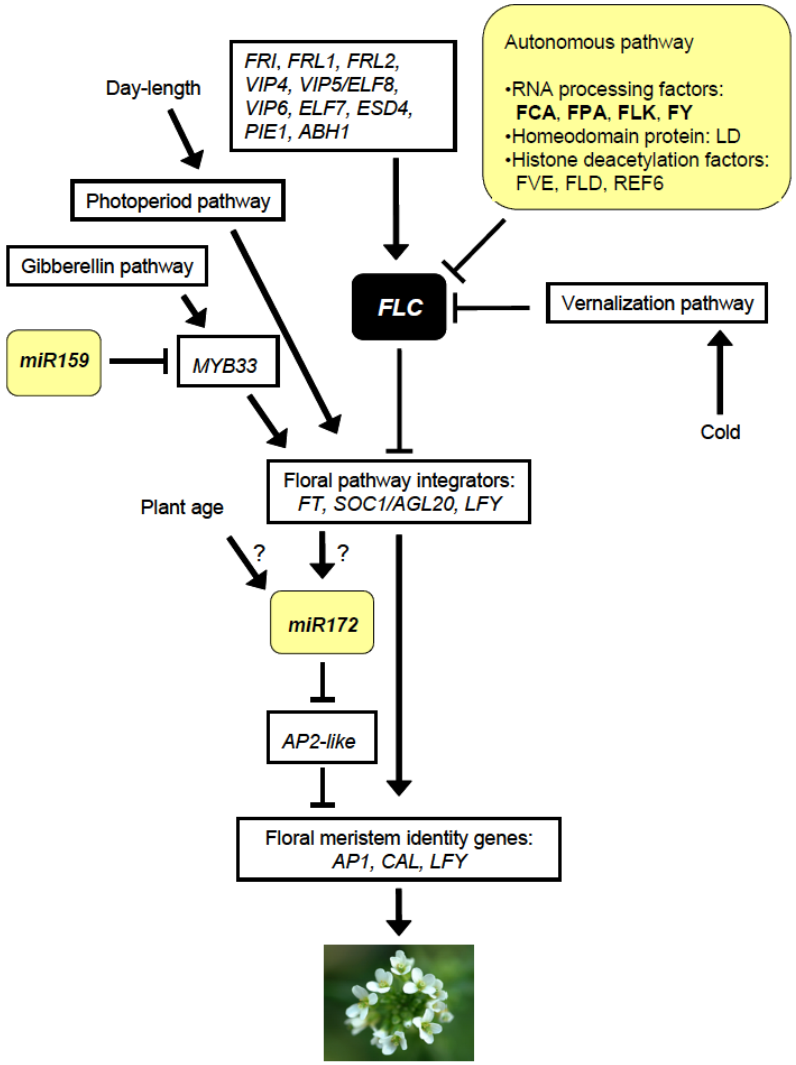

Fig. 6 The different pathways regulating flowering time in *Arabidopsis* (from Quesada et al. 2005).
Together with the photoperiod and gibberellic acid pathways, the various pathways regulating *FLC* converge on the expression of a small set of floral pathway integrator genes. *FLC*, the main inhibitor of flowering, is upregulated by diverse factors including *FRI* and downregulated by the autonomous pathway and the vernalization pathway. The floral pathway integrators in turn activate floral homeotic transcription factors like *APETALA1* (*AP1*), *CAULIFLOWER* (*CAL*) or *LEAFY* (*LFY*). The *miR172*-dependent age pathway also promotes the expression of these floral meristem identity genes. GA-dependent degradation of DELLA proteins has been shown to promote the miRNA family *miR159* which targets a subset of MYB transcription factors. However, due to controversial findings in *Arabidopsis*, the role of the *miR159*-MYB module in flowering time control is still under debate (discussed in Spanudakis and Jackson 2014). Not shown here is the *FLM*/*SVP*-dependent temperature pathway described in the text, which also feeds in the regulation of the integrator genes.

Typical *Arabidopsis* ecotypes used for laboratory analyses, like Columbia-0 (Col-0) or Landsberg *erecta* (L*er*), contain inactive *FRI* alleles and thus flower early without vernalization. In these accessions, the *FLC* expression is downregulated by the so-called autonomous pathway (Koornneef et al. 1991; **Fig. 6**), which will be described in detail in chapter 1.2.2. Natural allelic variation of the flowering inhibitor *FLC* itself contributes to differential flowering times observed in different *Arabidopsis* accession (Michaels et al. 2003). Although both Col-0 and L*er* contain *FRI* null alleles, L*er* flowers earlier than Col-0 due to a 30 bp-repeat and a transposon inserted in the FLC^{Ler} allele.

The described internal and external cues are integrated by the plant and ultimately lead to flowering under favourable conditions. Rather than acting strictly in parallel, the different pathways seem to be interconnected. Several miRNAs are involved in the crosstalk of the hormone, age and photoperiod pathways controlling flowering time (Wang 2014). Lastly, the various signals converge on one regulatory checkpoint: they regulate the expression of the few above mentioned floral pathway integrators (Simpson and Dean 2002). The FPIs then activate floral homeotic genes, also known as floral meristem identity genes, or are involved in flower development themselves (**Fig. 6**). The processes of signal integration and gene expression coordination leading to flower formation have been excellently reviewed by Posé et al. (2012) and Andrés and Coupland (2012).

1.2.2 The autonomous pathway

In the early 1990s, a set of proteins with variable functions has been demonstrated to influence the flowering of *Arabidopsis* independently from environmental factors. The combined action of these factors has been termed the constitutive or autonomous pathway (Amasino 1996). The first groundbreaking work that suggested the discrimination of different, partly independent pathways in the regulation of flowering was performed by Koornneef et al. (1991). Marten Koornneef and his colleagues identified 11 loci which they separated in three groups based on their behaviour under long-day (LD) and short-day (SD) conditions in combination with vernalization treatments. Four of the genes detected by Koornneef et al. (1991) grouped together and are part of the autonomous pathway: *FCA*, *FY*, *FPA* and *FVE* (these names are no abbreviations). Later four more members, termed *FLOWERING LOCUS K* (*FLK)*, *FLOWERING LOCUS D* (*FLD)*, *LUMINIDEPENDENS* and *RELATIVE OF EARLY FLOWERING 6* (*REF6*), were classified (Quesada et al. 2005; **Fig. 6**). Most of the pathway members are RNA-processing or chromatin-modifying factors. Mutants of these factors flower late due to increased *FLC* expression but are responsive to vernalization (Michaels and Amasino 2001).

The best described factors of the autonomous pathway are the RNA-processing factors *FCA* and *FPA*. *FCA* encodes a plant-specific protein containing both RNA- and protein-binding domains (Macknight et al. 1997). Interestingly, in addition to controlling *FLC* transcription, FCA regulates its own splicing and polyadenylation. Four *FCA* splice forms have been described, called *FCA*α to *FCA*δ (Macknight et al. 1997; **Fig. 7**). While *FCA*β is predominantly expressed early in development, only the splice form *FCAγ* encodes the functional FCA protein. The active protein promotes the selection of a proximal (i.e. more upstream) PAS in intron 3, which leads to the production of a truncated, inactive protein (Quesada et al. 2003; **Fig. 8**).

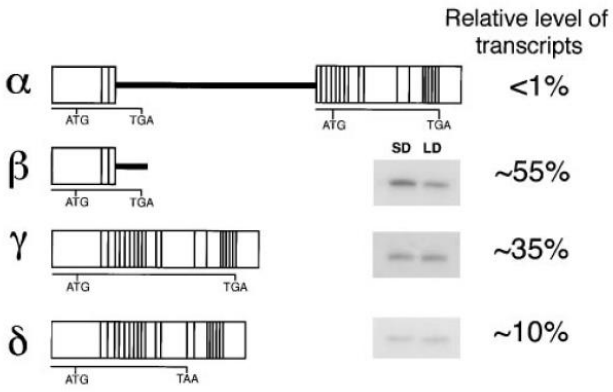

Fig. 7 Four *FCA* splice forms are expressed in *Arabidopsis* (from Macknight et al. 1997).
Exons are depicted as white boxes; retained introns are shown as black horizontal lines between the *exons*. Horizontal black lines underneath the illustrated mRNA represent possible open reading frames. *FCA* mRNA abundances were checked by RNAse protection assay and reverse transcription PCR with total RNA from plants grown under short day (SD) and long day (LD) conditions until they had reached the 2–3 leaf stage.

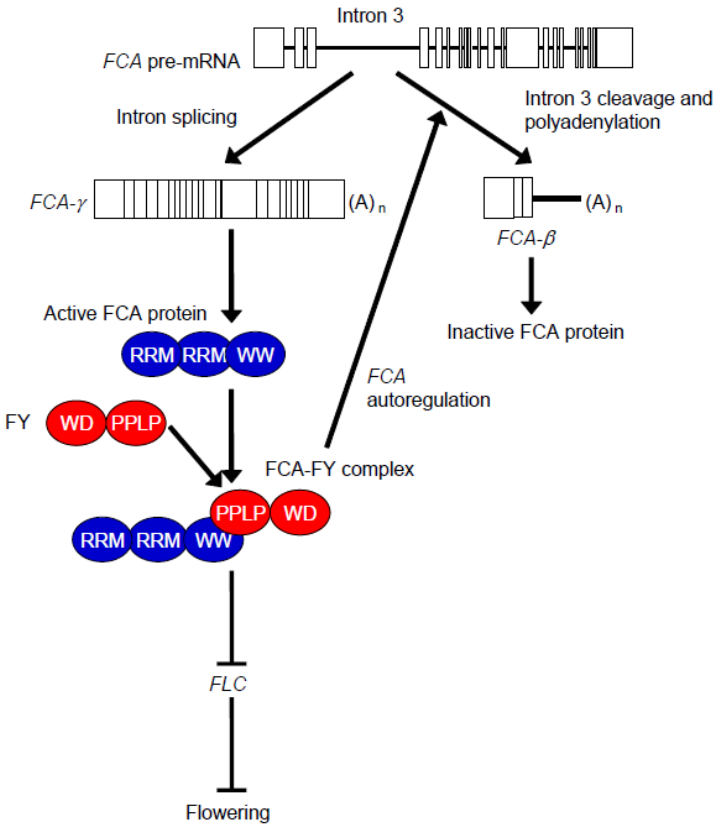

Fig. 8 The negative autoregulation of *FCA* controls flowering time (from Quesada et al. 2005).
The full-length mRNA *FCA-γ* encodes the functional FCA protein which contains two RNA recognition motifs (RRM) and a WW protein binding domain. FCA binds FY, a polyadenylation factor containing a WD and a PPLP domain. The FCA-FY complex inhibits the expression of the flowering inhibitor *FLC*, and in addition promotes the usage of an upstream intronic poly(A) site at the *FCA* locus by the 3' end processing complex. *FCA-β*, the resulting truncated mRNA, leads to a non-functional protein. This mechanisms regulates the FCA level in a temporal and spatial manner and is decisive to avoid premature flowering.

The upstream regulators that lead to the initial shift in PAS and splice site selection are still unknown (Rataj and Simpson 2014). However, the balance of the *FCA* splice forms in vegetative tissue is critical for the suppression of premature flowering (Macknight et al. 2002). In order to repress FLC activity and for the negative FCA autoregulation, FCA has to interact physically with the polyadenylation factor FY (Simpson et al. 2003). Both factors form an epistasis group (Koornneef et al. 1998).

The plant FY protein contains an essential WD repeat structure that is highly conserved in eukaryotic FY homologues. In addition, it contains a C-terminal extension to interact with FCA (Simpson et al. 2003; Henderson et al. 2005). While null mutations in *AtFY* are lethal, mutants with hypomorphic alleles are viable and show variability in the late-flowering phenotype. Like *fca* mutants, the *fy* mutants flower early in combination with a loss-of-function *FLC* allele (Henderson et al. 2005). An epistasis analysis with the hypomorphic allele *fy-5*, performed by Feng et al. (2011), raised the possibility of FY being involved in both repression and *FCA*-independent activation of *FLC*.

The 3’ end processing factor FPA regulates its own splicing besides the downregulation of *FLC*, a situation reminiscent to the autoregulation of *FCA* (Hornyik et al. 2010). However, FPA and FCA act in independent pathways (Hornyik et al. 2010; Bäurle and Dean 2008). The repressive mode of action by *FCA* and *FPA* will be discussed in chapter 1.2.3.

The chromatin remodelling factors *FLD*, *FVE* and *REF6* ensure the timely flowering of *Arabidopsis* by controlling the deposition of repressive marks on chromatin at the *FLC* locus (Quesada et al. 2005). Very little is known about the RNA-binding protein FLK which regulates *FLC* constitutively and independently from the photoperiod or vernalization pathway (Lim et al. 2004; Mockler et al. 2004). LUMINIDEPENDENS is a homeodomain-containing protein which is expressed in meristematic regions and putatively acts as a transcription factor (Lee et al. 1994; Aukerman et al. 1999).

The restriction of *FLC* transcription by the autonomous pathway represents an example of gene regulation that links the coordination of mRNA 3’ end processing and chromatin modification. Since the effects of *FLC* expression alterations are directly visible at the phenotypic level, *Arabidopsis* flowering time has developed to a subject of intensive investigation. Over the years it was revealed that many pathway members, especially the general 3’ end processing regulators, have multiple functions at both the cellular and the whole-plant level. *FCA* is for example also required for root development (Macknight et al. 2002). Veley and Michaels (2008) analysed a large set of autonomous pathway double mutants and found several factors to be involved in the regulation of plant growth and fertility.

Other factors involved in RNA metabolism and splicing have been implicated in the regulation of *FLC* but have not been characterized enough to be classified as autonomous pathway members (Rataj and Simpson 2014).

1.2.3 The regulation of *FLC* expression by non-coding *FLC* transcripts

Several components of the autonomous pathway machinery regulating *FLC* expression contain RNA-binding domains. While both *FCA* and *FPA* are involved in the negative autoregulation of their own expression (chapter 1.2.2), the direct RNA targets have not been identified yet. In *fca* and *fpa* mutants, the *FLC* sense transcript does not undergo alternative polyadenylation (Simpson et al. 2003; Duc et al. 2013). However, two alternatively polyadenylated *FLC* antisense RNAs have been discovered (Swiezewski et al. 2007; Liu et al. 2007). The mechanism by which these antisense RNAs regulate *FLC* sense transcription has been investigated in much detail in recent years. Whether the discovered RNAs have functional implications in *Arabidopsis* flowering time regulation or whether they are merely an artefact of sense transcription has ever since been a matter of debate.

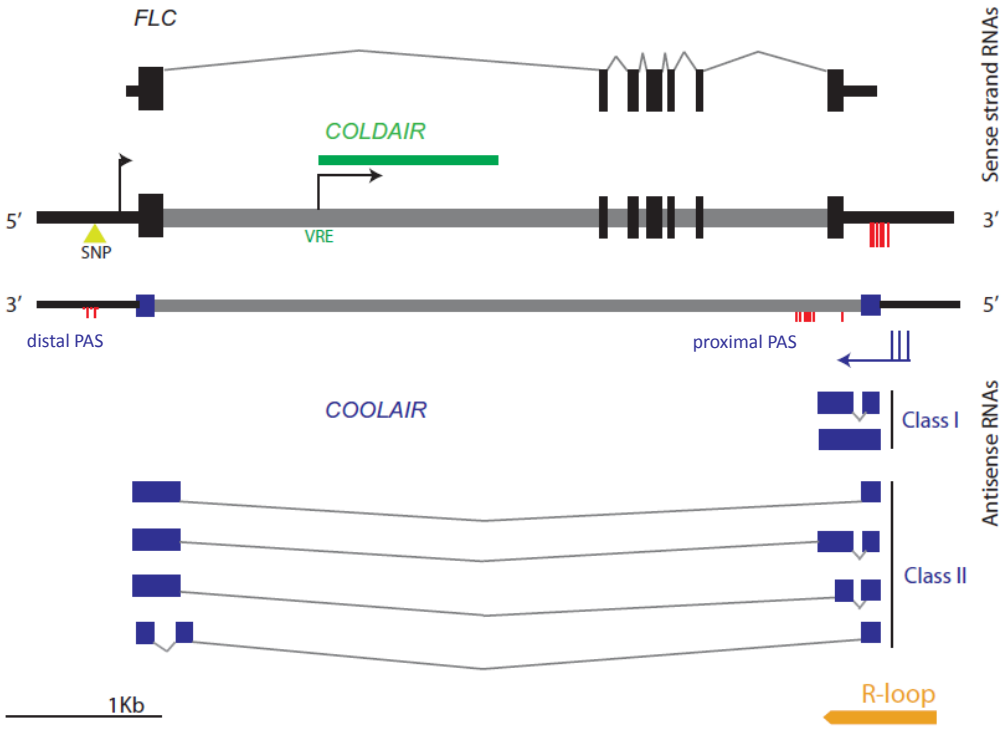

Fig. 9 Sense and antisense transcription at the *FLC* locus (from Rataj and Simpson 2014).
Depicted are the sense and antisense DNA strands of the chromosomal region around the *FLC* coding sequence. While only one *FLC* sense mRNA has been described, several splice forms of the *FLC* antisense RNAs termed *COOLAIR* have been identified (Swiezewski et al. 2009). *COOLAIR* contains two alternative polyadenylation sites. While *COOLAIR* class I is polyadenylated at a proximal PAS opposite to *FLC* sense intron 6, *COOLAIR* class II is polyadenylated at a distal PAS in the *FLC* sense promoter region. An intronic long non-coding RNA termed *COLDAIR* is expressed from the *FLC* sense strand and originates from the vernalization response element (VRE). Exons are indicated by boxes in black (sense strand) or blue (antisense strand). Red lines mark the position of antisense transcript cleavage sites identified by Duc et al. (2013). The orange pointed rectangle indicates an *FLC* region involved in the formation of R-loops. An R-loop consisting of *FLC* DNA and RNA was shown to inhibit *COOLAIR* transcription (Sun et al. 2013). The bright green triangle marks the only naturally occurring *FLC* single nucleotide polymorphism (SNP) that is associated with both altered flowering time and altered *COOLAIR* transcription levels (Coustham et al. 2012).

In relation to the animal non-coding RNA *HOTAIR*, which recruits chromatin modifiers to silence a locus in *trans*, the *FLC* antisense transcripts were termed *COOLAIR* (*COLD INDUCED LONG ANTISENSE INTRAGENIC RNA*) (Rinn et al. 2007; Swiezewski et al. 2009). The two *COOLAIR* PASs are located on the antisense strand opposite to the *FLC* intron 6 (proximal) and in the promoter region upstream of the *FLC* transcription start site (distal). The proximally polyadenylated *COOLAIR* transcript is termed antisense RNA class I, while the distally polyadenylated form is termed class II (Liu et al. 2007). Both classes are spliced alternatively (Swiezewski et al. 2009; Hornyik et al. 2010; **Fig. 9**).

A potential role for *COOLAIR* in flowering time regulation arose by the finding that increased *FLC* antisense levels were detected in plants treated with long-term cold. The putative *COOLAIR* promoter, located in the 3' region of the *FLC* sense gene, is indeed cold-responsive. The cold-induced expression of a p*COOLAIR*::antisense-*GFP* construct was sufficient to silence transcription of a *GFP* reporter gene (Swiezewski et al. 2009). Dynamic chromatin remodelling at the *FLC* locus during vernalization and several decisive proteins involved in the mechanism have long been discovered and have recently been reviewed in detail by Baulcombe and Dean (2014). Since *COOLAIR* expression peaks after two weeks of cold, it has been suggested to serve as an early repressor of *FLC* transcription in the cold (Swiezewski et al. 2009). Later, the so far transient silencing of *FLC* would be reinforced by chromatin modifications. However, this model was questioned by Helliwell et al. (2011), who discovered that the disruption of the *COOLAIR* promoter by a T-DNA does not abolish vernalization responsiveness.

Moreover, a second long non-coding RNA that responds to cold named *COLD ASSISTED INTRONIC NONCODING RNA* (*COLDAIR*) was discovered (Heo and Sung 2011; **Fig. 9**). The 1.1 kilo base pairs (kb) long RNA is capped but not polyadenylated and has been shown to recruit components of a polycomb group repressive complex to the *FLC* locus in response to cold. However, a recent analysis of the molecular processes during vernalization in perennial *Arabidopsis* species failed to detect *COLDAIR* (Castaings et al. 2014).

The *FLC* antisense RNAs have also been implicated in the regulation of the autonomous pathway. In *fca* and *fpa*, the ratio of *COOLAIR* transcripts shifts towards class II relative to the total *COOLAIR* amount (Liu et al. 2007, 2010; Hornyik et al. 2010). Moreover, mutants of the polyadenylation factor *CstF64* and of the histone demethylase *FLD* exhibit changes in *COOLAIR* 3' end processing (Liu et al. 2007, 2010). Like FCA, FPA binds *FLC* chromatin and has been suggested to act through *FLD* (Liu et al. 2007; Bäurle and Dean 2008). Moreover, proper alternative splicing of *COOLAIR* is required for *FLC* repression (Marquardt et al. 2014). A functional model which sought to combine these findings describes that both *FCA* and *FPA* promote the usage of the proximal polyadenylation site in concert with *CstF* and *FY* (Ietswaart et al. 2012; Sonmez and Dean 2012; **Fig. 10**). Increasing amounts of the

COOLAIR class I transcript then lead to the recruitment of *FLD* which initiates repressive chromatin changes at the *FLC* intron 6.

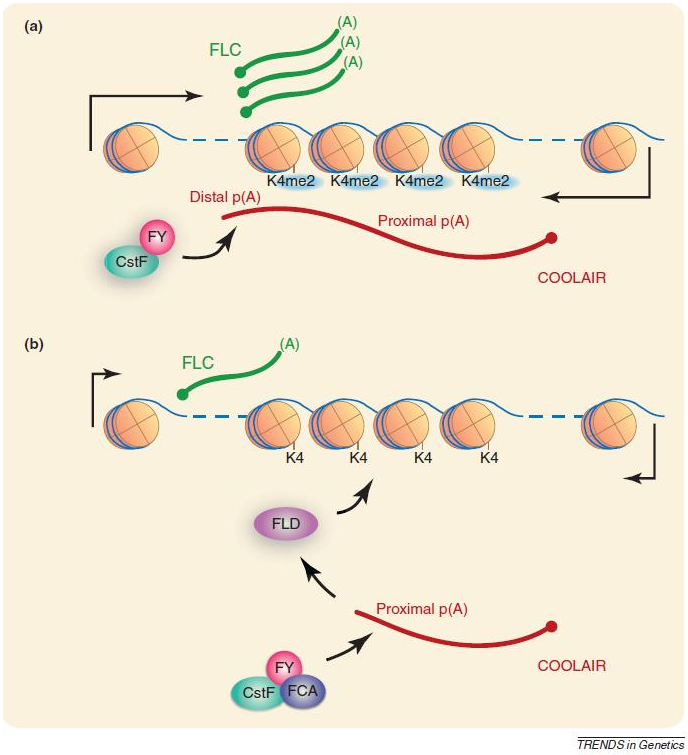

Fig. 10 Model for the repression of *FLC* by the autonomous pathway factor *FCA*.
The model was developed by Ietswaart et al. 2012. a) During the vegetative phase, the *FLC* antisense RNA *COOLAIR* (red) is polyadenylated at a distal PAS opposite the *FLC* sense-strand promoter. *FLC* transcription (green) is activated by histone 3 lysine 4 dimethylation (H3K4me2, in blue). b) In concert with the polyadenylation factors CstF and FY, the RNA-binding protein FCA promotes *COOLAIR* polyadenylation at the proximal PAS (Liu et al. 2010). This process is suggested to trigger the recruitment of the histone demethylase FLD to *FLC* chromatin, resulting in repression of sense-strand transcription by the removal of histone methylation.

The described model is challenged by various findings that have been summarized by Rataj and Simpson (2014). Amongst others, Rataj & Simpson argue that the late flowering phenotype of *fld* mutants is not completely epistatic to overexpressed *FCA* or *FPA* (Liu et al. 2007; Bäurle and Dean 2008), which opposes the idea of *FLD* acting constitutively downstream of *FCA* and *FPA.* Most strikingly however, Duc et al. (2013) could not confirm a reduced polyadenylation at the *COOLAIR* proximal PAS in *fpa* mutants using a single-molecule direct RNA sequencing approach. Instead, an increased amount of *COOLAIR* class II was detected. Rataj and Simpson (2014) suggest a model in which *FLC* antisense RNA polyadenylated at the distal PAS stimulates transcription of the *FLC* sense-strand in a self-reinforcing feedback loop. This phenomenon has been described in yeast before (Uhler et al. 2007; Crisucci and Arndt 2012). In this scenario, the proximal PAS of *COOLAIR* would only be promoted to prevent transcriptional read-through to the distal PAS, which would result in altered sense-strand transcription.

The various and seemingly heterogeneous results regarding the *FLC* antisense RNAs reflect technical difficulties that arise when several overlapping RNAs are transcribed from one locus. Furthermore, in contrast to the sense transcript, the *FLC* antisense RNAs are expressed at very low levels and undergo extensive alternative splicing and polyadenylation. Future work has to clarify whether both polyadenylation forms and the diverse splice forms indeed have functional implications. *COOLAIR* has been associated with the recruitment of chromatin remodeling factors in both the autonomous and the vernalization pathway. Contradictory results regarding the role of *COOLAIR* in both pathways are puzzling. So far, the exact mechanistic link between the antisense RNAs and the observed changes at the chromatin level remains to be elucidated.

1.3 Plant acclimations to stress

1.3.1 Plants are stressed constantly

When a young plant develops during germination or from a vegetative stolon, roots will usually be formed immediately to anchor the plant in the ground. From that point on, the plant is confronted with constantly changing environmental conditions. To what extent plants have to cope with fluctuations of temperature, light and humidity depends on the duration of the species' life cycle and on its location. The composition of the ground, which may be fertilized soil or stone covered only by a thin humus layer, determines the amount of accessible nutrients and trace elements and also osmolarity or the pH which plants have to adjust to. Lastly, plants are constantly subjected to predators, like feeding animals, fungi or bacterial pathogens. Every outer influence that compromises plant growth is termed stress. Stressful conditions might prevent an increase in biomass, optimal assimilation or even plant reproduction and survival. Acclimations designate short-term adjustments to changing conditions and are to be distinguished from genetic adaptations. To optimally use natural resources, plants evolved a variety of adaptation strategies regarding different aspects of plant growth or cell responses. These strategies are species- and habitat-specific. To increase yield, enhanced stress tolerance has ever since been selected by plant breeders and is still being improved (e.g. Araus and Cairns 2014; Kissoudis et al. 2014).

Plants constantly encounter multiple stress factors, which have to be recognized, integrated and transformed into signals that ultimately induce stress resistance or tolerance (**Fig. 11**).

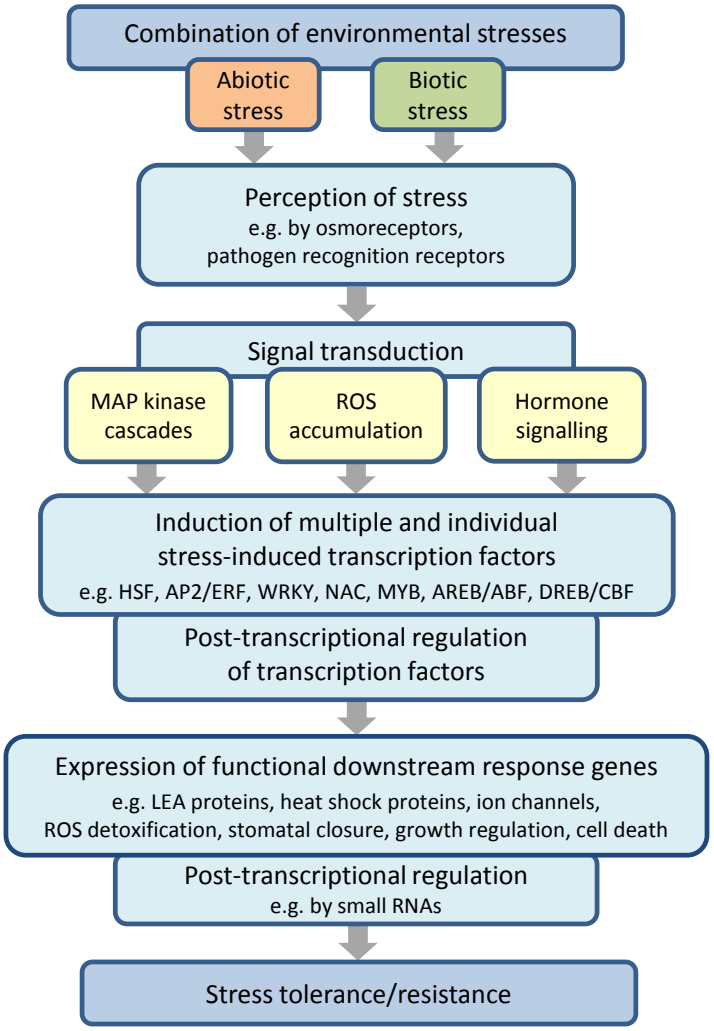

Fig. 11 Stress-induced signal transduction cascades in plants.
Plant resistance and tolerance responses to stress are regulated by intricate signalling cascades, involving e.g. receptors, second messengers and transcription factors as well as post-transcriptional and post-translational modifications (from Atkinson and Urwin 2012, modified).

Environmental signals can be perceived by the plasma membrane, for example by sensor proteins or by membrane fluidity, and can induce intracellular changes (Huang et al. 2012). The formation or release of second messengers like calcium ions (Ca^{2+}) or reactive oxygen species (ROS) results in the alteration of the cytosolic Ca^{2+} level, which induces calcium dependent signalling cascades (reviewed by Huang et al. 2012; Gilroy et al. 2014). Mitogen-activated protein kinases have been implicated in the crosstalk of calcium and ROS and serve as convergence points for different stress response pathways (Kissoudis et al. 2014). Moreover, phytohormones may be involved in stress signalling (reviewed e.g. by Atkinson and Urwin 2012). The signalling cascades ultimately lead to the activation of transcription factors and stress responsive genes. Extensive cross-talk between the diverse signalling cascades has been suggested, since many components have been shown to be shared by different stress pathways (reviewed e.g. by Atkinson and Urwin 2012; Kissoudis et al. 2014). Shared

signalling cascades might result from stresses that cannot be distinguished by the plant, or different stress types might require similar protective reactions (Knight and Knight 2001).

Post-transcriptional and post-translational processes add another layer of regulation to stress response pathways (reviewed by Mazzucotelli et al. 2008; **Fig. 12**). RNA secondary structure formation and alternative splicing of mRNAs encoding regulatory proteins in response to stress stimuli have been reported (Owttrim 2006; Staiger and Brown 2013). To reveal the impact of alternative splicing on stress resistance, global splicing patterns in stressed plants have been analysed (e.g. Ding et al. 2014a). Much less is known about alternative polyadenylation during stress adaptation. The polyadenylation factor CPSF30 determines PAS choice in response to oxidative stress (Zhang et al. 2008; Thomas et al. 2012). Mechanistic details about the CPSF30-dependent response pathway will be described in chapter 1.3.3.

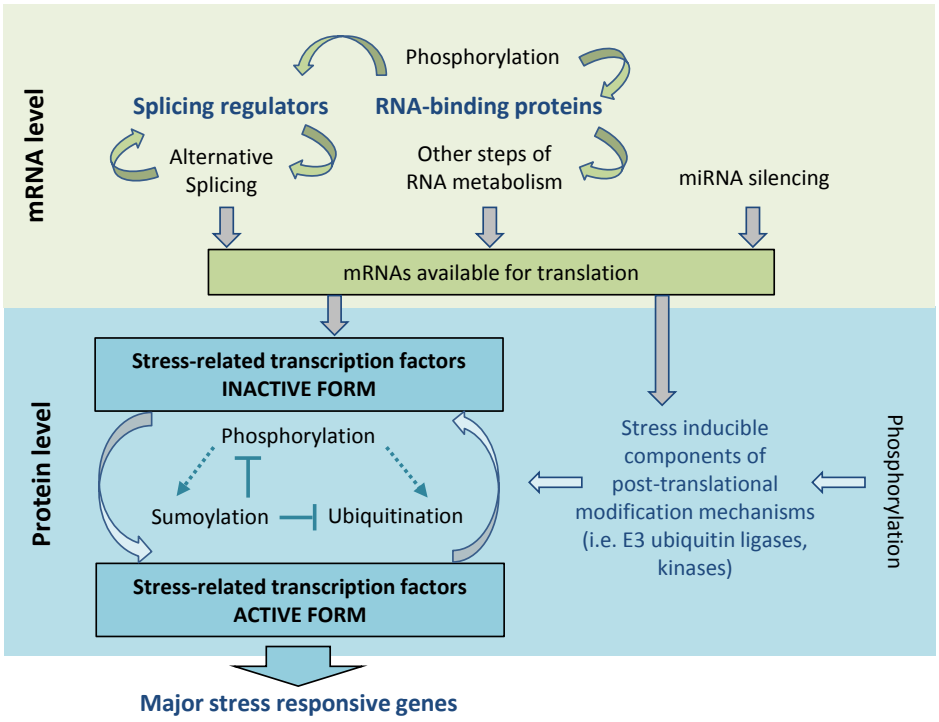

Fig. 12 RNA-processing and post-translational modification involved in plant stress responses.
Different RNA-processing steps and post-translational modifications are interconnected and contribute to the generation of responses to abiotic stress in plants (from Mazzucotelli et al. 2008, modified). Both post-transcriptional modification of stress-related mRNAs by alternative splicing or miRNA silencing add an additional regulatory layer to stress signalling pathways. Protein modifications like phosphorylation, sumoylation or ubiquitination regulate protein activities or mark proteins for degradation. Not mentioned here is the S-nitrosylation of proteins by nitric oxide, which has recently been characterized more in detail (reviewed by Trapet et al. 2014). Proteins involved in the regulation or modified themselves are marked in blue. Connections marked by dotted arrows have not been reported in plants.

In recent years, the potential of epigenetic mechanisms in the induction and maintenance of stress responses is being explored in more detail (reviewed by Baulcombe and Dean 2014; Kissoudis et al. 2014; Stief et al. 2014).

A vast amount of stress-induced signalling pathways and physiological plant stress responses has already been unravelled. It will be interesting to see whether further connections between the "classical" signalling cascades, 3' end processing factors and epigenetic modifications will be revealed in the future and which regulatory steps might serve as integration nodes in the regulatory networks.

1.3.2 Molecular acclimations of plant cells to oxidative stress

Since plants are photosynthetic organisms, large quantities of oxygen are constitutively being produced. As by-products, ROS, such as hydroxyl radicals, superoxide (O_2^-), singlet oxygen ($^1O_2$), or hydrogen peroxide (H_2O_2) are generated. Metabolic pathways like respiration impinge on the intracellular ROS pool. Peroxisomes produce large amounts of H_2O_2 during photorespiration as well, but simultaneously limit the ROS content (Mhamdi et al. 2012; Sandalio et al. 2013). Additionally, both biotic and abiotic stress stimuli affect the cellular redox status (reviewed e.g. by Foyer and Noctor 2005). Critical amounts of ROS result in oxidative damage due to radical cascade reactions that destroy cell components like membranes, proteins or DNA (Noctor and Foyer 1998). To prevent cell death, ROS-scavenging components and enzymes are being produced constantly. Plant cells contain a large set of antioxidant components: ascorbic acid, glutathione (GSH) or NADP(H), but also small proteins like thioredoxin or glutaredoxin, or metabolites likes sugars, phenolics, amino acids, carotenoids and tocopherols (Couée et al. 2006; Kissoudis et al. 2014). Several enzymes disarm ROS via a conversion to harmless components, like oxygen and water. Superoxide dismutases (SODs) and peroxidases act throughout the cell. SODs transform O_2^- into H_2O_2, whereas peroxidases detoxify H_2O_2 to water by using a reductant (Bowler et al. 1992; Noctor and Foyer 1998). The ascorbate peroxidase for example uses ascorbate as a substrate which is subsequently recovered in the ascorbic acid-GSH-cycle (Rausch and Wachter 2005). Catalases detoxify H_2O_2 with a higher catalytic activity but with a lower substrate specificity than peroxidases (Willekens et al. 1997). Characteristics of ROS-scavenging components and enzymes in plants have been summarized e.g. by Noctor and Foyer 1998; Rausch and Wachter 2005 and Meyer et al. 2009. Antioxidants are of particular importance in plastids due to thiol-regulated enzymes in photosynthesis-related processes. H_2O_2 oxidises thiol groups very rapidly. Thus, high amounts of peroxidases and catalases are present in chloroplasts (Kaiser 1979; Meyer et al. 2009).

Remarkably, ROS are not only potentially harmful but are also important signalling components. They are required for proper plant development or during acclimation and defence reactions. Foyer and Shigeoka (2011) reviewed the regulatory role of ROS in the improvement of photosynthesis and discussed the possibility of ROS-scavenging mechanisms having evolved to be "leaky" to allow ROS to act as signalling molecules. Among the huge amount of genes responsive to ROS in *Arabidopsis*, there are many transcription factors and protein kinases (Shigeoka and Maruta 2014). Diverse factors

encoded by these genes do not show an obvious connection to oxidative response pathways. Surprisingly, the exact mechanism by which ROS are perceived in plant cells has yet to be uncovered. ROS are unlikely to be bound by proteins, but rather act indirectly by oxidizing cysteine containing proteins (reviewed by Shigeoka and Maruta 2014; Wrzaczek et al. 2013). In a very rapid reaction with the O_2^- anion, the gas nitric oxide (NO) can be converted to peroxynitrite which has been suggested to act as a signalling component in plants (Foyer and Shigeoka 2011). As a signalling molecule and via post-translational S-nitrosylation of proteins, NO is involved in the crosstalk between Ca^{2+} and ROS (summarized by Trapet et al. 2014).

The redox state, which is defined as the balance of ROS and ROS-detoxifying components, ultimately determines cell fate. Deleterious ROS concentrations may results in cell death, while moderate concentrations elicit certain cellular responses. Apparently, subsets of plant genes are induced specifically by certain kinds of ROS that are produced at particular cell compartments, while others are generally ROS-responsive (Shigeoka and Maruta 2014).

ROS-induced gene expression may be caused by signalling cascades and involve second messengers like calcium (Rentel and Knight 2004). Moreover, since H_2O_2 easily permeates membranes, it has been suggested to directly modulate activities of redox-responsive transcription factors or protein kinases in the nucleus (Shigeoka and Maruta 2014). One of these proteins may be the polyadenylation factor CPSF30 which connects redox-sensitivity with alternative polyadenylation and plant resistance to oxidative stress.

1.3.3 CPSF30-mediated alternative polyadenylation regulates the response to oxidative stress

The dual role of ROS described above entails the tight regulation of ROS-responsive gene expression at several levels. Since a polyadenylation factor mutant has been identified in a screen for ROS-resistant *Arabidopsis* plants, the functional relation between 3' end processing and oxidative stress is being investigated in more detail.

To identify factors required for plant responses to increased amounts of oxidative molecules in both the chloroplast and the cytoplasm, a T-DNA insertion mutant library was tested for an enhanced resistance phenotype (Zhang et al. 2008). The root formation of plants growing on media containing methyl viologen or catalase and GSH synthesis inhibitors (described in chapter 3.2.4) was used as an indicator for resistance. Although the mutant *oxt6* was generally smaller, it exhibited longer roots than the wild type Col-0 on both media. Moreover, *oxt6* exhibited a higher dry weight after two weeks of oxidative stress. The *oxt6* mutant contains a T-DNA insertion in the first exon of *At1g30460*, which disrupts the formation of the polyadenylation factor subunit *CPSF30* (described in chapter 1.1.1). The *OXT6* locus encodes two transcripts that are spliced and polyadenylated alternatively (Delaney et al. 2006; **Fig. 13**). The proximal polyadenylation site is located in intron 2. The short

transcript encodes CPSF30, a protein with a molecular weight of 30 kDa. The splicing of intron 2 enables the transcription of the full-length mRNA and the resulting protein has a size of 68 kDa (Delaney et al. 2006). The larger protein version has been termed CPSF-YT521-B, due to the sequence similarities of the C-terminal extension with the yeast splicing factor YT521-B (Delaney et al. 2006).

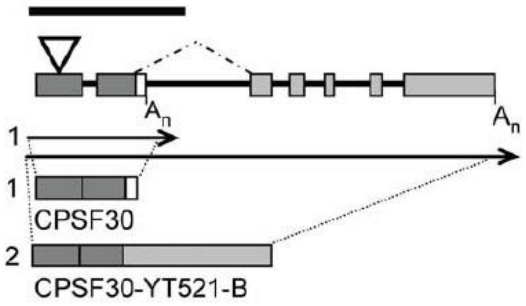

Fig. 13 Alternative polyadenylation at the *CPSF30* (*At1g30460*) locus (from Zhang et al. 2008).
The *CPSF30* gene contains 7 exons (boxes) and 6 introns (horizontal lines), encoding two alternatively polyadenylated mRNAs. Usage of the proximal polyadenylation site in intron 2 leads to the mRNA form "1" which encodes the active CPSF30 protein. CPSF30 has a molecular weight of ~30 kDa, and has Calmodulin/calcium-dependent RNA-binding activity. If intron 2 is spliced out, the full-length mRNA "2" is transcribed. The full-length protein, which is ~68 kDa large, lacks the last 13 C-terminal amino acids of CPSF30 (white box) and is termed CPSF30-YT521-B due to a large C-terminal domain (bright grey box) that shows sequence similarities to the human splicing factor YT521-B (Stoilov et al. 2002; Delaney et al. 2006). The T-DNA insertion site in *oxt6*, which is located 147 nt upstream of the start codon, is marked by a triangle.

CPSF30 is conserved among eukaryotes and its human and yeast counterparts are essential (Barabino et al. 1997). In *Arabidopsis*, the disruption of *CPSF30* affects genome-wide 3' end processing. The bulk mRNA polyadenylation is not altered in the *oxt6* T-DNA mutant, but a large subset of genes is alternatively polyadenylated, reflecting the function of CPSF in PAS selection (Zhang et al. 2008; Thomas et al. 2012). The expression of several thioredoxin- and glutaredoxin-related genes is upregulated in *oxt6*, which probably contributes to the observed stress-resistant phenotype (Zhang et al. 2008). While the *CPSF30* transcript is promoted by oxidative stress in the wild type, with a peak at ten hours after the induction, the expression of the full-length *CPSF-YT521-B* transcript remains unchanged. Accordingly, the introduction of the short *CPSF30* transcript into the *oxt6* mutant was sufficient to restore the wild type phenotype under oxidative stress (Zhang et al. 2008). However, with regard to both alternative polyadenylation and mRNA abundance, the large subset of genes deregulated in *oxt6* is not fully rescued in the absence of the full-length gene product (Zhang et al. 2008; Bruggeman et al. 2014). These findings indicate a functional significance of the large protein CPSF-YT521-B in gene expression regulation.

Certain structural features potentially indicate that the RNA-binding protein CPSF30 might be directly responsive to environmental cues (Hunt 2014). The C-terminal domain of the small protein exhibits unspecific endonucleolytic activity *in vitro* (Addepalli and Hunt 2007). Due to a disulfide bridge in this

region, the endonuclease function is inhibited by the sulfhydryl reagent dithiothreitol (DTT), but is not disturbed by the presence of reduced or oxidised glutathione (Addepalli and Hunt 2008). The functional significance of this protein feature *in vivo* remains to be elucidated.

Intriguingly, CPSF30 can also bind calmodulin. In the presence of calmodulin and calcium, the RNA-binding capacity of CPSF30 is abolished (Delaney et al. 2006). Calmodulin is a conserved calcium-sensor that is for example involved in the plant immune response (e.g. Perochon et al. 2011; Cheval et al. 2013). Thus, *CPSF30* provides a link between environmental influences, intracellular ROS and calcium levels and alternative polyadenylation (Xing and Li 2011). Indeed, similar to calmodulin, *CPSF30* is required for the salicylic-acid mediated plant immune response (Cheval et al. 2013; Bruggeman et al. 2014). Consequently, the *oxt6* mutant is more susceptible to *Pseudomonas syringae* infections than Col-0 (Bruggeman et al. 2014). Interestingly, *CPSF30* was not found to control the redox state of the intracellular glutathione pool.

In mammals it was shown that regulatory proteins can inhibit the complete polyadenylation complex by binding CPSF30. When the viral protein NS1 targets CPSF30 in influenza-virus infected cells, host mRNAs are not polyadenylated anymore and remain in the nucleus (Nemeroff et al. 1998). As a consequence, host gene expression is disrupted, while viral RNAs can still leave the nucleus. A different CPSF subunit, the human protein CPSF73, moves to the cytoplasm upon interaction with the ROS-responsive protein CSR1 (cellular stress response 1), which results in cell death (Han et al. 1998; Zhu et al. 2009). While CSR1 is an essential protein in *Arabidopsis*, the stress-induced translocation mechanism of CPSF73 has not been analysed in plants yet (Manabe et al. 2007). However, overexpressed CPSF30 has been detected in the cytoplasm of *Arabidopsis* cell cultures, indicating that CPSF subunits may not exclusively be located in the nucleus (Rao et al. 2009).

Clearly, similar regulatory mechanisms are likely to affect the activity and location of the remaining polyadenylation factor components as well. The example of CPSF30 provides a mechanistic link between oxidative stress and gene expression regulation. Likewise, 3’ end processing might play essential roles in the regulation of other stress responses.

1.4 Aim

To further investigate the regulatory potential of polyadenylation-controlled gene expression in *Arabidopsis*, the distinct functions of *AtPAPS1* and the two cPAPs *AtPAPS2* and *AtPAPS4* were characterized in detail in this thesis. Both *PAPS2* and *PAPS4* (in the following also termed *PAPS2/4*) share considerable amino acid sequence similarities, suggesting functional redundancy. Conclusions on the functional specificities of *PAPS1* and *PAPS2/4* were drawn from contrasting flowering time defects observed in different *paps* mutants. To identify the pathway disrupted in *paps* mutants, flowering times were determined under diverse growth conditions. Additionally, expression levels of key factors regulating flowering in *paps* mutants were analysed. In a different approach, *paps* mutations were combined with mutant alleles of flowering time factors, namely autonomous pathway components. The analysis aimed to reveal epistatic relationships and to further characterize the putative role of cPAPs in flowering time control.

To uncover additional *PAPS2/4* functions, a comparative analysis of *PAPS* expression was performed. Since *PAPS1* has been shown to be required for the mediation of biotic stress responses before (Trost et al. 2014), the *paps* mutant behaviour during a set of various short- and long-term stress exposures was analysed. An involvement of the polyadenylation factor *CPSF30* in the regulation of oxidative stress has been described (Zhang et al. 2008). The relation of *AtPAPS*s and *CPSF30* was tested by combining *paps* mutant alleles with the *oxt6* mutation. The response of *paps* single mutants and of the resulting *paps oxt6* mutants to oxidative stress was examined.

The transcriptome of *paps2 paps4* double mutant seedling was analysed and compared with the *paps1* transcriptome to uncover putative *PAPS*-specific target genes and to confirm the regulatory role of *PAPS2/4* in the response to various stresses.

Lastly, the PAPS1 and PAPS4 proteins were fused to yellow fluorescent protein (YFP) to confirm the nuclear localisation of PAPS proteins by microscopy and to gain the opportunity of validating alterations in PAPS abundances during certain growth conditions.

2. Material and Methods

2.1 Material

2.1.1 Chemicals

Chemicals were purchased from AppliChem (Darmstadt), Biozym Scientific GmbH (Hessisch Oldendorf), Difco (Detroit, USA), Duchefa Biochemie (Haarlem, The Netherlands), Frontier Scientific (Logan, USA), Lehle Seeds (Round Rock, USA), Merck (Darmstadt), Roche Diagnostics (Grenzach), Roth (Karlsruhe), Serva (Heidelberg), Sigma-Aldrich (St. Louis, USA), Thermo Fisher Scientific (Waltham, MA, USA) and VWR chemicals (Radnor, USA). Companies are based in Germany, if not indicated otherwise.

2.1.2 Technical equipment

The technical equipment is listed in Appendix A.

2.1.3 Disposable equipment

The disposable equipment is listed in Appendix B.

2.1.4 Microorganisms

The bacterial *Escherichia coli* (*E. coli*) strain XL-1 (Agilent Technologies/Stratagene, Santa Clara, USA) was used for vector amplification. The strain XL-1 can be selected by tetracyclin. The *Agrobacterium tumefaciens* strain GV3101 (Van Larebeke et al. 1974), which served to stably transform *Arabidopsis*, is resistant to gentamycin and rifampicin.

2.1.5 Enzymes and antibodies

Enzymes, like restriction endonucleases, polymerases etc. were purchased from Abchem (Cambridge, UK), Affymetrix (Santa Clara, CA, USA), Ambion/Life Technologies (Warrington, UK), Bioline Reagents (London, UK), Fermentas (St. Leon-Rot), Life Technologies (Carlsbad, CA, USA), New England Biolabs (NEB; Frankfurt am Main), Promega (Fitchburg, WI, USA), Qiagen (Surrey, UK) and Stratagene (Santa Clara, MO, USA) as indicated in the respective method chapter.

2.1.6 Plant materials

The *Arabidopsis thaliana* (L.) Heynh. ecotypes Landsberg *erecta* (L*er*) or Columbia-0 (Col-0) were used in all experiments. Plant mutants used in this work are summarized in **Table 2**.

Table 2 *Arabidopsis* mutants used in this thesis.
The mutant allele, the type of mutation and the *Arabidopsis* ecotype are indicated. References describing the mutation are given. The code of the T-DNA insertion lines obtained from the Nottingham *Arabidopsis* stock centre (NASC) are listed.

Mutant allele	Type of mutation	Ecotype	Reference
ahg2-1	5-bp deletion	Col-0	Nishimura et al. 2005
*cstf64-1**	point mutation	L*er*	Liu et al. 2010
*flc-2**	deletion	Col-0	Michaels and Amasino 1999
*flc-5**	point mutation	L*er*	Greb et al. 2007
*fca-9**	point mutation	Col-0	Page et al. 1999
*fy-2**	T-DNA insertion	Col-0	Henderson et al. 2005
*oxt6***	T-DNA insertion	Col-0	Zhang et al. 2008
paps1-1	T-DNA insertion	L*er* or Col-0^{+}	Vi et al. 2013
paps1-3	T-DNA insertion	Col-0	WiscDsLox413-416L14 (NASC)$^{++}$
paps1-3/ pPAPS1::PAPS1::YFP	T-DNA insertion	Col-0	Appendix E
paps1-4	T-DNA insertion	Col-0	WiscDsLox441G5 (NASC) $^{++}$
*paps2-3****	T-DNA insertion	Col-0	SALK_126395 (NASC)
paps2-6	T-DNA insertion	Col-0	SALK_003080 (NASC)
paps4-1	T-DNA insertion	Col-0	SALK_081180 (NASC)
paps4-2	T-DNA insertion	Col-0	WiscDsLox345-348M17 (NASC) $^{++}$
*paps4-3****	T-DNA insertion	Col-0	SALK_007979 (NASC)
paps4-3/ pPAPS4::PAPS4.5::YFP	T-DNA insertion	Col-0	Appendix E
paps4-3/ pPAPS4::PAPS4.8::YFP	T-DNA insertion	Col-0	Appendix E
paps4-4	T-DNA insertion	Col-0	SALK_117078 (NASC)
paps4-5	T-DNA insertion	Col-0	SALK_063790 (NASC)
paps2-3 paps4-3	T-DNA insertion	Col-0	obtained by crossing
paps2-3 paps4-3/ pPAPS4::PAPS4.5::YFP	T-DNA insertion	Col-0	Appendix E
paps2-3 paps4-3/ pPAPS4::PAPS4.8::YFP	T-DNA insertion	Col-0	Appendix E
paps2-3 paps4-3 ahg2-1	see above	Col-0	obtained by crossing
paps2-3 paps4-3 oxt6	see above	Col-0	obtained by crossing

* These mutant alleles were kindly provided by the laboratory of Caroline Dean.
** The *oxt6* mutant was kindly provided by Arthur Hunt.
*** The *paps2-3* and *paps4-3* alleles are termed *paps2-1* and *paps4-1* in previously published manuscripts, due to nomenclature standards.
+ The *paps1-1* allele was backcrossed to Col-0 for at least four times by Lang Son Vi.
++ WiscDsLox-T-DNA-insertion lines are resistant to glufosinolate and were pre-selected on PPT-containing media.

2.1.7 Antibiotics and herbicides

Antibiotics and herbicides were used to select mutant bacteria and Arabidopsis plants and are listed in **Table 3**. If not stated otherwise, the stock solutions were diluted 1:1000 (v/v) in the growth media. To select soil-grown plants with the herbicide Basta (glufosinolate; Bayer), a final concentration of 0.1 % (v/v) in water was applied with an aerosol can to plants that had grown for one to two weeks.

Table 3 Stock solutions of antibiotics and herbicides.
The name and type of the selective chemical are given. Stock solutions of the indicated concentrations were prepared with the indicated dissolvent.

Name	Type	Dissolvent	Stock solution
Ampicillin	antibiotic	ddH_2O	100 mg/ml
Chloramphenicol	antibiotic	ethanol	30 mg/ml
Gentamycin	antibiotic	ddH_2O	25 mg/ml
Kanamycin	antibiotic	ddH_2O	50 mg/ml
Tetracycline	antibiotic	ethanol	10 mg/ml
Rifampicin	antibiotic	DMSO	80 mg/ml
Phosphinothricin (PPT)	herbicide	ddH_2O	10 mg/ml

2.2 Plant cultivation

2.2.1 Cultivation on soil

Plants were cultivated on a soil mixture (3 parts *P-Erde*, 3 parts *T-Erde* and 1 part vermiculite). The empty pots were soaked with water containing the fungicide proPlant (Bayer). Before sowing out, seeds were gas-sterilized (chapter 2.2.3). Seeds on soil were stratified for three to five days at 4 °C. Plants were grown under long-day (LD) conditions (16 h light; 8 h darkness) in a growth room without temperature control with a photosynthetically active radiation (PAR) of 120 µmol photons/m^2/s, if not otherwise stated. The growth room is equipped with tubular fluorescent lamps (type Master TL-D 36W/840; Philips). During the first week of cultivation, the tray was covered with a transparent plastic lid to prevent high light stress. The humidity was kept between 50 % and 70 % in all experiments.

Experiments including *paps1-1* were performed in a climate growth chamber (day: 21 °C; night: 18 °C). The growth chamber is equipped with sodium vapour lamps (types SON-T AGRO 400W and HPI-T-Plus 400W, Philips), providing a PAR of 140 µmol photons/m^2/s. During the flowering time analysis with *paps1-1 paps4-3* lines, the PAR was reduced to 80 µmol photons/m^2/s.

All other flowering-related experiments including *paps1-1* were performed in a Percival at a PAR of 120 µmol photons/m^2/s (day: 22 °C; night: 20 °C). The settings during the short-day experiment were 8 h light and 16 h dark.

Flowering time analyses with *fca-9* and *fy-2* were performed under LD conditions in controlled environment rooms in a glass house, equipped with sodium vapour lamps providing a PAR of 160 µmol photons/m^2/s. The long-term hypoxia experiment and the flooding tolerance experiment were performed in the glass house at the Max-Planck-Institute of Molecular Plant Physiology.

2.2.2 Cultivation on plates

To cultivate seedlings under sterile conditions, seeds were wet-sterilized using the protocol described in chapter 2.2.4. Sterile seeds were sown out on 0.5× MS medium (Murashige and Skoog, Duchefa Biochemie; pH 5.8 with KOH, 7 g/l agar) in 100 × 100 mm plates or in plates with 100 mm Ø. Sugar (1 % w/v sucrose) was added to the solid media as indicated in the respective method chapter. Plates were sealed with breathable tape.

The plates were stratified and cultivated as described in chapter 2.2.1 or as indicated. In the growth room without temperature control, plates were irradiated by light-emitting diodes (LED) with a PAR of 120 µmol photons/m^2/s. In the climate growth chamber (day: 21 °C; night: 18 °C), plates were irradiated by sodium vapour lamps with a PAR of 120 µmol photons/m^2/s (lamp type see chapter 2.2.1). The oxidative stress experiment was performed in a Percival (day: 22 °C, night: 20 °C; 120 µmol photons/m^2/s).

2.2.3 Seed sterilization with chlorine gas

A small amount of seeds was transferred to a 1.5-ml tube and placed into a vacuum exsiccator. Next, 50 ml of sodium hypochlorite (12 %) was mixed with 1.5 ml concentrated hydrochloric acid (37 %) in a glass beaker. The beaker was transferred to the exsiccator immediately which was sealed with Parafilm for four hours. After that, the seeds were aerated overnight (O/N) to allow gas to evaporate.

2.2.4 Seed sterilization with sodium hypochlorite

Seeds were transferred to reaction tubes and the sterilization was performed in a clean bench. Seeds were soaked once in 1 ml 70 % (v/v) ethanol. Next, the seeds were incubated in 6 % (v/v) sodium hypochlorite (12 % solution mixed 1:2 with sterile ddH_2O). Subsequently, seeds were washed three times with 100 % ethanol and were transferred to a sterile filter paper with a sterile cut off tip to let the ethanol evaporate. The dry seeds were transferred back to the tube.

2.3 Cultivation of microorganisms

2.3.1 Growth media and bacteria cultivation

E. coli and *A. tumefaciens* were cultivated on solid LB medium in cell culture dishes (100 mm Ø). Liquid cultures were grown in sterile test tubes filled with 4 ml LB medium or flasks filled with 1/5 volume (vol) medium. Antibiotics were added to media in dependence of the used strains and vectors at the concentrations indicated in chapter 2.1.7. To amplify bacteria, both cell culture dishes and liquid cultures were incubated at 37 °C O/N.

LB medium	1 l
Bacto tryptone	10 g
Yeast extract	5 g
NaCl	10 g
pH 7.0	
To gain solid media, 15 g/l agar were added. Subsequently, the medium was autoclaved for 20 min.	

2.3.2 Preparation of *E. coli* stocks

To keep a library of vector stocks, a selected *E. coli* colony was amplified in 4 ml selective LB medium at 37 °C O/N. Next, 1 ml bacterial culture was transferred to a sterile screw-cap tube. 70 µl DMSO were added. Tubes were slowly inverted and transferred to a freezer (–70 °C). When needed, a small amount of the frozen culture was scraped off with a sterile tooth pick and streaked out on solid selective LB medium, or was directly transferred to a liquid culture.

2.4 DNA-related methods

2.4.1 Oligonucleotides

Oligonucleotides were ordered from LGC Genomics, Berlin. Names and sequences of the used oligonucleotides (or primers) are listed in Appendix C. The primer combinations used in all experiments and the individual annealing temperatures used in the related PCRs are listed in Appendix D.

2.4.2 Vectors and cloning strategy

The vectors used or produced in this thesis and the cloning strategy developed to produce vectors with *pPAPS:PAPS::venusYFP* constructs are summarized in Appendix E.

2.4.3 Isolation of plasmid DNA from *E. coli* cells by alkaline lysis (Miniprep)

To amplify a vector in *E. coli*, a 4 ml LB liquid culture (chapter 2.3.1) was inoculated with a single *E. coli* colony. The culture was incubated in a shaker at 37 °C rotating at 180 rpm. Subsequently, 2 ml of bacteria culture were transferred to a 2-ml tube and harvested by centrifugation (13,000 rpm, 2 min). The supernatant was discarded and the harvest was repeated with the rest of the liquid culture into the same tube. The cell pellet was resuspended in 100 µl E1 buffer. Next, 200 µl E2 buffer (or lysis buffer) were added to the resuspended cells. The tube was slowly inverted three to four times and incubated for not longer than five minutes. Subsequently, the reaction was neutralized by adding 150 µl E3 buffer. After several slow inversions of the tubes, the cell debris were precipitated by

centrifugation (13,000 rpm; 10 min; 4 °C). The supernatant was carefully transferred to a new 1.5-ml tube and 0.7 vol isopropanol were added. The tube was inverted to mix plasmid solution and alcohol, and the plasmid was harvested by centrifugation (13,000 rpm; 10 min; 4 °C). The pellet was washed with 70 % (v/v) ethanol and after harvesting the plasmid again by centrifugation (13,000 rpm; 5 min; 4 °C). The pellet was air-dried and subsequently dissolved in 50 µl ddH_2O.

E1 buffer
50 mM Tris-HCl (pH 8.0)
10 mM EDTA
0.1 mg/ml RNase A (NEB)

E2 buffer
0.2 M NaOH
1 % (w/v) SDS

E3 buffer
3.1 M sodium acetate (pH 5.5)

2.4.4 Isolation of plasmid DNA from *E. coli* cells by alkaline lysis (Midiprep)

To amplify low-copy vectors like pBarMAP, a large scale plasmid preparation, known as midiprep, was performed. The buffer compositions are given in chapter 2.4.3.

A 50 ml selective LB liquid culture was inoculated with a single *E. coli* colony and incubated O/N at 37 °C in a shaker (200 rpm). The culture was centrifuged in a sterile 50 ml tube to harvest the cells (7,500 rpm; 3 min; Beckman centrifuge, rotor type JLA 16.250). Having carefully discarded the supernatant, the pellet was resuspended in 5 ml E1 buffer. To lyse the cells, 5 ml E2 buffer were added and the tube was inverted carefully several times. Next, 7 ml E3 buffer were added, the tube was inverted and the solution was centrifuged (10,000 rpm; 10 min). The supernatant was carefully transferred to a new 50 ml tube and 1 vol isopropanol (about 17 ml) were added. The plasmid was precipitated by centrifugation (10,000 rpm; 15 min), washed with 5 ml 70 % (v/v) ethanol and harvested again (10,000 rpm; 5 min). Finally, the pellet was dissolved in TE buffer (including 0.1 mg/ml RNase A).

Prior to the experiment, an RNase A stock solution was prepared by dissolving 10 mg RNase A (NEB) in 1 ml 0.01 M sodium acetate. The solution was incubated for 20 min at 99 °C in a 1.5-ml safe-lock tube and let slowly cool down to room temperature (RT). After that, 0.1 vol (i.e. 100 µl) 1 M Tris-HCl (pH 7.2) was added to the solution. 100 µl of this RNase A stock solution were added to 100 ml of 1 × TE.

1× TE
10 mM Tris
1 mM EDTA
adjust pH to 8.0 with HCl

2.4.5 Fast plasmid preparation using the QIAprep Spin Miniprep kit

To receive a highly purified plasmid, the QIAprep Spin Miniprep Kit (Qiagen) was used. A 4 ml bacteria culture was grown O/N as described in chapter 2.4.3. The cells were harvested by transferring 2 ml culture into a fresh 2-ml tube and centrifuging the culture in a table centrifuge (13,000 rpm; 3 min). Subsequently, the plasmid was recovered according to the manufacturer's instructions.

2.4.6 DNA extraction from plant cells in a 96-well format

Prior to the harvest of plant material, a 96-well plate (1.2 ml volume per well) was filled with metal beads (one bead per well) using a bead dispenser. One *Arabidopsis* leaf sample (Ø about 0.5 cm) per tube was collected. First, 400 µl TNE buffer were added to the samples and the plate was sealed with cap strips. Samples were ground in a Retsch mixer mill for 2 min at 21/s. Plates were rotated once for 180° and ground again. The plate was centrifuged briefly to collect all liquid at the bottom (Beckman centrifuge, rotor type JS-5.9). To destroy cell membranes, 25 µl of 10 % SDS were added. The plate was sealed again and inverted twice. After centrifuging the plate (3,000 rpm; 5 min), 300 µl of the supernatant were carefully transferred to a new 96-well plate, filled with 300 µl isopropanol per well. The solution was mixed by inverting the plate five to ten times. The DNA was precipitated by centrifugation (3,000 rpm; 20 min). The supernatant was discarded and the pellet was washed with 70 % (v/v) ethanol. The plate was inverted and the DNA was precipitated again by centrifugation (3,000 rpm; 5 min). The alcohol was discarded and the pellets were dried for about 10 minutes. The DNA was dissolved in 30 µl 10 mM Tris (pH 8.5) and transferred to a 96-well PCR plate.
The plant DNA extraction protocol is based on the "Quick DNA extraction protocol" developed by Dr. Anahid Powell (Department of Genetics, University of Potsdam).

TNE buffer
200 mM Tris (pH 7.5)
250 mM NaCl
25 mM EDTA

2.4.7 Polymerase chain reaction (PCR)

PCR reactions were prepared in 250-µl 8-well-strips or 96-well-plates. For DNA fragment amplifications by PCR, the BIOTAQ DNA Polymerase (Bioline) was used if not stated otherwise. In cloning-related PCR reactions, the Phusion High-Fidelity DNA Polymerase (NEB), which has a proofreading activity, was used. Deoxyribonucleotides (dNTPs; dNTP Mix, Bioline) were used at a final concentration of 200 µM, while oligonucleotides were added to a final concentration of 0.2 µM. 50 mM $MgCl_2$ (Bioline) were added to a final concentration of 2.5 mM to all PCR reaction mixes. For

standard reactions, PCR reactions of a 20 µl volume were set up. If the PCR product had to be purified by gel extraction, e.g. for cloning purposes, a 50-µl PCR reaction was set up.
DNA denaturation temperatures were adjusted to the polymerase according to manufacturer's instructions. Annealing temperatures are listed in Appendix D. The elongation temperature was 72 °C Elongation times were adjusted to the length of the PCR product, based on an amplification rate of 1000 kb/min. Cycle numbers were adjusted to the purpose of the experiment and the efficiency of the individual PCR reactions achieved with specific primer combinations.
A positive control and a negative control (ddH_2O) were added in every PCR reaction.

2.4.8 Colony PCR

Prior to a plasmid preparation or a plant transformation, bacteria colonies were tested for the presence of a vector by colony PCR.
A small amount of an *E. coli* colony was picked and dissolved in 50 µl of ddH_2O. As template in a standard PCR reaction, 1 µl of the bacteria solution was used.
Agrobacterium tumefaciens cells have to be destroyed more stringently. Small amounts of individual colonies were dissolved in 10 µl of 20 mM NaOH. The bacteria solution was incubated at 37 °C for 5 min to disrupt the cell walls. The sample was briefly centrifuged and 1 µl of the supernatant was used as template in a standard PCR reaction (chapter 2.4.7).
As a positive control, 1 µl of a 1:1000 dilution of the respective vector was used as a PCR template. PCR products were analysed by agarose gel electrophoresis (chapter 2.4.13). Subsequently, the remaining *E. coli* solution of positively tested clones could be used to inoculate an LB liquid culture in preparation for a plasmid preparation (chapter 2.4.3).

2.4.9 Fusion of DNA fragments by PCR

The fusion of two PCR products served to synthesize a large fragment with novel features that should be cloned into a certain vector later. The two templates to be fused had been amplified by PCR before. The 3' end of PCR product 1 and the 5' end of PCR product 2 were overlapping. 20 ng of each PCR product served as templates in a 50-µl fusion PCR reaction using the Phusion High-Fidelity DNA Polymerase (NEB). Oligonucleotides binding the ends of the resulting full-length fusion PCR product were added. During the first PCR cycles the single strands of template 1 and 2 assembled via their complementary ends. The 3' ends of the overlapping single strands were extended. The resulting full-length fusion transcript served as template in the following amplification rounds. A high cycle number was chosen since the efficiency of the PCR is low in the beginning. The resulting PCR product was purified via an agarose gel (chapter 2.4.14).

2.4.10 Genotyping of *Arabidopsis* by PCR

Arabidopsis mutant alleles containing T-DNA insertions or insertion/deletion mutations were discriminated from the wild type alleles based on the different product sizes obtained by PCR. Alleles including single nucleotide polymorphisms were analysed by PCR combined with a subsequent restriction endonuclease digest (chapter 2.4.18).

Standard PCR reactions were performed (chapter 2.4.7) using 1 µl of *Arabidopsis* DNA (chapter 2.4.6) as template. The oligonucleotide combinations are listed in Appendix D. DNA samples of wild type and mutant control DNAs served as positive controls.

A modification of the standard protocol was applied when segregating T-DNA insertion lines were genotyped. To amplify the mutant and the wild type (WT) alleles simultaneously, three primers were added to the mix. Both the T-DNA-specific and the WT-allele-specific right-border primer were added to a final concentration of 0.1 µM. The final concentration of the gene-specific left-border primer, that serves to amplify both the mutant and the WT allele, was 0.2 µM.

PCR products were directly analysed by agarose gel electrophoresis (chapter 2.4.13). Alternatively, a restriction endonuclease digest was performed following the PCR reaction (chapter 2.4.18).

2.4.11 Genotyping of *Arabidopsis* by KASP

The *K*Biosciences Competitive *A*llele-*S*pecific *P*CR (KASP) assay was applied to discriminate *paps1-1* and *ahg2-1* mutant alleles from WT alleles in segregating populations. Both nucleotide polymorphisms could not reliably be discriminated by standard PCR-based assays. With the KASP technique, two alleles are simultaneously amplified using specific fluorescent primers. The fluorescent PCR-products can then be quantified and conclusions can be drawn to the plant genotypes. A prerequisite for the assay is a sufficient amount of control samples.

The gene-specific oligonucleotide mixes were ordered from KBiosciences (Hoddesdon, Herts, UK). The KASP reaction mix was ordered from LGC Genomics (Berlin). To genotype segregating plant populations, 1 µl *Arabidopsis* DNA (chapter 2.4.6) was mixed with 5 µl 2× KASP reaction mix and 0.06 µl gene-specific KASP primer mix in a total volume of 10 µl. For the setup, 384-well qPCR plates were used. The PCR reaction was run in a LightCycler 480 II (LC480; Roche) according to the manufacturer's instructions. Results were analysed with the LC480 software (version SW 1.5.0, 2011; tool Endpoint genotyping).

2.4.12 Quantitative real-time PCR (qPCR)

To compare relative transcript abundances in *Arabidopsis* plant material, the quantitative real-time polymerase chain reaction (qPCR or qRT-PCR) was performed. The qPCR method also served to

determine transcript abundances in the different fractions gained by poly(A) tail length-dependent RNA fractionation (chapter 2.5.8).

The qPCR is based on DNA intercalation of a fluorescent dye, e.g. SYBR green I, present in the PCR mix during the elongation phase of the qPCR cycles. The SYBR-green-I-DNA complex absorbs blue light at a wavelength of 497 nm and emits green light at 520 nm. The fluorescence signal of the individual samples is detected after every PCR cycle. Subsequently, the fluorescence is plotted against the cycle number. Conclusion to the transcript amount in the sample can be drawn regarding the slope of the resulting fluorescence curve.

Here, the SensiMix SYBR Low-ROX Kit (Bioline) was used according to the manufacturer's instructions. 2 µl of 1:10 diluted cDNA (chapter 2.5.5) served as a template in a 10-µl PCR mix which was set up in a 384-well qPCR plate. The qPCR was run in the LC480 with the program summarized in **Table 4**.

Table 4 qPCR program.

Phase	Temperature [°C]	Time [min:s]	Cycle number
Pre-Incubation	95	10:00	1
Amplification	60	00:15	45
	95	01:00	
Melting Curve	95	00:05	1
	65–97 (continuous)	01:00	
Cooling	40	00:30	1

The fluorescence data set obtained from the LC480 software was processed using the LC480 converter (chapter 2.13). The converted data were further analysed with the program LinRegPCR (version 2013.0, 2013; Ramakers et al. 2003; Ruijter et al. 2009), to obtain the PCR efficiency and the cycle threshold value of the individual samples. The program performs baseline corrections for each sample and determines the window-of-linearity for the whole amplicon. A straight line is fitted through the fluorescence values plotted against the cycle number of each sample. The individual PCR efficiencies are derived from the slope of the straight lines. Moreover, the individual cycle threshold (Ct) values are determined, which define the cycle at which the fluorescence primarily exceeds the background fluorescence.

The LinRegPCR data set was imported into Excel and the relative changes in transcript abundances were determined. First, the $\triangle$Ct was determined by subtracting the Ct value of the housekeeping gene (here *PDF2* was used) from the Ct value of the gene-of-interest. Then the average PCR efficiency for a given primer pair was included by calculating the (PCR efficiency$^{-\triangle Ct}$) values for each individual sample. Finally, the (PCR efficiency$^{-\triangle Ct}$) values of mutants and wild type were compared.

The transcript levels in the different fractions of the PAT-dependent RNA fractionation determined by qPCR could not be related to a housekeeping gene. Thus, individual (PCR efficiency^{-Ct}) values were

determined for the gene-of-interest in both WT and mutant and these values were compared to the abundances of the *in-vitro* transcribed control RNAs.

2.4.13 Agarose gel electrophoresis

The agarose gel electrophoresis was used to check the outcome of a PCR analysis, to separate DNA fragments of different sizes or to purify DNA fragments.
Horizontal gels containing 0.8–4 % (w/v) agarose were prepared by dissolving the appropriate amount of agarose in 50 ml, 100 ml or 400 ml 1× TAE buffer. The gel volume depended on the used agarose chamber which in turn dependent on the number of samples to be analysed. The agarose was completely dissolved in the buffer by heating in a microwave oven. When the liquid had cooled down to about 50 °C, ethidium bromide (3 µl/100 ml) was added. The liquid gel was mixed well and poured into the respective tray. DNA loading dye was added to the sample to visualize a dye front. An appropriate DNA marker was selected according to the expected fragment size (HyperLadder, Bioline). Gels were run in 1× TAE buffer at a voltage of 10 V/cm. Subsequently, DNA fragments were visualized and documented using a UV-transilluminator.

50× TAE
40 mM Tris base
40 mM acetic acid
1 mM EDTA

DNA loading dye
30 % (w/v) sucrose
0.2 % (w/v) cresol red
0.3 % (w/v) tartrazine
The solution was autoclaved for 20 min.

2.4.14 Purification of DNA fragments

PCR fragments and vectors to be sent to sequencing analyses were purified using the QIAquick PCR Purification Kit (Qiagen) according to the manufacturer's instructions.

2.4.15 Gel purification of DNA fragments

To purify DNA fragments from a fragment mix, an agarose gel electrophoresis was performed using low melting agarose (Biozym) (chapter 2.4.13). Next, the DNA fragment of the expected size was purified from the gel using the QIAquick Gel Extraction Kit (Qiagen) according to the manufacturer's instructions. Before the purified fragments were used for further experiments, an aliquot of the sample was tested for purity in a further agarose gel electrophoresis.

2.4.16 Determination of nucleic acid concentrations

Concentrations of DNA and RNA samples were determined using the Pico100 µl Spectrophotometer system.

2.4.17 Restriction digest of plasmid DNA

Vectors were digested with restriction endonucleases to analyse the result of a ligation reaction (chapter 2.4.20) or for cloning purposes (Appendix E). Restriction endonucleases were ordered from Bioline and were used according to the manufacturer's instructions. In an analytical setup, 1–2 µg plasmid DNA were digested in a 20-µl reaction mix for 2 h or O/N. Up to 8 µg plasmid DNA were digested O/N in a preparative restriction digest. The reaction volume was increased accordingly. Subsequently, the fragments were analysed by agarose gel electrophoresis (chapter 2.4.13). If the fragments had to be purified via the agarose gel, the whole restriction digest mix was loaded onto the gel (chapter 2.4.15).

2.4.18 Restriction digest to identify *Arabidopsis* by CAPS analysis

To identify specific point mutant alleles in segregating plant populations, the *C*leaved *A*mplified *P*olymorphic *S*equences (CAPS) method was applied. Single-nucleotide polymorphisms or insertion/ deletion mutations may create or abolish recognition sites of restriction endonucleases. First, the sequence surrounding the polymorphism is amplified by PCR. Subsequently, WT and mutant alleles can be discriminated by restriction fragment length polymorphism analysis. Alternatively, derived CAPS markers can be gained using mismatch primers to create a restriction site.

Genes identified by CAPS analysis can be found in Appendix D. *Arabidopsis* DNA was used as template in a gene specific PCR using a 20-µl reaction volume (chapter 2.4.10). The complete PCR reaction mix was subsequently digested by adding a 10 µl restriction enzyme mix to the sample. The restriction enzymes were ordered from Bioline and both mix and incubation conditions were adjusted according to the manufacturer's instructions. The resulting fragments were analysed by agarose gel electrophoresis (chapter 2.4.13). In dependence of the expected fragment sizes and the PCR efficiency of the used primer pair, the gel concentration and the sample volume loaded onto the gel were adjusted.

2.4.19 Dephosphorylation of linear plasmid DNA

Linearised vectors were dephosphorylated prior to a ligation reaction to avoid re-ligation of the vector. The antarctic phosphatase (NEB) was used to dephosphorylate an aliquot of linearised vector DNA according to the manufacturer's instructions.

2.4.20 Ligation of DNA fragments

DNA fragments were usually purified by agarose gel electrophoresis prior to a ligation (chapter 2.4.15). The ligation was performed using the T4 DNA ligase (NEB). In a standard setup, 50 ng vector

DNA and 150–200 ng insert were ligated in a 10 µl reaction mix using 0.5 µl T4 ligase and 1 µl 10× T4 buffer. The reaction was incubated O/N at RT or at 10°C for up to three days. Subsequently, a 1–2 µl aliquot of the ligation reaction was used to transform *E. coli* (chapter 2.7.2) and the rest was stored at –20 °C.

To ligate DNA fragments into pGEM-T (Promega) a 3' A-overhang at the insert is required. The Phusion DNA Polymerase (NEB) produces blunt ends. Thus, A-tails were added to the PCR product to be subcloned by adding 0.5 µl/10 µl of a housemade Taq polymerase producing 3' overhangs. The mix was incubated at 72 °C for 45 min followed by an agarose gel purification of the insert and a standard ligation reaction as described above.

2.4.21 Sequencing

The sequencing of plasmids or PCR products was performed by LGC Genomics (Berlin). The resulting sequences were analysed using the program Vector NTI (2.13).

2.5 RNA-related techniques

2.5.1 RNA extraction from *Arabidopsis* by phenol extraction (Mini hot phenol protocol)

Approximately 100–150 mg plant tissue (in 1.5-ml safe-lock tube) was frozen in liquid nitrogen. Subsequently, a small amount of glass sand was added and the tissue was ground to a fine powder using a homogenizer (Heidolph) or using mortar and pistil.

In preparation of the RNA extraction, fresh homogenisation buffer was prepared in a 50-ml tube and heated to 60 °C. The complete RNA extraction was performed using RNase-free, autoclaved material and filter-tips. Pipettes and the working space were cleaned with 6 % (v/v) bleach and ethanol.

First, 755 µl hot phenol mix were added to the ground plant tissue. The sample was mixed using a vortex and incubated for 15 min at RT under continuous shaking. 250 µl chloroform were added and the sample was shaken for further 15 min. A phase separation was induced by centrifugation (10 min; 13,000 rpm). The upper aqueous phase (about 550 µl) was transferred to a new 1.5-ml tube. 550 µl phenol:chloroform:isoamylalcohol (25:24:1) were added and the sample was shaken for 10 min at RT. The following steps were performed on ice. After centrifugation (10 min; 13,000 rpm), the aqueous phase was transferred to a new tube. Consecutively, 50 µl of 3 M sodium acetate and 400 µl isopropanol were added to the samples. After an incubation phase at –80 °C for 15 to 30 min and a centrifugation (14,000 rpm; 30 min; 4 °C) the supernatant was completely removed. The remaining pellet was air dried and subsequently resuspended carefully in 500 µl ddH_2O. After adding 500 µl 4 M LiCl, the sample was mixed and incubated on ice at 4 °C O/N to precipitate the RNA.

The following day, the RNA was precipitated by centrifugation (14,000 rpm; 30 min; 4 °C). After removal of the supernatant, the pellet was washed with 1 ml 80 % (v/v) ethanol. After centrifugation (14,000 rpm; 5 min; 4 °C), the supernatant was removed using a pipette and the pellet was air dried. When the pellet became glassy, the RNA was dissolved carefully in 30 µl DEPC-treated water. The RNA was stored at –80 °C.

Homogenisation buffer
100 mM Tris (pH 8.5)
5 mM EDTA (pH 8.0)
100 mM NaCl
0.5 % (w/v) SDS

Hot phenol mix
250 µl phenol
500 µl homogenisation buffer
5 µl β-mercaptoethanol

DEPC-treated water
0.1 % diethylpyrocarbonat
Incubate on a magnetic stirrer O/N; autoclave twice.

2.5.2 RNA extraction by TRIsure (Quick RNA isolation protocol)

Approximately 100–150 mg plant tissue (in 1.5-ml safe-lock tube) were frozen in liquid nitrogen. Subsequently, a small amount of glass sand was added and the tissue was ground to a fine powder using a homogenizer (Heidolph) or using mortar and pistil. First, 800 µl TRIsure reagent (Bioline) were added and the sample was mixed thoroughly with a vortex. The tube was incubated 5 min at RT and 5 min on ice. 200 µl chloroform were added. The sample was mixed well and incubated on ice for further 5 min. After centrifugation (13,000 rpm; 10 min; 4 °C) the upper soluble phase was transferred to a new tube containing 700 µl isopropanol. The sample was inverted several times and incubated for 20 min at RT. The RNA was precipitated by centrifugation (13,000 rpm; 30 min; 4 °C) and the supernatant was removed. The RNA pellet was washed with 1 ml 80 % (v/v) ethanol. After centrifugation (13,000 rpm; 5 min; 4 °C) the supernatant was removed completely and the pellet was air dried. The glassy pellet was dissolved in 30 µl DEPC treated water. The RNA was stored at –80 °C.

2.5.3 RNA purification by phenol:chloroform extraction

The RNA sample was filled up to a volume of 180 µl with DEPC-treated water. 20 µl 3 M sodium acetate (pH 5.2; 1/10 vol) were added and the sample was mixed thoroughly. Next, 1 vol of 1:1 phenol:chloroform mix (Roth) was added and the sample was mixed using a vortex. After centrifugation in a table centrifuge (13,000 rpm; 10 min), the aqueous phase was transferred to a new tube containing 1 vol chloroform. The extraction was repeated. The RNA was precipitated by adding 2 vol 100 % ethanol and an incubation phase at –20 °C for at least 30 min. After centrifugation

(13,000 rpm; 30 min), the supernatant was removed and the pellet was washed with 1 ml 70 % (v/v) ethanol. After brief centrifugation the ethanol was removed completely and the pellet was air dried. The RNA was dissolved in 30–50 µl DEPC-treated water or 0.1 mM EDTA and stored at –80 °C.

2.5.4 DNase digest of RNA samples

To digest remaining DNA in RNA samples, the TURBO DNA-free Kit (Ambion/Life Technologies) was used. In the standard procedure, 10 µg total RNA were used in a 50-µl setup. First, the RNA was filled up to a volume of 22.5 µl with RNase-free water provided in the kit. 2.5 µl TURBO DNase buffer were added. Simultaneously, a mix of 21.5 µl water, 2.5 µl TURBO DNase buffer and 2.5 µl TURBO DNase (10 u/µl) was prepared and added to the RNA sample. After an incubation at 37 °C for 30 min, 5 µl of DNase inactivation reaction were added. The sample was incubated at RT for 2 min. After centrifugation in a table centrifuge (13,000 rpm; 1 min), the supernatant was carefully transferred to a new tube. The result of the DNase digest was tested by PCR (chapter 2.4.7), adding Col-0 DNA as a positive control.

2.5.5 cDNA synthesis by reverse transcription PCR (RT-PCR)

SuperScript III Reverse Transcriptase (Invitrogen) was used to synthesize cDNA from RNA. 2–3 µg total RNA were filled up to a volume of 12.2 µl with water. For standard cDNA synthesis, 0.8 µl 100 µM oligo $(dT)_{17}$ primer (LGC Genomics) were added. For the cDNA synthesis after the mRNA fractionation (chapter 2.5.8), 1.5 µl RNA were filled up to a volume of 12 µl with water and 0.5 µl Random Hexamer Primer (Qiagen) were added. Next, 1 µl 10 mM dNTPs (Bioline) was added and the sample was incubated for 5 min at 65 °C. After incubation on ice for 5 min, 4 µl 5× First strand buffer, 1 µl 0.1 M DTT (provided with the enzyme) and 1 µl SuperScript III were added. The cDNA synthesis was carried out at 50 °C for 60 min in a thermocycler followed by the enzyme inactivation at 75 °C for 15 min. The cDNA was stored at –20 °C. For a subsequent qPCR, the samples were tested for an equal cDNA concentration by PCR (chapter 2.4.7). A 1:10 cDNA dilution was used as a qPCR template.

2.5.6 Poly(A) tail test (PAT)

For measurements of the poly(A) tail length by PCR (PAT test), the Affymetrix Poly(A) Tail-Length Assay Kit was used according to the instructions. RNA was extracted by the hot phenol method (chapter 2.5.1). For the PCR, HotStart-IT Taq DNA Polymerase (Affymetrix) was used according to the instructions. Primers used for the detection of specific genes (*At1g19180*, *At1g72450*, *At2g18700*) are listed in Appendix C. PCR products were visualized by agarose gel electrophoresis (chapter 2.4.13) using 3 % agarose gels. For PAT-test samples, Ficoll DNA loading dye based on Orange G-dye was used to avoid concealing any DNA bands in the UV transillumination analysis.

10× Ficoll DNA loading dye	10 ml
Ficoll-400	2.5 g
1 M Tris-HCl (pH 7.4)	1 ml
0.5 M EDTA	2 ml
Dissolve in a water bath at 65 °C.	
Orange G	25–50 mg

2.5.7 *In-vitro* transcription

Control RNA with defined poly(A) tail sizes was transcribed *in vitro* with the T7 RNA Polymerase (NEB). First, 2 µg vector DNA (pGT2d, pGT3b or pGT5; see **Table 10**) were filled up to a volume of 13.6 µl with RNase-free water. Subsequently, 4 µl 5 mM NTP solution (Bioline), 4 µl 10x T7 transcription buffer (NEB) and 2 µl BSA (2 mg/ml BSA) were added. The sample was mixed gently and 2 µl RNase Inhibitor (Promega) and 0.4 µl T7 Polymerase (NEB) were added. The sample was incubated at 37 °C for 2 h. The reaction was stopped by adding 1.5 µl TURBO DNase (Ambion) and a further incubation at 37 °C for 30 min. Subsequently, the RNA was purified by phenol:chloroform extraction (chapter 2.5.3) and dissolved in 50 µl 0.1 mM EDTA.

2.5.8 Poly(A) tail length-dependent RNA fractionation

The poly(A)-tail-dependent mRNA fractionation protocol based on the method, developed by Meijer and de Moor (2011), was modified and adjusted to an RNA amount of 20 µg. The PolyATtract® System 1000 (Promega) was used.

RNA was extracted by the hot phenol method (chapter 2.5.1). Three control RNAs with a defined poly(A) tail length of 29, 75 or 124 A's, respectively, were prepared by *in-vitro* transcription (chapter 2.5.7). An RNA control mix with a final concentration of 1 ng/µl for each control RNA was prepared.

All chemicals and buffers were allowed to reach RT prior to the experiment. In preparation for the fractionation, 41 µl BME were added to 1 ml GTC, and 20.5 µl BME were added to 1 ml DIL. The DIL/BME-mix was preheated to 70 °C. A 0.085× SSC dilution was prepared from the 0.5× SSC buffer stock.

First, 1 µl *in-vitro* RNA control mix was added to 20 µg total RNA in a 2 ml tube (in a maximum volume of 20 µl). The RNA was mixed with 200 µl GTC/BME. Then 7.5 µl biotinylated oligo (dT) (Promega) and 408 µl preheated DIL/BME were added. The mix was incubated at 70 °C for 5 min, followed by centrifugation in a table centrifuge (13,000 rpm; 10 min; RT).

Simultaneously, the paramagnetic beads (Streptavidin MagneSphere® Paramagnetic Particles, Promega) were carefully resuspended and a 300 µl aliquot was transferred to a fresh 2-ml tube. Tubes containing beads were placed into a magnetic stand, which was slowly tilted to a horizontal position to collect the beads at the magnetic tube side. The storage buffer was removed carefully (by

pouring, or better, by removal with a pipette) and the beads were resuspended in 300 µl the 0.5× SSC buffer. The washing procedure was repeated twice.

The SSC buffer was removed from the beads and after spinning the RNA sample the supernatant was added to the beads. To allow the biotinylated oligo (dT) to bind the beads, the tubes were incubated on a rotator at RT for 15 min. Subsequently, the beads were captured by placing the tube in the magnetic stand and the supernatant, i.e. the unbound mRNA fraction, was transferred to a fresh tube which was kept on ice in the following. The beads were washed three times with 0.5× SSC buffer as described above and rotated for at least 5 min between each wash step. To obtain the short-tailed mRNA fraction, the beads were resuspended in 200 µl 0.085× SSC buffer, which induces the release of mRNAs with tails shorter than 50 A's from the oligo (dT)-bound beads. After a 5 min rotation, the beads were captured and the supernatant, i.e. the "short fraction", was collected in a new tube. The beads were washed three times in 0.5× SSC buffer with a 5 min rotation between each wash step. To release the remaining mRNAs, the beads were resuspended in 200 µl nuclease-free water. The tubes were rotated for 5 min and after capturing the beads the supernatant containing the mRNAs with tail longer than 50 A's was collected. This step was repeated twice and the three eluates were merged, resulting in the "long fraction".

To remove any transferred beads, all samples were centrifuged (14,000 rpm; 10 min; 4 °C). For RNA precipitation, 0.1 vol Co-precipitant Pink buffer (BioLine) was added to each sample and after thorough mixing, 15 µg (or 3 µl) Co-precipitant pink (BioLine) were added. Samples were mixed with a vortex and 1 vol 100 % ethanol was added. After incubation (30 min or O/N, –20 °C) the RNA was precipitated by centrifugation (14,000 rpm; 10 min; 4 °C). The supernatant was removed. The RNA pellet was washed with 500 µl 80 % (v/v) ethanol, air dried and dissolved in 10 µl DEPC-treated water.

Subsequently, 1.5 µl RNA were used for cDNA synthesis (chapter 2.5.5) and the abundances of target and control genes in the different fractions were determined by qPCR (chapter 2.4.12).

2.6 Protein techniques

2.6.1 Protein extraction from *Arabidopsis*

For protein extraction, exactly 100 mg *Arabidopsis* seedlings were harvested in 1.5-ml tubes, which were immediately frozen in liquid nitrogen. The sample weight was determined with a high-accuracy scale, since the protein measurement was performed on the basis of equal sample fresh weight. A small amount of glass sand was added and the seedlings were ground to a fine powder with a homogenizer (Heidolph). After adding 2 vol of preheated SDS sample buffer and thorough mixing, the samples were boiled at 95 °C for 5 min and cooled on ice for 5 min. Cell debris was removed by

centrifugation in a table centrifuge (13,000 rpm; 10 min; 4 °C). Equal volumes of supernatant (20 µl) were separated by SDS-PAGE (chapter 2.6.2).

SDS sample buffer	10 ml
Stacking buffer	1.4 ml
Glycerol	1.0 ml
ddH_2O	5.1 ml
10 % (w/v) SDS	2.0 ml
β-mercaptoethanol	0.5 ml
Bromphenol blue	0.001 %

Stacking buffer
0.5 M Tris
0.4 % (w/v) SDS
adjust pH to 6.8 with HCl

2.6.2 SDS polyacrylamide gel electrophoresis (SDS-PAGE)

Prior to a Western blot, protein extracts were separated by SDS polyacrylamide gel electrophoresis (SDS-PAGE). The SDS-PAGE was performed according to the Tris-glycin buffer system (Laemmli 1970) using the Mini-Protean® 3 Cell-System (Biorad). Since the expected size of PAPS-YFP proteins was 114–116 kDa, an 8 % (w/v) polyacrylamide gel was prepared as separating gel. The stacking gel contained 5 % (w/v) polyacrylamide. A 10-slot comb was used and 20 µl *Arabidopsis* protein extract (chapter 2.6.1) per slot were loaded. The Prestained Protein Molecular Weight Marker (5 µl; Fermentas) served as protein size control. The electrophoresis was run in 1× electrophoresis buffer at 120 V for 1–2 h until the dye front had reached the end of the gel. Subsequently, the gel was stained with Coomassie protein dye (chapter 2.6.3) or a Western blot was performed (chapter 2.6.4).

8 % (w/v) separating gel	10 ml
1.5 M Tris-HCl (pH 8.8)	2.5 ml
30 % (w/v) acrylamide/ bis-acrylamide	2.7 ml
ddH_2O	4.6 ml
10 % (w/v) SDS	100 µl
10 % (w/v) APS	100 µl
TEMED	60 µl

5 % (w/v) stacking gel	5 ml
0.5 M Tris-HCl (pH 6.8)	0.63 ml
30 % (w/v) acrylamide/ bis-acrylamide	0.83 ml
ddH_2O	3.40 ml
10 % (w/v) SDS	50 µl
10 % (w/v) APS	50 µl
TEMED	5 µl

10× electrophoresis buffer	1 l
Tris	30 g
Glycin	144 g

1× electrophoresis buffer	1 l
10× electrophoresis buffer	100 ml
10 % (w/v) SDS	10 ml

2.6.3 Coomassie staining of protein gels

A polyacrylamide gel was incubated in Coomassie staining solution for 1 h or O/N on a rotator. Proteins in the gel were detected by shaking the gel several times in destaining solution.

Coomassie staining solution	500 ml
Coomassie blue R-250	120 mg
Methanol	250 ml
Acetic acid	4 ml

Destaining solution	1 l
Methanol	450 ml
Acetic acid	100 ml

2.6.4 Western blot

Proteins were transferred from a polyacrylamide gel to a nitrocellulose membrane (0.2 µm pore size; 0.15 ± 0.05 mm membrane strength) using a wet-blot system (Mini Trans-Blot Cell; Bio-Rad). Both membrane and blotting paper were cut to the size of the gel and were wet in 1× transfer buffer. The blotting holder cassette was assembled stacking a wet pad, three layers of wet blotting paper, the wet membrane, the gel, again three layers of wet blotting paper and a wet pad. The blotting module was put in the blotting tank with the nitrocellulose membrane oriented towards the anode to allow proteins to move towards the positive pol. An ice-filled container was added, the chamber was filled with 1× transfer buffer and the blot was run at 100 V for 90 min.

Empty binding sites were blocked by incubating the membrane in 5 % (w/v) milk powder (in 1× TBST) on a rotator (4 °C; 1 h). The milk powder solution was removed by washing the membrane twice in 1× TBST buffer for 10 min. Next, the membrane was incubated with the primary antibody on a rotator (4 °C; O/N). A polyclonal anti-GFP antibody from rabbit (ab290, Abchem) was diluted 1:2000 in 1× TBST buffer. The membrane was washed three times in 1× TBST for 20 min and incubated with the second antibody, a horseradish peroxidise-coupled anti-rabbit antibody (A6154-1ML, Sigma) diluted 1:5000 in 1× TBST (4 °C; 2 h). The membrane was washed two times in 1× TBST for 20 min and once in 1× TBS for 10 min.

For chemiluminescence detection, the membrane was covered completely with luminol reagent and the luminol signal was detected with a CCD camera (NightOWL LB 983 NC100; Berthold Technologies).

10× transfer buffer	1 l
Tris	30 g
Glycin	144 g

1× transfer buffer	1 l
10× transfer buffer	100 ml
Methanol	200 ml
10 % (w/v) SDS	10 µl

10× TBS buffer	1 l
Tris	15 g
NaCl	72 g
pH 7.4 with HCl	

1× TBS buffer	1 l
10× TBS buffer	100 ml

1× TBST buffer	1 l
10× TBS buffer	100 ml
Tween 20	1 ml

Luminol reagent	
Solution A	2 ml
Solution B	200 µl
35 % (v/v) H_2O_2	0.6 µl

Solution A	200 ml
Luminol	50 mg
0.1 M Tris-HCl (pH 8.6)	200 ml

Solution B	100 ml
p-hydroxycoumaric acid	11 mg
DMSO	10 ml

2.7 Transformation techniques

2.7.1 Preparation of electro-competent bacteria

To prepare a pre-culture, 50 ml selective LB liquid medium was inoculated with a single bacteria colony (strains see chapter 2.1.4, antibiotics see **Table 3**). The culture was incubated O/N on a shaker (200 rpm; 37 °C for *E. coli*; 28 °C for *Agrobacterium*). 400 ml pre-warmed, selective LB medium was inoculated with 4 ml pre-culture, resulting in an optical density (at 600 nm) of about 0.1. The culture was shaken at the respective temperature until an optical density of 0.3–0.4 was reached (about 2 h for *E. coli*, about 4 h for *Agrobacterium*). The culture was cooled on ice for 15 min. The following steps were performed on ice in a cold room (at 8 °C). The cells were harvested by centrifugation in two pre-cooled centrifuge tubes (4,000 rpm; 10 min; 4 °C; Beckman centrifuge, rotor type JLA 16.250). The supernatant was discarded and the cells of the remaining culture were harvested likewise in the same tubes. The cell pellet was carefully resuspended in 10 ml cold, autoclaved water. The volume was filled up to 100 ml with water and the cells were harvested by centrifugation (4,000 rpm; 10 min; 4 °C). The washing was repeated. The bacteria were resuspended in 10 ml 10 % (v/v) glycerol (cold, autoclaved) and transferred to two 50-ml tubes. After centrifugation (4,000 rpm; 10 min; 4 °C) the supernatant was discarded and the cells were resuspended in 3 ml 10 % (v/v) glycerol (cold, autoclaved) per tube. Aliquots of 50 µl were directly frozen in liquid nitrogen and stored at –80 °C.

2.7.2 Transformation of electro-competent *E. coli* or *Agrobacterium* cells

In preparation for a transformation, electroporation cuvettes were chilled on ice (1 mm gap for *E. coli*; 2 mm gap for *Agrobacterium*). The bacteria were slowly thawed on ice and 1 µl of a plasmid DNA (1:100 diluted, about 5 µg) or 1–2 µl of a ligation mix were added. The cell/DNA mix was transferred to the cuvette. The cuvette was wiped with a tissue and quickly placed in the electroporator. The pulse was immediately triggered (1.8 kV for *E. coli*; 2.5 kV for *Agrobacterium*; 200 Ω resistance and 25 µF capacitance) and the bacteria were quickly resuspended in 1 ml pre-warmed SOC medium. The bacteria were transferred to a fresh tube and incubated for 30 min to 1.5 h dependent on the antibiotics used (37 °C for *E. coli*; 28 °C for *Agrobacterium*). After centrifugation, the cell pellet was dissolved in 100 µl of the remaining medium. The culture was plated on selective solid LB medium. The agar plates were incubated O/N at 37 °C (*E. coli*) or for two to three days at 28 °C (*Agrobacterium*) to allow colony formation.

SOC-Medium	1 l
Bacto trypton	20 g
Yeast extract	5 g
NaCl	0.5 g
1 M KCl	2.5 ml
pH 7.0	
After autoclaving for 20 min, the following substances were added:	
2 M $MgCl_2$	10 ml
2 M glucose	10 ml
Aliquots of 1 ml were stored at –20 °C.	

2.7.3 Transformation of *Arabidopsis* by floral dip

Plants were grown until they had reached the reproductive phase, producing at least three inflorescences. To prepare a pre-culture, 4 ml liquid LB medium containing gentamycin to select the *Agrobacterium* strain GV3101 and antibiotics selecting for the binary vector (**Table 10**) were inoculated with a single bacteria colony and incubated in a shaker (200 rpm; 28 °C; O/N). 400 ml selective LB medium were inoculated with 1 ml pre-culture and were shaken to allow bacteria growth (200 rpm; 28 °C; O/N). The culture was transferred to centrifuge tubes and harvested by centrifugation in a Beckman centrifuge (4,000 rpm; 15 min; 18 °C; rotor type JLA 16.250). The supernatant was discarded and the cell pellet was resuspended in 10 ml transformation medium. The cell culture was transferred to a beaker (2 litre volume) and filled up to one litre with the remaining transformation medium. After adding Silwet L-77, an adjuvant that lowers surface tension, the *Arabidopsis* inflorescences were dipped into the bacterial suspension for 20 s. The plants were placed horizontally in a tray and the tray was put into a plastic bag in order to keep up humidity. The bagged plants were incubated in the dark O/N. The following day, the plants were removed from the bag and were subsequently grown under standard conditions until the T1 seeds developed.

Transformation medium	1 l
Sucrose	50 g
MS salts	2.15 g
Silwet L-77 (to be added after resuspension of the bacterial pellet)	500 µl

2.8 Physiological methods

2.8.1 Crossing of *Arabidopsis*

Two to four larger floral buds of a mother plant inflorescence were selected. Other open flowers and siliques were removed from the shoot. Using a microscope, smaller buds were removed from the

inflorescence. The remaining buds were carefully opened using forceps and all stamens were removed. Two days later, pollen of the father plant was placed on the receptive stigmas.

2.8.2 Flowering time analysis

Flowering times were assessed according to the instructions by Möller-Steinbach et al. (2010). Plants were cultivated on soil under standard conditions (chapter 2.2.1) or as indicated. If segregating plant lines were used in the flowering time analysis, plants were genotyped when four primary leaves had developed (chapters 2.4.10; 2.4.11; 2.4.18). If a whole leaf had been used for the DNA extraction, the plant was marked. Plants were observed regularly until bolting. As soon as the shoot had reached a height of 1 cm, primary and cauline leaves were counted to determine the total leaf number. Leaves used for DNA extraction were considered. The flowering date was noted to calculate the plant age. The age was measured from the date plants were transferred to the growth chamber after stratification. A high correlation between total leaf number and flowering time in days to bolting can be observed if plants exhibit wild-type like leaf initiation rates (Koornneef et al. 1991).

2.8.3 Salicylic acid treatment of plants

Plants were grown on soil under standard conditions (chapter 2.2.1). Starting at ten days after germination (DAG), the plants were sprayed with salicylic acid solutions every other day until all leaves were completely bedewed. The solutions contained 0.5 mM or 1 mM salicylic acid in 0.1 % (v/v) Tween 20. As a control, plants were sprayed with a mock solution containing 0.1 % (v/v) Tween 20.

2.8.4 Leaf initiation rate determination

Plants were grown on soil in single pots in a Percival (chapter 2.2.1). The temperature was kept stable (22 °C day/ 20 °C night). The plants were observed daily and the initiation of a newly developed leaf was noted when the leaf primordia were 1 mm long.

2.8.5 Vernalization

The vernalization treatment was performed as described before (De Lucia et al. 2008). Sterile seeds were sown out on 0.5× MS media plates (without sugar), stratified and cultivated under standard LD conditions (chapter 2.2.2). To obtain non-vernalized control plants for the flowering time analysis, seeds from the same sterilized seed batch were directly sown out on soil and grown under standard conditions (chapter 2.2.1). Late-flowering plants were grown in pots with a diameter of 10 cm. At six DAG, the plates were transferred to 4 °C for vernalization. In the cold room, plates were irradiated by LEDs with a PAR of 120 µmol photons/m^2/s under short-day (SD) conditions (8 h light, 16 h darkness).

After six weeks, the plates were returned to standard LD conditions. To analyse the flowering time, plants were transferred to soil after five days of recovery at warm ambient temperatures.
To extract RNA for a qPCR analysis, both control plants and vernalized plants were sown out on 0.5× MS media plates. After stratification, the plates were transferred to standard LD conditions (chapter 2.2.2) as described above. Unvernalized control plants were harvested at ten DAG. Cold-treated plants were vernalized as described above. Seedlings were harvested after two, four or six weeks directly in the cold room. Alternatively, the plates were transferred to standard conditions and the plants were harvested after five days of recovery.

2.8.6 Biotic stress treatment

Pathogen infection assays were performed by the lab of Cyril Zipfel (John Innes Center, Norwich, UK). The *Arabidopsis* treatment with the fungus *Hyaloperonospora arabidopsidis* was carried out as described before (Tör et al. 2002). Treatments with the bacterial elicitor flg22 were performed by Lena Stransfeld as described before (Zipfel et al. 2004).

2.8.7 Oxygen depletion stress by submergence

To test flooding tolerance of the *paps* mutants, a submergence experiment was performed. Plants cultivated under standard LD conditions for four weeks in a glass house (Max-Planck-Institute of Molecular Plant Physiology; chapter 2.2.1) were transferred to plastic boxes. The boxes were filled with water until all plants were completely submerged and were closed with lids. Control plants were kept in boxes that had not been filled with water. To ensure complete darkness, the boxes were covered with aluminium foil. After 72 h, the boxes were opened and plants were returned to standard growth conditions. After three days of recovery, the plant phenotype was documented by photography.

2.8.8 Long-term oxygen depletion stress by hypoxia

The long-term hypoxia experiment was performed under supervision from Joost van Dongen at the Max-Planck-Institute of Molecular Plant Physiology. The experiment was performed in a glass house under standard LD conditions. Three-week-old plants were transferred to plexiglass boxes. In the boxes, the pots were placed on trays containing a layer of felt cloth that served to store water. The plexiglass boxes were sealed with tape. A gas mixture containing 400 ppm CO_2, 10 % O_2, and N_2 (Air Liquide, Berlin) was blown into the boxes. Control boxes were streamed with ambient air (later termed 21 % O_2 boxes). The flow rate was kept between 0.25 and 1 l/min/box and was monitored daily. A hole in the boxes sealed with putty served to irrigate the plants and to monitor temperature and gas conditions inside the boxes. Water was poured into the boxes with a syringe until the felt

cloth was completely soaked. The temperature and the gas concentration inside of the boxes was monitored regularly using an electrode (LI-800 Gas Hound Analyzer, LI-COR; Microx TX2, PreSens; software TX2 Oxyview V4.16). Simultaneously, control plants were grown under standard conditions outside of the boxes.

The plants were observed regularly. The flowering time of all plants was noted during the experiment. After 32 days of hypoxia, all plants had bolted and the plexiglass boxes were opened. The individual leaf diameter and the plant shoot fresh weight were measured immediately. To determine the plant dry weight, plant shoots were transferred to paper bags and dried using a vacuum drying oven (Binder).

2.8.9 Oxygen depletion stress by anoxia

To test the plant response to complete anoxia, plants were grown on 0.5× MS media plates (chapter 2.2.2). After stratification for four days, plates were transferred to a Percival and cultivated under standard LD conditions. At nine DAG, the anoxic treatment was carried out. The plates were transferred to boxes that were streamed with pure N_2 in complete darkness (Air Liquide, Berlin). Control plates were kept in dark under normoxic conditions during the treatment. After 5–8 h plates were returned to standard conditions. After six days of recovery, the plant development was documented by photography.

2.8.10 Drought stress induction

Plants were cultivated on soil under standard LD conditions in a growth chamber (chapter 2.2.1). Each pot was kept in a weighing boat and was daily irrigated with a defined amount of water. At 14 DAG, the irrigation was interrupted and plants were kept under complete drought. Control plants were continuously watered. After 14 days, the plant phenotype was documented by photography and the dry plants were irrigated again, to monitor the plant phenotype during the recovery phase.

2.8.11 Induction of osmotic stress by mannitol

The sugar alcohol mannitol was used to induce osmotic stress in plants as described before (Nishimura et al. 2004). Sterile seeds were sown out on 0.5× MS media plates containing 200–400 mM mannitol or on control plates without mannitol (chapter 2.2.2). Five plates per condition were poured. The plates were divided into four squares and 25 seeds of Col-0, *paps1-4* and *paps2-3 paps4-3* were sown out on every plate. The last square was filled with *paps2-3* or *paps4-3* seeds.

After stratification, plates were cultivated under standard LD conditions. To avoid water evaporation from the media, which would have resulted in an increase of the mannitol concentration, the plates

were illuminated by LEDs. At eleven DAG the seedling fresh weight was determined using a high-accuracy scale. For the measurement, all 25 seedlings per genotype were pooled in a weighing boat.

2.8.12 Application of cold stress

Seeds were sown out on 0.5× MS media plates, stratified and cultivated under LD conditions in a climate growth chamber (chapter 2.2.2). Since the *paps1-1* mutant germinates late the *paps1-1* containing plates were transferred to the growth chamber two days before the other plates. At five DAG, the plates were transferred to 4 °C for four weeks. In the cold room, plates were irradiated by LEDs with a PAR of 120 µmol photons/m^2/s under SD conditions. Eight days before the cold-treatment ended, the control plates were sown out, stratified and cultivated under LD conditions. Five days after returning the cold-treated plates back to 21 °C, the phenotype of the cold-treated and the ten-day-old control plants was documented by photography. Immediately after photographing the plates, the seedling fresh weight was determined using a high-accuracy scale. For the measurement, ten seedlings per genotype were pooled on a weighing boat.

2.8.13 Induction of oxidative stress

Oxidative stress was induced using methyl viologen or 3-amino-1, 2, 4-triazole (AT) and buthionine-S, R-sulfoximide (BSO) as described before (Zhang et al. 2008). Seeds were sown out on 0.5× MS media plates, stratified and pre-grown for seven days in a Percival (chapter 2.2.2). At seven DAG, seedlings were transferred to 0.5× MS media plates supplemented with 1 % (w/v) glucose and the stress-inducing chemicals (40 mM MV; 1 µM AT + 200 µM BSO; 2 µM AT + 400 µM BSO; control without supplements). A slice of medium (2 cm width) had been removed from the plate. The seedlings were placed on the upper side of the cut medium and plates were placed horizontally in the Percival to allow horizontal root growth. After 14 days, all plates were photographed for the root length analysis. The fresh weight of every individual seedling was immediately determined using a high-accuracy scale. The individual root length was determined using the software ImageJ (Abràmoff et al. 2004).

2.9 Plant photography

Plants and plates were photographed on a black cloth using a Canon SX220 HS Powershot camera. The sensitivity (ISO) was kept at 100, the exposure time was kept at 1/60 s, and the relative aperture (f-stop) was adjusted.

2.10 Microscopy

Arabidopsis seedlings expressing *pPAPS:PAPS::YFP* constructs were monitored using a fluorescence microscope (Axiovert200M; Carl Zeiss) or a laser-scanning microscope (LSM510 Axioplan2; Carl Zeiss). Scale bars were included using the program ImageJ (Abràmoff et al. 2004).

2.11 Statistical means

Replicate numbers are indicated for every experiment. At least three replicates were used for all measurements. To analyse the data, mean and standard deviation were determined as a measure for data variation. The standard error of the mean (SEM) respects the sample size. Significant differences between treatments or genotype-specific phenotypes were assessed using the two-sided Student's t-test and applying Bonferroni-correction.

Mean:

$$\bar{x} = \frac{1}{n}\sum_{i=1}^{n} x_i$$

Standard deviation:

$$s = \pm\sqrt{\frac{1}{n-1}\sum_{i=1}^{n}(x_i - \bar{x})^2}$$

Standard error of the mean

$$SE_{\bar{x}} = \frac{s}{\sqrt{n}}$$

n = Number of values (sample size)
x_i = The i's of values
i = Running index from 1 to *n*

2.12 Transcriptome analysis

2.12.1 Sequencing

For the transcriptome analysis, ten-day-old seedlings and flowers of *paps2-3 paps4-3* and Col-0 were harvested. Four replicates per genotype and per tissue were collected. RNA was extracted using the hot phenol protocol (chapter 2.5.1). DNA was digested using RQ1 RNase-free DNase (Promega) according to the manufacturer's instructions. Subsequently, samples were purified by phenol:chloroform extraction (chapter 2.5.3). The RNA was sequenced using the EXPRSS method (Rallapalli et al. 2014). Four flower and four leaf samples for both *paps2-3 paps4-3* double mutants and Col-0 wild type were barcoded and sequenced on two Illumina Genome Analyzer II (GAII) lanes. Four flower samples for both *paps1-1* and L*er* wild type were barcoded and sequenced on half a GAII lane (Trost 2014, PhD thesis).

2.12.2 Data preprocessing

Data were demultiplexed using fastq-multx. rRNA reads were removed using RiboPicker (Schmieder et al. 2012). Sequencing reads were mapped against the TAIR10 reference genome using TopHat2 (Kim et al. 2013) with a reference annotation from TAIR10. Output files were further processed using samtools (Li et al. 2009) before counting reads per gene using htseq-count (Anders et al. 2014).

2.12.3 Gene expression investigation

Expression analyses were done using R (chapter 2.13). Count data were further processed using DESeq2 (Love et al. 2014). Data were transformed to stabilize variance, clustered using euclidean distance and then visualized as a heat map to test for proper grouping of biological replicates. Differential gene expressions were assessed using DESeq2. Genes with log2 fold changes above 1 and BH-adjusted (Benjamini and Hochberg 1995) p-values below 0.05 were considered significant when doing binary comparisons. Overlap of differentially expressed genes were visualized using the limma vennDiagram function (Smyth 2005). Functional category analyses were done using the MapMan ontology (Thimm et al. 2004). Affected categories were identified using Wilcoxon rank-sum test and Kolmogorov-Smirnov test, p-values were BH corrected. Differentially expressed genes were overlapped with the top 200 up- and top 200 down-regulated genes within microarray experiments re-analyzed for MASTA (Reina-Pinto et al. 2010). Overlaps in the same and opposite sense were addressed.

2.13 Software and online tools used for the data analysis

The database PubMed from the National Center for Biotechnology Information (NCBI) served for literature research:

http://www.ncbi.nlm.nih.gov/pubmed/

The LC480 converter (version 2.0, 2012) was used to convert qPCR data obtained with the LC480 (Roche):

http://www.hartfaalcentrum.nl/index.php?main=files&sub=0

The software Image J (version 1.44p, 2011) was used to analyse plant phenotypes and to analyse images gained by microscopy:

http://rsbweb.nih.gov/ij/

Arabidopsis genome information published at *The Arabidopsis Information Resource* (TAIR) website was used to obtain *Arabidopsis* gene sequences, coding sequences, cDNA data and enhanced sequence tag data

http://arabidopsis.org/

The comparison of DNA and protein sequences with published genome and protein data was performed with the Basic Local Alignment Search Tool of the data base NCBI:

http://blast.ncbi.nlm.nih.gov/Blast.cgi

DNA sequences were translated into amino acid sequences using the Translate tool of the ExPASy Proteomics Server of the Swiss Institute of Bioinformatics:

http://web.expasy.org/translate/

The Vector NTI Advance software (version 11.0, 2008; Invitrogen Corp.) was used to analyse gene sequence data:

http://www.lifetechnologies.com/de/de/home/life-science/cloning/vector-nti-software.html

The software R (version 3.1.2, 2014) was used to analyse large data sets:

http://www.r-project.org/

The basic plant biology version of Genevestigator was used to analyse plant gene expression patterns and to compare RNA-seq data with published transcriptome data (tools indicated below):

https://www.genevestigator.com/gv/doc/plant/featured_tools.jsp

The reference manager Mendeley desktop (version 1.12.1, 2008-2014) was used to insert citations:

http://www.mendeley.com/

3. Results

3.1 Poly(A) polymerases ensure the timely flowering of *Arabidopsis*

3.1.1 Poly(A) polymerase mutants exhibit contrasting flowering time phenotypes

When the *paps1-1* mutant was identified in a screen for EMS-induced mutations causing growth defects, the question arose whether plants with defects in the other nuclear poly(A) polymerases would exhibit specific phenotypes as well. However, a set of homozygous mutants with T-DNA insertions at different sites in either the *PAPS2* or the *PAPS4* gene was phenotypically indistinguishable from the wild type Col-0 (**Fig. 14, Fig. 15**). Since a complete knockout of the *PAPS1* function in the *paps1-3* mutant leads to gametophytic lethality due to an insertion in the centre of the catalytic domain (Vi et al. 2013), even lethality caused by the disruption of *PAPS2* or *PAPS4* function was considered beforehand. As mentioned above, the PAPS2 and PAPS4 amino acid sequences exhibit a high overall similarity, which indicates a functional redundancy of these cPAPs. The two *paps* alleles carrying T-DNA insertions in the centre of their catalytic regions, termed *paps2-3* and *paps4-3,* were crossed. By semi-quantitative RT-PCR the resulting double mutant was proved to lack *PAPS2/4* expression (Vi 2013, PhD thesis). Surprisingly, in contrast to *paps1* mutants, the *paps2-3 paps4-3* double mutants did not show phenotypic anomalies with regard to the plant architecture or with regard to leaf or flower shape or size (**Fig. 15**; Vi et al. 2013).

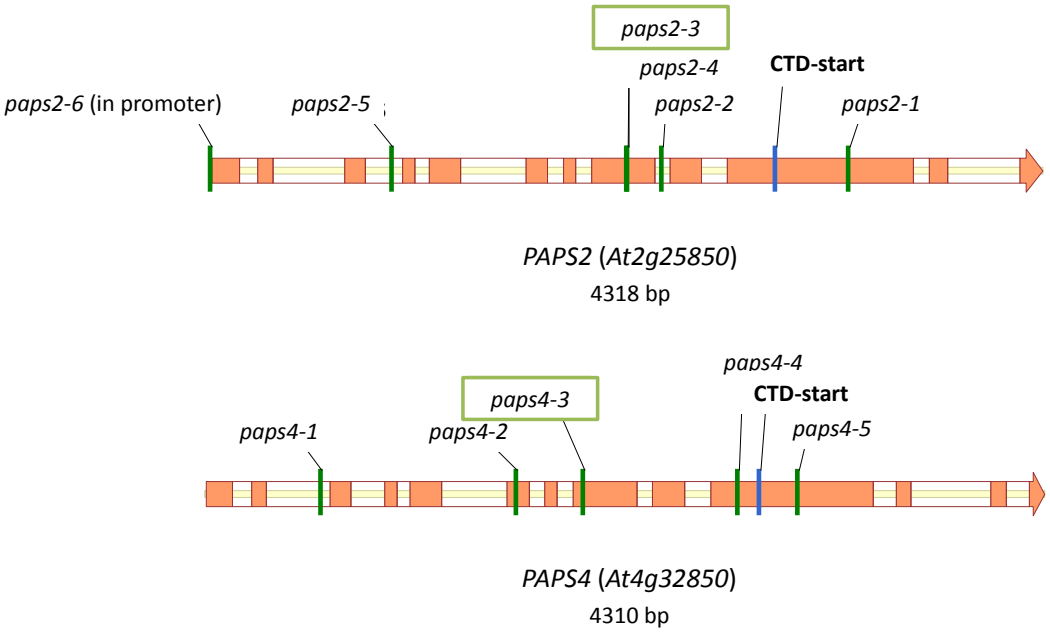

Fig. 14 T-DNA insertion sites in the *PAPS2* and *PAPS4* genes.
All available *paps* mutant lines are indicated. *paps2-3* and *paps2-4* have T-DNA insertions at similar positions in the gene. The highly conserved catalytic core domain ends at the marked beginning of the CTD (CTD-start). Most experiments of this thesis were performed with *paps2-3* and *paps4-3* (highlighted by green boxes).

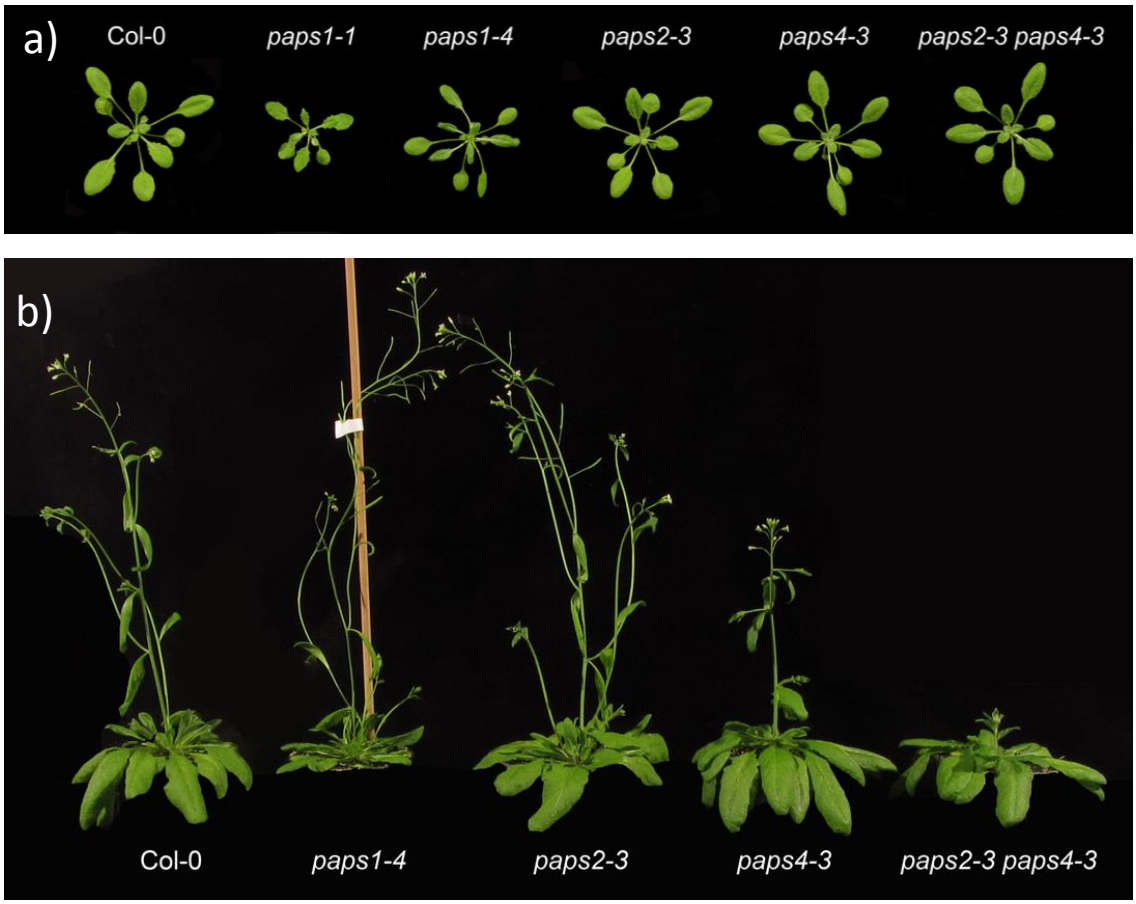

Fig. 15 Phenotype of *paps* mutants in Col-0 background.
a) *paps1-1* and *paps1-4* mutants have smaller leaves than the wild type, while *paps2-3*, *paps4-3* and the double mutant *paps2-3 paps4-3* do not show a specific phenotype. Shown are 21-day-old plants grown under LD conditions (22 °C day; 20 °C night). b) 35-day-old *paps* mutants grown under LD conditions. *paps4-3* and *paps2-3 paps4-3* flower later than Col-0, while *paps1-4* flowers early.

The only striking observation was a moderately delayed flowering of *paps2 paps4* compared to the wild type (**Fig. 15**). The same effect was seen for the *paps4-3* single mutant, albeit to a lesser degree. To quantify the observed effects, a flowering time analysis (FTA) was performed under standard LD conditions (**Fig. 16**). All five accessible *paps4* lines were tested in comparison to the wild type and to *paps2-3 paps4-3*. Since *paps2* mutants had no visible defect, only two lines with T-DNA insertions in the promoter region and in the catalytic centre were examined in the FTA. The total leaf number (TLN), consisting of visible rosette and cauline leaves, was noted when the plants were bolting with a shoot of approximately 1 cm length. Box plots were chosen to present the flowering time data. Box plots display the interquartile range, i.e. the central 50 % of the data. The median, dividing the lower and upper half of the samples, separates the box into the second and third quartile. The box's whiskers range from the minimum to the maximum value. Both *paps2* lines flowered similar to the wild type with an average TLN of 12 (**Fig. 16**). All *paps4* mutant lines flowered significantly late with 14 to 15 leaves. Strikingly, with an average TLN of 17 the *paps2-3 paps4-3* double mutant flowered later than all individual *paps2* or *paps4* single mutants.

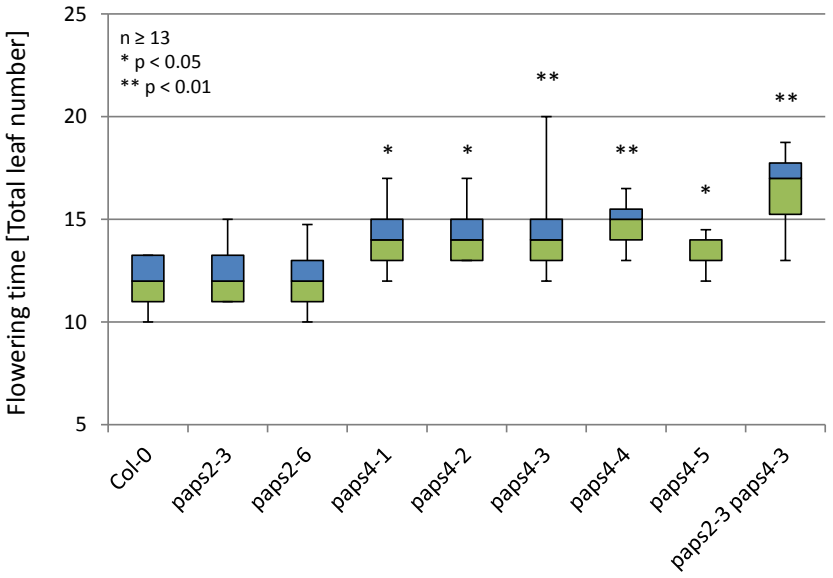

Fig. 16 Flowering time of *paps2* and *paps4* mutant lines under LD conditions.
Plants were grown under standard LD conditions. The box plot depicts the interquartile range (the central 50 % of the data) in a box which is separated into the second (green) and third (blue) quartile by the median. The box whiskers reach from minimum to maximum of all data. Two *paps2* mutant lines with flowering times identical to the wild type are shown as representative examples. All *paps4* mutant lines are flowering two to three leaves later than Col-0, while a double mutant of *paps2-3* and *paps4-3* is flowering later than all individual *paps4* single mutant lines. P-values indicate significant difference to Col-0 and are Bonferroni-corrected.

Subsequently, a more detailed comparative FTA with two different *paps2 paps4* mutant lines was performed to confirm that the observed phenotype is a general feature of *paps* mutants (**Fig. 17**). Moreover, two *paps1* mutant knockdown lines were analysed. *paps1-1* is a strong mutant allele with a point mutation in the CTD; *paps1-4* is a weaker allele with a T-DNA insertion in the beginning of the NTD. Both mutants exhibit a reduced leaf size (**Fig. 16**) and larger floral organs. The *paps1-1* point mutant was originated in a Landsberg *erecta* (L*er*) background. It had been backcrossed to Col-0 for several generations. The *paps1* mutants used in the following analyses and throughout the thesis contained the FLC^{Col} allele which is stronger than the FLC^{Ler} allele (Michaels et al. 2003).

Although the average TLN of all lines was shifted slightly towards higher values in this experiment, the late flowering phenotype of the *paps2-3 paps4-3* double mutant could be confirmed (**Fig. 17**). While Col-0 flowered with an average TLN of 16, *paps2-3 paps4-3* flowered with a TLN of 23. In a preliminary experiment, the alternative mutant *paps2-2 paps4-2*, that contains T-DNA insertions in the centre of the catalytic domain as well, flowered even later than *paps2-3 paps4-3* (data not shown). In the comparative FTA, the alternative double mutant did not flower as late as *paps2-3 paps4-3*, but still flowered moderately late similar to the *paps4* single mutant (**Fig. 17**). Despite the phenotypic fluctuations of *paps2-2 paps4-2*, the late flowering phenotype was considered to be caused specifically by the lack of the poly(A) polymerases *AtPAPS2* and *AtPAPS4*.

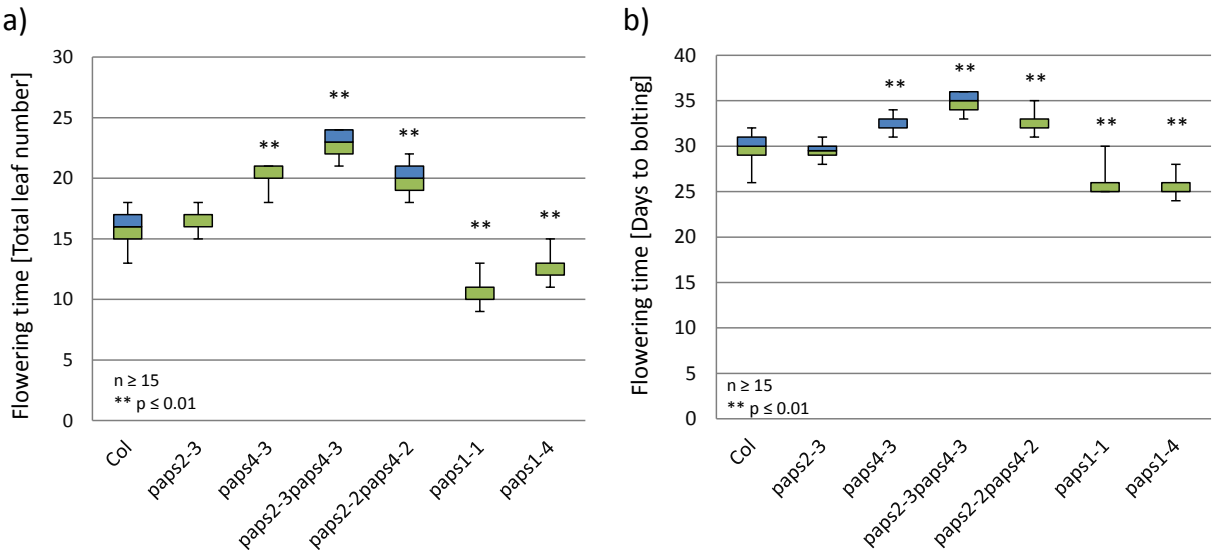

Fig. 17 Comparative flowering time analysis of *paps* single and double mutants.
A comparative flowering time analysis with representative *paps* mutant lines was performed under LD conditions. In this experiment, the temperature was kept stable (22 °C day/ 20 °C night). The total leaf number (a) and the plant age in days (b) were determined when the plants were bolting. P-values indicate significant difference to Col-0 and are Bonferroni-corrected.

Interestingly, with a TLN of 11 and 13, respectively, both *paps1* mutants flowered significantly earlier than the wild type. While a strong correlation between the TLN and age of the bolting plants was observed for most of the analysed plant lines, a discrepancy was noticed for the two *paps1* mutant lines (**Fig. 17**). Both *paps1* lines flowered exactly four weeks after germination (**Fig. 17 b**). However, with regard to the TLN *paps1-1* is flowering two leaves earlier than *paps1-4* (**Fig. 17 a**). To examine this divergence in more detail, the leaf initiation rates of the analysed lines were determined. Since the leaf initiation rate of the wild type and of two *paps2 paps4* (in the following *paps2/4*) double mutant lines were found to be almost identical, the late flowering phenotype cannot be caused by a delayed leaf emergence (**Fig. 18 b**). Similarly, *paps2-3* and *paps4-3* single mutants (data not shown) and *paps1-4* (**Fig. 18 a**) exhibit leaf initiation rates identical to the wild type. In contrast, *paps1-1* shows delayed initiation of the first three leaves. Later, the dynamics are similar to the wild type again (**Fig. 18 a**). This finding indicates pleiotropic phenotypes caused by the strong *paps1-1* mutant allele and explains the discrepancy between plant age and TLN observed for bolting *paps1* mutants.

Subsequently, it was checked whether the *paps* mutant phenotypes could be enhanced by plant growth under SD conditions (8 h light/16 h darkness). Both photoperiod pathway and circadian clock regulate the amount of the diurnally expressed *CONSTANS* (Yanovsky and Kay 2002). High CONSTANS protein levels, which are achieved under LD conditions in summers, can upregulate the transcription of *FT*, an important activator of flowering also described as “florigen” (e.g. Corbesier et al. 2007). The plant circadian clock consists of several interdependent transcriptional and translational feedback loops, involving dawn- and evening-activated genes and rhythmic changes in chromatin structure (described in detail in Farré 2012; Barneche et al. 2014). The lack of *AtPAPS* might cause a

deregulation of day length perception or of the entrainment of the circadian clock, leading to a moderate phenotype under LD conditions and an enhanced late flowering phenotype under SD conditions.

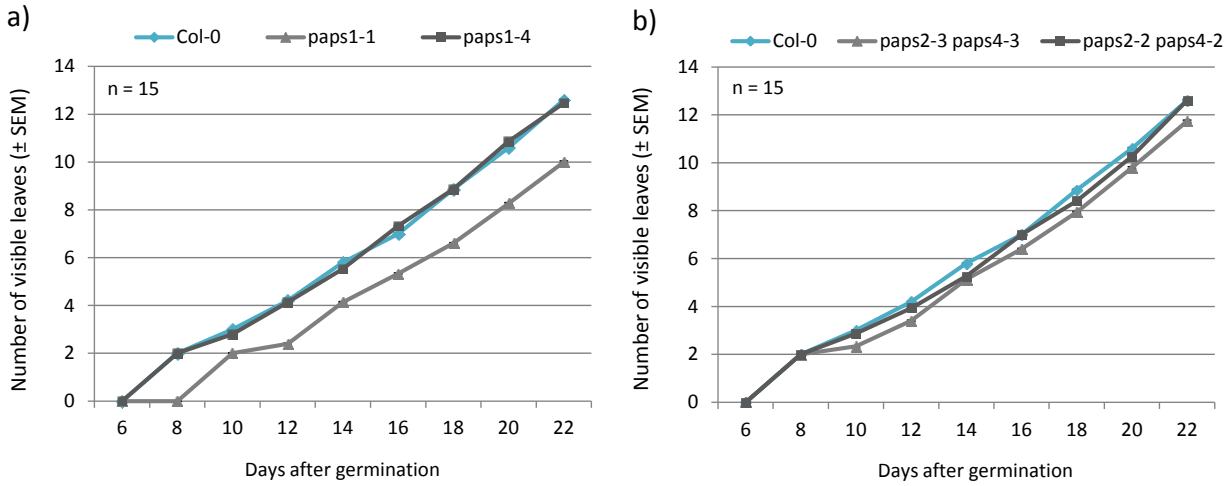

Fig. 18 Leaf initiation rate of *paps* mutants.
The rosette leaf emergence of different *paps1* and *paps2 paps4* double mutants was observed on plants grown under LD conditions. The temperature was kept stable (22 °C day/ 20 °C night). Leaf initiation was noted when the leaf primordia were 1 mm long. SEM error bars are very short and thus hardly visible. a) *paps1-4* shows the same leaf initiation rate like the wild type Col-0. In contrast, *paps1-1* shows a delayed emergence of the first two to three leaves. Leaves 4 to 13 are emerging at similar rates in wild type and mutant. b) Two different *paps2 paps4* lines exhibit a leaf initiation rate that is highly similar to that of the wild type.

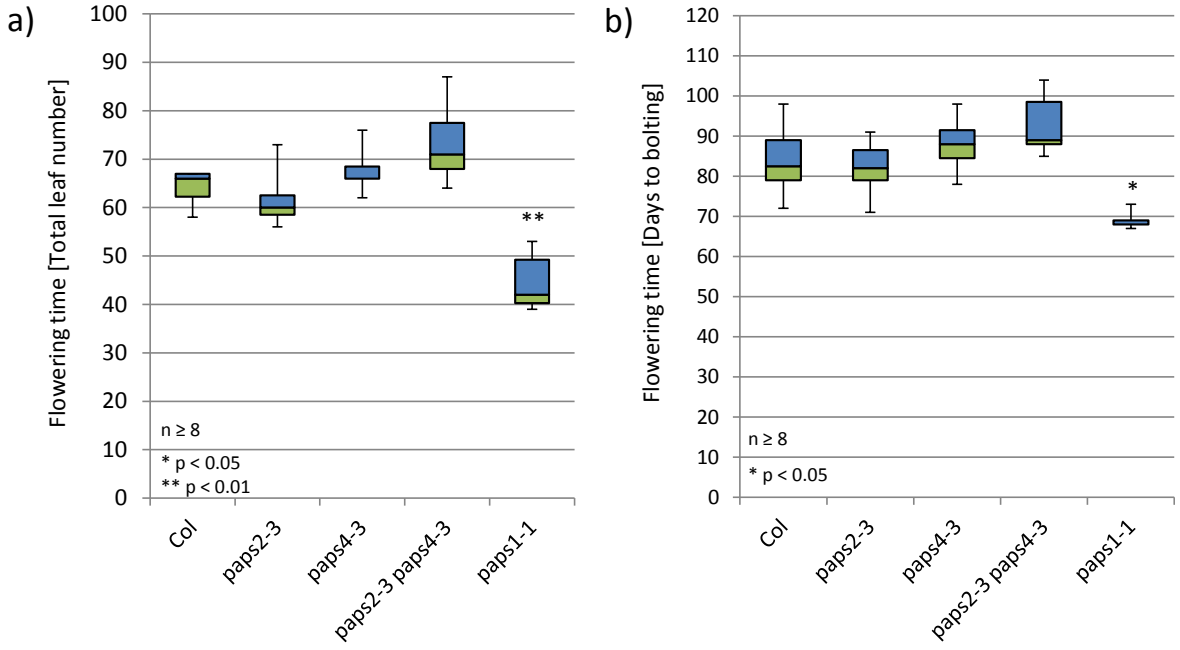

Fig. 19 Flowering time of *paps* mutants under SD conditions.
The total leaf number (a) and plant age in days to bolting (b) were determined when plants started to flower under SD conditions (8 h light, 22 °C/ 16 h darkness, 20 °C). While the *paps2*, *paps4* and *paps2 paps4* mutants behave similarly in LD and SD conditions, the early flowering phenotype of *paps1* is enhanced compared to the phenotype under LD conditions (**Fig. 17**). P-values are Bonferroni-corrected and indicate significant differences to Col-0.

A standard FTA was performed under SD conditions and both TLN and age of the bolting plants were noted (**Fig. 19**). Under SD conditions, the wild type Col-0 flowered with an average leaf number of 64 (and a median of 66). Both the *paps2* and *paps4* single and double mutants did not flower significantly different to Col-0 (**Fig. 19**). However, a trend towards late flowering of *paps2 paps4* is notable. Under SD, the *paps2/4* average TLN was increased by nine leaves compared to Col-0. The median TLN difference (ΔTLN) of both lines was five leaves, which is similar to the value measured under LD conditions (**Fig. 17, Fig. 19**). The *paps1* mutant is responsive to the shorter light period, but flowers again significantly earlier than Col-0, a phenotype reminiscent of that seen for the *flc-3* mutant under SD conditions (Michaels & Amasino 2001). Moreover, an enhanced leaf initiation rate defect might explain that the *paps1-1* TLN is reduced more strongly than the age at bolting.

To determine whether the *paps1* or the *paps4* allele would dominate the flowering phenotype, a double mutant was generated. If the mutations cause defects in different pathways, the resulting flowering time could have been intermediate. However, when first analysed under standard growth conditions, the *paps1-1 paps4-3* double mutants were severely impaired in growth (**Fig. 20 a**). Neither the rosette nor the inflorescences developed properly. The experiment was thus repeated with plants grown under lower temperatures and at low light conditions. The mutant PAPS1 protein in the *paps1-1* line was previously proved to show strongly reduced activity at temperatures above 24 °C. Thus, the protein activity should be stabilized at a lower ambient temperature (18 °C at night, 21 °C during the day). Using low light conditions, oxidative stress in the leaves caused by excess light should be reduced. Indeed, *paps1-1* and the double mutant lines developed much better (**Fig. 20 b**). Resembling the control, the *paps1 paps4* double mutants exhibited slightly serrated leaves. However, the offspring of two homozygous F3 lines behaved differentially (**Fig. 20 b**). Some individuals looked similar to *paps1-1*, while others showed pleiotropic growth defects. These plants did not develop proper shoots and inflorescences and were dwarf-like with bushy rosettes.

To note putative flowering defects, the flowering time of the two F3 lines was determined (**Fig. 21**). With regard to the TLN, one line flowered with an average TLN intermediate between *paps1* and *paps4*, while the second line flowered similar to the *paps1-1* control. This discrepancy arose from the pleiotropic growth phenotypes observed in some individuals. The TLN could not be determined reliably. Regarding the plant age, both lines flowered similarly to *paps4-3.* However, since the shoots and inflorescences were partially stunted, it was not always possible to measure the plant age when the stem was 1 cm long. In this cases flowering was defined as the day when shoot growth arrested. The phenotyping difficulties are reflected by the high variation of both TLN and plant age at bolting.

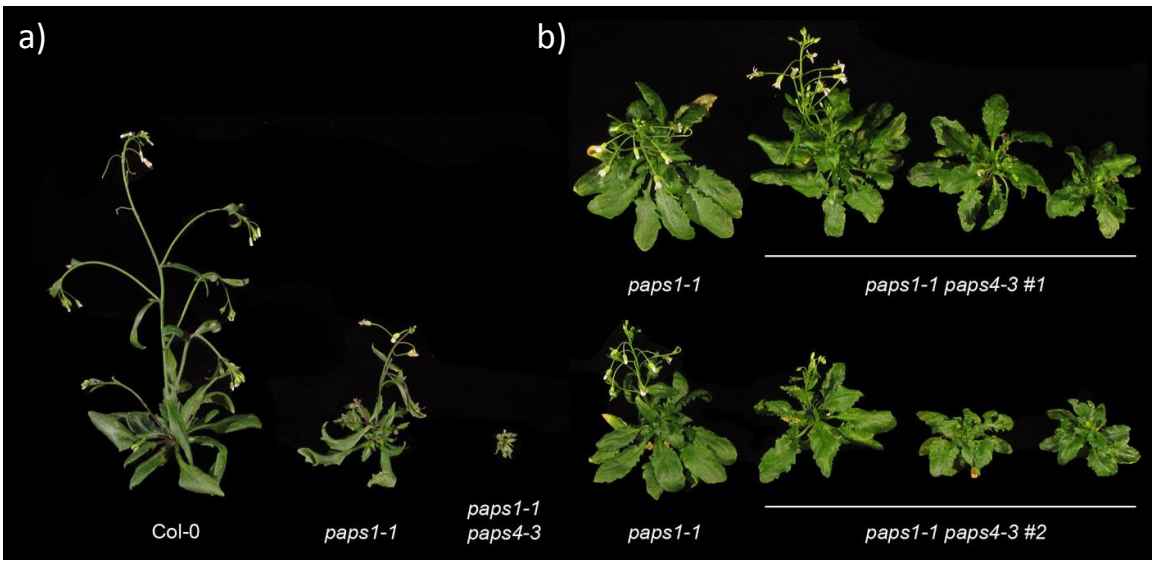

Fig. 20 The double mutant *paps1-1 paps4-3* exhibits growth defects.
Growth phenotype and flowering time of homozygous *paps1-1 paps4-3* lines were tested under different growth conditions. a) Under standard conditions (LD; PAR 120 µmol photons/m^2/s; temperature up to 24 °C), the *paps1-1 paps4-3* rosette leaves could not develop properly. b) The double mutants were germinated on ½ MS medium and transferred to soil after seven days. Under low light and lower temperatures (LD; PAR 80 µmol photons/m^2/s; 21 °C D/ 18 °C N), the double mutants grow larger, but partly still show stunted growth and leaf deformations.

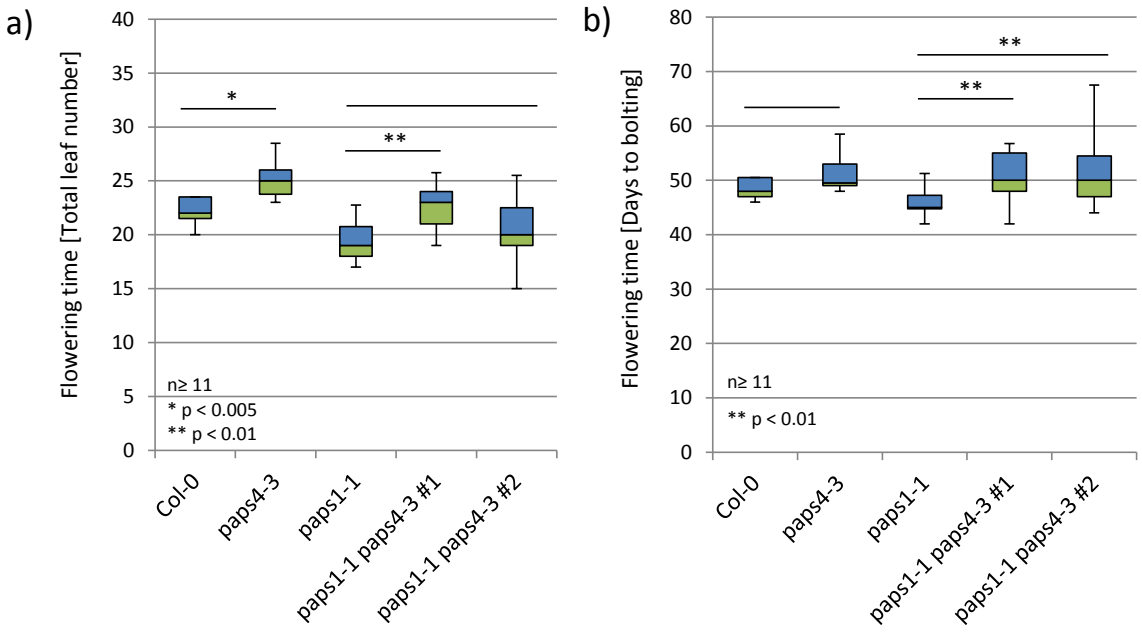

Fig. 21 The flowering time of *paps1-1 paps4-3* mutants varies between different lines.
A flowering time analysis under low light and low temperature conditions was performed with two independent *paps1-1 paps4-3* F3 lines (LD; PAR 80 µmol photons/m^2/s; 21 °C D/ 18 °C N). a) TLN and b) days to bolting were determined when the plants started to flower. While double mutant line 1 flowers with an intermediate leaf number between the *paps1* and *paps4* control lines, double mutant line 2 flowers with a TLN similar to *paps1-1*. However, with regard to the plant age, both lines flower as late as *paps4-3*. P-values are Bonferroni-corrected.

In addition to the homozygous double mutant lines, the offspring of four F2 *paps1-1/paps1-1 paps4-3/+* lines were tested. In an FTA, these lines also behaved very differently with regard to TLN and days to bolting (data not shown). The proportion and degree of growth defects varied in the four lines, increasing the difficulties to interpret the data.

3.1.2 Salicylic acid treatment does not change the *paps* mutant flowering time phenotype

Plants flower early under diverse stress conditions. Martínez et al. (2004) found that early flowering induced by excess UV-C light is mediated by the plant hormone salicylic acid (SA). Since overexpression of the SA-degrading enzyme NahG, a salicylate hydroxylase, led to a moderate delay in flowering under LD conditions (with Col-0 flowering with 11–12 leaves, and *35S::NahG* mutants flowering with 15–16 leaves), SA also seems to regulate flowering time in non-stressed plants (Martínez et al. 2004; Lawton et al. 1995). The early flowering phenotype was found to be independent from *FLC*. Consistently, late flowering autonomous pathway mutants were not responsive to spraying with SA. Since the moderately late flowering phenotype of *35S::NahG* plants is reminiscent of the *paps2/4* phenotype, it was tested whether *paps* mutants are responsive to SA.

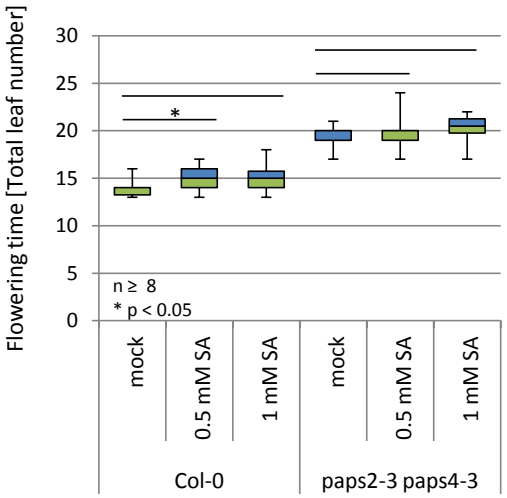

Fig. 22 Flowering time of *paps2-3 paps4-3* and wild type plants sprayed with 0.5 mM or 1 mM SA.
Plants were grown under standard LD conditions and, starting at 10 DAG, sprayed with SA every other day. The SA treatment did not rescue the *paps* mutant phenotype. Instead, there was a trend towards a slight delay of flowering in SA-treated plants, which is significant in the wild type Col-0, but not in the mutant. P-values indicate significant difference to the mock-treated plants and are Bonferroni-corrected.

In a rescue experiment, plants were sprayed with low SA concentrations of 50 and 100 µM every other day, a method used by Martínez et al. (2004). However, neither *paps-1* nor *paps2-3, paps4-3* or *paps2-3 paps4-3* exhibited altered flowering times compared to the non-treated control (data not shown). Subsequently, the SA concentrations were increased to 0.5 and 1 mM. The *paps2/4* double mutant did still not exhibit a change in flowering time upon spraying with SA (**Fig. 22**).

Instead, the flowering of Col-0 was slightly delayed by the treatment with 0.5 mM SA, but not with 1 mM SA. In contrast, Martínez et al. (2004) observed a very slight shift towards early flowering in Col-0 sprayed with low concentrations of 50 and 100 µM SA. In either direction, the observed phenotype is too subtle to explain the late flowering of the *paps2 paps4* double mutant.
Interestingly, the SA content of *paps1-1* was indistinguishable from that of the wild type (Trost 2014, PhD thesis). Moreover, the phenotype of *paps1-1* remained unchanged when the plant SA level was reduced by the overexpression of *NahG*. These findings indicate that both the late flowering and the early flowering phenotypes observed in different *paps* mutants are not caused by alterations in the level of or the responsiveness to SA.

3.1.3 The *paps* mutant phenotype is based on a deregulation of *FLC*

Next it was asked, which flowering-regulating pathway could be deregulated in *paps1* and in *paps2 paps4*. The focus was first set on the *paps2/4* late flowering phenotype. Based on the mutant growth phenotype and based on the performed FTAs (chapter 3.1.1), certain pathways could be ruled out. Since the *paps2/4* morphology is indistinguishable from that of the wild type, a defect in GA synthesis or signalling is unlikely. The result of the SD-FTA indicates that the photoperiod pathway is not involved. The leaf size and the leaf-initiation rate of the *paps2/4* mutants are identical to the wild type (Vi et al. 2013; chapter 3.1.1). Since misexpressions of *miR156* and of *SPL* genes are often associated with changes in leaf size or leaf initiation rate (Wang et al. 2008b; Wu et al. 2009), the age-dependent pathway was left out of consideration. The reduction of *PAPS1* activity results in a reduced leaf size (Vi et al. 2013; Vi 2013, PhD thesis). A slight retardation of the primary leaf development could only be observed for the *paps1-1* mutant, but not for *paps1-4* (**Fig. 18**), indicating that the age-pathway is not causing the early flowering phenotype either. During experiments performed during summers, *paps2/4* plants grown under non-controlled temperature conditions showed a reduced late flowering phenotype. It was concluded that temperature perception is not impaired. In conclusion, a defect in the autonomous pathway seemed very likely.
First, the expression level of *FLC*, the main inhibitor of flowering, was tested. In a microarray performed with *paps1-1* and L*er* RNA extracted from 10-day-old seedlings, the *FLC* mRNA level was found to be reduced in *paps1* (not shown). Reduced *FLC* expression or instability of the *FLC* transcript in *paps1-1* could indeed explain the observed early flowering phenotype. In nine-day-old seedlings, a trend towards a lower *FLC* mRNA steady state level in *paps1-1* could be confirmed by qPCR, but the difference to the wild type L*er* is not significant (**Fig. 23**). Since the FLC^{Ler} allele is weak and the Landsberg accession flowers naturally early (Michaels et al. 2003), the experiment was repeated with *paps1-1* that had been backcrossed to Col-0. Indeed, the *FLC* mRNA level was strongly decreased in *paps1-1* expressing FLC^{Col} compared to Col-0, but again the difference remained a trend.

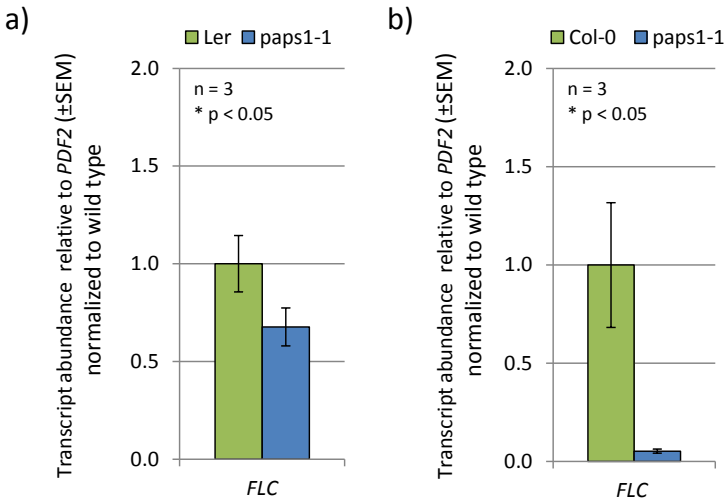

Fig. 23 A trend towards decreased *FLC* mRNA abundance can be observed in *paps1-1*.
Seedlings used for the RNA extraction were grown at 21 °C under LD conditions for nine days. By qPCR, the *FLC* mRNA levels in *paps1-1* in L*er* (a) or Col-0 (b) background and in the respective wild type were determined. While the *FLC* abundance is decreased in *paps1-1*, in Col-0 even stronger than in L*er*, the decrease remains an insignificant trend.

The *FLC* transcript level could be altered in *paps2/4* as well. Indeed, nine-day-old *paps2-3 paps4-3* seedlings exhibit a two-fold upregulated *FLC* mRNA level compared to Col-0, which could explain the flowering inhibition observed (**Fig. 24 a**). In accordance, several floral pathway integrators were found to be lowly expressed in the double mutant at nine DAG (**Fig. 24 b**). The transcript abundances of the FPIs *SOC1* and *FT* were significantly reduced in *paps2/4*. A trend towards lower expression of *AP1* and *LFY* could also be observed.

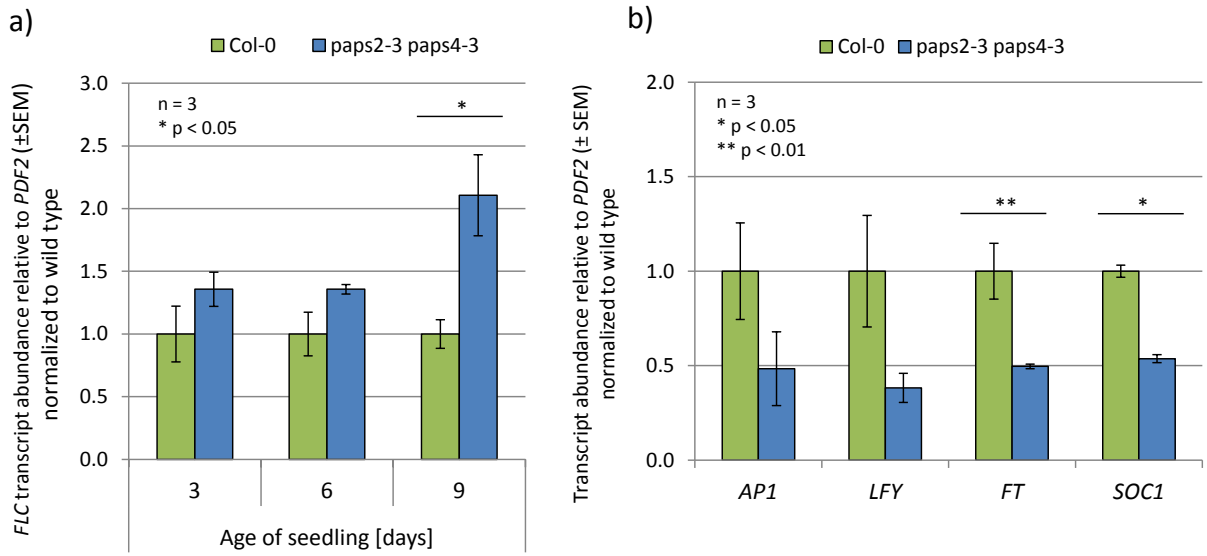

Fig. 24 Expression levels of *FLC* and of floral pathway integrators in *paps2 paps4*.
The *FLC* mRNA abundance is increased in the *paps2-3 paps4-3* double mutant. Floral pathway integrators show reduced expression levels. a) Col-0 and mutant seedlings were grown under LD conditions and were collected simultaneously for the measurement at three, six and nine DAG. b) Seedlings were grown under LD conditions and harvested at nine DAG. *FT* and *SOC* mRNA abundances are significantly reduced in *paps2-3 paps4-3*. *AP1* and *LFY* are not reduced significantly, but a trend towards lower expression levels can be observed.

To find out whether other flowering inhibitors might be involved in causing the *paps2/4* phenotype, transcript levels of *SVP*, *FLM* and *MAF2* were inspected. The MADS box factor SVP represses the expression of floral pathway integrators and directly interacts with FLC and FLM (Hartmann et al. 2000; Scortecci et al. 2003; Li et al. 2008). In *Arabidopsis*, five *MAF* (*MADS AFFECTING FLOWERING*) transcription factors have been described. *FLM*, also termed *MAF1*, controls flowering in response to ambient temperatures. Temperature-dependent alternative splicing of *FLM* leads to the splice variants *FLMβ* and *FLMδ*. At lower temperatures the dominant form FLMβ interacts with SVP (Lee et al. 2013; Posé et al. 2013). The repressive FLMβ-SVP complex binds promoters of FPI genes, like *FT* or *SOC1*. As temperatures increase, the *FLMδ* splice variant is predominantly produced. The FLMδ-SVP complex has a lower DNA-binding capacity, which antagonizes the flowering-inhibiting effect of SVP.

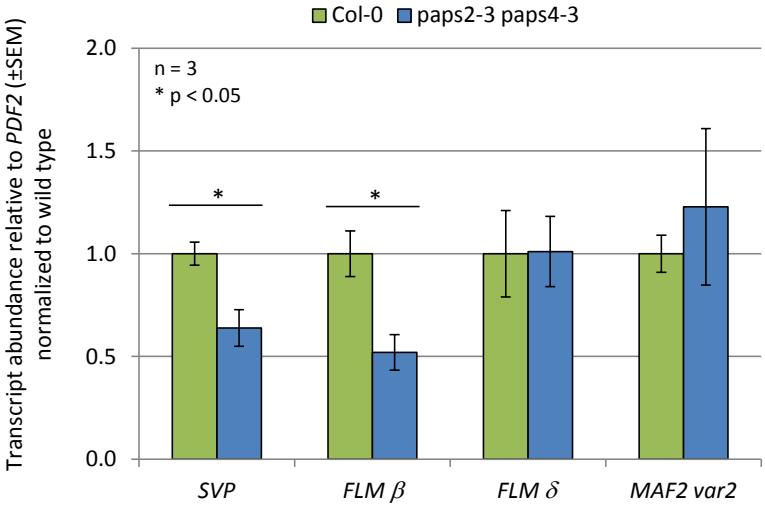

Fig. 25 Expression levels of *SVP*, *FLM* and *MAF2* in *paps2 paps4*.
The *SVP* and *FLMβ* mRNA abundances are reduced in *paps2-3 paps4-3*. *FLMδ* and *MAF2* do not show altered expression levels. Seedlings were grown under LD conditions and harvested at nine DAG. The *SVP* mRNA abundance is significantly reduced in *paps2 paps4*. While the *FLMβ* splice variant is produced to a significantly lesser extent in *paps2 paps4*, the *FLMδ* splice variant and the *MAF2* splice variant 2 (*MAF2 var2*) levels are unchanged. *MAF2* splice variant 1 was not detected in the studied genotypes. P-values indicate significant difference

Surprisingly, the transcript levels of *SVP* and the *FLMβ* splice form were found to be halved in *paps2/4* (**Fig. 25**). *svp* mutants have been described to flower early due to increased FPI gene expression (Li et al. 2008). The abundance of the *FLMβ* splice form is reduced while the level of *FLMδ* is unchanged (**Fig. 25**). Interestingly, also in the wild type the ratio of *FLMβ* to *FLMδ* is less than one (**Table 5**). Increased *FLMδ* values indicate high ambient temperatures (Posé et al. 2013). The samples for the experiment were collected in June 2013 in a growth chamber without temperature control, which exhibited slightly elevated ambient temperatures. Indeed, in a simultaneously performed flowering time analysis the average ΔTLN between Col-0 and *paps2-3 paps4-3* was only three to four leaves (**Fig. 32 a**), while in earlier experiments a ΔTLN of eight had been determined (**Fig. 17**).

Table 5 Relative expression values of the *FLM* splice variants *β* and *δ*.
Expression levels are indicated by [PCR efficiency $^{(-\Delta Ct)}$] values. ΔCt (threshold cycle) values reflect *FLM* Ct values normalized to *PDF2* Ct values.

	FLMβ	***FLMδ***	**ratio *β*/*δ***
Col-0	0.064	0.084	0.76
paps2-3 paps4-3	0.033	0.085	0.39

The other four *Arabidopsis MAF* genes are arranged in a tandem array on chromosome V. *MAF2* is a further flowering inhibitor which is also alternatively spliced in a temperature-dependent manner. While the *MAF2* splice variants (var) 2 and 4 are predominantly expressed under higher ambient temperatures, but have hardly any effect on flowering time when overexpressed, the *MAF2* splice variant 1 is induced by cold and promotes flowering when overexpressed (Rosloski et al. 2013). In general, only var 1 and var 2 can be detected specifically by qPCR. In nine-day-old *paps2-3 paps4-3* seedlings, *MAF2* var 2 expression was not altered compared to the WT (**Fig. 25**). As expected, *MAF2* var 1 could not be amplified under ambient temperatures.

MAF3, *4* and *5* have so far not been characterized in detail. All three *MAFs* are putatively weak flowering inhibitors that play minor roles in addition to *FLC* (Ratcliffe et al. 2003). Therefore, these factors were not considered further in this study. In conclusion, the late flowering of *paps2/4* seemed to be mainly caused by increased *FLC* mRNA levels. Similarly, decreased *FLC* transcript levels were putatively involved in the early flowering phenotype of *paps1-1*.

Next it was tested how the loss of functional *FLC* would affect the *paps* mutant phenotype. The *paps2-3 paps4-3* mutant was crossed with the point mutant *flc-5*, an *flc* null allele in the L*er* background (Greb et al. 2007). The resulting triple mutant exhibited a mixed Col-0/ L*er* background. To reduce the background variation, two F2 lines that were fixed for the *paps2-3* and *flc-5* mutations but still segregating for *paps4-3* were analysed. The *paps2-3 flc-5* plants from the segregating population served as a line-specific early flowering control. Regarding the plant TLN when bolting, both analysed lines indeed exhibited a complete rescue (**Fig. 26 a**). The *paps2-3 paps4-3 flc-5* triple mutants flowered with the same TLN like the corresponding *paps2-3 flc-5* plants. With regard to the plant age when bolting one line similarly exhibited a complete rescue, while the offspring of the second line showed a strongly reduced but still significant flowering time difference (**Fig. 26 b**). The *paps2-3 flc-5* plants were expected to show the same flowering time like the *flc-5* control line, which was confirmed in terms of the plant age when flowering (**Fig. 26 a**). However, both *paps2-3 flc-5* lines exhibited a higher TLN than *flc-5*, which supposedly is a consequence of the mixed background. Nonetheless, the rescue of the *paps2/4*-dependent flowering delay by the loss of functional *FLC* was demonstrated.

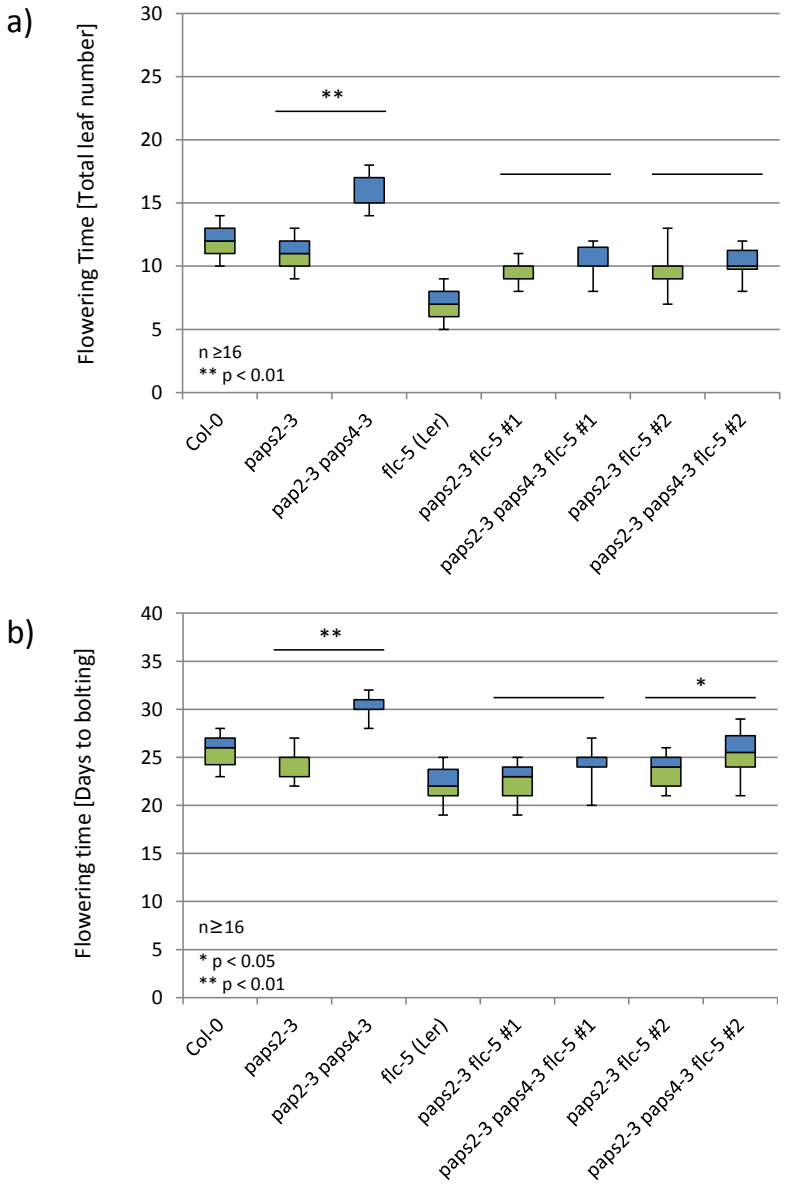

Fig. 26 The late flowering phenotype of *paps2-3 paps4-3* is rescued by the *flc-5* (L*er*) mutation.
The *paps2-3* and *paps4-3* alleles are in Col-0. *flc-5* is a point mutant null allele in the L*er* background. To reduce background variation, an FTA was performed comparing the homozygous offspring of two *paps2-3 paps4-3/+ flc-5* lines. a) Regarding the TLN at bolting, the late flowering phenotype of *paps2-3 paps4-3* was completely abolished by the loss of *FLC* activity. b) With regard to the age when bolting, line 1 exhibited a complete rescue, while the *paps2-3 paps4-3 flc-5* triple mutant derived from line 2 shows a strongly reduced phenotype.

To confirm the rescue without background variation and to gain insights into the genetic interaction of *PAPS1* and *FLC*, the *paps1-1* and *paps2-3 paps4-3* mutants were crossed with the Col-0 allele *flc-2*. Due to a 30 kb deletion, the *FLC* activity is completely eliminated in the fast-neutron *flc-2* mutant (Michaels and Amasino 1999; Michaels et al. 2003). A comparative FTA under LD conditions revealed that the loss of *FLC* did not enhance the early flowering phenotype of *paps1-1* (**Fig. 27 a, c**). The double mutant *paps1-1 flc-2* and the respective single mutants flowered early with an identical TLN. This finding underlines that reduced *FLC* expression levels cause the early flowering phenotype observed in *paps1* mutants.

Next, the offspring of two *paps2-3 paps4-3/+ flc-2* lines was analysed. As expected, in a Col-0 background the *paps2-3 flc-2* plants flowered as early as *flc-2* with regard to both TLN and age when bolting (**Fig. 27 b, d**). However, surprisingly the reduction of the flowering time difference between *paps2-3 flc-2* and *paps2-3 paps4-3 flc-2* was less pronounced compared to the results gained with the *flc-5* allele. While the average ΔTLN between *paps2-3* and *paps2-3 paps4-3* was seven, in the *flc-2* background the ΔTLN was reduced to three to four leaves (**Fig. 27 b**). Regarding the plant age, the flowering difference of seven days in the FLC^{Col} background was reduced to four days in line 1, but still comprised six days in line 2 (**Fig. 27 d**).

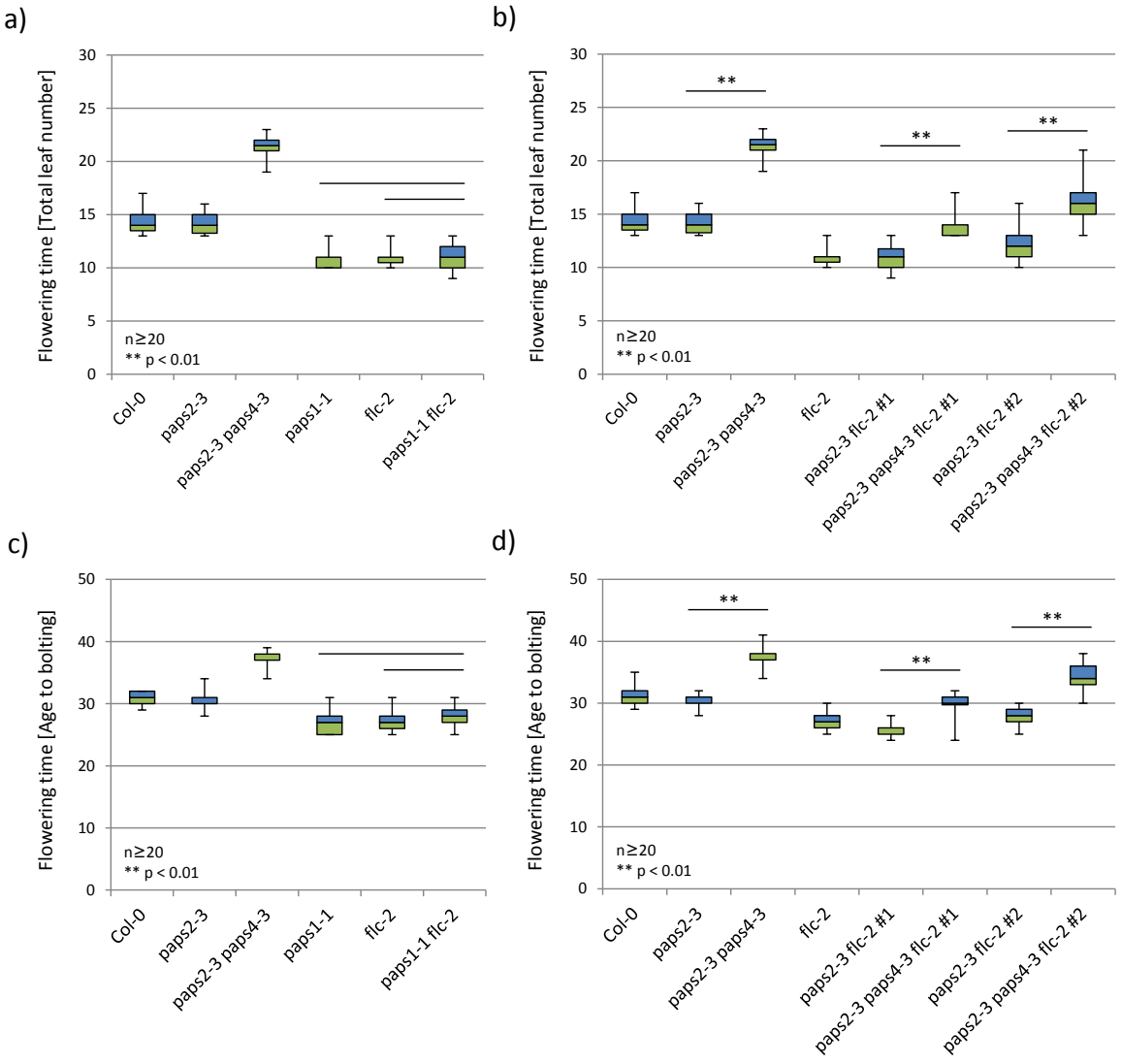

Fig. 27 Flowering time of *paps* mutants in an *flc-2* (Col-0) background.
A comparative flowering time analysis with representative *paps* and *flc-2* mutant lines was performed under LD conditions and stable temperatures (22 °C day/ 20 °C night). a, c) The loss of functional *FLC* does not enhance the early flowering phenotype of *paps1-1*. b, d) The offspring of two *paps2-3 paps4-3/+ flc-2* lines was analysed. Comparing *paps2-3 flc-2* and *paps2-3 paps4-3 flc-2*, the deletion of the *FLC* gene partially rescues the late flowering phenotype of *paps2 paps4*. The total leaf number (a, c) and the plant age in days (b, d) were determined when the plants were bolting. P-values indicate significant difference and are Bonferroni-corrected.

These results indicate that the increased *FLC* transcript level detected in *paps2/4* is not the only component responsible for the late flowering phenotype. Other yet unidentified factors seem to contribute to the phenotype. In contrast, the early flowering phenotype of *paps1* was not additive with the loss of *FLC* activity. Supposedly, *PAPS1* is required to maintain *FLC* expression or *FLC* transcript stability.

3.1.4 *PAPS1* and *PAPS2/PAPS4* act independently from *CstF64* and *FY*

Since knocking down the function of essential polyadenylation factors like *CstF64* and *FY* results in a delay of flowering (Henderson et al. 2005; Liu et al. 2010), it was checked whether these components act in the same pathway like *PAPS1* and *PAPS2/4*. The mutant *cstf64-1* was identified as a *sof* (*s*uppressor of *o*verexpressed *FCA*) mutant in the L*er* background. With a ΔTLN of 10 when bolting compared to L*er*, *cstf64-1* exhibits a moderate delay in flowering (Liu et al. 2010). An alternative mutant allele *cstf64-2*, a T-DNA insertion line in Col-0, shows pleiotropic defects including reduced fertility (Liu et al. 2010). Thus, the *cstf64-1* allele was used for the genetic analysis. While *paps1-1 cstf64-1* double mutants are embryo lethal (Vi et al. 2013), *paps2 paps4 cstf64-1* triple mutants are viable. Importantly, only F2 plants containing the FLC^{Col} allele were selected for the flowering time analysis in the following experiments. First, the phenotypic effects caused by *cstf64-1* in a mixed Col-0/L*er* background were determined examining two *cstf64-1/+* F2 lines (**Fig. 28 a**).

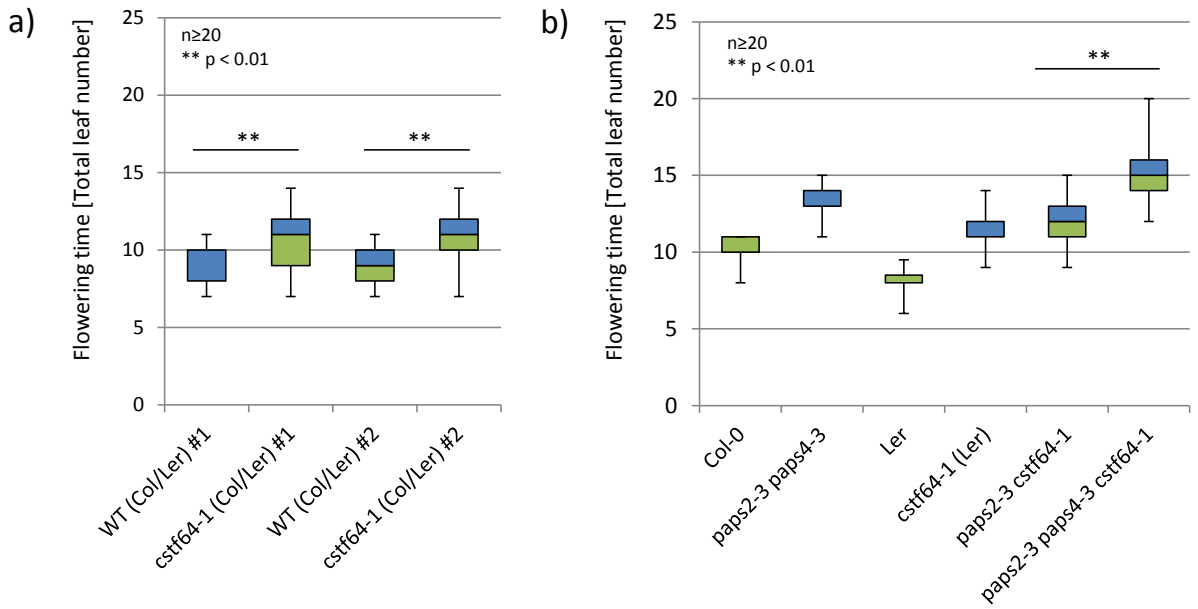

Fig. 28 Regarding flowering time, *PAPS2/PAPS4* and *CstF64* act in independent pathways.
a) In a mixed background of Col-0 and L*er*, the *cstf64-1* mutation delays flowering for two to three days. Two independent *cstf64-1/+* lines homozygous for FLC^{Col} were tested under LD conditions. b) The effect of the loss of *Cstf64* on *paps2 paps4* mutants was tested with a *paps2-3 paps4-3/+ cstf64-1* line homozygous for FLC^{Col}. While *paps2-3 cstf64-1* flowers like *cstf64-1,* the triple mutant *paps2-3 paps4-3 cstf64-1* flowers significantly later than the individual control lines. P-values are Bonferroni-corrected.

With a ΔTLN of two to three leaves, the flowering time delay caused by the loss of *CstF64* activity was less pronounced in the mixed background than in the L*er* background, but is still significant. Next, a comparative FTA was performed with an F2 line homozygous for the FLC^{Col}, *cstf64-1* and *paps2-3* alleles and heterozygous for *paps4-3* (**Fig. 28 b**). The flowering times of the homozygous *paps4-3/paps4-3* and *PAPS4/PAPS4* F3 plants were compared. While *paps2-3 cstf64-1* flowers like the *cstf64-1* single mutant, *paps2-3 paps4-3 cstf64-1* triple mutants flower later than all individual single mutants. This result indicates that *CstF64* and *PAPS2/4* act independently from each other.

Next, the effect of reduced *FY* activity in the *paps* mutant background was tested. Complete null mutations in *AtFY* result in embryo lethality. Therefore, *paps1* and *paps2/4* were crossed to the knockdown mutant *fy-2* (Col-0), a T-DNA insertion mutant that flowers with approximately 55 leaves (Henderson et al. 2005). Homozygous *paps1-1 fy-2* and *paps2-3 paps4-3 fy-2* lines were used for a comparative FTA (**Fig. 29**). The large-scale experiment was performed in spring in a glass house under LD conditions. The *fy-2* control line flowered with a TLN of 33, earlier than documented (Henderson et al. 2005). The flowering behaviour of all *paps* mutant control lines corresponded to previous experiments (e.g **Fig. 17**). Interestingly, the combination of mutant *paps1* and *fy* knockdown alleles is not lethal, although *FY* is an important and multifunctional polyadenylation factor. While the *paps1-1 fy-2* double mutant shows a flowering phenotype intermediate to the two controls, the effects of *paps2-3 paps4-3* and *fy-2* are additive. Both double and triple mutant phenotypes can be interpreted as additive in a multiplicative manner, which indicates that all three *PAPSs* act independently from *FY*. Thus, both *CstF64* and *FY* are functional in *paps* mutant backgrounds and do not seem to cause the mutant flowering phenotypes.

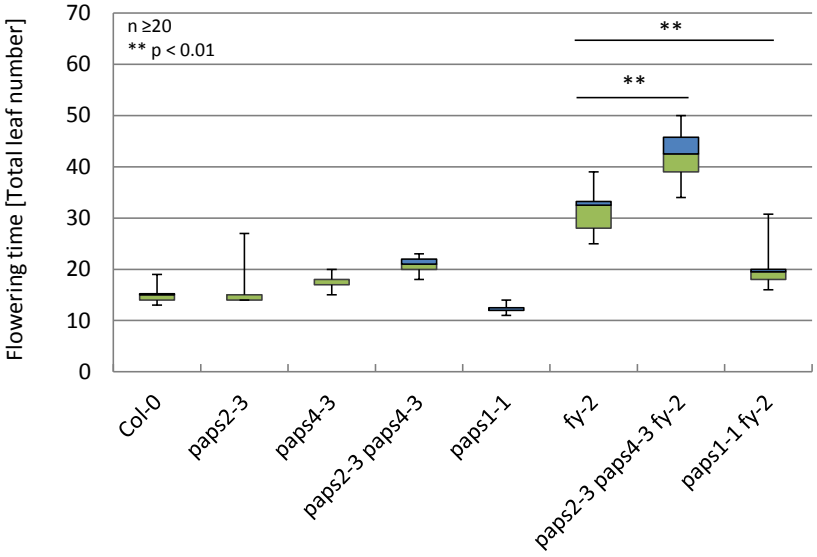

Fig. 29 Regarding flowering time, *FY* acts independently from *PAPS1* and *PAPS2*/*PAPS4*.
The experiment was performed under LD conditions in a glass house. While the *paps1-1 fy-2* mutant shows an intermediate phenotype between *paps1-1* and *fy-2*, the *paps2-3 paps4-3 fy-2* triple mutant flowers later than *paps2-3 paps4-3* or *fy-2.* P-values are Bonferroni-corrected.

3.1.5 *FCA* is epistatic to *PAPS2/4*, but not to *PAPS1*

To analyse whether the *FCA* function might be impaired in *paps2-3 paps4-3* or *paps1-1*, the strong mutant allele *fca-9* (in Col-0) was introduced into the *paps* mutant background. The *fca-9* allele contains a point mutation that results in a truncated FCA protein (Page et al. 1999). A large-scale experiment under LD conditions was performed in a glass house, similar to the *fy-2* experiment (**Fig. 30**). Both *fca-9* and *paps2-3 paps4-3 fca-9* flowered with an average TLN of 74. The *fca-9* mutation is clearly epistatic to *paps2-3 paps4-3*, indicating that *PAPS2/4* and *FCA* act in a common pathway. The fact that *paps2/4* mutants do not nearly flower as late as the *fca-9* single mutant suggests that *PAPS2* and *PAPS4* act downstream of *FCA* and that there are additional factors through which *FCA* can influence flowering in *paps2/4* mutants. Accordingly, the transcript abundance of *FCAγ*, which encodes the active protein isoform, was found to be unchanged in *paps2/4* (not shown). The ratio of *FCA* splice forms supposedly would have been changed, if *PAPS2/4* were required for the correct polyadenylation of one or several *FCA* mRNA isoforms.

In combination with the *paps1-1* mutation, the *fca-9* mutation leads to an intermediate phenotype, underlining that *PAPS1* functions independently from *FCA*. Again the early flowering effect caused by reduced *PAPS1* activity is very pronounced.

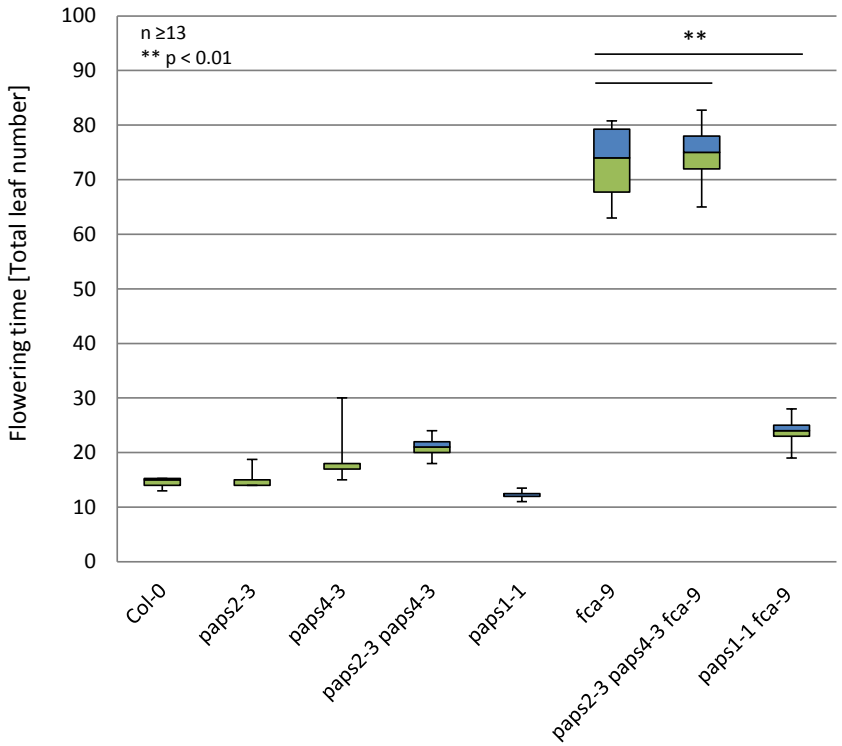

Fig. 30 *FCA* is epistatic to *PAPS2/PAPS4*, but not to *PAPS1*.
The experiment was performed under LD conditions in a glass house. While the *paps1-1 fca-9* mutant shows an intermediate phenotype between *paps1-1* and *fca-9* with a strong shift towards the *paps1* phenotype, *paps2-3 paps4-3 fca-9* triple mutants flower similar to *fca-9*, indicating an epistatic interaction of *FCA* and *PAPS2/PAPS4*. P-values are Bonferroni-corrected.

The flowering time of the *paps1-1 fca-9* double mutant is strongly shifted towards the early flowering phenotype of *paps1-1*, which most likely reflects the defective *FLC* expression in *paps1* that has been shown before (**Fig. 23, Fig. 27**). Next, the effect of the loss of *PAPS1* or *PAPS2/PAPS4* was tested in an *FCAγ*-overexpressing (OE) background, in which the *FLC* steady state abundance is strongly decreased, resulting in early flowering (Macknight et al. 2002). Indeed, the *35S::FCAγ*-OE line flowers on average three leaves and five days earlier than the wild type Col-0 (**Fig. 31**).

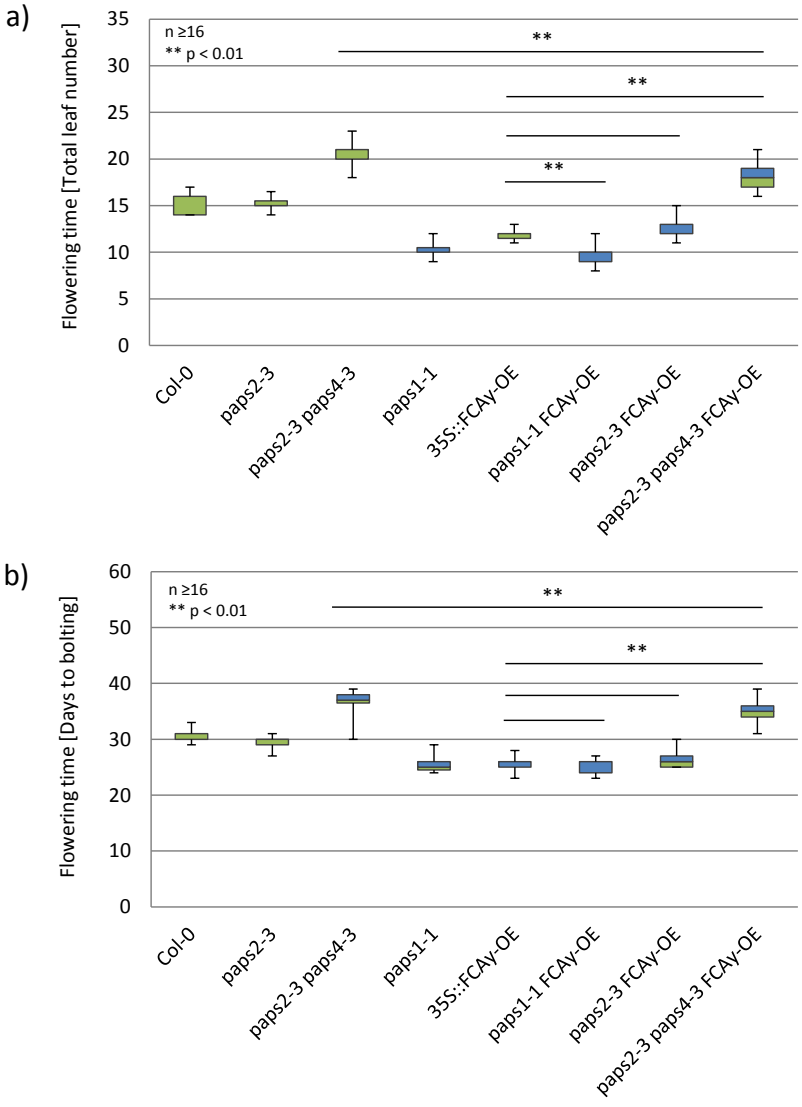

Fig. 31 Overexpression of *FCA* splice form *γ* in *paps* mutants.
The overexpression of *FCA* does not rescue the *paps2-3 paps4-3* late flowering phenotype and does not increase the early flowering phenotype of *paps1-1*. In the early flowering *35S::FCAγ*-OE line, the splice form *FCAγ* encoding the functional FCA protein is overexpressed. To analyse the overexpression effect in a *paps* mutant background, the offspring of *paps2-3 paps4-3/+ 35S::FCAγ* and *paps1-1 35S::FCAγ* were analysed. a) Regarding the TLN when flowering, the *paps1-1 FCAγ*-OE line flowers as early as *paps1-1*. While the *paps2-3 35S::FCAγ*-OE flowers early, the *paps2-3 paps4-3 35S::FCAγ*-OE plants derived from the same parental line are only partially rescued. b) With regard to the plant age when flowering, the control lines *paps1-1* and *35S::FCAγ* flower at the same time like the *paps1-1 35S::FCAγ*-OE mutant. The experiment was performed under LD conditions with controlled temperature (22 °C D/20 °C N). P-values are Bonferroni-corrected.

An identical acceleration of flowering was observed upon loss of *FLC* activity (**Fig. 27**). If residual *FLC* activity was still present in *paps1-1*, the *paps1-1 FCAγ*-OE double mutant would be expected to exhibit an additive phenotype. With an average ΔTLN of two leaves, the *paps1-1 FCAγ*-OE flowered indeed significantly earlier than the *35S::FCAγ*-OE control, but with regard to the plant age when bolting, both lines flowered at the same time (**Fig. 31**). This discrepancy reflects the leaf initiation rate defect conferred by the *paps1-1* mutation (**Fig. 18**). The identical age of *paps1-1* and *paps1-1 FCAγ*-OE when flowering underlines the virtual lack of functional *FLC* in *paps1*.

In contrast, the late flowering phenotype of *paps2-3 paps4-3* is only partially rescued by the OE of *FCAγ* (**Fig. 31**). The flowering time difference between Col-0 and the *FCAγ*-OE line comprises on average three leaves, the median ΔTLN are four leaves (**Fig. 31**). Both median and average ΔTLN between *paps2 paps4* and *paps2 paps4 FCAγ*-OE triple mutant are significantly different but comprise only two leaves, meaning that both phenotypes are not simply additive. Since the *FCAγ* transcript that is expressed from the *35S*-promoter does not contain the *FCA*-specific 3' UTR, it cannot be directly affected by altered polyadenylation due to the loss of *PAPS2/4*. Apparently, the FCAγ protein is functional but due to the lack of *PAPS2/4* activity it cannot exhibit its function completely. If the defective polyadenylation of *FCA* in *paps2/4* had caused the late flowering phenotype, the *35S::FCAγ* should have rescued the mutant phenotype completely.

It is more likely that *PAPS2/4* indeed act downstream of *FCA*. It has been suggested before that *FCAγ* downregulates *FLC* by regulating the alternative 3' end processing of the two *COOLAIR* antisense RNAs that are required for the downregulation of the *FLC* sense expression (e.g.Liu et al. 2010; chapter 1.2.3). *PAPS2/4* might for example aid this regulatory mechanism by polyadenylating *COOLAIR*. The low *FLC* sense transcript abundance observed in *paps1* could reflect a function of *PAPS1* in polyadenylating *FLC* sense mRNA. In concert with *FCA*, *PAPS2/4* might in turn be required for the timely repression of *FLC* expression.

3.1.6 The vernalization pathway is functional in *paps* mutants

Independent of the autonomous pathway, the vernalization pathway regulates the expression of *FLC* in response to cold. In autonomous pathway mutants, the vernalization response is not impaired since the two pathways do not share major components. Instead, prolonged cold leads to chromatin modifications at the *FLC* locus by a polycomb group complex (Andrés and Coupland 2012). Moreover, two *FLC* antisense RNAs termed *COOLAIR* and an intronic lncRNA termed *COLDAIR* are involved in the regulation of the vernalization response (Swiezewski et al. 2009; Heo and Sung 2011). The antisense mRNAs are implicated in both the autonomous and the vernalization pathway. To analyse whether the vernalization response is impaired in the *paps* mutant background, an active *FRI* allele from the accession San Feliu-2 (Sf-2) was crossed into *paps2-3 paps4-3* to strongly increase the *FLC* expression.

The experiment could not be performed with *paps1-1* mutants, because *paps1* plants are cold-sensitive (Kappel et al., submitted; chapter 3.2.2).

As reflected by the strong increase in flowering time, the FRI^{Sf-2} allele entailed a massive upregulation of the *FLC* expression in *paps2/4* (**Fig. 32 a**). Interestingly, despite a high degree of flowering time variation, *paps2-3 paps4-3* FRI^{Sf-2} did flower significantly later than Col-0 FRI^{Sf-2}. After a six-week period of growth at 4 °C, the flowering time of *paps2-3 paps4-3* FRI^{Sf-2} was strongly reduced (**Fig. 32 b**). However, both in the presence and absence of the FRI^{Sf-2} allele, the late flowering phenotype of *paps2-3 paps4-3* was only partially reduced by prolonged cold (**Fig. 32 b**).

An explanation for the incomplete rescue could be a defective vernalization response and thus an incomplete downregulation of *FLC*. Alternatively, the unknown components delaying flowering of *paps2/4* might not be responsive to vernalization. Therefore, it was checked whether the observed flowering time changes were reflected by altered *FLC* steady state abundances. Indeed, the prolonged cold leads to a strong reduction in the *FLC* transcript amount (**Fig. 33**). However, several discrepancies between the measured *FLC* level and the FTA were revealed. Compared to the FRI^{Col-0} containing control lines, even after six weeks of vernalization and five days of recovery under elevated ambient temperatures, the *FLC* mRNA level was not fully downregulated in the FRI^{Sf-2} lines. This was an unexpected result, considering that previously published analyses documented a complete downregulation of *FLC* expression during this time period (e.g. Sung and Amasino 2004; Angel et al. 2011). In a repetition of the experiment, even after eight weeks of vernalization and five days of recovery the *FLC* level was still significantly upregulated in the FRI^{Sf-2} lines compared to the FRI^{Col-0} lines (data not shown).

Regarding the control lines Col-0 and *paps2-3 paps4-3* after six weeks of vernalization, there is still a significant difference in the *FLC* transcript abundance, which is reflected by a ΔTLN of two leaves (**Fig. 32 b**). With an introduced FRI^{Sf-2} allele the ΔTLN between both lines is increased to four leaves. However, this flowering time difference is not reflected by significantly different *FLC* levels (**Fig. 33**).

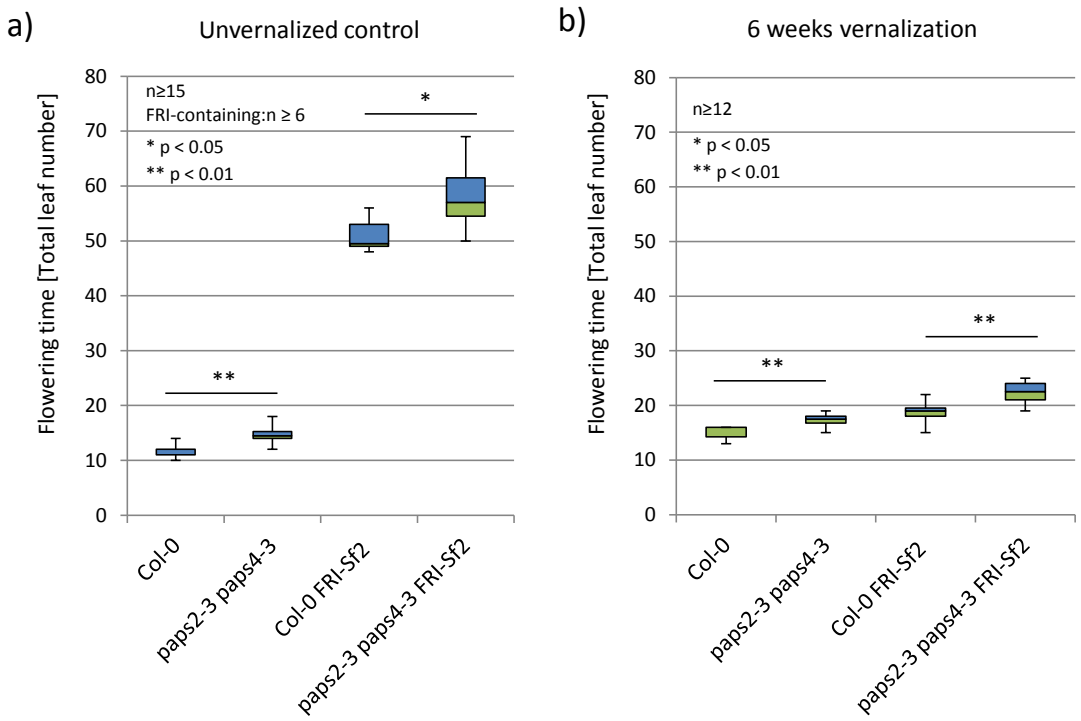

Fig. 32 The vernalization pathway is functional in *paps2-3 paps4-3*.
a) *paps2/4* containing an active *FRI*$^{Sf-2}$ allele (FRI-Sf2) flowered approximately one week later than Col-0 *FRI*$^{Sf-2}$ plants. The flowering time variation of the very late flowering plants is much larger than that of plants containing *FRI*$^{Col-0}$, while viability is reduced (explaining the low sample number). b) After a six-week long growth period at 4 °C (vernalization), all genotypes flower early. However, the moderate delay of flowering of *paps2-3 paps4-3* and of *paps2-3 paps4-3 FRI*$^{Sf-2}$ could not be overcome by cold. The flowering time analysis was performed under LD conditions; the vernalization was performed under SD conditions. p-values are Bonferroni-corrected.

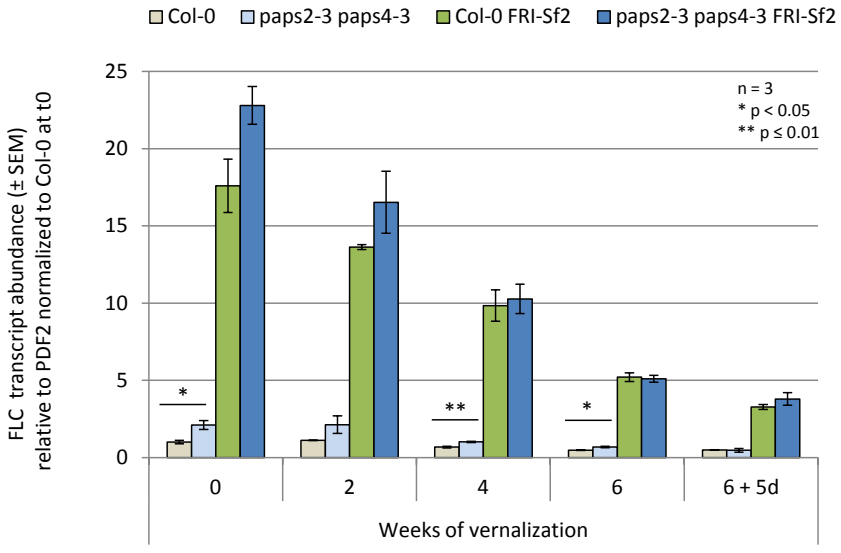

Fig. 33 Regarding the *FLC* mRNA abundance, *paps2 paps4* mutants respond to vernalization.
RNA was extracted from seedlings grown for 10 DAG (22 °C, LD, 0 weeks of vernalization), directly after the indicated period of vernalization (4 °C, SD) or after a five-day recovery phase (22 °C, LD). The *FLC* mRNA abundance is strongly increased in a *FRI*$^{Sf-2}$ (FRI-Sf2) background and is reduced during vernalization. Only in the *FRI*$^{Col-0}$ background, *FLC* levels are significantly enriched in *paps2 paps4*. This enrichment is not overcome by vernalization. When plants were set back to 22 °C for five days after vernalization, the downregulation of *FLC* is still not complete compared to Col-0 (6 + 5d).

This result implies that flowering time inhibitors other than *FLC* exhibit a defective regulation in *paps2-3 paps4-3*. This view becomes even more likely considering that the six-fold increased *FLC* transcript amount in Col-0 FRI^{Sf-2} compared to Col-0 is transduced into a similar ΔTLN of four leaves when bolting. Apparently, at such low levels even significant variations in the total amount of *FLC* transcript do not influence flowering times to a high extent anymore.

As observed before, unusual *FLC* levels can result from defective processing of the abovementioned *FLC* antisense RNAs (Liu et al. 2010). Thus, in parallel to the *FLC* measurements, the *FLC* antisense (AS) RNA amounts were determined (**Fig. 34**). Before vernalization, the *COOLAIR* RNA abundance was very low in all genotypes. Regarding the normalized Ct-values obtained by qPCR, the expression of both AS RNAs was two orders of magnitude lower than the expression of the *FLC* sense transcript. These values are consistent with previously published data (Duc et al. 2013; Rataj and Simpson 2014). Interestingly, the expression of *FLC* AS class II was significantly increased in both FRI^{Sf-2} containing lines compared to the FRI^{Col} lines (**Fig. 34 b,** not marked in the figure).

As described before, the expression of *FLC* AS class I was strongly induced in all backgrounds upon cold exposure (Swiezewski et al. 2009). However, in contrast to the previous findings, the *COOLAIR* expression did not decrease after two weeks in the FRI^{Sf-2} lines, but remained at high levels during the entire cold period. After six weeks of cold, the abundance of *FLC* AS class I was significantly higher in *paps2-3 paps4-3* compared to Col-0 (**Fig. 34 a**). This observation could be explained by a decelerated decrease of *FLC* AS class I expression over time. When returned to 22 °C after six weeks of cold, the *FLC* AS class I was downregulated in all genotypes.

In contrast, the *COOLAIR* class II abundance was downregulated over time in the cold in all backgrounds. Analysing the *FLC* AS class II in *paps2/4* compared to Col-0, there were only very minor and sometimes contradictory changes in the expression behaviour. These subtle differences are probably due to the generally low *COOLAIR* transcript abundance. Strikingly, when the plants were returned to warm ambient temperatures, the *FLC* AS class II abundance reversed in *paps2/4* compared to Col-0. Regardless of the *FRI* allele, the transcript level was significantly increased in *paps2/4*.

To test whether the oligonucleotides from Hornyik et al. (2010) that were used for this experiment indeed only amplified the desired fragments, the melting curves determined by the LC480 were analysed. While there was only one PCR product amplified in the *COOLAIR* class I samples, two peaks appeared in *FLC* AS class II PCR samples that were harvested in the cold. These qPCR products were analysed on an agarose gel (**Fig. 35**).

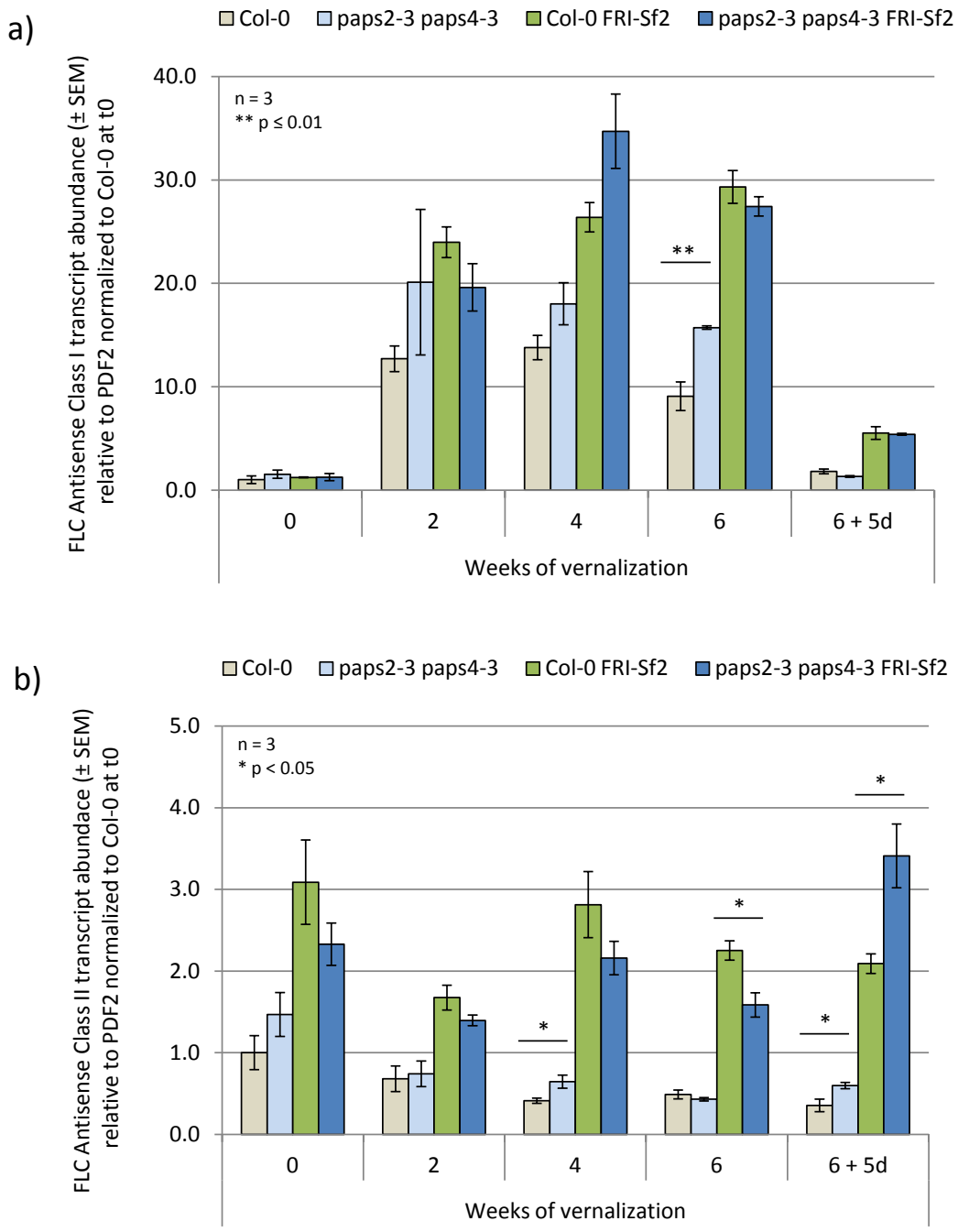

Fig. 34 Transcript abundances of the *FLC* antisense classes I and II behave oppositely during vernalization.
RNA was extracted from seedlings grown for 10 DAG (22 °C, LD, 0 weeks of vernalization), directly after the indicated period of vernalization (4 °C, SD) or after a five-day recovery phase (22 °C, LD). a) The *FLC* antisense class I mRNA abundance is increased during vernalization. Only after six weeks of vernalization a significant increase in expression can be observed in *paps2 paps4 FRI*$^{Col-0}$ seedlings compared to Col-0. b) In a *FRI*$^{Sf-2}$ background, the *FLC* antisense class II mRNA content is increased. The expression level decreases over time during the period of cold. After returning seedlings to 22 °C, the abundance is significantly increased in *paps2 paps4* mutant lines.

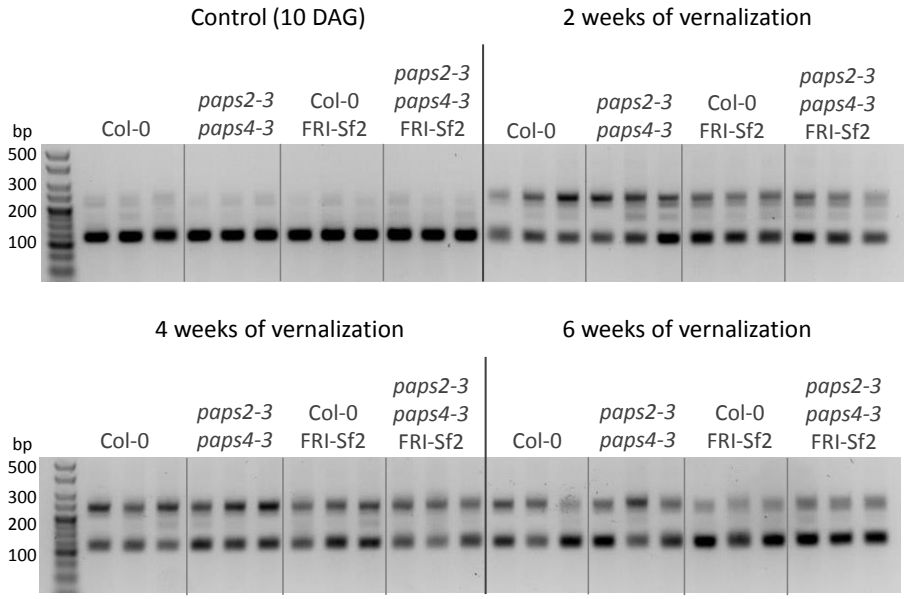

Fig. 35 Upon vernalization, a second splice form of *FLC* antisense class II appears.
A quantitative real time-PCR was performed for 40 cycles and PCR products were separated on an agarose gel. RNA was extracted from seedlings grown on ½ MS medium at ten DAG (22 °C, LD) or after the indicated period of vernalization (4 °C, SD).

Indeed, upon cold exposure, a larger PCR product appears. Alternative splicing of *FLC* AS class II had been observed by Hornyik et al. (2010) and the documented product sizes that were gained with the primer pair used are consistent with the PCR products obtained in this experiment. Samples that had been returned to 22 °C for five days predominantly expressed the shorter splice form (data not shown). To get a higher resolution and to see possible differences in abundance between *paps2/4* and the wild type more in detail, *COOLAIR* class II was amplified with a reduced cycle number by semi-qPCR. However, due to the very low expression levels of *COOLAIR* class II, the attempt failed. There was hardly any amplification and the bands in the agarose gels were too thin to discriminate between wild type and mutant (data not shown).

Thus, it can be concluded that the overall *COOLAIR* class II transcript abundance is increased in the *paps2/4* mutant samples compared to Col-0 upon return to warm ambient temperatures, but no conclusion can be drawn with regard to alternative splicing patterns. However, no significant difference in *COOLAIR* transcript abundance between mutant and wild type could be observed at time point zero, which corresponds to ten day-old-seedlings grown under standard LD conditions (**Fig. 34**). This might imply that *COOLAIR* expression is not defective in *paps2/4*. Similarly, the very low *COOLAIR* expression levels complicate the detection of genotype-specific abundance differences, especially regarding the alternative splicing patterns. It can furthermore be stated that the vernalization pathway is functional in *paps2/4* double mutants. Both the upregulation of *FLC* expression by active *FRI* and the drastic drop of *FLC* transcript levels upon prolonged cold exposure can be observed despite the lack of *PAPS2* and *PAPS4* function.

3.1.7 *FLC* and *COOLAIR* poly(A) tail lengths are not altered in *paps2 paps4*

An obvious effect to be expected in a poly(A) polymerase mutant are changes in poly(A) tail (PAT) lengths of mRNAs, which would be most certainly shortenings. As described in the introductory chapter 1.1.4, altered tail lengths might cause defects in mRNA stability, translatability or nuclear export. To address the question whether altered transcript abundance levels in *paps* mutants might be due to defective polyadenylation, a fractionation of RNA isolated from Col-0 and *paps2-3 paps4-3* according to PAT lengths was performed in a small-scale approach. The mRNA fractionation method used is explained in detail in chapter 3.4.2. It had previously been applied in a large-scale procedure to detect global PAT changes in *paps1-1* and was validated in detail by a bioinformatics analysis (fractionation performed by Gerda Trost; Kappel et al. submitted). Since the strongest increase in *FLC* abundance in *paps2/4* had been observed at nine DAG (**Fig. 24 a**), mutant and wild type plants were grown for nine days in LD before the harvesting samples for RNA extraction. Total RNA of three biological replicates per genotype was subsequently separated into pools of mRNAs with long tails (> 50 A; termed “long fraction”) and with short tails (> oligo A but < 50 A; termed “short fraction”). Transcript abundances of *FLC* and *COOLAIR* contained in both fractions were tested in a subsequent qPCR analysis. Since this method does not allow normalization of a given transcript amount to a housekeeping gene, already small technical errors are reflected directly at the transcript abundance level. Thus, a high standard error was anticipated. However, PAT changes caused by the loss of *PAPS* activity should still be detectable (see chapter 3.4.2).

Regarding the *FLC* sense transcript, both mutant and wild type contained a similarly high amount of long-tailed *FLC* mRNA (**Fig. 36**). This was unexpected since previous sequencing and RACE-PCR analyses had revealed rather short A-tails in Col-0 (communication with Szymon Swiezewski, unpublished). Moreover, *paps2/4* had been expected to exhibit a higher proportion of long-tailed *FLC* than the wild type. The finding suggests that the higher *FLC* transcript level detected in *paps2/4* compared to Col-0 originates from increased *FLC* expression rather than from altered transcript stability. In contrast, *paps1-1* was expected to predominantly contain short-tailed *FLC* mRNAs compared to the respective wild type. However, looking at the global fractionation data set, the mutant did not exhibit significant changes in the *FLC* PAT length compared to the wild type L*er* at ten DAG (data not shown).

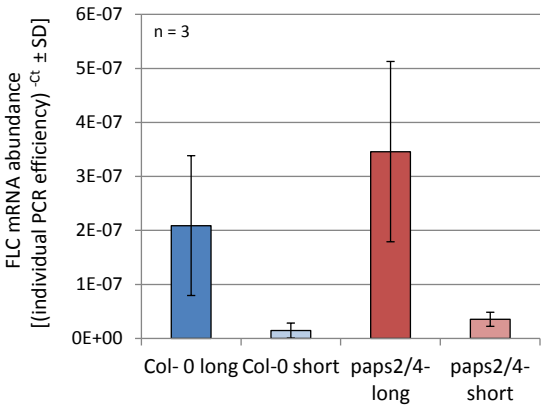

Fig. 36 *FLC* mRNAs have long poly(A) tails in both wild type and *paps2 paps4*.
Total RNA of Col-0 and *paps2-3 paps4-3* (paps2/4) of 9-day-old seedlings was separated into pools of mRNAs with long tails (> 50 A; long) and with short tails (> oligo A but < 50 A; short).

Next, the PAT length of both *COOLAIR* classes was analysed. As expected, the *COOLAIR* transcript abundance was very low. The *FLC* AS class I mRNA was mainly found in the long fraction (**Fig. 37 a**). Regarding the *FLC* AS class II, the PAT was balanced between short and long tails in Col-0, while there seemed to be a trend towards longer PATs in *paps2/4* (**Fig. 37 b**). This would be in consistence with a slight but insignificant trend towards a higher *COOLAIR* class II level in the mutant at ten DAG (**Fig. 34**). However, the finding from the fractionation analysis has to be treated with caution since the analysis of spike-in control RNAs revealed that the total amount of input RNA must have been higher in the *paps2/4* samples (chapter 3.4.2). Moreover, the very low transcript abundance and the presence of more than one splice form might additionally obscure subtle changes in PAT length.

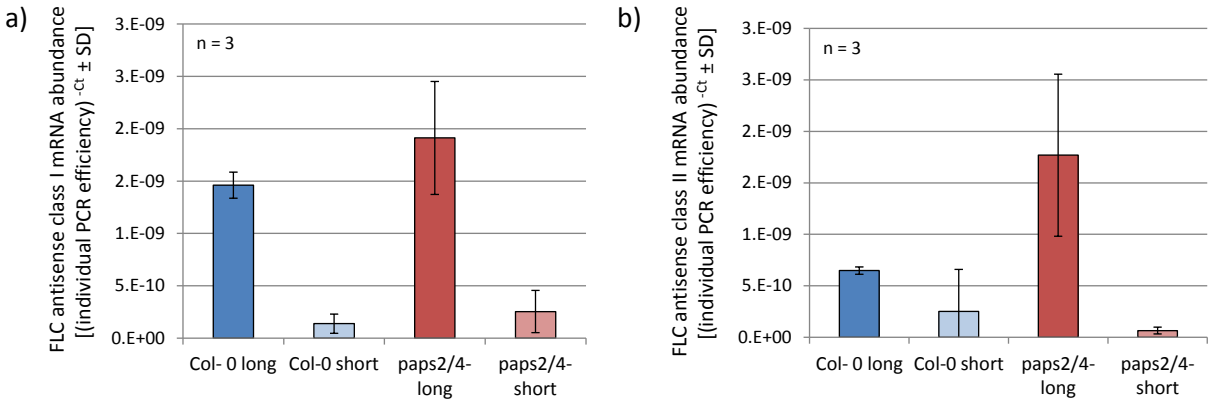

Fig. 37 Poly(A) tail lengths of *FLC antisense* mRNAs do not differ between wild type and *paps2 paps4*.
Total RNA of Col-0 and *paps2-3 paps4-3* (paps2/4) of 9-day-old seedlings was separated into pools of mRNAs with long tails (> 50 A; long) and with short tails (> oligo A but < 50 A; short).

3.2 Poly(A) polymerases mediate the response to distinct stress conditions in *Arabidopsis*

3.2.1 An *AtPAPS* expression analysis indicates functions in specific stress response pathways

To identify conditions under which *PAPS2* or *PAPS4* might be up- or downregulated and thereby define possible *PAPS* specificities, an expression analysis was performed with the Genevestigator tool "Pertubations" (**Fig. 38, Fig. 39**). At first sight it is noticeable that both *PAPS2* and *PAPS4* expression levels change differentially under stress conditions. Among the 25 most-upregulating conditions for *PAPS2*, seven studies were related to treatments with the bacterium *Pseudomonas syringae* and four studies involved a treatment with the fungus *Golovinomyces cichoracearum* (**Fig. 38**). Both species are typical plant pathogens used to test plant reactions to biotic stress. Furthermore, nine studies are related to the bacterial elicitor flg22, a short peptide derived from flagellin which triggers plant immune responses. The expression of either *PAPS1* or *PAPS4* was also slightly upregulated under certain conditions. However, the upregulation of *PAPS2* can be observed consistently and seems to be stronger.

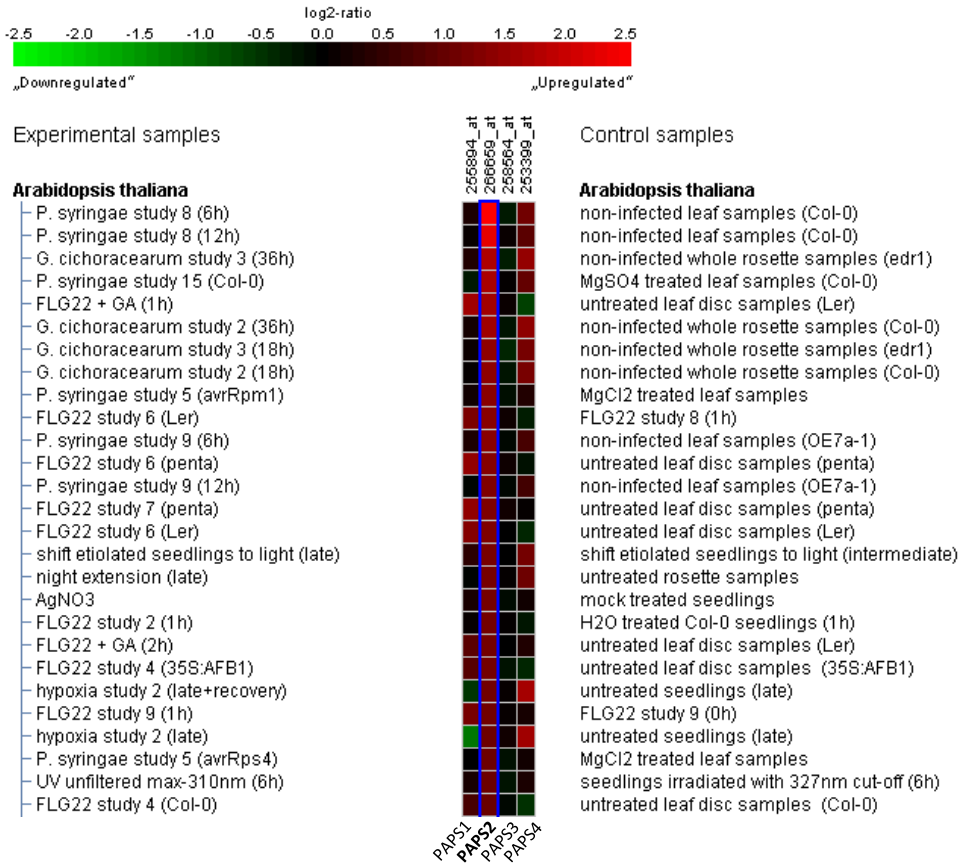

Fig. 38 *PAPS2* expression is upregulated mainly under biotic stress conditions.
Shown are the 25 most up-regulating conditions for *PAPS2* (*At2g25850*) in comparison to the three other canonical *AtPAPSs*. The Condition Search Tool „Pertubations" from Genevestigator was used for the analysis (screen shot from 2011, modified).

Regarding the 30 most-upregulating conditions for *PAPS4*, one third of the studies was related to hypoxia or anoxia treatments (**Fig. 39**). Another third of the studies involved biotic stress treatments similar to the *PAPS2*-upregulating conditions. Other treatments triggering *PAPS4* expression involved drought stress or different light conditions. Under all listed conditions, the *PAPS1* expression remained unchanged or was even slightly downregulated.

These observations indicated that both *PAPS2* and *PAPS4* might act redundantly to control the response to biotic stress and that specifically *PAPS4* might be required to exhibit an appropriate response to abiotic stresses.

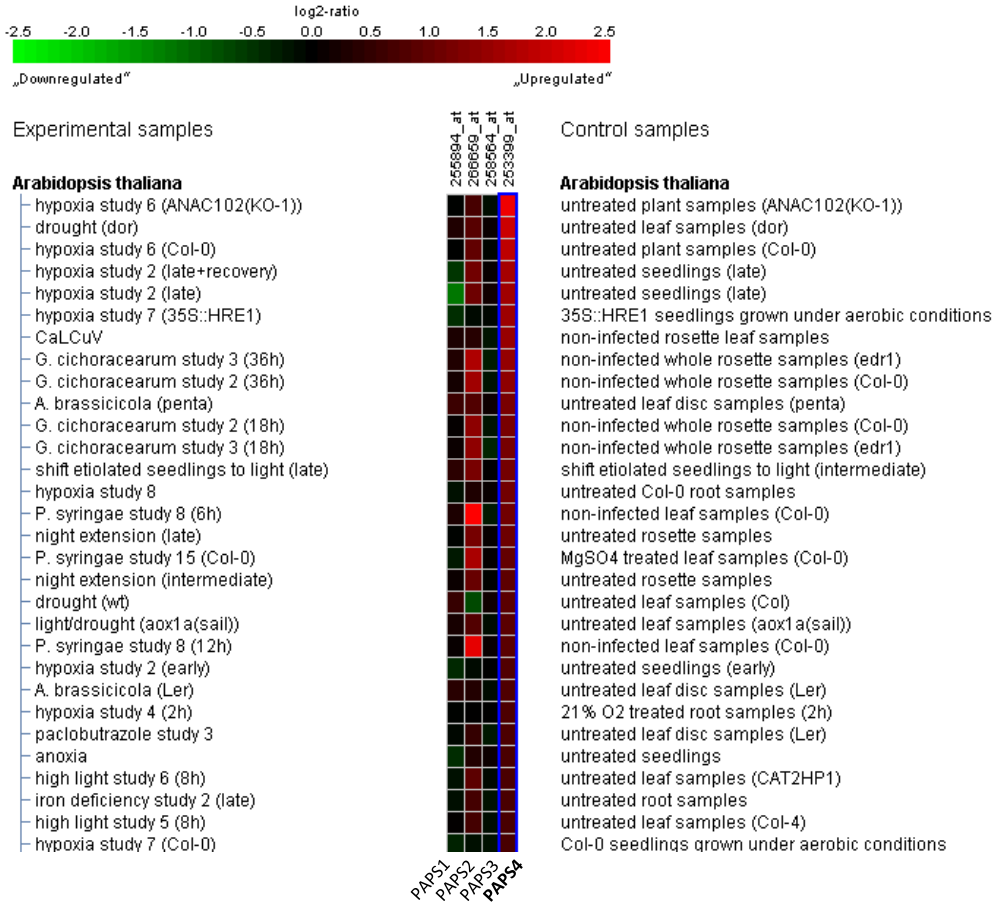

Fig. 39 *PAPS4* expression is upregulated under abiotic stress conditions, specifically under hypoxia.
Shown are the 30 most up-regulating conditions for *PAPS4* (*At4g32850*) in comparison to the three other canonical *AtPAPSs*. The Condition Search Tool „Pertubations" from Genevestigator was used for the analysis (screen shot from 2011, modified).

3.2.2 Search for stress-induced phenotypes of *paps* mutants

Based on the Genevestigator analysis and on a transcriptome analysis performed with *paps1-1* RNA (not shown), diverse stress experiments were performed with *paps1* and with *paps2* and *paps4* single and double mutants. First, the biotic stress response of *paps* mutants was tested by the research group of Cyril Zipfel at the John Innes Centre (Norwich). Plant reactions to treatments with flg22 or

with the biotrophic oomycete *Hyaloperonospora arabidopsidis* were examined. An impaired resistance of the *paps2/4* mutant was expected. Instead, while *paps1-1* proved to be hyper-resistant to the fungus, *paps2-3 paps4-3* showed no differential response to the wild type (Trost et al. 2014). While the experimental outcome of repeated flg22 treatments was not homogeneous (data not shown), it was obvious that *paps2/4* mutants were not significantly more susceptible to biotic stress than Col-0.

Since oxygen-stress related studies were predominantly found to upregulate *PAPS4* expression, oxygen-depletion stress was tested in various set ups in collaboration with the research group of Joost van Dongen (Max Planck Institute for Molecular Plant Physiology, Potsdam Golm). Plants were submerged for up to 72 h, treated with complete anoxia for up to 8 h and grown at low oxygen conditions for six weeks in a long-term experiment.

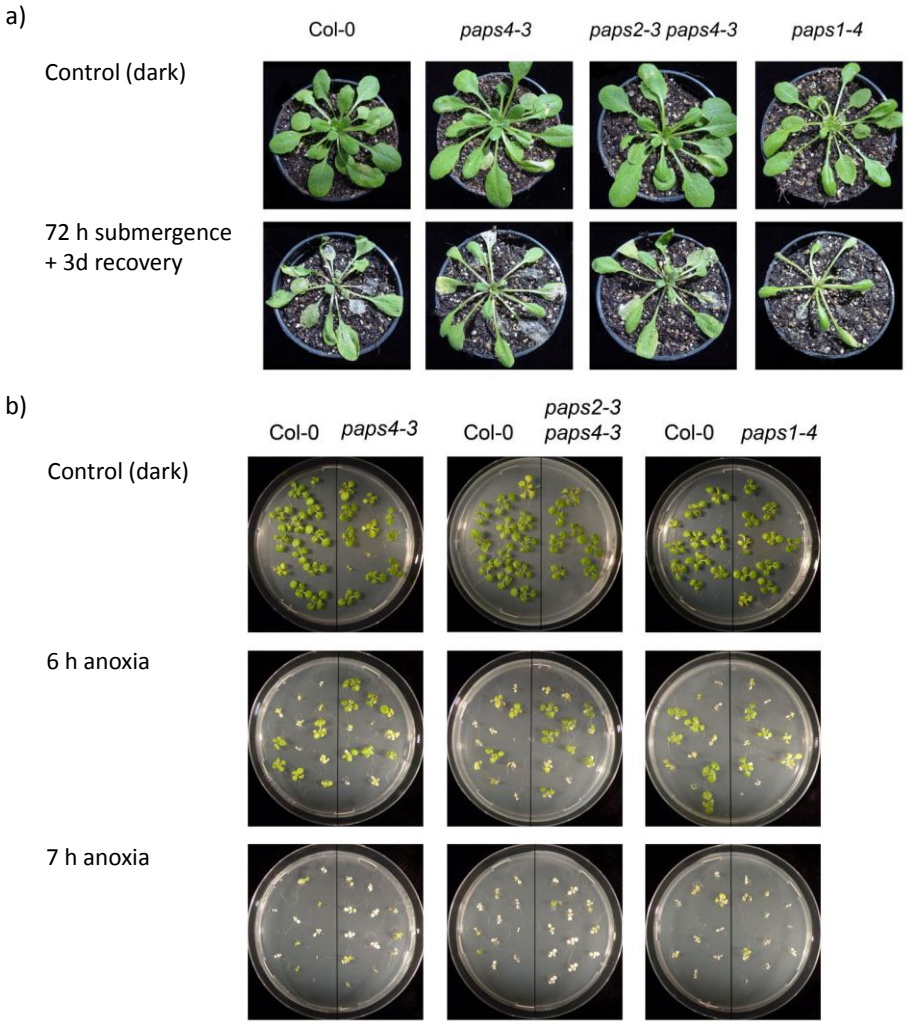

Fig. 40 Short-term oxygen depletion does not lead to a differential stress response in *paps* mutants.
a) 28-day-old plants were kept in the dark (control) or were submerged in the dark for 72 h. Darkness prevented oxygen production by photosynthesis. Photos were taken after three days of recovery under standard conditions in the glass house. b) Seven-day-old seedlings grown on ½ MS medium under standard conditions were transferred to complete anoxia (gas treatment with nitrogen) in the dark for the indicated period of time. Photos were taken after five days of recovery under standard growth conditions.

First, four-week-old plants were submerged for several days in the dark to avoid plant oxygen production. Interestingly, when the submergence was terminated after 60 h, the plants recovered almost completely (data not shown). When the plants had been submerged for three days, plants were more affected. However, among all genotypes, there were plants that recovered quickly and plants that showed bleaching or turgor loss (**Fig. 40 a**). To detect more subtle defects, the fresh weight and dry weight could have been determined after a short recovery phase.

Next, seven-day-old seedlings grown on MS plates were stressed with complete anoxia which was generated by a gas treatment with nitrogen for several hours. Subsequently, the plates were transferred back to standard growth conditions for five days of recovery. Plants that sustained 5 h of anoxia were relatively mildly affected (not shown). Longer anoxia treatments of 6–7 h successively provoked stronger lesions that resulted in growth retardation, bleaching and death of seedlings (**Fig. 40 b**). While *paps2 paps4* looked slightly better than Col-0 after five days of recovery, this observation was not homogeneous throughout the four replicate plates. Moreover, as seen on the control plates, the germination rate of the four genotypes was not homogeneous. A fresh weight determination could have helped to interpret the findings. The anoxia treatment of 8 h duration was too strong for all genotypes and led to a complete growth arrest and bleaching (not shown).

After that, a long-term hypoxia treatment was set up with 21-day-old plants in the glass house. To create a low-oxygen atmosphere, the pots were kept in plexiglass boxes that were sealed and aerated with 400 ppm of CO_2 and 21 % or 8 % of oxygen in N_2 for four weeks (**Fig. 41 e, f**).

Since Col-0 does not show a phenotype down to an oxygen concentration of 10 % (communication with Joost van Dongen), a concentration below that threshold was chosen to provoke a phenotype in the wild type and to be able to see both a putative hyper-sensitivity or a hyper-resistance of *paps* mutants. Next to the control plants in the boxes, additional control plants were grown under standard conditions outside the boxes. The plants and boxes were observed regularly. If the gas pressure was set too low, the humidity in the boxes became very high (**Fig. 41 f**). Moreover, fungi and fungus gnats began to develop in all boxes after three weeks of treatment. After four weeks of hypoxia, the boxes were opened and the leaf diameter, the fresh weight and the dry weight (FW and DW) of all plants were determined.

The leaf diameter of the hypoxia-treated plants was normalized to either the non-treated control (NTC) or the plants grown at 21 % O_2 in the boxes. Both normalized leaf diameters did not reveal significant growth differences between mutants and Col-0 (Table **6**). Except for *paps1-1*, the plants grown in the boxes generally showed a larger diameter than the NTC plants, which was probably caused by light depletion. Probably due to the increased temperatures and the high humidity, *paps1-1* plants exhibited a strong diameter decrease in the boxes compared to the control plants grown outside.

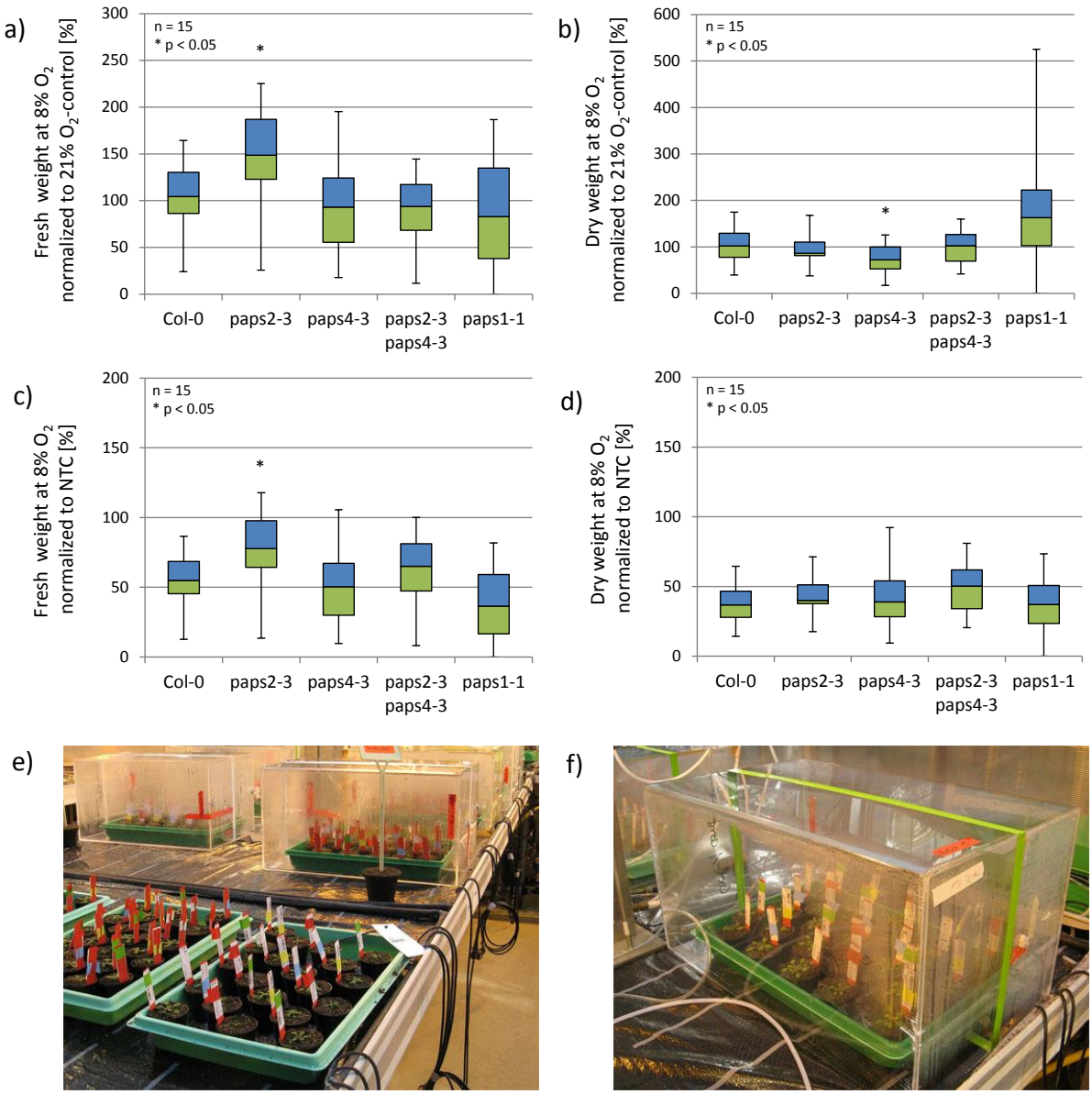

Fig. 41 Hypoxia-treated *paps* mutants and Col-0 exhibit similar weight changes.
21-day old plants were transferred to plexiglass boxes treated with 21 % O_2 or 8 % O_2 for 4 weeks or were kept under standard conditions as non-treated control (NTC) plants. a, b) Fresh and dry weight of hypoxia-treated plants normalized to weight of plants grown in 21 %-control boxes. c, d) Fresh and dry weight of hypoxia-treated plants normalized to weight of NTC plants. e, f) Setup of control plants and plexiglass boxes. P-values indicate significant difference to Col-0, but do not withstand Bonferroni-correction.

Usually, temperatures between 22 °C and 23 °C were measured inside of the boxes, but the temperature increased up to 26 °C during sunny days. The flowering time was determined during the regular examination of all pots. It was similar inside and outside of the boxes (data not shown).

The *paps* mutant phenotypes were still visible in the boxes. Both FW and DW were generally reduced under oxygen stress (Table **6, Fig. 41**). Regarding the normalized weight data, *paps2-3* grown at 8 % O_2 showed a significantly increased FW compared to Col-0. This indicates an increased resistance to hypoxia. However, the difference is subtle and the significance does not withstand Bonferroni-correction. Normalized to the plants grown in boxes at 21 % O_2, the *paps4-3* mutant exhibits a

reduced DW compared to Col-0, but again the difference is not significant applying Bonferroni-correction. In summary, apart from subtle growth variations there was no significant difference between *paps* mutants and wild type in their response to oxygen depletion.

Table 6 Phenotype of *paps* mutants under hypoxia conditions.
Diameter, fresh and dry weight from seven-week-old plants grown in the glasshouse under LD conditions were determined. Plants grown in boxes under hypoxia (8 % O_2) from 21 DAG until the time point of measuring (49 DAG) were compared to plants grown in boxes under standard conditions (21 % O_2) or to a non-treated control (NTC, 49 DAG). SD, standard deviation; *n* = 15.

		Diameter [cm]			Fresh weight [g]			Dry weight [g]		
		Average	Median	SD	Average	Median	SD	Average	Median	SD
Col-0	NTC	12.2	12.5	1.1	4.7	4.7	0.6	0.73	0.73	0.10
	21 % O_2	13.5	13.5	2.6	2.5	2.5	1.6	0.26	0.26	0.10
	8 % O_2	**12.4**	**12.2**	**2.2**	**2.6**	**2.6**	**1.0**	**0.28**	**0.27**	**0.10**
paps2-3	NTC	11.7	12.2	1.2	3.7	3.8	0.6	0.57	0.57	0.08
	21 % O_2	13.6	13.6	2.4	2.0	1.9	1.1	0.26	0.25	0.07
	8 % O_2	**12.6**	**12.5**	**2.4**	**2.8**	**2.9**	**1.1**	**0.25**	**0.23**	**0.09**
paps4-3	NTC	11.6	12.2	1.4	4.2	4.0	0.8	0.51	0.51	0.14
	21 % O_2	13.1	14.1	3.3	2.3	2.3	1.5	0.28	0.30	0.09
	8 % O_2	**12.1**	**11.6**	**2.9**	**2.1**	**2.1**	**1.5**	**0.20**	**0.20**	**0.10**
paps2-3 paps4-3	NTC	12.4	12.6	0.8	3.7	3.6	0.7	0.42	0.40	0.08
	21 % O_2	13.3	14.0	2.1	2.6	2.6	1.0	0.21	0.21	0.06
	8 % O_2	**12.3**	**12.6**	**1.9**	**2.2**	**2.4**	**1.0**	**0.21**	**0.21**	**0.08**
paps1-1	NTC	9.3	9.7	1.4	3.3	3.5	0.8	0.54	0.59	0.15
	21 % O_2	7.7	7.5	1.9	1.4	1.4	0.8	0.12	0.13	0.06
	8 % O_2	**8.6**	**8.1**	**2.4**	**1.4**	**1.2**	**0.9**	**0.21**	**0.20**	**0.15**

Since drought stress appeared as a condition under which *PAPS4* was upregulated in the Genevestigator analysis (**Fig. 39**), the *paps* mutant responses to drought and osmotic stress conditions were tested. Plants were watered with exactly defined volumes per pot for 14 DAG and were subsequently kept under complete drought for 14 further days. No difference in the response to drought was noticed between Col-0 and *paps2* and *paps4* single and double mutants (**Fig. 42 a**). Also after re-watering, the plants did not exhibit differential phenotypes (not shown).

The germination rate and FW of seedlings grown on different concentrations of mannitol, which provokes osmotic stress, were determined. To avoid a bias regarding the mannitol concentration in the MS plates, the plates were kept under LED lights which do no emit heat leading to water evaporation from the media. Since LED lights were only available without temperature control, in this experiment the *paps1-4* allele rather than the heat-sensitive *paps1-1* mutant was used. While no difference between *paps2*, *paps4*, *paps2 paps4* and Col-0 could be noticed, the *paps1-4* mutant turned out to be more resistant to up to 400 mM of mannitol (**Fig. 42 b**). Both germination rate (not shown) and FW were significantly increased in a mutant with reduced *PAPS1* activity at eleven DAG, indicating a novel, specific function for *PAPS1*.

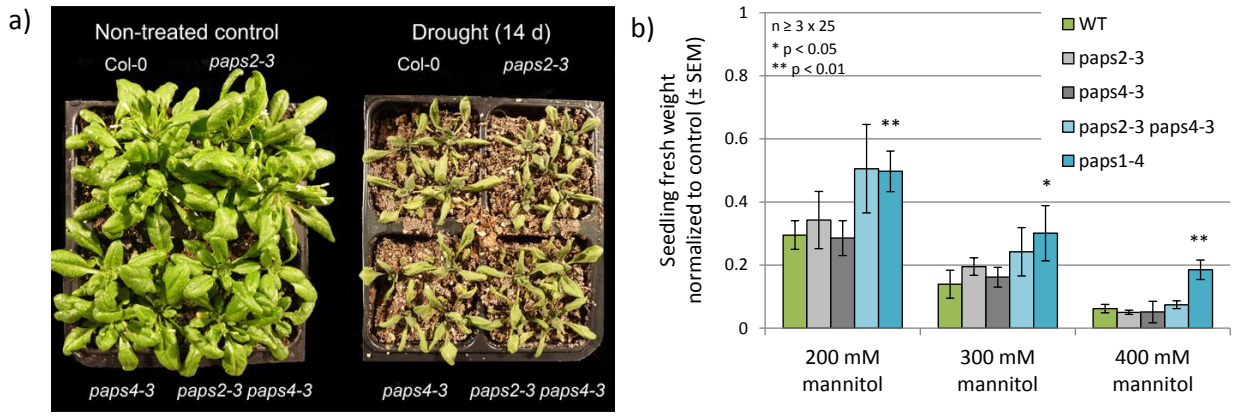

Fig. 42 The *paps* mutant phenotype under drought and osmotic stress.
PAPS1 regulates the response to osmotic stress, while *PAPS2* and *PAPS4* are not involved in the regulation of drought or osmotic stress. a) *paps* mutants and Col-0 were irrigated with defined volumes of water. At 14 DAG, the plants were kept under drought, while control plants were continuously watered (*n* = 3 pots per condition). After 14 days of drought no difference between wild type (WT) and mutants was observed. b) Seedlings were germinated on ½ MS medium containing the indicated concentrations of mannitol. At eleven DAG the average FW of seedlings was determined. Relative to the non-treated control, *paps1-4* shows a significantly higher FW compared to the wild type. P-values indicate significant difference to Col-0 and are Bonferroni-corrected.

Finally, the *paps* mutant response to salt stress was addressed by determining the germination rate on MS medium containing different concentrations of NaCl. However, in three experimental replicates the results varied vastly and no clear phenotype could be observed (not shown).

3.2.3 *PAPS1* regulates the response to cold stress

To gain insights into the functional specificity of *PAPS1*, a MASTA analysis was performed with the data set of the aforementioned global sequencing analysis of the *paps1-1* long and short mRNA fractions (see chapter 3.1.7; Trost 2014, PhD thesis). Using the MASTA tool (Reina-Pinto et al. 2010), 400 genes with the strongest fold-changes of PAT length in *paps1-1* were compared with 600 published microarray data sets. Interestingly, genes that exhibit altered expression under cold conditions showed the strongest overlay, indicating that *PAPS1* might be involved in the regulation of the response to cold stress. In comparison to Col-0, *paps1-1* and *paps2-3 paps4*-3 were grown for six days at 22 °C (LD) and were then transferred to 4 °C (SD) for four weeks. After six days of recovery under ambient temperatures, the FW was determined. Seedlings grown for twelve days at 22 °C and thus lacking the cold period served as a control, since six-week-old plants grown at LD at 22 °C would have developed strong developmental differences. In particular the early flowering *paps1-1* mutant would have shown signs of senescence already. Indeed, *paps1-1* showed impaired growth under cold-stress (**Fig. 43 a, b**). While both Col-0 and *paps2/*4 still grew and gained weight in the cold, which is consistent with observations made during the vernalization experiment, *paps1* growth almost arrested and the seedlings exhibited bleaching. An essential role of *PAPS1* in the response to cold stress could thus be confirmed.

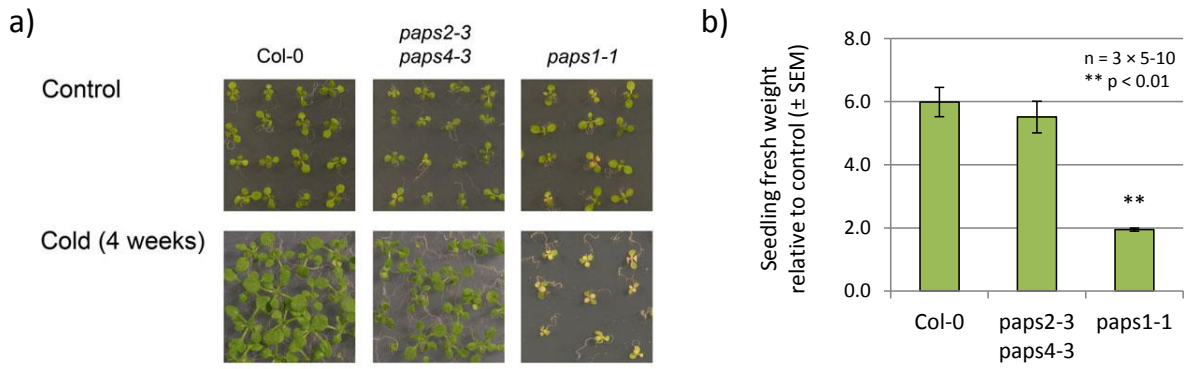

Fig. 43 *paps1-1* but not *paps2-3 paps4-3* shows an impaired response to cold.
Seedlings were grown for six days (LD, 22 °C), then transferred to cold conditions for four weeks (4 °C, SD) and returned to 22 °C for six days of recovery. Control seedlings (LD, 22 °C) were sown out during the ongoing cold treatment and were harvested at twelve DAG simultaneously with the cold-treated plants, when images were taken (a) and the fresh weight was determined (b). While *paps1-1* development arrested during the cold-treatment and the seedlings exhibited bleaching, *paps2-3 paps4-3* grew like Col-0. P-values indicate significant difference to Col-0 and are Bonferroni-corrected.

3.2.4 *PAPS1* and *PAPS2/4* regulate the response to oxidative stress in different pathways

Another MASTA comparison with the *paps1* mRNA fractionation data set was performed using 400 genes that exhibited the most significant changes in *paps1-1* (i.e. the lowest p-values in a comparison of the short-tail and long-tail fractions of mutant and wild type) (see chapter 3.2.3; Trost 2014, PhD thesis). The analysis revealed a high overlap with several experiments, in which the cellular redox state was modulated. Genes showing differential PAT lengths in *paps1-1* overlapped significantly with plants overexpressing a thylakoid-localized ascorbate peroxidase (tAPX), an enzymes that detoxifies H_2O_2. As a *35S::tAPX* line had previously been shown to be resistant to oxidative stress provoked by a treatment with paraquat (Murgia et al. 2004), a similar ROS-resistance phenotype could be expected for *paps1* mutants. Moreover, a set of genes with altered PAT length in *paps1-1* overlapped with genes that were deregulated in the *CPSF30* mutant *oxt6* which is resistant to both oxidative stress in the cytoplasm and the chloroplast (Zhang et al. 2008; Kappel et al. submitted).

In a preliminary test starting at seven DAG, plants were sprayed with 100 mM H_2O_2 every other day. A similar degree of leaf necrosis formation was observed in Col-0, *paps1-1* and *paps2-3 paps4-3* (not shown). However, with regard to the irregular shape and size of *paps1-1* leaves, the necrosis formation was difficult to quantify.

Zhang et al. (2008) provoked cytoplasmic ROS stress by a combination of the chemicals 3-amino-1, 2, 4-triazole (AT) and buthionine-S, R-sulfoximide (BSO). AT inhibits catalases and thus indirectly increases intracellular H_2O_2 levels, which entails increased glutathione levels (May and Leaver 1993). BSO in turn inhibits the glutathione synthesis, which in combination with AT, provokes strong cytoplasmic ROS stress (Griffith and Meister 1979). Moreover, the group tested the plant response to oxidative stress in the chloroplast using methyl viologen (MV) which is also known as the herbicide

paraquat. MV accepts electrons from the photosystem I. The resulting paraquat radical reduces O_2 molecules to ROS and the free paraquat cation can accept new electrons. This circuit continues until chloroplasts are completely damaged. In the sun, paraquat-treated plants will bleach and dry out.

First, the development of *paps* mutants was tested on MS media containing BSO and AT concentrations as used by Zhang et al. (2008). In addition, lower concentrations were tested. The *oxt6* mutant served as a positive control. At standard growth conditions (on soil, 22 °C, LD) the reduced size of *oxt6* that had been described before was confirmed (**Fig. 44 a**). At seven DAG the seedlings were transferred from standard MS plates to stress media. After 14 days of treatment, root length and FW were determined and indeed Col-0 was more affected by the treatment than *oxt6* (**Fig. 44 b, c**). Moreover, as expected, *paps1-1* clearly exhibited an enhanced resistance to cytoplasmic ROS stress. At lower chemical concentrations, the phenotype is more pronounced. In contrast, the weight of *paps2-3 paps4-3* is as impaired as that of the wild type.

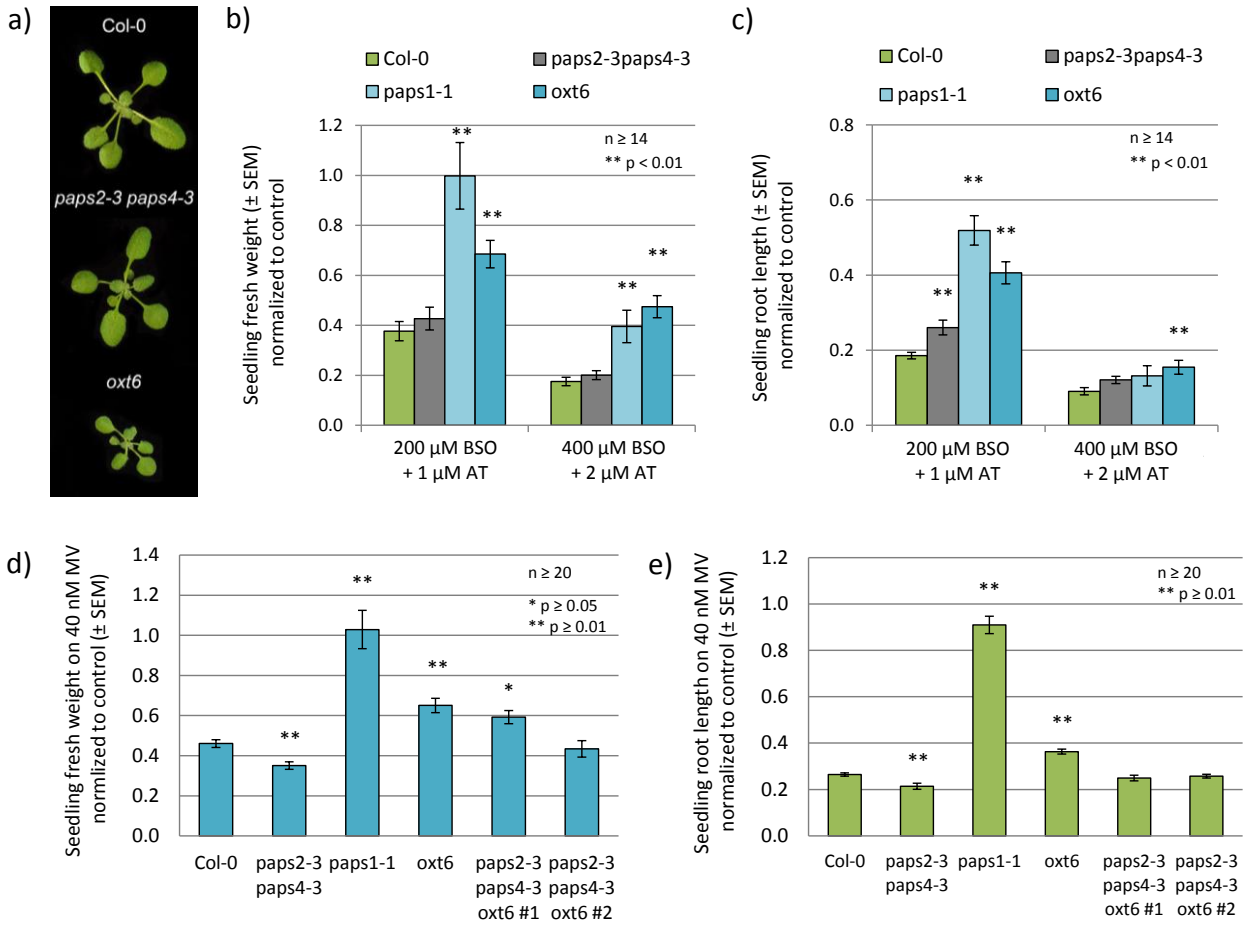

Fig. 44 *PAPS1* and *PAPS2/PAPS4* regulate the response to oxidative stress in different pathways.
a) Phenotype of 20-day-old plants grown under standard growth conditions (LD, 22 °C). b)–e) Seven-day-old seedlings were transferred to ½ MS containing sucrose and BSO/AT (b, c) or MV (d, e). Fresh weight (b, d) and root lengths (c, e) were determined after 14 days of treatment. *paps1-1* is more resistant to cytoplasmic and chloroplast stress, similar to *oxt6*. *paps2-3 paps4-3* is less resistant to chloroplast ROS stress than Col-0. Two *paps2-3 paps4-3 oxt6* triple mutant lines have an intermediate phenotype between *paps2 paps4* and *oxt6* on chloroplast ROS stress. P-values are Bonferroni-corrected.

The *paps2/4* double mutant exhibits slightly longer roots than the wild type, but this phenotype is very subtle and is abolished at high BSO and AT concentrations (**Fig. 44 c**).

Next, a comparative growth analysis was performed on 40 nM MV. Preliminary studies revealed that both 80 and 100 nM of MV impaired plant growth too severely to see differential stress responses. As observed for the cytosolic ROS stress, *paps1-1* and *oxt6* were more resistant than Col-0, with *paps1-1* being even stronger than *oxt6* (**Fig. 44 d, e**). In contrast, with regard to both FW and root length, the *paps2-3 paps4-3* growth was impaired significantly more strongly than the wild type development. These results indicate that *PAPS1* and *PAPS2/4* are required for a proper response to oxidative stress.

Both *paps1-1* and *oxt6* exhibit a reduced size under standard growth conditions and are more resistant to oxidative stress in several cellular compartments. To reveal the genetic interactions of *PAPS1*, *PAPS2/4* and *CPSF30*, the *paps* mutants were crossed to *oxt6*. Since *PAPS1* and *CPSF30* are both located on chromosome 1, several recombinant F2 lines were used to search for double mutants. However, among the analysed individuals (238 F3 plants derived from *paps1-1*/*paps1-1 oxt6*/+ lines and among 333 F3 plants derived from *paps1-1*/+ *oxt6*/*oxt6* lines), no homozygous double mutant could be detected. This finding indicates that the combination of the loss of CPSF30 function with reduced PAPS1 activity results in embryo or gametophytic lethality.

In contrast, two *paps2-3 paps4-3 oxt6* triple mutants could be isolated in the F2 generation. The stress response of the F3 generations on MV were tested, to address the question, whether one mutant allele would be epistatic in the stress test or whether the resulting phenotype was intermediate. Interestingly, the FW of one triple mutant line was indeed intermediate between *oxt6* and *paps2-3 paps4-3*, while the other mutant line showed an enhanced resistance like *oxt6* (**Fig. 44 d**). In contrast, both lines exhibited a root length that was intermediate between the single mutants (**Fig. 44 e**).

The results imply that *PAPS1* and *CPSF30* may act together in a common pathway to downregulate the response to oxidative stress in both chloroplast and cytoplasm, while *PAPS2/4* act in a different pathway to enhance the resistance to ROS stress mainly in the chloroplast.

3.2.5 *paps1* and *paps2/4* react differentially to the loss of a poly(A) ribonuclease

A different stress mutant phenotype caused by deregulated poly(A) tail processing is exhibited by the mutant *ABA-hypersensitive germination 2-1* (*ahg2-1*). This *ahg2* mutant contains a point mutation in a gene encoding a mitochondria-localized poly(A) ribonuclease named PARN and exhibits increased sensitivity to salinity and osmotic stress (Nishimura et al. 2005). Interestingly, the combination of mutant *paps1-1* and *ahg2-1* alleles is lethal (Trost 2014, PhD thesis). The triple mutant *paps2-3 paps4-3 ahg2-1* is viable but very weak (**Fig. 45**).

While *ahg2-1* germinates late and exhibits a stunted growth phenotype, the additional loss of *PAPS2/4* function caused even stronger growth impairments. Since the triple mutant hardly produced seeds, no stress assays could be performed. Apparently, the defect of the mitochondrial PARN and the double knockout of *PAPS2* and *PAPS4* results in too much cellular mis-regulation to keep up a growth rate that is at least similar to the *ahg2-1* mutant. However, the fact that reduced *PAPS1* activity has an even stronger impact on the *agh2-1* mutant again underlines that *PAPS1* and *PAPS2/4* most certainly act on differential subsets of mRNAs.

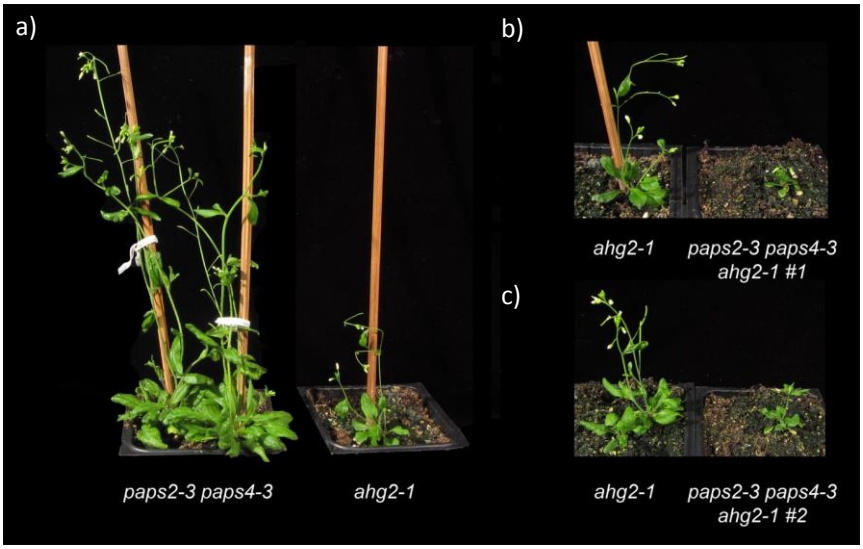

Fig. 45 Phenotype of *paps2 paps4 ahg2-1* triple mutants.
Plants were grown under standard LD conditions. The knockdown of a mitochondrial poly(A) ribonuclease in a *paps2 paps4* mutant background results in strong developmental defects. a) *ABA-hypersensitive germination 2-1* (*ahg2-1*) mutants with reduced poly(A) ribonuclease activity in mitochondria germinate late and exhibit reduced growth compared to the *paps2-3 paps4-3* mutant that shows no growth difference compared to Col-0. b, c) In a *paps2 paps4* mutant background the *ahg2-1* mutant phenotype is enhanced. Triple mutants are even smaller and less developed than *ahg2-1* single mutants.

3.3 Molecular characterisation of *PAPS1* and *PAPS2/PAPS4*

3.3.1 Establishing *PAPS1*- and *PAPS4*-specific antibodies

As outlined above, under certain conditions the phenotype of all *paps* mutant is different from that of the wild type. Changing expression levels, as predicted by the Genevestigator analysis (**Fig. 38, Fig. 39**), might be reflected by altered PAPS protein levels. Since PAPS proteins are essential enzymes in every nucleus and thus are assumed to be rather abundant, changes in the protein level might be detectable in a Western blot. The *paps1* mutants exhibited diverse strong phenotypes, and the *paps4* phenotype was more pronounced than that of *paps2*. Therefore, these two *AtPAPSs* were chosen to prove the putatively altered or opposing PAPS protein contents.

In a first attempt to attain specific antibodies, the C-terminal domains of PAPS1 and PAPS4 were tagged with hexa-histidine and overexpressed in *Escherichia coli*. However, the His-tagged proteins could not be purified using nickel agarose. Proteins bound to nickel agarose columns were washed stringently using buffer containing high imidazole concentrations (The QiaExpressionist handbook, 2003, Qiagen). However, even after diverse protocol optimizations, the obtained protein solution was still contaminated with *E. coli* proteins.

In an alternative approach, specific synthetic-peptide antibodies were ordered. The antibodies were directed against two 15 amino-acid long PAPS-specific peptides which were synthesized by Genescript (Piscataway, NJ, USA). A Western blot with crude protein extracts from *E. coli* overexpressing the PAPS-CTDs confirmed that the peptide antibodies were highly specific for PAPS1 and PAPS4, respectively. However, in a Western blot with *Arabidopsis* protein extracts from seedlings both antibodies bound a high amount of other proteins unspecifically. Even when concentrated in purified nuclei, the *PAPS* protein levels were still too low to visualize them against the background noise. The possibility that the proteins were not denaturated properly was ruled out by using strongly reducing protein extraction buffer which contained 4 M urea. After all, the PAPS protein content seemed to be lower than expected for enzymes exhibiting a very basic cellular function.

Fig. 46 Protein coding gene models for *PAPS1* (a) and *PAPS4* (b).
While only two *PAPS1* (*At1g17980*) splice forms that differ in the 5' end are known (a), *PAPS4* (*At4g32850*) expresses at least ten different splice forms (b). The splice forms differ in their 3' end and exhibit alternative polyadenylation sites and stop codons. When annotated expressed sequence tags (ESTs) for *PAPS4* were analysed to look for predominant splice forms, *At4g32580.5* and *At4g32850.8* were identified as the main forms that are being expressed at similar levels (arrows). The stop codon of splice form 5 is located in an intron of splice form 8 (green boxes).

Since these attempts to raise PAPS-specific antibodies failed, the PAPS-CTDs were tagged with venus-YFP (vYFP), an optimized version of yellow fluorescent protein. Only two *PAPS1* splice forms that differ in the 5' UTR are known. In contrast, ten *PAPS4* transcripts have been documented. All forms are alternatively spliced and polyadenylated at their 3' end (**Fig. 46**).

To identify possible coding sequences and sites at which the YFP could be inserted without being spliced out, expressed sequence tags annotated at *The Arabidopsis Information Resource* (TAIR, www.arabidopsis.org) were analysed by sequence comparison. Two transcripts were found to be predominantly expressed. Splice form *At4g32850.5* shows an alternative 3' acceptor site of the last intron, which results in a shorter coding sequence. The splice form *At4g32850.8* has an extended last intron and a longer coding sequence. Since the stop codon of splice form 5 is located in the partially retained intron that is spliced out of sequence 8, two *pPAPS4:PAPS4::YFP* sequences with alternative 3' ends were constructed by site-directed mutagenesis.

Since *paps1-1* still exhibits reduced *PAPS1* activity, the *paps1-3* mutant was transformed with *pPAPS1:PAPS1::YFP*. *paps1-3* is a knockout allele that results in male gametophytic lethality. The complementation of *PAPS1* function by the construct was shown by successful pollination of Col-0 plants with pollen from *paps1-3*/ *pPAPS1:PAPS1::YFP* lines (Ramming 2014, MSc thesis). The *paps1-3* mutant pollen had regained its functionality.

The *pPAPS4:PAPS4::YFP* constructs were transformed into *paps4-3* and *paps2-3 paps4-3*. A rescue of *PAPS4* function should result in flowering times similar to the wild type (see **Fig. 17**). As a first assay for *pPAPS:PAPS::YFP* expression, seedlings from four T2 lines per transformed mutant line were tested for YFP signals using confocal laser scanning microscopy.

Only lines transformed with *PAPS4* splice form 5 (*PAPS4.5*) emitted YFP signals which were weak compared to the YFP emission from the simultaneously analysed *paps1-3*/ *PAPS1::YFP* lines (data not shown). In parallel, a Western blot with protein crude extracts from seedlings was performed with a polyclonal anti-GFP antibody (**Fig. 47**).

In *pPAPS4:PAPS4.5::YFP*-expressing samples, a specific thin protein band ran at 130 kDa (**Fig. 47 b**). This band appeared directly below an unspecific band and was not observed in the Col-0 control. In accordance with the microscopy results, this band was not visible in samples transformed with *PAPS4.8*. The predicted protein sizes of PAPS4.5::YFP and PAPS4.8::YFP are 114 and 116 kDa, respectively. Similarly, the predicted PAPS1-YFP size was 113 kDa, but the recombinant protein ran at 130 kDa in a Western blot (Ramming 2014, MSc thesis). The proteins supposedly exhibit a different size due to post-translational modifications or the amino acid composition results in an anomalous electrophoretic behaviour.

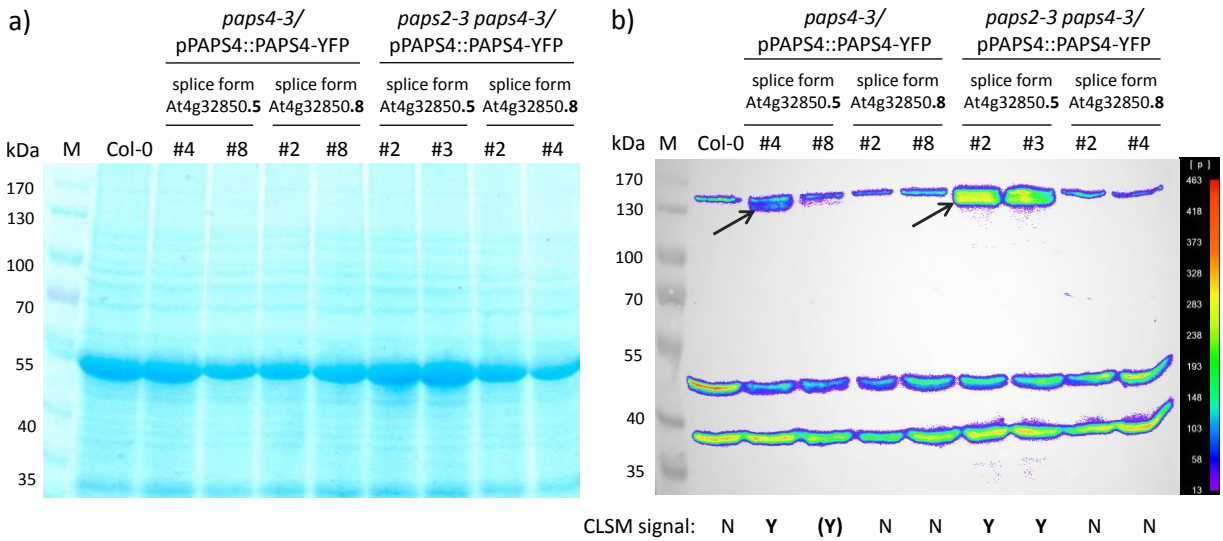

Fig. 47 The *PAPS4* splice form 5 is translated, while splice form 8 is non-coding.
A Western blot was performed with protein crude extracts of eleven-day-old seedlings. Col-0 and *paps4-3* or *paps2-3 paps4-3* expressing two different *PAPS4-YFP* constructs (*At4g32850.5* or *At4g32850.8* with C-terminal *venusYFP*) from the *PAPS4*-promoter were analysed. Two T2 lines per combination were tested. a) Coomassie staining was performed as a loading control. b) A Western blot was performed using a polyclonal anti-GFP antibody. A band that does not appear in Col-0 can be seen in samples transformed with *PAPS4* splice form 5 (arrow), but not with splice form 8. The predicted protein size is 114 kDa, the observed band runs at 130 kDa. The lines were tested for YFP signals with a confocal laser scanning microscope (CLSM signal; N - no signal; Y - signal; (Y) - weak signal). The observed signal strength is in accordance with the strength of the putative PAPS4-YFP protein band.

In future experiments, the flowering time of homozygous *PAPS4.5-YFP* expressing T3 lines should be analysed to test for a complete complementation. Moreover, PAPS protein abundances under oxidative stress conditions should be tested.

3.3.2 Localization and Expression of the PAPS1 and PAPS4 proteins

The cellular localization of the PAPS proteins was addressed using *pPAPS:PAPS::YFP*-expressing T2 lines. So far, the nuclear localization of *PAPS1* and *PAPS2/4* had only been shown by transient overexpression of *PAPS-GFP* in onion cells (Meeks et al. 2009). This finding should be confirmed with *PAPS1* and *PAPS4* expressed from the gene-specific promoters. Since T2 lines are still segregating for the transgene, the *PAPS4::YFP*-expressing plants were pre-selected based on their resistance to the herbicide BASTA (**Table 10**). The *PAPS1::YFP*-expressing lines had been tested for homozygosity before. First, roots from eleven-day-old seedlings were analysed by fluorescence microscopy. Indeed, the nuclear localization of both PAPS1 and PAPS4 could be confirmed (**Fig. 48**). In accordance with the Western blot (**Fig. 47**), *PAPS4* splice form 5, but not splice form 8, was found to be expressed *in vivo*. The PAPS1-YFP signal was generally stronger than the PAPS4-YFP signal. With regard to the *AtGenExpress*-analysis (**Fig. 5 b**), *PAPS4* was expected to be expressed more strongly. However, since the *PAPS4*-expressing lines might contain only one copy of the transgene, this might not necessarily

reflect the expression pattern in the wild type. Roots of the *paps1-3/PAPS1::YFP* lines were shorter and had more lateral roots, which might be due to the selection with PPT and kanamycin. Looking directly into the microscope it was observed that the expression of *PAPS4* was enhanced in the *paps2/4* lines compared to the *paps4* lines. The loss of the supposedly redundant *PAPS2* gene might result in an enhanced expression of the transgene. However, this expression difference could not be captured in images.

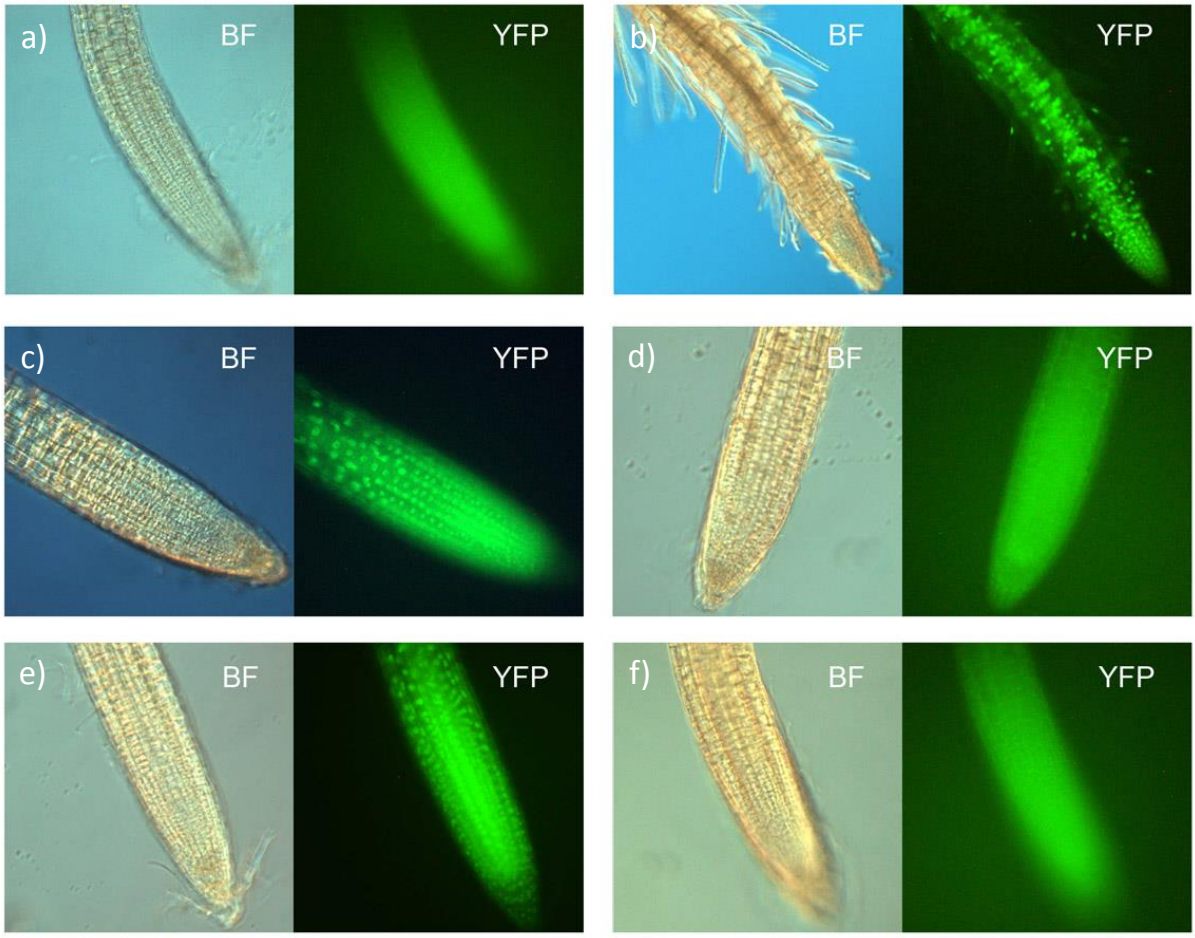

Fig. 48 PAPS1 and PAPS4 are localized in the nucleus.
Not all *PAPS4* splice forms encode functional PAPS4. Bright field (BF) and fluorescence microscopy (YFP) of a) Col-0, b) *paps1-3/PAPS1::YFP*, c) *paps4-3/PAPS4.5::YFP*, d) *paps4-3/PAPS4.8::YFP*, e) *paps2-3 paps4-3/PAPS4.5::YFP* and f) *paps2-3 paps4-3/PAPS4.8::YFP*. Specific YFP-signals can only be observed for *PAPS1* and *PAPS4* splice form 5. The magnification is 20×. Illumination times were 1 s (b) or 5 s (a, c–f).

Next, the *PAPS1* and *PAPS4*-expressing lines that had exhibited the strongest signals were analysed by confocal laser scanning microscopy in more detail (**Fig. 49**). To gain insights into potential *PAPS* expression patterns in specific cell types, the PAPS::YFP signals were observed in roots of 14-day-old plants. Again, the PAPS1::YFP signal was much stronger than that of PAPS4::YFP (**Fig. 49 a, d**). The PAPS4 protein was found to be more abundant at initiation sites of newly developing lateral roots, which was not observed for PAPS1. PAPS4 was also enriched in phloem companion cells. However,

the complemented *paps1-3* lines showed a very compact and branched root phenotype on the selective media (**Fig. 48**). To provide equal root development, the analysis has to be repeated with homozygous lines grown on standard MS media without selective supplements. Moreover, only one *PAPS4* splice form is expressed in the analysed lines. Other alternative splice and polyadenylation forms might be expressed specifically in different tissues or cell types. Differential *cPAP* transcripts have for example been documented in specific mouse tissues (Zhao and Manley 1996).

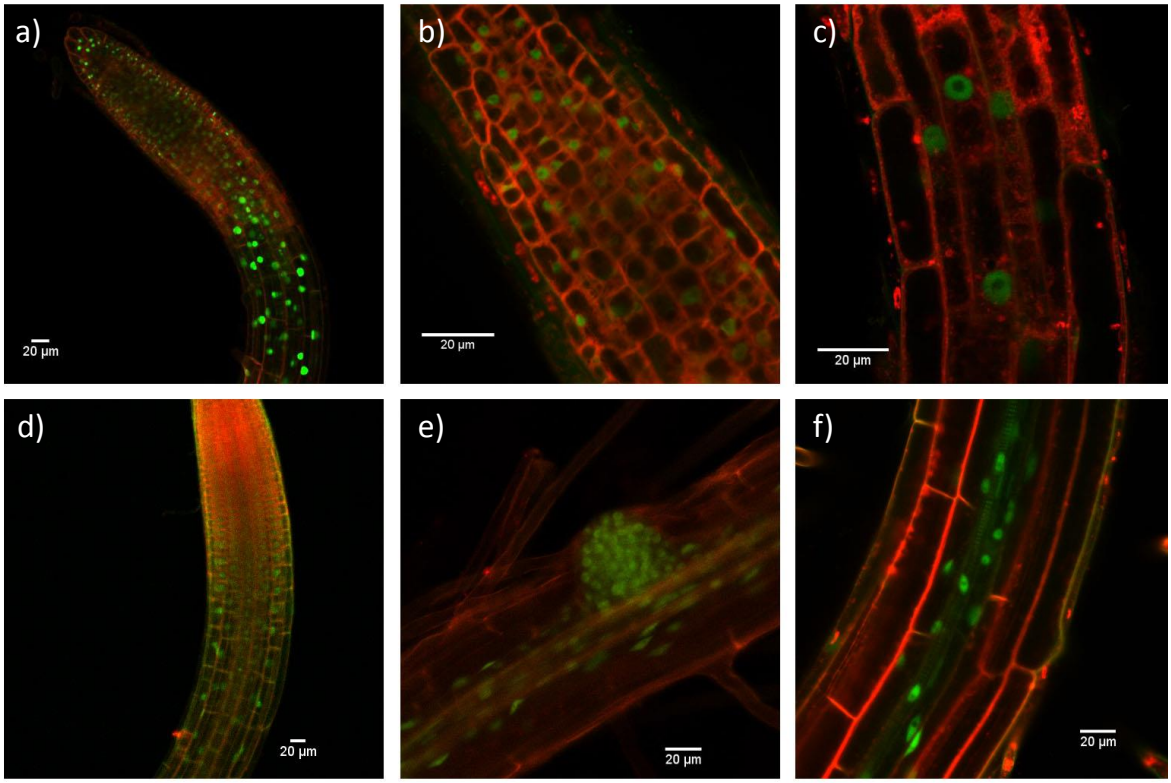

Fig. 49 PAPS1 and PAPS4 proteins are localized in nuclei and show enrichment in certain tissues.
Confocal laser scanning microscopy of a–c) *paps1-3/PAPS1::YFP*; d–e) *paps4-3/PAPS4.5::YFP* and f) *paps2-3 paps4-3/PAPS4.5::YFP*. The PAPS1 protein is more abundant than PAPS4 (a, d). PAPS4 is enriched at the initiation site of lateral roots (e) and in phloem companion cells (f). Membranes were stained with the dye FM-64. The scale bar marks 20 µm.

3.4 The search for *PAPS2/PAPS4*-specific target genes

3.4.1 A PCR-based PAT test did not reveal specific target genes

In order to detect putative *PAPS*-specific mRNA subsets, a microarray was performed with RNA extracted from *paps1-1* seedlings (Vi et al. 2013). Later, a transcriptome analysis with *paps2-3 paps4-3* RNA was carried out additionally. The two data sets were compared, assuming that altered PAT lengths might be reflected by altered expression levels. Genes with deregulated expression levels in *paps2/4* that exhibited no or opposite expression changes in *paps1-1* were determined. Based on strong and significant changes in gene expression levels, a set of 20 genes was selected for a PCR-based PAT length test.

For the PAT test, RNA is extended with a G/I adaptor at the 3' end by a mutant yeast PAP. After RT with an adaptor-specific oligonucleotide, RNA tail lengths can be determined by PCR using a gene-specific and an adaptor-specific primer. To receive a tail-free PCR product as a baseline, a control pool of RNA is treated with RNase H in the presence of an oligo (dT) primer prior to the adaptor ligation. Gene-specific primers were derived from cDNAs annotated at TAIR (www.arabidopsis.org). The PAT test had been validated before in the context of *SAUR* mRNA characterization in *paps1-1* (Vi et al. 2013). Unfortunately, in several cases no or unspecific products were amplified by PCR, probably due to unfavourable features of the gene-specific primer. In other cases the baseline PCR product did not show the expected size (**Fig. 50 a**).

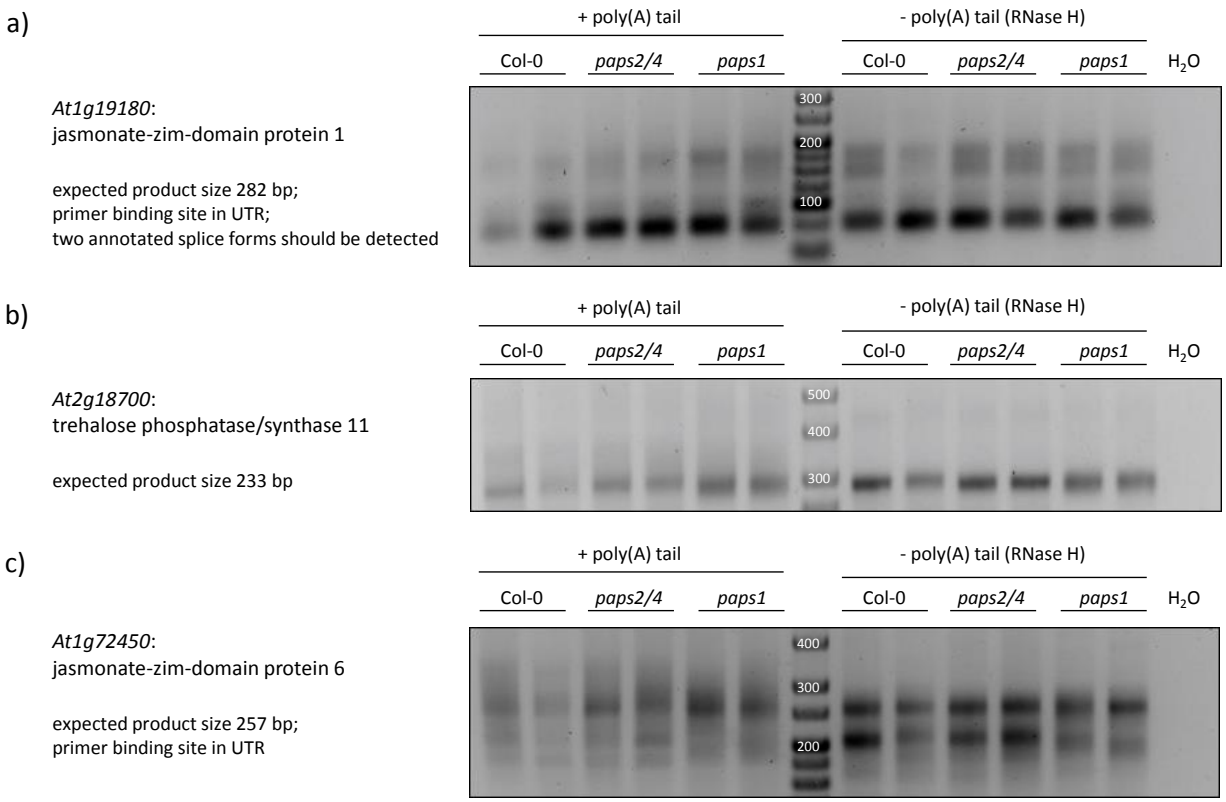

Fig. 50 Poly(A) tail test with putatively *PAPS2/4*-specific candidate genes.
To find mRNAs with deregulated poly(A) tails in *paps2-3 paps4-3* (*paps2/4*) but not *paps1-1* (*paps1*), a PCR-based poly(A) tail test was performed. Based on microarray and transcriptome data of *paps* mutants, candidate genes were determined. No differential PAT size could be observed for 20 genes. Shown here are three candidate genes with reduced expression in *paps2-3 paps4-3* and unchanged (a, b) or increased (c) expression in *paps1-1*.

Since the primer binding site must be located within 150 bp 5' to the PAS, correct annotation of the 3' UTR is essential for the PAT test. For some of the selected genes specific PCR products could be amplified. However, no differences in PAT lengths were observed between the *paps* mutants (**Fig. 50 b, c**). In summary, based on the transcriptome analysis, the PAT-test did not reveal specific targets for *PAPS2/4*.

3.4.2 Fractionation of mRNAs into pools according to their poly(A) tail length

An alternative approach was tested in order to detect mRNAs with differential poly(A) tails in the *paps2/4* mutants. As addressed in chapter 3.1.7, total RNA extracted from Col-0 and *paps2-3 paps4-3* was fractionated into pools according to their PAT length. This method was developed by Meijer and de Moor (2011) and is usually applied in a large scale to perform RNA blots. Much less RNA is required for a reverse transcription and a subsequent test on transcript abundance by qPCR. Therefore, the fractionation was performed in a small scale with 20 µg of total RNA as input.

Prior to the fractionation, biotinylated oligo (dT) probes were bound to paramagnetic streptavidin particles. Next, the RNA samples were incubated with the pre-treated magnetic beads. The poly(A) tail-containing mRNAs were bound by the oligo (dT) probes. After capturing the beads by a magnet, the unbound fraction was washed off. This fraction contains all kinds of non-polyadenylated RNAs. There should only be little DNA left, since the RNA was extracted by the so-called hot phenol method and was precipitated specifically with lithium chloride. Subsequently the mRNAs were eluted with differentially concentrated buffers. First, a "short" fraction containing mRNAs with oligo(A)-tails and tails with up to 50 A's is collected. Then the "long" fraction is obtained with a more stringent wash buffer, removing all mRNAs containing longer tails.

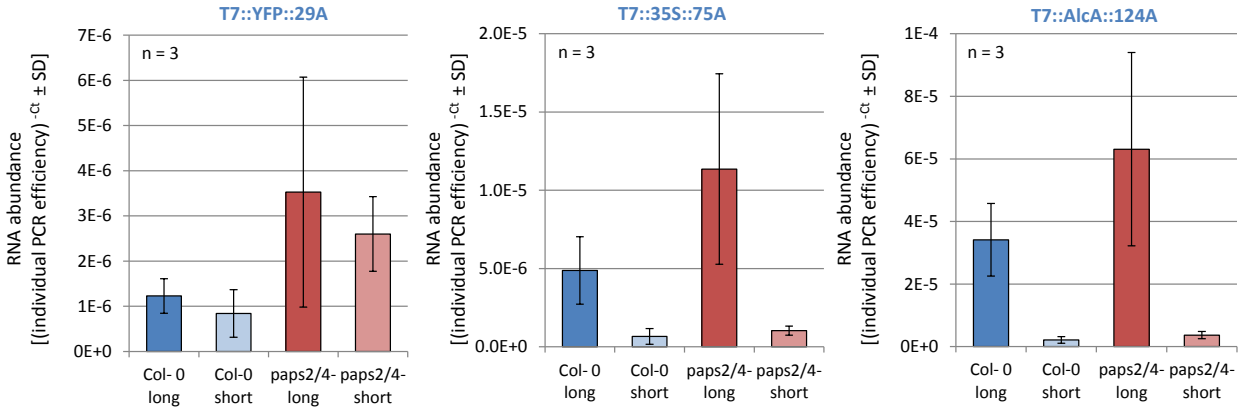

Fig. 51 Control RNAs with longer poly(A) tails are enriched in the long fraction.
Total RNA of Col-0 and *paps2-3 paps4-3* (paps2/4) of 9-day-old seedlings was separated into pools of mRNAs with long tails (> 50 A; long) and with short tails (> oligo A and < 50 A; short). The abundances of *in vitro*-transcribed control RNAs were tested by qPCR.

As a control, *in vitro*-transcribed RNAs with defined 3' PAT lengths had been added to all RNA samples prior to the fractionation. To validate the method, the control RNA abundances were tested by qPCR (**Fig. 51**). While the short-tailed control RNA was partly still found in the long fraction, RNAs with longer poly(A) tails were not detected in the short fraction anymore. Thus, in principle the separation of mRNAs according to their PAT length is possible. Trends in changes of PAT lengths of putative *PAPS*-specific target RNAs should be visible. However, it can also be seen that the *paps2/4*

samples contain higher RNA amounts, which indicates that the input RNA amount must have been higher than that of the wild type. Since no normalization against a housekeeping gene can be carried out, the method is based on equal volumes. Thus, despite a high accuracy of the experimenter, the outcome is very sensitive to slight technical variations. Therefore, in contrast to a standard qPCR, the fractionation method reveals mainly trends rather than abundance differences.

The abundances of *FLC* and *COOLAIR* in the long and short fractions have been examined by qPCR (chapter 3.1.7). Since the reduced mRNAs levels of *SVP* and *FLM* splice form β in *paps2/4* might be based on shortened poly(A) tails, the abundances of these factors were also tested in the fractionated mRNA pools (**Fig. 52**). However, neither *SVP* nor the two *FLM* splice forms exhibit PAT length alterations, suggesting that *PAPS2/4* specifically polyadenylate a factor upstream of these flowering regulators.

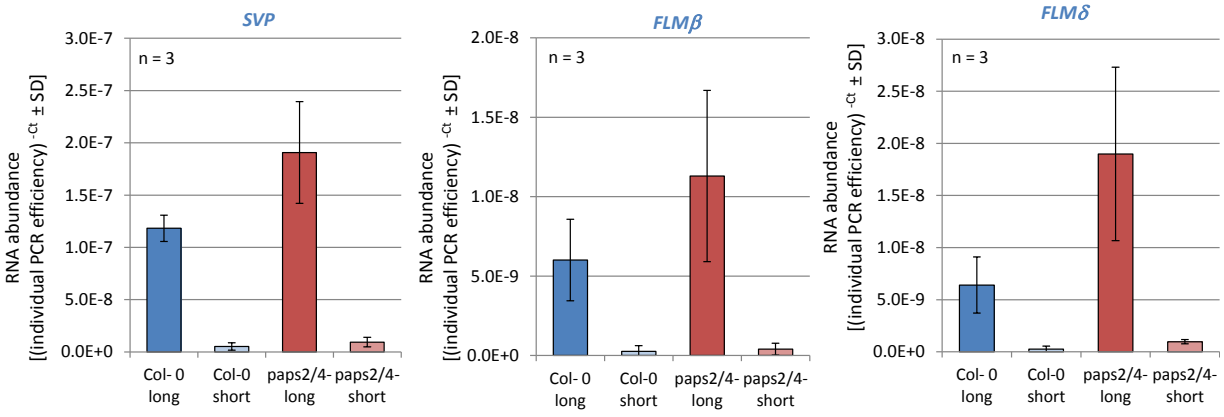

Fig. 52 *SVP* and *FLM* do not exhibit altered poly(A) tail lengths in *paps2 paps4*.
The transcript abundances of *SVP* and *FLM* splice form β are reduced in *paps2 paps4* (paps2/4; see **Fig. 25**). However, the mRNAs poly(A) tails of *SVP* and both *FLM* splice forms β and δ are not shortened or extended in the double mutant. The trend towards higher PAT length in *paps2 paps4* is based on an RNA abundance shift that can also be observed for control RNAs (**Fig. 51**).

3.4.3 A transcriptome analysis underlines an involvement of *PAPS2/PAPS4* in stress responses

A detailed analysis of the differential gene expression was performed with an RNA sequencing (RNA-seq) data set based on RNA extracted from ten-day-old *paps2-3 paps4-3* and Col-0 seedlings. With regard to the *PAPS2* and *PAPS4* upregulating conditions (**Fig. 38, Fig. 39**), defective expression of stress-related genes was expected. Instead, an analysis of the seedling transcriptome using the MapMan tool revealed that mainly genes related to RNA processing, translation and metabolism exhibited the most significant expression changes (**Table 7**). While abiotic stress genes were not affected, a subset of biotic stress-related genes was deregulated.

Table 7 The ten most significantly deregulated gene categories in *paps2-3 paps4-3* compared to Col-0 as determined by MapMan.
First, the significantly deregulated genes in *paps2 paps4* were filtered using the Kolmogorov-Smirnov test (KS-test) or using the Wilcoxon rank-sum test (Wilcoxon-test). Significantly deregulated gene categories were determined using the MapMan tool. The significance is indicated by the p-values detected by the two statistical methods. No stress-related gene categories can be found within the most significantly affected gene classes.

Description	p-value (KS-test)	p-value (Wilcoxon-test)
protein synthesis; ribosomal protein; eukaryotic; 60S subunit	5.7^{-8}	3.7^{-06}
DNA synthesis/chromatin structure; retrotransposon/transposase	4.1^{-7}	0.3
micro RNA, natural antisense etc	3.9^{-6}	1.2^{-4}
hormone metabolism	7.3^{-6}	0.2
RNA regulation of transcription	2.5^{-5}	3.7^{-7}
protein degradation; ubiquitin E3 RING	1.2^{-3}	4.9^{-4}
mitochondrial electron transport / ATP synthesis	2.8^{-3}	0.1
development	4.7^{-3}	2.5^{-3}
RNA processing	7.4^{-3}	4.9^{-4}
photosynthesis	9.3^{-3}	0.2

Next, significantly deregulated genes uncovered by the RNA-seq analysis were compared with the 200 most up- and downregulated genes of all experiments collected in the MASTA database. Interestingly, the analysis revealed strong opposite overlaps of the *paps2/4* transcriptome with stress-treated plants and stress-related mutants (**Table 8**). This means that genes upregulated during the stress treatments were downregulated in *paps2/4* and vice versa. Moreover, many of the experiments revealed by the comparison were related to short-term stress in the range of several hours, indicating that *PAPS2/4* might be required for immediate stress-responses.

In an alternative approach, the 200 most significantly deregulated genes and the 200 genes with the strongest fold-changes in *paps2/4* were analysed with the Genevestigator “Signature Tool”. This program searches for similarities with published *Arabidopsis* transcriptome data sets. As mentioned before, the transcriptomes of diverse stress-treated plants and stress-related mutants were overlapping with *paps2/4,* independently from the selections of input genes mentioned above (data not shown). As seen in the previous analyses, no specific stress condition could be determined.

Previously, gene expression changes in *paps1-1* were analysed based on a microarray with ten-day-old *paps1-1* and L*er* seedlings (Vi et al. 2013). In order to determine the degree of overlap between the two transcriptomes, the differentially expressed genes in *paps2/4* and *paps1* were compared. The analysis revealed that the transcriptomes almost did not overlap at all (**Fig. 53**).

The surprisingly low number of similarly deregulated genes in the mutants suggests that *PAPS1* and *PAPS2/4* polyadenylate different target genes. However, the number of significantly deregulated genes determined by RNA-seq was much lower than the number of differentially expressed genes

detected by the microarray. Moreover, these results have to be treated with caution since not the same *Arabidopsis* accessions were used in the two experiments.

Table 8 Opposite overlap of significantly deregulated genes in *paps2-3 paps4-3* relative to Col-0 with published microarray experiments as determined by MASTA.
The MASTA terms of 16 experiments with the highest opposite overlap to *paps2 paps4* are given. Types and times of the treatments are in bolt. Genes upregulated in *paps2 paps4* are downregulated under the indicated experimental conditions and vice versa. The type of the experiments as annotated by MASTA (encoded to ensure the possibility of tracking the exact experiment), and the number of oppositely overlapping genes are indicated.

Experiment as annotated by MASTA	Type of experiment	Number of oppositely overlapping elements
S851&**cold**_wt-wt_**3h**	stress	23
S8411&**cold**_soil_**1h**	stress	18
S852&**cold**_wt-wt_**6h**	stress	15
S411&**wounding**_sh_**15m**	stress	15
S121&**drought**_Col-Col	stress	13
S854&**cold**_ice1-ice1_**3h**	stress	13
S113&**drought**_sh_**1h**	stress	13
S831&**heat**_rt_**15m**	stress	13
S8414&**cold**_plate_**1h**	stress	13
M133&**BTHwrky18**_8h-BTHwt_8h	mutants	13
M172&**35SMBF1**-wt	mutants	13
S412&**wounding**_sh_**30m**	stress	12
E163&**elf26**_wt-wt_**30m**	elicitors	12
S855&**cold**_ice1-ice1_**6h**	stress	11
M125&**antisenseFBP1**-wt	mutants	11
S312&**osmotic**_sh_**1h**	stress	11

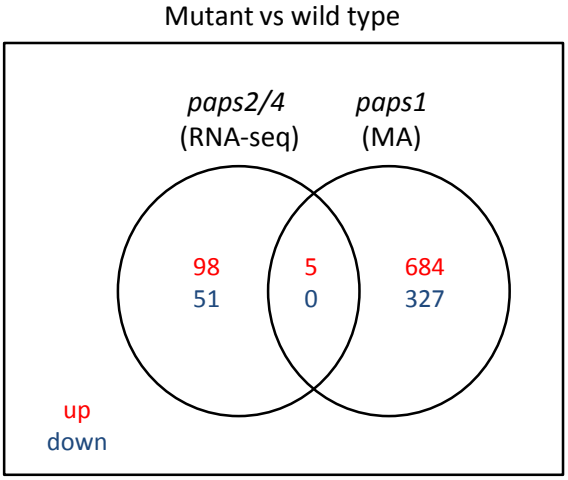

Fig. 53 Differentially expressed genes in *paps2-3 paps4-3* and *paps1-1* do not overlap.
Significantly up- and downregulated genes in *paps2-3 paps4-3* (*paps2/4*; in Col-0 background) and *paps1-1* (*paps1*; in *L*er background) are depicted in a Venn diagram. Only five genes are similarly deregulated in both *paps* mutants, suggesting that *PAPS1* and *PAPS2/4* polyadenylate different target genes. MA – microarray

4. Discussion

4.1 *PAPS1* and *PAPS2/4* regulate similar developmental processes in different pathways

Based on the *Arabidopsis* poly(A) polymerase mutant *paps1*, which exhibits smaller leaves but larger petals than the wild type, the question arose how reducing the activity of a constitutively expressed enzyme with a basic cellular function could result in this very specific growth phenotype. Molecular analyses revealed that the bulk mRNA 3' end processing is unaffected in *paps1-1*. Instead, the phenotype is caused by a small subset of mRNAs which exhibited defective polyadenylation (Vi et al. 2013). For the first time it was demonstrated that cPAPs can have an influence on the expression of specific genes. Consequently, the modulation of *PAPS* gene expression or of PAPS protein activity bears an obvious regulatory potential. The results gained in this thesis confirmed the essential role of *AtPAPS1* and revealed novel and specific functions for the plant cPAPs *AtPAPS2* and *AtPAPS4*.

A complete knockout of *PAPS1* function results in male gametophytic lethality in *Arabidopsis* (Vi et al. 2013), which reveals the essential character of *PAPS1*. In contrast, the loss of *PAPS2* and *PAPS4* function results in viable plants with a moderate delay of flowering (**Fig. 17**). The differential *paps* mutant phenotypes observed under standard growth conditions indicate that cPAPs regulate various developmental processes. Different *paps2* single mutants do not exhibit a phenotype (**Fig. 15, Fig. 16**). Consistently, the *PAPS2* promoter was found to be inactive in a GUS reporter analysis (Meeks et al. 2009; Son Vi, data unpublished). Moreover, *paps1-1 paps2-3* double mutants are indistinguishable from *paps1-1* (data not shown). *paps1-1 paps4-3* plants exhibit severe pleiotropic defects and only grow under very mild light and temperature conditions, which indicates that the *PAPS1* rest activity provided from the *paps1-1* allele is required for survival (**Fig. 20**). However, the loss of *PAPS2* function enhances the phenotype of *paps4* mutants (**Fig. 17**). Thus, *PAPS2* exhibits polyadenylation activity under certain conditions.

The cPAPs might be guided to specific mRNA substrates by polyadenylation complex components or other yet unidentified regulatory proteins. These might simultaneously bind the divergent PAPS-CTDs and detect certain mRNA signals. While a *pPAPS1::PAPS4* construct did not rescue the *paps1-1* phenotype, the domain swap construct *pPAPS1::PAPS4^{NTD}::PAPS1^{CTD}* complemented *paps1-1* (Vi 2013, PhD thesis). This experiment revealed the functional significance of the PAPS-specific CTDs.

As outlined in the introduction (chapter 1.1.1), both animal and plant cPAPs are bound by diverse proteins involved in gene regulation. The combination of mutant *CPSF30* or *CstF64* alleles with *paps1-1* results in lethality. So far, no direct interaction of these factors with *PAPS1* has been shown. However, *paps2/4 cstf64* and *paps2/4 oxt6* mutants are viable, which supports the idea that *PAPS1* and *PAPS2/4* act in different genetic pathways. Plants encode more than one functional isoform of

several polyadenylation factor subunits, e.g. *CPSF73 I* and *II* (Xu et al. 2006; see **Table 1**). This opens up the possibility that plants possess various differentially assembled 3' end processing complexes.

In order to reveal unique and novel interaction partners, a yeast-two-hybrid screen has been performed (Bartholomäus 2012, MSc thesis). The PAPS1- and PAPS4-CTDs were used as bait proteins in a library-scale mating approach. However, none of the detected putative interaction partners could be confirmed *in vivo* using bimolecular fluorescence complementation (Ramm 2013, MSc thesis). Although NTD and CTD of the bovine cPAP appear to form separate globular structures (Martin et al. 2004), a repetition of the screen using full length AtPAPS proteins might be required. Alternatively, a co-immunoprecipitation (Co-IP) with the *PAPS::YFP* expressing plant lines could be performed. The fusion proteins could be detected in a Western blot using anti-GFP antibodies (**Fig. 47**). However, since the polyadenylation complex is very large and some factors might act as bridges between the cPAPs and other regulatory proteins, certain genetic relations might be missed by Co-IP. An immunoaffinity isolation of the whole supramolecular protein complex in combination with a subsequent mass spectrometric analysis could be considered. This method has been used successfully to identify novel components in *Xenopus* protein complexes (Conlon et al. 2012; Greco et al. 2012) and an adapted protocol for plant material is available (Núria Sánchez-Coll, oral communication).

Since the nuclear *AtPAPSs* are constitutively expressed (**Fig. 5 b**) and cPAPs take over essential and basic cellular functions, both *PAPS1* and *PAPS4* might be considered as housekeeping genes (Tsukaya et al. 2013). A Western blot with protein extracts from *PAPS::YFP* expressing seedlings revealed that PAPS proteins are present at surprisingly low abundances (**Fig. 47**). To compare the exact protein levels of PAPS1 and PAPS4, the Western blot has to be repeated with homozygous T3 lines. Moreover, the flowering time of the *PAPS4.5::YFP*-expressing *paps4* and *paps2/4* lines has to be tested. If the transgene does not completely rescue the mutant phenotype, other alternatively polyadenylated *PAPS4* splice forms might also be translated and exhibit regulatory functions. While only one *PAPS1* splice form exists, *PAPS4* exhibits at least ten transcript isoforms that are alternatively spliced and polyadenylated in the 3' region of the gene. Interestingly, only one of the two most abundant transcript forms is translated into a protein (**Fig. 47, Fig. 48**). Alternative splicing and polyadenylation of cPAP genes has been observed in other eukaryotes before. However, in both zebrafish and mouse the use of an alternative intronic PAS leads to substantial shortening of the resulting transcript. The short isoform of the mouse cPAP can only be detected in some tissues and is not translated into a protein (Zhao and Manley 1996). The short supposedly non-coding *PAPOLB* isoform detected in some zebrafish tissues has been suggested to be produced in favour of exclusive mRNA polyadenylation by *PAPOLG* (Ulitsky et al. 2012). This scenario could be transferred to *Arabidopsis*. The production of non-coding transcripts for regulatory purposes has been observed

before. Prominent examples are the alternative processing events of *FCA* and *FPA* which have been described in detail in the introduction (chapter 1.2.2). To analyse *FCA* transcript abundances, an RNase protection assay was proved to reveal all splice forms efficiently (e.g. Macknight et al. 1997). Since the *AtPAPS4* transcript isoforms have very similar sequences and sizes, the exact transcript amounts cannot easily be detected by PCR or Northern blot. Whether all *PAPS4* splice forms annotated at TAIR are present in Col-0 under standard conditions could be tested by single molecule direct sequencing, an approach that has been used successfully to precisely describe alternative 3' end processing in *fpa* mutants (Duc et al. 2013). In zebrafish, the 3' terminome was determined by poly(A)-position profiling by sequencing (Ulitsky et al. 2012). These methods might be sensitive enough to capture the exact *PAPS4* polyadenylation forms present in Col-0.

Interestingly, in a Western blot analysis both the PAPS1::YFP and PAPS4::YFP proteins were around 15 kDa larger than predicted (chapter 3.3.1, **Fig. 47**). Mobility shifts in SDS-PAGEs can be caused by certain amino-acid side chains, like prolins and tyrosines, which are indeed abundant in both cPAPs (Garfin 2003). Shifts in migration behaviour could also indicate post-translational protein modifications. Phosphorylation of the animal PAPα has been reported (Martin and Keller 2007). However, protein phosphorylations are easily being lost during sample preparation if no phosphatase inhibitor is used. Moreover, it changes the molecular mass only by around 80 Da (mass changes listed on www.sigma-aldrich.com). Additionally, PAPα was shown to be sumoylated (Vethantham et al. 2008). Sumoylation of proteins can be tested *in vitro*. One SUMO does indeed result in a size increase of 15 to 17 kDa in SDS-PAGEs (Park-Sarge and Sarge 2009). In plants, sumoylation has for example been shown to be implicated in stress resistance and flowering time (Miura et al. 2007; Jin and Hasegawa 2008). However, since the mobility shift was observed for both PAPS1 and PAPS4, potential protein modifications do not seem to determine *PAPS*-specificity. It would be interesting to see whether the PAPS protein migration behaviour in an SDS-PAGE changes under certain plant growth conditions.

The nuclear localization of PAPS1 and PAPS4 was confirmed by microscopy (**Fig. 48, Fig. 49**). Seedlings expressing *PAPS1::YFP* generally exhibited a stronger YFP signal than seedlings expressing *PAPS4::YFP*, although the offspring of the earliest flowering *paps4* and *paps2/4* T1 lines was used in the analysis. The expression levels of both cPAPs were found to be similar (**Fig. 5 b**). Thus, at least equal signal strengths had been expected. The low PAPS4 signal strength observed could be based on the insertion site of the transgene in the tested mutant lines. An expression analysis has to be repeated with homozygous lines that show the best complementation.

4.2 An optimized PAT test is required to reveal mRNA specificity of cPAPs

The identification of the *PAPS1*-specific polyadenylation of *SAUR* mRNAs was the first direct proof of cPAP isoform-dependent gene regulation in plants. Indirect support for the concept is provided by the finding that *FLC* transcript abundances are decreased in *paps1-1* but are increased in *paps2/4* (**Fig. 23, Fig. 24**). Thus, *Arabidopsis* cPAPs are not completely interchangeable.

In the *paps1* mRNA fractionation, *FLC* was not found to exhibit an altered PAT length (not shown). Since the fractionation was performed with RNA from ten-day-old L*er* and *paps1-1* seedlings, the *FLC* expression level might have been too low to observe significant differences between the transcript amounts in the long and short fractions. An RNA immunoprecipitation (RIP) with the *PAPS::YFP*-expressing lines could be considered in order to identify further specific targets. A real-time PCR-based method to detect low abundance RNAs subsequently to an *Arabidopsis* RIP has been described (Rowley et al. 2013). It remains possible that *PAPS1* represses flowering by specifically polyadenylating components that are required for the upregulation of *FLC*. A parallel RIP-seq with *PAPS1::YFP*- and *PAPS4::YFP*-expressing lines might be suitable to identify *PAPS*-specific target RNAs at a global scale, but might miss low abundance and antisense RNAs.

The significant increase of the *FLC* transcript level in *paps2/4* led to the idea that either *FLC* or *COOLAIR* might exhibit an altered PAT length in the mutant. However, so far no altered PAT lengths were detected by the fractionation of *paps2/4* mRNAs into pools of short-tailed and long-tailed mRNAs (**Fig. 36, Fig. 37**). A *paps2/4* transcriptome analysis revealed strong global gene expression changes (chapter 3.4.3). This could mean that the wrong transcripts were looked at in the fractionation analysis. Alternatively, significant PAT alterations of lowly expressed transcripts like *COOLAIR* in *paps2/4* or *FLC* in *paps1* might in general not be captured by the RNA fractionation. Since housekeeping genes cannot be used for normalization, the output for a given sample is its primer efficiency to the power of the negative cycle threshold value determined by qPCR. Subtle PAT changes become easily blurred by small technical variations which are unavoidable regarding the fractionation protocol. Since all samples were treated equally and equal amounts of the *in vitro*-transcribed RNAs were pipetted to all samples, it is difficult to recapitulate why the *paps2/4* samples contained higher RNA amounts than the Col-0 samples (**Fig. 36, Fig. 37, Fig. 51**).

The attempt to reveal tail changes of mRNAs in *paps2/4* using a PCR-based PAT test described in chapter 3.4.1 failed, although the test was successfully used with regard to the *SAUR* mRNAs in *paps1* (Vi et al. 2013). An amplification bias towards shorter PCR products, i.e. transcripts with shorter tails, is inherent to PCR-driven PAT tests. Since *SAUR* mRNAs almost completely lack A-tails, the PAT test was suitable in this case. Subtle differences especially with regard to tail elongations are difficult to catch. Similarly to the RNA fractionation, only strong trends can be substantiated by this method.

As discussed in Jalkanen et al. (2014), all methods that aim to determine PAT sizes exhibit a higher accuracy with regard to more strongly expressed genes. The classic RNase H/ Northern blot method is very time-consuming, requires large amounts of RNA and is still not reliable for transcripts with a low abundance. An anchor-based alternative to the G/I-tail based PAT test used here is the so called extension PAT test (ePAT; Jänicke et al. 2012). Prior to the cDNA synthesis, an oligo (dT) anchor with a 3'-overhang is hybridized to the poly(A) tails of mRNAs. The mRNA 3' end is extended complementary to the anchor sequence using a Klenow polymerase, followed by an RT-PCR that starts at the anchor. Subsequently, specific PAT lengths can be determined using a gene-specific and an anchor-specific primer. In combination with a nested PCR, the ePAT has recently successfully been used to show PAT length changes of three more *PAPS1*-specific target genes in the *paps1* mutant (Kolbe 2014, BSc thesis). Thus, more putative *PAPS2/4*-target genes should be examined with the optimized ePAT to confirm the mRNA specificity of these cPAPs.

4.3 *PAPS1* represses flowering by promoting *FLC* expression

The early flowering phenotype of *paps1-1* was found to be associated with reduced *FLC* transcript levels (**Fig. 23**), which indicates that *PAPS1* is involved in the regulation of *FLC* expression. Supporting this idea, the loss of *FLC* or the overexpression of *FCAγ* do not enhance the early flowering of *paps1* (**Fig. 27, Fig. 31**). As mentioned above, the *FLC* PAT size was unchanged in *paps1*, which indicates that *PAPS1* might not directly polyadenylate *FLC*.

A simple explanation for the reduced *FLC* level could be elevated levels of *FCAγ* in *paps1*. PAPS1 activity might be required for the functional autoregulation of *FCA* expression. There is no flowering time difference between *35S::FCAγ paps1-1* and *35::FCAγ* plants (**Fig. 31**). Additional support for this scenario is provided by the recent finding that, like *paps1*, *35S::FCAγ* plants are resistant to oxidative stress induced by paraquat (Lee et al. 2014; **Fig. 44**). However, the *paps1-1* mutant is not epistatic to *fca-9* or *fy-2,* which indicates that an independent pathway is deregulated in *paps1*.

Alternatively, *PAPS1* might specifically polyadenylate an *FLC*-promoting factor (reviewed e.g. by Henderson and Dean 2004; Rataj and Simpson 2014). Some *FLC* activators can be excluded because the early flowering mutants exhibit pleiotropic defects that were not observed in *paps1*. The loss of *ESD4* for example results in elevated SA levels (Villajuana-Bonequi et al. 2014), but SA-levels are unchanged in *paps1* (Trost et al. 2014). Several chromatin remodelling factors are required for the initial expression of *FLC* (reviewed e.g. by Rataj and Simpson 2014). The expression level of these and other less-known *FLC* activators in *paps1* could be tested. Mutants of two cap-binding complex factors and of the cap-associated protein *SERRATE* flower early and exhibit serrated leaves, which is reminiscent of the *paps1* phenotype (reviewed by Rataj and Simpson 2014). However, these factors mediate the *FRI*-dependent *FLC* upregulation, a pathway not active in Col-0. It would still be

interesting to examine the effect of *FRI* in *paps1*. An F2 generation segregating for *paps1-1* and FRI^{Sf-2} was vernalized prior to genotyping before the *paps1-1* cold-sensitivity had been revealed. Accordingly, no homozygous *paps1* FRI^{Sf-2} plants survived a cold treatment of four weeks. To see whether the *FRI*-mediated *FLC*-upregulation is defective in *paps1*, the experiment should be repeated without vernalization treatment.

4.4 *PAPS2* and *PAPS4* ensure timely flowering in a common pathway with *FCA*

In contrast to *paps1* mutants, single and double mutants of the cPAPs *PAPS2* and *PAPS4* are indistinguishable from the wild type under standard growth conditions (**Fig. 15**). However, all analysed *paps4* and *paps2 paps4* lines flowered moderately late (**Fig. 16, Fig. 17**). Apparently, the two redundant cPAPs *PAPS2* and *PAPS4* promote flowering in *Arabidopsis*. Growth under short photoperiods did not increase or rescue the *paps2/4* mutant phenotype (**Fig. 19**). As described in detail in chapter 3.1.3, the mutant phenotype does not seem to be caused by altered GA or SA levels or by deregulation of the temperature and age pathways. Therefore, deregulation of the autonomous pathway was considered.

While the *FLC* transcript level was indeed found to be twofold upregulated in *paps2/4*, neither the loss of *FLC* nor the overexpression of *FCAγ* could completely rescue the late flowering phenotype (**Fig. 27, Fig. 31**). Surprisingly, the point mutant *flc-5* (in L*er* background) suppressed the late flowering phenotype almost completely, but the deletion mutant *flc-2* rescued only partially. An explanation for this discrepancy could be that the effect of the loss of *PAPS2/4* is less pronounced in the mixed background of Col-0 and L*er*. The flowering time difference between *cstf64-1* and wild type was slightly reduced in mixed background in comparison to the pure Landsberg background (**Fig. 28**). The flowering time of the homozygous offspring of a *paps2-3*/+ *paps4-3*/+ (Col/L*er*) should have been determined. However, the elevated *FLC* levels and the decreased floral pathway integrator levels detected in *paps2*/*4* motivated a further search for deregulation of the autonomous pathway.

Apparently, other flowering inhibitors are involved in the late flowering of *paps2/4*. While *MAF2* and the *FLMδ* were not affected, the transcript levels of *SVP* and *FLMβ* were significantly reduced (**Fig. 25**). Reduced *SVP* and *FLMβ* levels are typically associated with early flowering under higher ambient temperatures due to enhanced *FT* and *SOC1* expression (Posé et al. 2013). Moreover, the loss of *SVP* function is accompanied by an early flowering time, even in the presence of high *FLC* levels (e.g. Li et al. 2008). Consistent with the late flowering of *paps2/4* even under higher ambient temperatures, the expression levels of several floral pathway integrators were significantly decreased (**Fig. 24**). It appears that the inhibitory effect of *FLC* and other yet unidentified MAFs on the FPIs exceeds the flowering promoting effect based on the loss of the SVP-FLMβ protein complex in *paps2/4.* It has been documented before that different FPI-regulating factors can outweigh each other. Mutants of

the E3 ubiquitin ligase *CUL4* for instance exhibit high *FT* mRNA levels and thus flower early despite simultaneously increased *FLC* expression (Pazhouhandeh et al. 2011). The finding that *SVP* and *FLM* PAT lengths are not altered in *paps2/4* (**Fig. 52**) suggests that one or more yet unidentified upstream factors are direct *PAPS2/4* target genes.

While *paps2/4* responded to vernalization and the *FLC*-level was indistinguishable between wild type and mutant after an extended cold period, the flowering delay was still not completely rescued (**Fig. 32, Fig. 33**). Other vernalization-independent flowering inhibitors might be upregulated in *paps2/4*. *MAF3* is downregulated and *MAF5* is upregulated by cold, but *MAF4* expression is indeed not affected by vernalization (Ratcliffe et al. 2003). Although both overexpression and knockout of *MAF4* have only little physiological consequences in Col-0, a *maf4* mutant could rescue the late flowering phenotype of the PRC1 RING-finger protein mutant *Atring1a* due to altered FPI gene expression (Ratcliffe et al. 2003; Shen et al. 2014). Moreover, the *MAF4* and *MAF5* chromatin structures differ from the other MAFs, and the two factors respond differentially to activity changes of certain chromatin remodelling factors (Jiang et al. 2008; Xu et al. 2013; Shen et al. 2014). In combination with other deregulated factors in *paps2/4*, *MAF4* could indeed cause a moderate delay of flowering.

Next, the genetic interactions of *PAPS2/4* with *FCA* and *FY* were analysed. Interestingly, *PAPS2/4* were found to act in the same pathway like *FCA*, but independently from *FY* (**Fig. 29, Fig. 30**). Accordingly, the *FY* expression level was not altered in *paps2/4* (not shown). Similarly, the transcript abundance of *FCAγ*, encoding the active FCA protein isoform, was unchanged in *paps2/4* (not shown). The fact that *paps2/4* mutants do not flower as late as *fca* mutants suggests that *PAPS2/4* act downstream of *FCA*. To confirm this result, the FCA protein abundance in *paps2/4* could be checked in a Western blot (Quesada et al. 2003).

In unvernalized seedlings, *FCA* promotes the polyadenylation of *COOLAIR* class I in concert with *FY* and *CstF64* (Ietswaart et al. 2012). Since *cstf64-1* and *fy-2* are not epistatic to *paps2/4* and the *COOLAIR* class I expression is not deregulated (**Fig. 28, Fig. 29, Fig. 34 a**), this pathway is not affected by the loss of *PAPS2/4*. Instead, *FCA* and *PAPS2/4* seem to regulate the expression of flowering inhibitors in a novel, so far unidentified pathway that has a minor, but still significant impact on timely flowering. The overexpression of *FCAγ* repressed the *paps2/4*-mediated flowering delay only partially (**Fig. 31**). An explanation for this puzzling observation might be that the *FLC* expression is completely suppressed in *paps2/4 35S::FCAγ*, but the *PAPS2/4*-dependent deregulation of the yet unidentified flowering inhibitor is not rescued. *FLC* and for example *MAF4* expression levels in *paps2/4 35S::FCAγ* could be checked by qPCR.

As *paps2/4 fca-9* is completely epistatic to *fca-9* (**Fig. 30**), *FCA* should control the expression level of all flowering inhibitors downstream of *PAPS2/4*. Indeed, the *MAF4* expression level might be slightly increased in *fca-9* (Ratcliffe et al. 2003). Double mutants of *fca* and *flc* do not flower later than *flc*

single mutants (Michaels and Amasino 2001), indicating that the deregulation of other MAFs is not reflected at the level of flowering time in *fca*. However, the only comparative flowering time analysis of *fca flc* and *flc* was performed in a mixed background of Col-0 (*flc-3*) and Wassilewskija (*fca*). Since *MAF4* expression varies in different *Arabidopsis* accessions (Ratcliffe et al. 2003), this analysis should be repeated in a complete Col-0 background. Strikingly, accession-dependent *MAF4* variation might also explain the flowering time differences of *paps2 paps4 flc-2* and *paps2 paps4 flc-5*.

The findings regarding the regulatory role of *AtPAPSs* in the flowering time network have been summarized in **Fig. 54**.

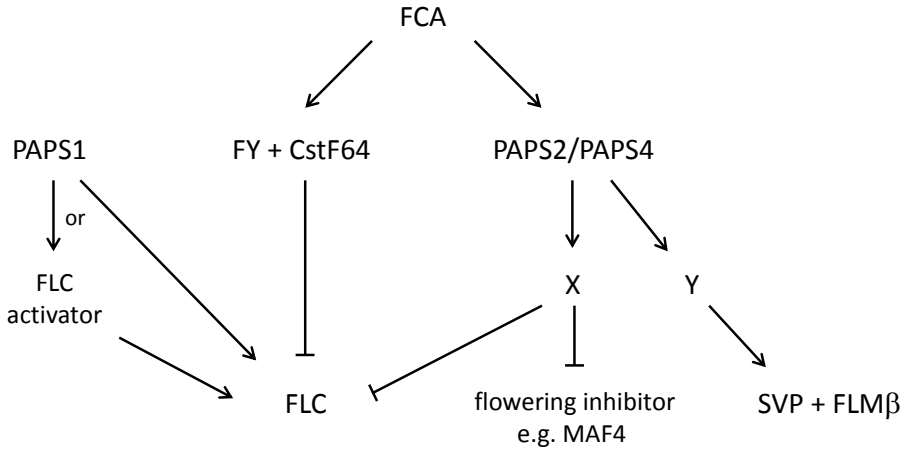

Fig. 54 *PAPS1* and *PAPS2/PAPS4* ensure timely flowering in *Arabidopsis*.
PAPS1 represses flowering by promoting *FLC* expression. It polyadenylates *FLC* mRNA directly or polyadenylates an essential *FLC* activator. In contrast, PAPS2 and PAPS4 promote flowering by suppressing *FLC* transcription and other flowering inhibitors, probably by polyadenylating a factor (X) required for the transcriptional downregulation of these inhibitors. While FCA acts in concert with PAPS2/PAPS4, these two cPAPs act independently from FY and CstF64. PAPS2/PAPS4 are moreover implicated in the upregulation of the temperature-dependent flowering inhibitors SVP and FLMβ via the polyadenylation of one or more so far unidentified direct target genes (Y).

4.5 Putative *PAPS2/PAPS4* targets that inhibit *FLC* and *MAF* expression

Since *FLC* mRNA does not exhibit an altered PAT length in *paps2/4*, the question arises, which component might be regulated by *FCA* and polyadenylated by *PAPS2/4* in order to inhibit *FLC* and *MAF* expression. Remarkably, the *COOLAIR* class II expression was significantly upregulated in both *paps2/4* and *paps2/4 FRI*$^{Sf\text{-}2}$ mutants when the plants were transferred to warm temperatures after growing at 4 °C for six weeks. Accordingly, a trend towards a PAT size increase in *paps2/4* was observed for *COOLAIR* class II (**Fig. 37 b**) and the mutants do still flower late after the vernalization treatment (**Fig. 32**). The distally polyadenylated *FLC* antisense transcript has been associated with the promotion of *FLC* transcription before (Hornyik et al. 2010; Rataj and Simpson 2014). A functional significance of *COOLAIR* class II in the molecular regulation of vernalization is further indicated by the

alternative splicing pattern observed in this study (**Fig. 35**). Although the different *COOLAIR* splice forms have been documented before (Hornyik et al. 2010), this is the first report on cold-induced intron retention in *COOLAIR* class II. Recently, defective splicing of *COOLAIR* class I has been implicated in flowering time regulation (Marquardt et al. 2014). A similar mechanism is conceivable for the class II transcript. It is tempting to speculate that *PAPS2/4* might regulate flowering time by suppressing *FLC* AS class II. However, several observations argue against this scenario. First, the unvernalized *paps2/4* plants flower late but do not exhibit *COOLAIR* upregulation (**Fig. 34**). Second, the high *COOLAIR* level was not associated with higher *FLC* levels after the vernalization treatment (**Fig. 33**). It can also not be excluded that the *FLC* level drops faster in Col-0 than in *paps2/4* after return to the warmth. A high-resolution time course analysis of both *FLC* and *COOLAIR* abundances until flowering would be interesting. However, as suggested before, increased levels of the distally polyadenylated transcript might simply be an artefact due to defects in *COOLAIR* processing (Marquardt et al. 2014). Interestingly, *COOLAIR* class I has been implicated in the vernalization response in several *Arabidopsis* species, but class II upregulation during vernalization has only be observed in *Arabidopsis thaliana* (Castaings et al. 2014). Similar to *MAF4*, *COOLAIR* class II expression might vary in different *Arabidopsis* accessions and species. After all, the relatively small flowering shift caused by the loss of *PAPS2/4* suggests an involvement in a regulatory fine-tuning mechanism.

RNA-processing factors have been implicated in the regulation of flowering time before. The autonomous pathway component *FPA* is an RNA-binding protein that has also been shown to be involved in the 3' end processing of *COOLAIR*. However, *FPA* acts genetically independently from *FCA* and is most likely not involved in the *PAPS2/4*-mediated *FLC* and *MAF* expression regulation (Hornyik et al. 2010).

Pcsf4, an Arabidopsis homologue of the yeast polyadenylation factor Paf1c, forms a complex with *FY* and controls *FCA* transcript processing. Interestingly, *pcsf4* mutants exhibit a moderately late flowering phenotype very similar to *paps2/4* (Xing et al. 2008b). The delay is increased by *FRI*, but only partially rescued by vernalization and by *flc-3*. Moreover, *FLC* is upregulated, FPIs are downregulated and the *FY* expression is unaffected. The molecular phenotype of *pcfs4* is thus completely identical to *paps2/4*. *Pcfs4* could be a direct target of *PAPS2/4* and both expression level and PAT length of this factor in *paps2/4* should be examined. However, *Pcfs4* binds *FY*, but *PAPS2/4* have been shown to act independently from *FY* (**Fig. 29**). Unfortunately, the phenotype of *pcfs4 fy* and *pcfs4 fca* double mutants has not been examined. It would be relevant to compare the phenotype of *paps2/4 pcfs4*, *paps2/4 fy* and *pcfs4 fy* mutants and to analyse the *FCA* transcript abundances in these mutants, e.g. by Northern blot. Similarly, *paps2/4 fca* and *pcfs4 fca* mutants should be compared. Lastly, it is notable that the deregulation of *FCA* processing does not necessarily

result in very strong flowering delays as seen for complete loss-of-function *fca* mutants. This re-opens the possibility that *PAPS2/4* act upstream of *FCA* and might be involved in *FCA* processing.

Several chromatin remodelling factor mutants exhibit *FLC*-dependent late flowering phenotypes. The autonomous pathway components *FLD* and *FVE* are involved in histone deacetylation at the *FLC* locus. Associated in a multiprotein complex, FVE binds *FLC* chromatin (Jeon and Kim 2011). Similarly, the mammalian homologue to FLD is part of a histone deacetylase complex (He et al. 2004). Histone deacetylation is a chromatin mark related to the repression of gene expression (Berger 2007). Consistently, *fld* and *fve* mutants exhibit histone hyperacetylation in *FLC* chromatin (He et al. 2004). Similarly, *ref6* mutants flower late due to enhanced acetylation of the *FLC* chromatin (Noh et al. 2004), indicating that the Jumonji/zinc-finger-class transcription factor *REF6* is involved in chromatin remodelling despite the absence of typical DNA-binding domains. Although these autonomous pathway factor mutants usually exhibit very high *FLC* levels, deregulations of these factors in *paps2/4* cannot be excluded.

Interestingly, next to histone deacetylation both FVE and FLD have also been shown to be involved in histone demethylation. Trimethylation of lysine 4 of histone 3 (H3K4me3) triggers transcriptional activation and *FLD*-mediated histone demethylation contributes to the repression of *FLC*. *FCA* requires *FLD* to exert its repressive effect on *FLC* (Liu et al. 2007). The loss of *FCA* and *FLD* was associated with reduced *COOLAIR* class I expression. Liu et al. (2007) drew this conclusion regarding reduced ratios of class I to class II in *fca* and *fld* mutants. Remarkably, the reduced ratio could also result from an elevated class II level while the class I abundance remained unchanged (Gordon Simpson, oral communication). The total transcript abundance values would have been more meaningful. If *PAPS2/4* was for example required for the polyadenylation of *FLD*, increased H3K4me3 level should be detected at the *FLC* locus in *paps2/4*.

In contrast, the autonomous pathway factor *FVE* (also termed *MSI4*) does not function as a histone demethylase itself, but is part of a large complex that regulates the demethylation of *FLC* chromatin at lysine 27 of histone 3 (H3K27). The FVE protein interacts with a factor termed DDB1 which in turn binds an E3 ligase termed CUL4 (Pazhouhandeh et al. 2011). The CUL4-DDB1^{FVE} complex represses *FLC* gene activity by binding a PRC2-like complex which contains the methyltransferase CLF. Strikingly, CLF-mediated H3K27 trimethylation is also implicated in the regulation of *MAF4* expression (Jiang et al. 2008; Alexandre and Hennig 2008). It is difficult to decipher a putative role of *PAPS2/4* in this pathway, especially since *clf* and *cul4* mutants also exhibit increased H3K27me3 levels at the *FT* locus. Thus, both *clf* and *cul4* flower early due to high *FT* expression in spite of simultaneously high *FLC* expression (Pazhouhandeh et al. 2011; Jiang et al. 2008). While such a phenomenon has not been observed in *paps2/4*, moderately reduced *FVE* and/or *CLF* levels might still be responsible for the upregulation of *FLC* and putatively *MAF4*.

4.6 *PAPS1* and *PAPS2/4* are involved in the regulation of different stress response pathways

Since *PAPS2* and *PAPS4* were found to be upregulated during diverse stress treatments (**Fig. 38, Fig. 39**), a number of stress tests were performed to learn more about the specific cPAPs functions in *Arabidopsis*. Unexpectedly, the *paps2/4* mutants did not exhibit hyper-resistance or hyper-sensitivity during osmotic or salt stress, cold stress or drought (chapter 3.2.2). Several RNA-seq data suggested a regulatory function of these two cPAPs in the response to biotic stress, but *paps2/4* did not display specific reactions to treatments with a bacterial or a fungal elicitor. In particular the upregulation of *PAPS4* under hypoxia implicated that this cPAP has an essential function in the response to oxygen depletion stress. Surprisingly, the *paps2*, *paps4* and *paps2/4* mutants did not react with specific sensitivity or resistance to hypoxia, submergence or even complete anoxia (**Fig. 40, Fig. 41**). Instead, the double mutants exhibited sensitivity to oxidative stress induced by methyl viologen (**Fig. 44**), which will be discussed in the next chapter.

The comparison of deregulated genes in *paps2/4* with published transcriptome data sets indicated an involvement of *PAPS2* and *PAPS4* in short-term stress regulation (**Table 8**). Amongst others, plants treated with cold, heat or drought for 15 minutes or for a few hours exhibited the highest opposite transcriptome overlap to *paps2/4*. This suggests that *PAPS2/4* are required for the polyadenylation of early stress-response components. Changes in the PAT size have direct consequences with regard to mRNA localisation, stability or translatability (see chapter 1.1.4). While both *PAPS1* and *PAPS2/4* might be exchangeable during long-term stress acclimation, *PAPS2/4* might specifically polyadenylate target mRNAs to adjust gene expression immediately upon stress perception. In mammals, functional consequences of PAT size changes of specific mRNAs during stress were shown. Hyperadenylation of mRNAs in response to viral or abiotic stress is triggered by cytoplasmic poly(A) binding proteins that move to the nucleus upon stress perception (Kumar and Glaunsinger 2010). The hyperadenylated mRNAs are retained in the nucleus and thus cannot be translated. Similar mechanisms are conceivable in plants, since the polyadenylation machineries of animals and plants exhibit analogous compositions (see chapter 1.1.1). Since prompt cellular stress acclimations are not reflected at the phenotypic level, the expression level of indicator genes should be checked in *paps2/4* directly after the beginning of the stress treatment.

Alternatively, the extensive changes in the *paps2/4* transcriptome might result in a compensatory reaction to stress. *Arabidopsis* plants in which both ascorbate peroxidase and catalase mRNAs are targeted for decay by antisense constructs are less sensitive to oxidative stress than the respective single antisense mutants (Rizhsky et al. 2002). The double antisense mutants exhibited a compensation response due to certain metabolic adjustments that were not induced in the single mutants. Apparently, plants can adapt to the loss of certain cellular components required for a stress

response by inducing alternative defence pathways (Foyer and Noctor 2005). Again, testing the expression level of certain stress marker genes might give insights into the molecular processes altered in *paps2/4*. Since the abundance of the majority of stress-related genes does not change in *paps2/4* (**Table 7**), these two isoforms might indeed polyadenylate only few early downstream stress-response genes that are responsible to fine tune the plant tolerance or resistance to environmental stimuli.

In contrast to *paps2/4*, several stress-related phenotypes of the *paps1* mutants have been uncovered in this thesis. In accordance to the strong overlap of deregulated genes in *paps1-1* with the transcriptome of cold-treated plants, the loss of *PAPS1* activity causes enhanced sensitivity to prolonged cold (**Fig. 43**). Moreover, *paps1-1* seedlings did not survive a vernalization treatment. Since the MASTA analysis was performed with genes that exhibited altered PAT sizes in *paps1-1,* the detected phenotype validates the large-scale mRNA fractionation as a means to identify specific *AtPAPS* functions. Cold is an important environmental factor limiting plant growth, and plants developed a variety of strategies to acclimate to unfavourably low temperatures (reviewed e.g. by Theocharis et al. 2012; Huang et al. 2012). Upon cold perception, signalling cascades involving alterations of the intracellular calcium and ROS levels are induced. A variety of cold-responsive transcription factors are expressed. The membrane composition changes and cellular protectants are synthesized. Lastly, plant metabolism and photosynthesis are adjusted to chilly temperatures. Since *paps1-1* seedlings bleached during the cold-treatment, metabolic acclimations might be defective. Putative *PAPS1*-target genes might be detected among the genes that exhibit a differential tail size in *paps1-1* and overlapped with the transcriptome of cold-treated plants in the MASTA analysis. Indeed, all of the 46 genes deregulated in *paps1* and overlapping in their expression patterns with the transcriptome of cold-treated plants exhibit shorter A-tails in the mutant (Kappel et al. submitted). Of these genes 37 are upregulated and nine are downregulated by cold. The expression level of interesting candidate genes should be determined in the *paps* mutants under standard and cold conditions. After all, the cold experiment should be repeated with alternative *paps1* alleles, since the mutant PAPS1 protein expressed in *paps1-1* exhibits heat sensitivity. Although to our knowledge no study has been published so far in which a heat-sensitive protein also exhibits cold-sensitivity, a growth defect due to further reduction of PAPS1 activity should be excluded.

Compared to Col-0, the *paps1-4* mutant exhibited increased resistance to mannitol (**Fig. 42**). Thus, a novel function of *PAPS1* in the response to osmotic stress was uncovered. Mannitol-induced drought and high salt concentrations partially lead to similar cellular reactions (Knight et al. 1997), but *paps1* was not found to be more resistant to NaCl than the wild type (not shown). However, only the germination rate on salt-containing media was tested. In the mannitol experiment, the determination of the fresh weight gave more reliable insights regarding the hyper-resistance

phenotype of *paps1*. Moreover, the *paps1* reaction to drought stress by water depletion should be tested. The observation of a cross-tolerance might facilitate the search for specific components that depend on polyadenylation by *PAPS1*. Intriguingly, cold, drought and salt stress are partially regulated via common signalling pathways since these stress types evoke cellular dehydration (Knight and Knight 2001; Huang et al. 2012). Certain MAP kinases have been shown to be upregulated by both low temperatures and osmotic stress (Ichimura et al. 2000). However, since *paps1* mutants are less resistant to cold and more resistant to osmotic stress, probably specific downstream components of the individual pathways are deregulated rather than common upstream factors. Notably, stress-related genes containing the dehydration-responsive element (DRE) are responsive to a class of transcription factors named DRE-binding proteins (DREB) (Huang et al. 2012). Since DREB are differentially responsive to cold and drought, the expression levels and PAT sizes of these factors should be checked in *paps1*.

4.7 *PAPS1* and *PAPS2/4* regulate the response to oxidative stress in different pathways

Since the *CPSF30* mutant *oxt6* exhibits unspecific resistance to oxidative stress (Zhang et al. 2008), the response of *paps* mutants to increased ROS release in the cytoplasm or the chloroplast was examined (**Fig. 44**). Interestingly, the *paps1-1* mutant behaved very similar to ROS stress like *oxt6*. Double mutants of *paps1-1* and *oxt6* are not viable, which indicates that both *PAPS1* and *CPSF30* might act in a common pathway to negatively regulate the reaction to ROS stress in the wild type. In accordance, the bulk of alternatively polyadenylated genes and transcripts with altered abundances in *oxt6* exhibited significantly shorter PAT sizes in *paps1* (Kappel et al. submitted).

In contrast, *paps2/4* mutants reacted sensitively to ROS-stress induced by MV and *paps2/4 oxt6* triple mutants had an intermediate phenotype. Apparently, *PAPS2/4* act in a different pathway independently from *CPSF30* to promote resistance against oxidative stress generated in the chloroplast. The fact that *paps1* reacts to both MV and BSO/AT, while *paps2/4* only shows a differential phenotype in response to MV confirms that the chemicals induce ROS-production only in the specific cell compartments.

The loss of *PAPS1* and *PAPS2/4* has a great influence on ROS sensitivity and the question arises whether a direct detoxification mechanism or a signalling pathway requires specific cPAP activity in *Arabidopsis*. It is tempting to speculate that the cPAPs polyadenylate specific stress-related genes in response to elevated ROS levels. For *paps1* mutants, a transcriptome correlation was detected with plants overexpressing *tAPX* (chapter 3.2.4, Kappel et al. submitted). This enzyme scavenges H_2O_2 in the chloroplast. Most of the genes overlapping between the two mutant transcriptomes are more strongly induced, which indicates that these genes are usually repressed by H_2O_2 in the wild type. The redox status of *paps1* was tested with a redox-sensitive form of GFP that was specifically

expressed in the cytosol or the chloroplast (Kappel et al. submitted). While the cytosolic redox state was not altered compared to wild type, a more oxidizing environment was discovered in the chloroplast. However, no elevated H_2O_2 levels were detected in *paps1* leaves using 3,3'-Diaminobenzidine (DAB) staining (Trost et al. 2014). Thus the molecular changes induced by the loss of *PAPS1* seem to be more intricate.

As outlined in the introduction (chapter intro 1.3.2), diverse antioxidant components and enzymes are constantly being produced by plant cells. In the chloroplast, efficient ROS detoxification by ascorbate and reduced glutathione is essential to ensure optimal photosynthetic efficiency (Foyer and Shigeoka 2011). Thioredoxin reductases are implicated in cytosolic and mitochondrial ROS scavenging (Meyer et al. 2009). Some components required for these cyclic detoxification networks might directly depend on polyadenylation by a specific cPAP, especially regarding the unspecific ROS resistance exhibited by *paps1-1*. The loss of *CPSF30* results in a defective expression of a subset of thioredoxin- and glutaredoxin-related factors (Zhang et al. 2008). However, none of these genes was deregulated in the *paps* mutants (not shown).

Alternatively, certain redox-responsive signalling components might be defective in the *paps* mutants. The molecular acclimations of plants in response to ROS stress are highlighted in chapter 1.3.2. The ROS-induced signal transduction could be impaired in both *paps1* and *paps2/4* mutants, although the defects would have to affect factors of opposite functions. Regarding the very specific growth defect of *paps2/4* that is only observed during paraquat-induced ROS-production in the chloroplast, a defective downstream factor in the signalling chain depending specifically on polyadenylation by *PAPS2/4* seems likely. Accordingly, the bulk of stress-related genes was not significantly deregulated in the *paps2/4* transcriptome (**Table 7**). Since the mutant transcriptomes were determined under standard growth conditions and in particular *pap2/4* mutants do normally not show phenotypic abnormalities, an analysis of gene expression changes in the *paps* mutants during the oxidative stress treatment could reveal further *PAPS*-dependent molecular mechanisms (Laloi et al. 2007).

The question remains how *PAPS1* and *CPSF30* might act together. A direct binding of *CPSF30* and *PAPS1* has not been shown so far. Instead, a yeast-two-hybrid based screen for direct protein interactions of *Arabidopsis* 3' end processing factors revealed an interaction of *CPSF30* with *PAPS2* and *PAPS3* (Hunt et al. 2008). However, since promoter studies revealed that these two cPAPs are almost not expressed in *Arabidopsis* leaves (Meeks et al. 2009), the physiological role of this interaction seems negligible. The unique features of *CPSF30*, described in chapter 1.3.3, turn this polyadenylation factor into a putative sensor of ROS and other environmental stimuli that simultaneously influences APA. The activity of both the short and the long CPSF30 protein isoform might not only be influenced by the cellular redox or calcium states, but also by interacting proteins.

Several CPSF30 binding partners have been identified in *Arabidopsis*. It has been shown that CPSF30 binds Fip1 (also termed AtFIPS5) (Forbes et al. 2006). Fip1 acts as a bridge to other polyadenylation factors, to the nuclear poly(A) binding protein and to PAPS itself (Forbes et al. 2006; Hunt et al. 2008). Conformational changes or changes in the CPSF30 activity might influence the PAS choice of the polyadenylation complex, and potentially even the poly(A) tail length, although altered tail lengths were not observed in the *oxt6* mutant. Moreover, AtCPSF30 can interact with itself, and the formation of homodimers or heteromeric complexes of both CPSF30 variants in response to certain impacts might change features of the whole polyadenylation complex (Delaney et al. 2006; Zhao et al. 1999). *PAPS*-specific target mRNAs supposedly contain distinct *cis* elements (described in chapter 1.1.1), which might be detected by specifically composed complexes. Thus, although PAPS1 and CPSF30 do not directly interact, their functions are intimately linked at the level of mRNA processing and a molecular bridge could be provided by other polyadenylation factors.

So far, not much is known about the putative functions of the long CPSF30-YT521-B protein (**Fig. 13**). As mentioned above, the C-terminal protein domain is highly similar to a human splicing factor. The mammalian YT521-B homologue is involved in pre-mRNA splicing and binds other regulatory proteins, e.g. other splicing factors (Stoilov et al. 2002). In other words, the long polypeptide encoded by the *CPSF30* gene combines RNA-binding activity, and all CPSF30 protein features described above with the potential regulation of splicing (Xing and Li 2011). Proteins containing YTH-domains (for *YT*521-B *h*omology) are abundant in plants (Stoilov et al. 2002), but only one yeast YTH protein has been identified so far. The yeast YTH protein Pho92 is not involved in splicing but decreases the stability of an mRNA via interaction with a deadenylase complex (Kang et al. 2014). Pho92-binding to the 3’ UTR of its target decreases the mRNA half-life, probably due to PAT degradation. Interestingly, Pho92 is responsive to intracellular phosphate levels. Thus, the YTH-domain protein Pho92 putatively functions in 3’ processing and is responsive to certain cellular stimuli. These findings indicate the regulatory potential of CPSF30-YT521-B and it is only a matter of time until this protein will be investigated more in detail.

Lastly, the AtPAPS protein levels might be altered in response to certain environmental stimuli, which might have consequences regarding the PAT length of PAPS-specific target mRNAs. As outlined above (chapter 1.1.2), abundance changes of certain factors influence the PAS choice and thus mRNA fate. Indeed, cPAPs are targeted by diverse protein modifications, which might result in activity changes or in altered protein binding capacities. Putative changes of PAPS abundances could be traced with the homozygous offspring of *pPAPS::PAPS:YFP*-expressing lines.

5. Conclusion

The detailed analysis of *Arabidopsis paps* mutants revealed novel and specific functions of two different canonical poly(A) polymerase subsets in plants. *PAPS1* is implicated in the repression of flowering by activating the main flowering inhibitor *FLC*. In contrast, the two redundant cPAPs *PAPS2* and *PAPS4* promote flowering in a novel regulatory pathway downstream of *FCA*. To repress *FLC* and other flowering inhibitors, *PAPS2/4* probably polyadenylate factors involved in transcriptional downregulation, like chromatin remodelling factors. It could not be excluded that *PAPS2/4* ensure timely flowering by modulating the abundance of *COOLAIR* transcripts which have been implicated in the regulation of both the autonomous pathway and vernalization before.

Moreover, the loss of *PAPS1* activity confers plant resistance to osmotic and oxidative stress and simultaneously results in cold sensitivity. *PAPS2/4* are required to maintain a balanced redox state by promoting ROS detoxification in the chloroplast and probably regulate early cellular stress responses. The individual *paps* mutant phenotypes provide new evidence for an additional layer of gene regulation based on *PAPS*-specific polyadenylation of selected mRNAs in response to internal and environmental stimuli. While *PAPS1* exhibits a more global role regarding plant growth, development and defence, *PAPS2/4* seem to be required for the fine-tuning of flowering and stress responses.

The exact transcripts that specifically depend on *PAPS1* or *PAPS2/4* polyadenylation in the aforementioned pathways remain elusive. In the future, a reliable assay measuring poly(A) tail lengths will be essential to confirm the models developed above. The cellular localization of two cPAPs could be confirmed with *paps* mutants that were transformed with *PAPS1*- and *PAPS4-YFP* rescue constructs. These plant lines could be used to gain further insights into changes of PAPS protein abundances during stress treatments. The existence of non-coding *PAPS4* splice forms in *Arabidopsis* indicates that furthermore an autoregulatory mechanism may be involved in balancing the cellular PAPS4 protein content. It will be exciting to reveal further details about the intricate gene regulation mechanisms based on cPAP specificity.

Since yeast encodes only one cPAP and mutations in mammalian cPAPs result in lethality, the investigation of the differential functions of poly(A) polymerase isoforms in plants provides an important addition to the research field of 3’ end processing. The polyadenylation apparatus of mammals and plants exhibit very similar compositions. It is thus conceivable that similar cPAP-based regulatory mechanisms will be revealed in other organisms in the future.

Appendix A Technical equipment

Name	Type; company (located in Germany or as indicated)
Agarose gel chambers	PerfectBlue Gel System; Peqlab Biotechnologie GmbH, Erlangen
Autoclave	3850 EL; Systec, Wettenberg
Bead dispenser	TissueLyser; Qiagen, Venlo, The Netherlends
Camera	SX220 HS Powershot; Canon, Tokio, Japan
Centrifuge	Avanti J-25; Beckman Coulter, Brea, California USA
Clean benches	Holten Lamin Air 1.8; Thermo Scientific, Waltham, USA Nuaire; Integra Biosciences GmbH, Fernwald
Confocal laser scanning microscope	LSM 710; Carl Zeiss, Jena
Cooling centrifuge	5417R; Eppendorf AG, Hamburg
Electroporation apparatus	Micropulser; Bio-rad Laboratories; Hercules, USA
Fluorescence Microscope	BX51; Olympus, Tokio, Japan
Gas monitoring system	LI-800 Gas Hound Analyzer; LI-COR, Lincoln, Nebraska USA Microx TX2; PreSens Precision Sensing GmbH, Regensburg
Gel documentation system	BioDocAnalyze; Biometra, Göttingen
Homogenizer	RZR2020; Heidolph/ Heidrive, Kelheim
Incubator/ shaker	Ecotron; Infors HT, Bottmingen, Schweiz
Laboratory high-accuracy scale	AB104-S; Mettler-Toledo GmbH, Gießen
Laboratory scales	BL150S, BL6100; Sartorius, Göttingen
Laser-scanning microscope	LSM510 Axioplan2; Carl Zeiss, Jena
Light Sensor	Lightscout #3415FX Light Sensor Reader; Spectrum Technologies, Inc., Aurora USA
Magnetic stand, 6 Tube	AM10055; Applied Biosystems, Foster City, CA, USA
Magnetic stirrer	heat-stir SB162; Stuart, Stone, Staffordshire, UK
Mini Centrifuge	Biofuge pico; Heraeus GmbH, Hanau
Mixer mill	Mixer mill MM301; Retsch GmbH, Haan
PCR Machines	PTC200; MJ Research, St. Bruno, Quebec, Canada Mastercycler nexus eco, Mastercycler pro 384; Eppendorf AG; Hamburg
pH meter	pH210; Hanna instruments, Kehl am Rain
Pipettes	Eppendorf AG; Hamburg
Plant incubator	Percival incubator; Percival, Perry, USA
Plate centrifuge	4K15; Sigma Laborzentrifugen GmbH, Osterode im Harz
Plate rotator	KS 260 basic; IKA-Werke, Staufen
Power supplies	MP-300V; Major Science, Saratoga, CA, USA
SDS-PAGE system	Mini-Protean Tetra System; Bio-rad Laboratories, Hercules, USA
Spectrophotometer	Pico100; Biozym Scientific GmbH; Hessisch Oldendorf
Stereo microscope	Stemi 2000-C; Carl Zeiss, Jena
Table centrifuge	Biofuge pico; Heraeus GmbH, Hanau
Thermomixer	Thermomixer comfort; Eppendorf
Tube rotator	SB3; Stuart, Stone, Staffordshire, UK
UV transilluminator	UVstar 312 nm; Biometra, Göttingen
Vacuum drying oven	VD 115; Binder GmbH, Tuttlingen
Vortex	Vortex Genie 2; Scientific industries, Bohemia, NY, USA
Western Blot Visualization System	NightOWL LB 983 NC100; Berthold Technologies GmbH & Co. KG, Bad Wildbad
Wet-Blot Apparatus	Mini Trans-Blot Cell; Bio-Rad Laboratories, Hercules, USA

Appendix B Disposable equipment

Disposable product	Company (located in Germany or as indicated)
96-well PCR plates, 0.2 ml	ABgene, Epsom Surrey, UK
96-well plates, 1.2 ml (Collection microtubes, racked) and cap strips	Qiagen GmbH, Hilden
384-well PCR plates	Applied Biosystem
384-well qPCR plates for LC480	Biozym Scientific GmbH; Hessisch Oldendorf
Blotting paper (Rotilabo®; strength 0.35 mm)	Carl Roth, Karlsruhe
Cell culture dishes Ø 100 mm	Sarstedt, Nümbrecht
Cell culture dishes 100 × 100 mm	Greiner Bio-One GmbH, Frickenhausen
Combitips plus, 0.1 – 0.2 ml	Eppendorf, Hamburg
Electroporation cuvettes (1 or 2 mm gap)	PeqLab Biotechnologie GmbH, Erlangen
Glass beads, unwashed, ≤106 µm (glass sand)	Sigma-Aldrich, St. Louis, USA
Inoculating loops	Carl Roth, Karlsruhe
Metal beads 0.25 mm	Carl Roth, Karlsruhe
Nitrocellulose membrane (Roti-NC©; 0.2 µm pore size; 0.15 ± 0.05 mm membrane strength)	Carl Roth, Karlsruhe
Parafilm® M	Bemis, Neenah, WI, USA
PCR-Softstrips 0.2 ml	ABgene, Epsom Surrey, UK
Pipette tips, with or without filter (Tipone system)	Starlab GmbH, Hamburg
Polypropylene tubes 50 ml	VWR, Radnor, PA, USA
Polypropylene tubes 15 ml	VWR, Radnor, PA, USA
Reaction tubes (1.5 ml/ 2 ml)	Sarstedt, Nümbrecht
Sealing-film for PCR	ABgene, Epsom Surrey, UK
Sealing-film for 384-well qPCR plates for LC480	Biozym Scientific GmbH; Hessisch Oldendorf
Serapore adhesive tape, breathable	Seradem GmbH, Krefeld
Silicone compression mats for PCR	Kisker Biotech GmbH & Co. KG, Steinfurt
Soil, *P-Erde* and *T-Erde*	Gebrüder Patzer, Einheitserde, Sinntal-Altengronau
Sterile filters (0.2 µm pore size)	Whatman Schleicher & Schuell, München
Syringes	B. Braun Melsungen AG, Melsungen
UVpette P10 pipette tips	Biozym Scientific GmbH, Hessisch Oldendorf
Vermiculite	Kausek GmbH, Mittenwalde

Appendix C Oligonucleotide list

Code	Name (Reference)	Sequence (5‘-3‘)
GTO27	pSV1c_seq_P1_fw	GGAAACCAAGTGATTGAGCAGA
GTO28	pSV1c_seq_P2_rev	GTAGAGAGTAATTTAGCATATAGCAT
GTO40	SALK Lba	TGGTTCACGTAGTGGGCCATCG
GTO41	cstf64.fw	ATTCAGATTAGTTACGGATAGAGA
GTO42	cstf64.rev	ACGGGTTTTGTCAGTGC
GTO379	30A_YFP_fw	GGACGACGGCAACTACAAGA
GTO380	30A_YFP_rev	GAACTCCAGCAGGACCATGT
GTO381	75A_35s_fw	CGACACGCTTGTCTACTCCAA
GTO382	75A_35s_rev	GAAGGATAGTGGGATTGTGCG
GTO383	134A_AlcA_fw	CTTCGGGATAGTTCCGACCT
GTO384	134A_AlcA_rev	CGTCCTCTCCAAATGAAATGA
GTO370	PAP13-Genotyping	TTGGCAATGTAGGGAAAAGC
HBo6	T7	TAATACGACTCACTATAGGG
HBo84	PDF2-qPCRfor	GCATTTCACTCCTCTGGCTAAG
HBo85	PDF2-qPCRrev	GGCACTTGGGTATGCAATATG
MLo1076	paps1-4_geno_L	CCAGTTGATGGGAAGAAGAGAAAA
MLo1077	paps1-4_geno_R	CTTCGAATGGAGGTATAGTTGCAGTA
oHC1	FLC_cDNA_393F	AGCCAAGAAGACCGAACTCA
oHC2	FLC_cDNA_550R	TTTGTCCAGCAGGTGACATC
oHC5	SK-003080_LP	ACACCACTGTGAGCCTCTTTG
oHC6	SK-003080_RP	ATGAGAAAAATGAATTGGGGG
oHC7	SK-117078_LP	CCCGAAACCCTGTAAAAACTC
oHC8	SK-117078_RP	AGATTTATTGGCTTGGAAGGG
oHC14	FT_qRTF	ACAACTGGAACAACCTTGGCAATGAG
oHC15	FT_qRTR	CCTCCGCAGCCACTCTCCCTCTG
oHC16	SOC1_qRTF	AGCTCTCTGAAAAGTGGGGATCTCAT
oHC17	SOC1_qRTR	TTTCTTGAAGAACAAGGTAACCCAATG
oHC18	LFY_qRTF	TGCCCCACCAAGGTGACGAACC
oHC19	LFY_qRTR	TTCTTCGTCTAGGCAGTGGAGAGCGT
oHC20	AP1_qRTF	AGGGAAAAAATTCTTAGGGCTCAACAG
oHC21	AP1_qRTR	CTTCTTGATACAGACCACCCATGTTGA
oHC23	FLC_AS_qRTF (Hornyik et al. 2010)	CTCGATGCAATTCTCACACG
oHC24	FLC_AS1_qRTR (Hornyik et al. 2010)	TCCTTGGATAGAAGACAAAAAGAGA
oHC25	FLC_AS2_qRTR (Hornyik et al. 2010)	TTCTCCTCCGGCGATAAGTA
oHC32	SVP_qRTF (Li et al. 2008)	CAAGGACTTGACATTGAAGAGCTTCA
oHC33	SVP_qRTR (Li et al. 2008)	CTGATCTCACTCATAATCTTGTCAC
oHC38	flc5_DCAP_40R	AACCATAGTTCAGAGCTTTTGACTGAAGATC
oHC39	flc5_19+F	TTAAAGCCTTGGTAATACAAACATT
oHC48	SK-081180_LP	CATCAACATGCAAACAAGCAC
oHC49	SK-081180_RP	AGGGACTCTACGAGAGCAAGG
oHC55	FY4	CTGTTGGAAAGGGTTGTTGTAGCCTGGAATC
oHC56	LB3	TAGCATCTGAATTTCATAACCAATCTCGATACAC
oHC57	CL_FRI_10	CAT GTC GTA ATC ATG CAA CC
oHC58	UJ43_FRI prom	GAA GAT CAT CGA ATT GGC
oHC76	FY_exon16_fw	GAACAAGGTTTTGGTCGC
oHC101	GSO379	TGTTGAGATGGTGAAACTGTG
oHC102	Rlfca9	TCTTTGGCTCAGCAAACC
OHC-112	NotI-linker-vYFP_ORF_fw	CTACTAGCGGCCGCCCCAGGAGCAGGAGCAGGAG CAGGAGC
OHC-113	vYFP-Stop-NotI_rev	TAGTAGGCGGCCGCTTATAACTTGTACAGCTCGTC CA
OHC-114	PAP4_P1_fw	CTGTGTTATAACTTGCCTTGTG
OHC-115	PAP4-NotI_P3_rev	GCCTAGAGGACGTTCAGGCGGCCGCCACAGTGGA CTTTAAGCTTAACC

OHC-116	NotI-PAP4_P4_fw	GCGGCCGCCTGAACGTCCTCTAGGCTATTG
OHC-117	pSV5a_P2-rev	AAAAACGAGAGACAAGGAGGC
OHC-118	PAP4-NotI_P5_rev	TCCATATTAAAAATTCACTTAGGCGGCCGCCCAAA AGCTTCTGGACTCTGTCG
OHC-119	NotI-PAP4_P6_fw	GCGGCCGCCTAAGTGAATTTTTAATATGG
oHC121	p745	AACGTCCGCAATGTGTTATTAAGTTGTC
oHC127	AT1G19180_PAT	GTTATTGTCGCCTGTCTAAATCC
oHC128	AT1G72450_PAT	ACGATCGAGTTCACGTTTCTAG
oHC136	AT2G18700_PAT	ACAATGTCGAAAGAAAGCATAG
oHC161	FLC_transposon_rev (Gazzani et al. 2003)	AAACAATCTGGACAGTAGAGGCTTAT
oHC162	FLC_transposon_fw (Gazzani et al. 2003)	CAGGCTGGAGAGATGACAAAA
oHC163	FLC_30bp repeat_fw (Gazzani et al. 2003)	AAATGTAAGCCACATTAATTGGGAAA
oHC164	FLC_30bp repeat_rev (Gazzani et al. 2003)	ATTAAATCATAATTAAGACCAGGAG
OHC-165	NPT-5′ (Zhang et al. 2008)	CCTGTCCGGTGCCCTGAATG
OHC-167	At1g30460_oxt6_fw	GAGGATGCTGATGGACTTAG
OHC-168	At1g30460_oxt6_rev	AATCCTGCTCTCGACATTC
oHC187	MAF2 var1_qRTF (Rosloski et al. 2013)	TAGAAATAGTCCAAAGCAAGCTTGAAGAATC
oHC188	MAF2 var1_qRTR (Rosloski et al. 2013)	CGTCTACGAAGGTACAATAAAGATCTACTAT
oHC189	MAF2 var2_qRTF (Rosloski et al. 2013)	TAGCACAAAGACACTTTTATCTCCCTC
oHC190	MAF2 var2_qRTR (Rosloski et al. 2013)	CTATAACCAGAAACGTCTTCTTCCC
oHC191	FLC-3436.R	GCGTCGTGGAAGATGTGTAACTC
oHC192	FLC-3569.F	GTCAAAACTCAAGCCTCAAAACC
oHC204	3045-FY qPCR-F1 (Feng et al. 2011)	TCGTCAGCTTCTTCCACTAACATC
oHC205	3046-FY qPCR-R1 (Feng et al. 2011)	GTGTATGCTTTCTCATTCGTTTCG
oHC212	FLM-β_G-30796 (F2) (Posé et al. 2013)	CATGCTGATGAACTTAGAGCCTTAGATC
oHC213	FLM-β_G-28156 (R2) (Posé et al. 2013)	CAGCAACGTATTCTTTCCCAT
oHC214	FLM-δ_G-28150 (F2) (Posé et al. 2013)	GATAGAAGCGCTGTTCAAGC
oHC215	FCAγ-RT-PCR-F	GCTCTTGTCGCAGCAAACTC
oHC216	FCAγ-RT-PCR-R	GATCCAGCCCACTGTTGTTT
oSV110	At4g32850_5R	TGCATCTGCTGCCACTATATC
oSV111	At4g32850_6F	TTGCTGAAGCTGTAGGGTCTG
oSV120	SK126395_LP	ACATGGAGATGTTGAACTGCC
oSV121	SK126395_RP	CCACTGTTCCACGTATATCAAAC
	universal PAT	Affymetrix Poly(A) Tail-Length Assay Kit

Appendix D Oligonucleotide combinations

Experiment	Method chapter	Gene or allele	Oligonucleotide combination (+ restriction endonuclease, if CAPS/dCAPS marker)	T_m [°C]	product sizes [bp]
Genotyping of polyadenylation factor mutants	2.4.10	OXT6, WT allele	oHC167 + oHC168	60	319
		oxt6	oHC165 + oHC167	60	4000
		paps1-4	MLo1076 + MLo1077 + oHC121	60	388 (WT)
		paps2-3	oSV120 + oSV121 + GTO40	60	1348 (WT)
		paps2-6	oHC5 + oHC6 + GTO40	60	1168 (WT)
		paps4-1	oCH48 + oHC49 + GTO40	60	1061 (WT)
		paps4-2	oSV110 + oSV111 + oHC121	60	1130 (WT)
		paps4-3	oSV110 + oSV111 + GTO40	60	1070 (WT)
		paps4-4	oHC7 + oHC8 + GTO40	60	1125 (WT)
		paps4-5	oHC7 + oHC8 + GTO40	60	1125 (WT)
Genotyping of flowering time mutants; Discriminating FRI^{Col-0} and FRI^{Sf-2} (Johanson et al. 2000)	2.4.10, 2.4.18	*35S::FCAγ*	oHC63 + oHC68	58	461
		FRI, 16 bp indel	oHC59 + oHC60	58	208; 224
		FRI, promoter	oHC57 + oHC58	58	250; 550
		fy-2	oHC55 + oHC56 + oH76	58	500; 800
		cstf64-1	GTO41 + GTO42 (Hpy188I)	58	175; 100 + 75
Discriminating FLC^{Col-0} and FLC^{Ler} alleles (Gazzani et al. 2003)		*fca-9*	oHC101 + oHC102 (StyI)	58	~230; ~200 + 30
		flc-2	oHC191 + oHC192 (WT band; no amplification in flc-2)	60	~150
		flc-5	oHC38 + oHC39 (BglII)	58	220; 200 + 20
		FLC, 30 bp-repeat	oHC163 + oHC164	60	342; 372
		FLC, transposon	oHC161 + oHC162	60	570; 1740
qPCR analysis of flowering time genes with *Arabidopsis* cDNA	2.4.12	*AP1*	oHC20 + oHC21	60	163
		COOLAIR class I	oHC23 + oHC24	60	402
		COOLAIR class II	oHC23 + oHC25	60	171
		FCAγ	oHC215 + oHC216	60	159
		FLC	oHC1 + oHC2	60	222
		FLMβ	oHC212 + oHC213	60	290
		FLMδ	oHC213 + oHC214	60	312
		FT	oHC14 + oHC15	60	230
		FY	oHC204 + oHC205	60	106
		LFY	oHC18 + oHC19	60	123
		MAF var1	oHC187 + oHC188	60	527
		MAF var2	oHC189 + oHC190	60	296
		PDF2	HBo84 + HBo85	60	97
		SOC1	oHC16 + oHC17	60	145
		SVP	oHC32 + oHC33	60	104
Poly(A) tail test	2.5.6	*At1g19180*	oHC127 + universal PAT	60	282
		At2g18700	oHC136 + universal PAT	60	233
		At1g72450	oHC128 + universal PAT	60	257
qPCR analysis of fractionation control RNAs	2.5.8, 2.4.12	*YFP::29A*	GTO379 + GTO380	60	367
		35S::75A	GTO381 + GTO382	60	357
		AlcA::124A	GTO383 + GTO384	60	296

Appendix E Cloning strategy and vector list

Methods used for cloning

Vectors used and produced are listed in **Table 10**. Specific fragments were amplified by PCR (chapter 2.4.7) using the oligonucleotide combinations listed in **Table 9**. Oligonucleotide sequences can be found in Appendix C. The Phusion High-Fidelity DNA Polymerase (NEB) was used for all PCRs. Two PCR products were fused by fusion PCR (chapter 2.4.9). PCR fragments were subcloned into pGEM-T via ligation (chapter 2.4.20). *E. coli* (strain XL-1) was transformed with dilutions of vectors or with ligation mixes (chapter 2.7.2). The protocol to produce electrocompetent bacteria is described in chapter 2.7.1. Bacteria colonies containing the transgene were selected by colony PCR (chapter 2.4.8). Vectors were amplified in *E. coli* and purified by mini prep (chapters 2.4.3, 2.4.5). DNA sequences were controlled with specific oligonucleotides (chapter 2.4.21) and analysed using Vector NTI (chapter 2.13). Restriction digests were performed to linearise vectors or to cut fragments from vectors (chapter 2.4.17). The resulting fragments were purified via agarose gels (chapter 2.4.15). Linearised vectors were dephosphorylated to avoid self-ligation. The binary low-copy vectors were amplified via midi prep (chapter 2.4.4). Following a transformation of *Agrobacterium tumefaciens* (chapter 2.7.2), colonies positive for the transgene were selected by agrobacteria colony PCR (chapter 2.4.8). These clones were used to transform *Arabidopsis* (chapter 2.7.3).

Cloning of the construct *pPAPS1:PAPS1::vYFP* and plant transformation

The *PAPS1* promoter (*pPAPS1*) and the full-length *PAPS1* gene had been cloned by cloned by Lang Son Vi (PhD thesis). By site-directed mutagenesis, an NcoI restriction site had been inserted behind the stop codon by Gerda Trost (unpublished), resulting in the vector pGT1a. The *venusYFP* sequence (*vYFP*; 750 bp) was amplified from the vector ML850 with the primers oHC112/oHC113 which added NotI restriction sites to both 3' and 5' end of *vYFP*. The PCR product was subcloned into pGEM-T, resulting in pHC31. The *vYFP* sequence was checked using the T7 primer. Both pHC31 and pGT1a were digested with NcoI and pGT1a was dephosphorylated. The *vYFP* fragment was ligated into pGT1a, resulting in the vector pHC26. *E. coli* colonies positive for the transgene were identified using primers oHC112/oHC113. The correct insertion of *YFP* in pHC26 was checked by sequencing the plasmid with primers GTO27, GTO28 and GTO370. The complete *pPAPS1:PAPS1::YFP* construct was cut out of the vector using the restriction endonuclease AscI. The fragment mix was separated on an agarose gel and the fragment of the correct size was purified. The vector ML1231b was linearised with AscI and dephosphorylated. The *pPAPS1:PAPS1::YFP* construct was ligated into ML1231b, resulting in the vector pHC32. Positive *E. coli* clones were selected by colony PCR with the primers oHC112/oHC113. The vector was amplified by midi prep and transformed into agrobacteria (strain

GV3101). Clones positive for the transgene were used to transform heterozygous *Arabidopsis paps1-3* mutants. Positive *paps1-3* transformants were selected using Km (to select for the vector) and BASTA (to select for the mutant *paps1-3* allele).

Cloning of the constructs *pPAPS4:PAPS4.5::vYFP* and *pPAPS4:PAPS4.8::vYFP* and plant transformation

The *PAPS4* promoter (*pPAPS4*) and the full-length *PAPS4* gene had been cloned by cloned by Lang Son Vi (PhD thesis) and were present in vector pSV5. First, a NotI restriction site was introduced 5' to the stop codon present in *PAPS4* splice form *At4g32850.5* and 5' to the stop codon present in *PAPS4* splice form *At4g32850.8* via site-directed mutagenesis. Unique restriction sites flanking the *PAPS4* stop codon were identified (5': BsgI; 3' PshAI). Primers were designed to individually amplify the fragments between the respective restriction site and the stop codon and to simultaneously add a NotI site 5' to the stop codon. The individual fragments were amplified in SDM-PCR1 to SDM-PCR4 (**Table 9**) using pSV5 as a template. Subsequently, the fragments were fused by PCR. In SDM-PCR5, the PCR products from SDM-PCR 1 and 2 or the PCR products from SDM-PCR 3 and 4 were both used as a template to amplify the complete construct including the new restriction site 5' to the stop codon for both *PAPS4* splice forms (BsgI-site:: *At4g32850*::NotI-site::stop-codon::*At4g32850*::PshAI-site). The constructs were purified, subcloned into pGEM-T and sequenced with the T7 primer. Constructs with the correct sequence were cut out of pGEM-T by BsgI and PshAI. Simultaneously, pSV5a was digested with these two enzymes and the backbone fragment of the correct size was purified. The construct ligation into pSV5a resulted in the vectors pHC27 and pHC28. The correct insertion was confirmed using the primers oHC114 and oHC117. Next, pH27, pHC28 and pHC31, which included *vYFP* between two NotI restriction sites, were digested with NotI. pHC27 and pHC28 were dephosphorylated and *vYFP* was ligated into both vectors, resulting in the vectors pHC29 and pHC30. The complete constructs were cut out of pHC29 and pHC30 with AscI and were ligated into pAS25. Agrobacteria (strain GV3101) were transformed with the resulting vectors pHC35 and pHC36 and clones tested positively for the transgene by colony PCR were used to transform *Arabidopsis paps4-3* and *paps2-3 paps4-3* mutants. Plant transformants were selected with PPT.

Table 9 Oligonucleotide combinations used for cloning.

Experiment	Gene or allele	Oligonucleotide combination	T_m [°C]*	product size [bp]	Method chapter
Amplification of NotI-site::*vYFP*::NotI-site	*venusYFP*	oHC112 + oHC113	58	794	2.4.7
SDM-PCR1	*At4g32850*	oHC114 + oHC115	62	344	
SDM-PCR2	splice form 5	oHC116 + oHC117	62	468	
SDM-PCR3	*At4g32850*	oHC114 + oHC118	62	438	
SDM-PCR4	splice form 8	oHC117 + oHC119	62	376	
SDM-PCR5 (Fusion PCR)	*At4g32850*	oHC114 + oHC117	62	850	2.4.9

Table 10 Vector list.

Name	Vector construct	bacteria selection	plant selection	Features
ML850	pCHF10:pRPL3::RPL3-linker-vYFP-StrepII	unknown	-	Containing *YFP* connected to linker (Prolin, 4x Gly-Ala repetition)
ML939	pBlueMLPUCAP	Amp	-	Subcloning vector, multiple cloning site flanked by AscI restriction sites and PacI restriction sites
ML1231b	pBI101:XPB::pA	Km	Km	Binary vector to transform plants, low copy, containing AscI restriction site
pAS25	pBarMAP	Km	BASTA	Binary vector to transform plants, low copy, containing AscI restriction site
pGEM-T	-	Amp	-	Subcloning vector by Promega
pGT1a	AscI-site::pPAPS1::gPAPS1::NotI-site::UTR::AscI-site in ML939	Amp	-	NotI-restriction site inserted 5’ to *PAPS1* stop codon
pGT2d	pT7::YFP::29A stretch in pJill_SV1 (35s:omega removed by NcoI)	Amp	-	Used for in-vitro transcription
pGT3b	pT7::35s::omegaLeader::75A stretch::YFP in pJill_SV1 (75A_55 colony PCR1)	Amp	-	Used for in-vitro transcription
pGT5	pT7::124A inserted in pGT4 (AlcA::124A tail in pBlueML)	Amp	-	Used for in-vitro transcription
pHC26	pPAPS1:gPAP1::NotI-site::vYFP::NotI-site in pGT1a	Amp	-	*vYFP* introduced 5’ to *PAPS1* stop codon via NotI restriction site
pHC27	pSV5a::pPAPS4:gPAP4-NotI-Stop .5 in pGT1a	Amp	-	NotI restriction site 5’ to Stop codon of *PAPS4* splice form *At4g32850.5*
pHC28	pSV5a::pPAPS4:gPAPS4-NotI-Stop .8 in pGT1a	Amp	-	NotI restriction site 5’ to Stop codon of *PAPS4* splice form *At4g32850.8*
pHC29	pSV5a::pPAPS4:gPAPS4:vYFP-Stop .5 in pGT1a	Amp	-	*vYFP* insertion 5’ to Stop codon of splice *PAPS4* form *At4g32850.5*
pHC30	pSV5a::pPAPS4:gPAPS4:vYFP-Stop .8 in pGT1a	Amp	-	*vYFP* insertion 5’ to Stop codon of *PAPS4* splice form *At4g32850.8*
pHC31	pGEM-T::NotI-site::vYFP::NotI-site	Amp	-	contains *vYFP* and linker flanked by NotI-sites
pHC32	pPAPS1:gPAPS1::NotI-site::vYFP::NotI-site in ML1231b	Km	Km	binary vector with pPAPS1::gPAPS1 fused to vYFP 5’ to stop codon
pHC35	pAS25::pPAPS4::gPAPS4::vYFP-Stop.5	Km	BASTA	pBarMAP::pPAP4:gPAP4:vYFP with Stop 5’ to of splice form *At4g32850.5*
pHC36	pAS25::pPAPS4::gPAPS4::vYFP-Stop.8	Km	BASTA	pBarMAP::pPAP4:gPAP4:vYFP with Stop codon of splice form *At4g32850.8*
pSV5a	NcoI-site::pPAPS4::gPAPS4::NcoI-site in ML939	Amp	-	

References

Abràmoff MD, Magalhães PJ, Ram JS. 2004. Image Processing with ImageJ. *Biophotonics Int* **11**: 36–42.

Addepalli B, Hunt AG. 2007. A novel endonuclease activity associated with the Arabidopsis ortholog of the 30-kDa subunit of cleavage and polyadenylation specificity factor. *Nucleic Acids Res* **35**: 4453–63.

Addepalli B, Hunt AG. 2008. Redox and heavy metal effects on the biochemical activities of an Arabidopsis polyadenylation factor subunit. *Arch Biochem Biophys* **473**: 88–95.

Addepalli B, Meeks LR, Forbes KP, Hunt AG. 2004. Novel alternative splicing of mRNAs encoding poly(A) polymerases in Arabidopsis. *Biochim Biophys Acta* **1679**: 117–28.

Al Husini N, Kudla P, Ansari A. 2013. A role for CF1A 3' end processing complex in promoter-associated transcription. *PLoS Genet* **9**: e1003722.

Alexandre CM, Hennig L. 2008. FLC or not FLC: the other side of vernalization. *J Exp Bot* **59**: 1127–35.

Amasino RM. 1996. Control of flowering time in plants. *Curr Opin Genet Dev* **6**: 480–487.

Amrani N, Minet M, Le Gouar M, Lacroute F, Wyers F. 1997. Yeast Pab1 interacts with Rna15 and participates in the control of the poly(A) tail length in vitro. *Mol Cell Biol* **17**: 3694–701.

Anders S, Pyl PT, Huber W. 2014. HTSeq - A Python framework to work with high-throughput sequencing data. *Bioinformatics* 1–4.

Andrés F, Coupland G. 2012. The genetic basis of flowering responses to seasonal cues. *Nat Rev Genet* **13**: 627–39.

Angel A, Song J, Dean C, Howard M. 2011. A Polycomb-based switch underlying quantitative epigenetic memory. *Nature* **476**: 105–8.

Araus JL, Cairns JE. 2014. Field high-throughput phenotyping: the new crop breeding frontier. *Trends Plant Sci* **19**: 52–61.

Atkinson NJ, Urwin PE. 2012. The interaction of plant biotic and abiotic stresses: from genes to the field. *J Exp Bot* **63**: 3523–43.

Aukerman MJ, Lee I, Weigel D, Amasino RM. 1999. The Arabidopsis flowering-time gene LUMINIDEPENDENS is expressed primarily in regions of cell proliferation and encodes a nuclear protein that regulates LEAFY expression. *Plant J* **18**: 195–203.

Barabino SM, Hubner W, Jenny a, Minvielle-Sebastia L, Keller W. 1997. The 30-kD subunit of mammalian cleavage and polyadenylation specificity factor and its yeast homolog are RNA-binding zinc finger proteins. *Genes Dev* **11**: 1703–1716.

Barneche F, Malapeira J, Mas P. 2014. The impact of chromatin dynamics on plant light responses and circadian clock function. *J Exp Bot* **65**: 2895–913.

Bartholomäus L. 2012. Yeast Two-Hybrid Based Interaction Study of Growth-Related Proteins of Arabidopsis thaliana. University of Potsdam.

Baulcombe DC, Dean C. 2014. Epigenetic regulation in plant responses to the environment. *Cold Spring Harb Perspect Biol* **6**: a019471.

Bäurle I, Dean C. 2008. Differential interactions of the autonomous pathway RRM proteins and chromatin regulators in the silencing of Arabidopsis targets. *PLoS One* **3**: e2733.

Beelman CA, Parker R. 1995. Degradation of mRNA in eukaryotes. *Cell* **81**: 179–83.

Bell S a, Hunt AG. 2010. The Arabidopsis ortholog of the 77 kDa subunit of the cleavage stimulatory factor (AtCstF-77) involved in mRNA polyadenylation is an RNA-binding protein. *FEBS Lett* **584**: 1449–54.

Benjamini Y, Hochberg Y. 1995. Controlling the false discovery rate: a practical and powerful approach to multiple testing. *J R Stat Soc Ser B* **57**: 289–300.

Bentley DL. 2014. Coupling mRNA processing with transcription in time and space. *Nat Rev Genet* **15**: 163–75.

Berger SL. 2007. The complex language of chromatin regulation during transcription. *Nature* **447**: 407–12.

Bernstein P, Peltz SW, Ross J. 1989. The poly(A)-poly(A)-binding protein complex is a major determinant of mRNA stability in vitro. *Mol Cell Biol* **9**: 659–70.

Bowler C, Montagu M, Inze D. 1992. Superoxide dismutase and stress tolerance. *Annu Rev Plant Biol* **43**: 83–116.

Bruggeman Q, Garmier M, de Bont L, Soubigou-Taconnat L, Mazubert C, Benhamed M, Raynaud C, Bergounioux C, Delarue M. 2014. The Polyadenylation Factor Subunit CLEAVAGE AND POLYADENYLATION SPECIFICITY FACTOR30: A Key Factor of Programmed Cell Death and a Regulator of Immunity in Arabidopsis. *Plant Physiol* **165**: 732–746.

Castaings L, Bergonzi S, Albani MC, Kemi U, Savolainen O, Coupland G. 2014. Evolutionary conservation of cold-induced antisense RNAs of FLOWERING LOCUS C in Arabidopsis thaliana perennial relatives. *Nat Commun* **5**: 4457.

Chang H, Lim J, Ha M, Kim VN. 2014. TAIL-seq: genome-wide determination of poly(A) tail length and 3' end modifications. *Mol Cell* **53**: 1044–52.

Cheval C, Aldon D, Galaud J-P, Ranty B. 2013. Calcium/calmodulin-mediated regulation of plant immunity. *Biochim Biophys Acta* **1833**: 1766–71.

Choi K, Kim J, Hwang H-J, Kim S, Park C, Kim SY, Lee I. 2011. The FRIGIDA complex activates transcription of FLC, a strong flowering repressor in Arabidopsis, by recruiting chromatin modification factors. *Plant Cell* **23**: 289–303.

Choi YH, Hagedorn CH. 2003. Purifying mRNAs with a high-affinity eIF4E mutant identifies the short 3' poly(A) end phenotype. *Proc Natl Acad Sci U S A* **100**: 7033–8.

Colgan DF, Murthy KG, Prives C, Manley JL. 1996. Cell-cycle related regulation of poly(A) polymerase by phosphorylation. *Nature* **384**: 282–5.

Colgan DF, Murthy KG, Zhao W, Prives C, Manley JL. 1998. Inhibition of poly(A) polymerase requires p34cdc2/cyclin B phosphorylation of multiple consensus and non-consensus sites. *EMBO J* **17**: 1053–62.

Conlon FL, Miteva Y, Kaltenbrun E, Waldron L, Greco TM, Cristea IM. 2012. Immunoisolation of protein complexes from Xenopus. eds. S. HOPPLER and P.D. Vize. *Methods Mol Biol* **917**: 369–90.

Corbesier L, Vincent C, Jang S, Fornara F, Fan Q, Searle I, Giakountis A, Farrona S, Gissot L, Turnbull C, et al. 2007. FT protein movement contributes to long-distance signaling in floral induction of Arabidopsis. *Science* **316**: 1030–3.

Couée I, Sulmon C, Gouesbet G, El Amrani A. 2006. Involvement of soluble sugars in reactive oxygen species balance and responses to oxidative stress in plants. *J Exp Bot* **57**: 449–59.

Coustham V, Li P, Strange A, Lister C, Song J, Dean C. 2012. Quantitative modulation of polycomb silencing underlies natural variation in vernalization. *Science* **337**: 584–7.

Crisucci EM, Arndt KM. 2012. Paf1 restricts Gcn4 occupancy and antisense transcription at the ARG1 promoter. *Mol Cell Biol* **32**: 1150–63.

Dávila López M, Samuelsson T. 2008. Early evolution of histone mRNA 3' end processing. *RNA* **14**: 1–10.

Davis R, Shi Y. 2014. The polyadenylation code: a unified model for the regulation of mRNA alternative polyadenylation. *J Zhejiang Univ Sci B* **15**: 429–37.

De Lucia F, Crevillen P, Jones AME, Greb T, Dean C. 2008. A PHD-polycomb repressive complex 2 triggers the epigenetic silencing of FLC during vernalization. *Proc Natl Acad Sci U S A* **105**: 16831–6.

Decker CJ, Parker R. 1993. A turnover pathway for both stable and unstable mRNAs in yeast: evidence for a requirement for deadenylation. *Genes Dev* **7**: 1632–1643.

Delaney KJ, Xu R, Zhang J, Li QQ, Yun K, Falcone DL, Hunt AG. 2006. Calmodulin interacts with and regulates the RNA-binding activity of an Arabidopsis polyadenylation factor subunit. *Plant Physiol* **140**: 1507–21.

Deng W, Ying H, Helliwell CA, Taylor JM, Peacock WJ, Dennis ES. 2011. FLOWERING LOCUS C (FLC) regulates development pathways throughout the life cycle of Arabidopsis. *Proc Natl Acad Sci U S A* **108**: 6680–5.

Ding F, Cui P, Wang Z, Zhang S, Ali S, Xiong L. 2014a. Genome-wide analysis of alternative splicing of pre-mRNA under salt stress in Arabidopsis. *BMC Genomics* **15**: 431.

Ding Y, Tang Y, Kwok CK, Zhang Y, Bevilacqua PC, Assmann SM. 2014b. In vivo genome-wide profiling of RNA secondary structure reveals novel regulatory features. *Nature* **505**: 696–700.

Dower K, Kuperwasser N, Merrikh H, Rosbash M. 2004. A synthetic A tail rescues yeast nuclear accumulation of a ribozyme-terminated transcript. *RNA* **10**: 1888–99.

Duc C, Sherstnev A, Cole C, Barton GJ, Simpson GG. 2013. Transcription termination and chimeric RNA formation controlled by Arabidopsis thaliana FPA. *PLoS Genet* **9**: e1003867.

Elkon R, Ugalde AP, Agami R. 2013. Alternative cleavage and polyadenylation: extent, regulation and function. *Nat Rev Genet* **14**: 496–506.

Elliott BJ, Dattaroy T, Meeks-Midkiff LR, Forbes KP, Hunt AG. 2003. An interaction between an Arabidopsis poly(A) polymerase and a homologue of the 100 kDa subunit of CPSF. *Plant Mol Biol* **51**: 373–84.

Farré EM. 2012. The regulation of plant growth by the circadian clock. *Plant Biol* **14**: 401–10.

Feng W, Jacob Y, Veley KM, Ding L, Yu X, Choe G, Michaels SD. 2011. Hypomorphic alleles reveal FCA-independent roles for FY in the regulation of FLOWERING LOCUS C. *Plant Physiol* **155**: 1425–34.

Forbes KP, Addepalli B, Hunt AG. 2006. An Arabidopsis Fip1 homolog interacts with RNA and provides conceptual links with a number of other polyadenylation factor subunits. *J Biol Chem* **281**: 176–86.

Ford LP, Bagga PS, Wilusz J. 1997. The poly(A) tail inhibits the assembly of a 3’-to-5' exonuclease in an in vitro RNA stability system. *Mol Cell Biol* **17**: 398–406.

Foyer C, Noctor G. 2005. Redox homeostasis and antioxidant signaling: a metabolic interface between stress perception and physiological responses. *Plant Cell Online* **17**: 1866–1875.

Foyer CH, Shigeoka S. 2011. Understanding oxidative stress and antioxidant functions to enhance photosynthesis. *Plant Physiol* **155**: 93–100.

Fuke H, Ohno M. 2008. Role of poly (A) tail as an identity element for mRNA nuclear export. *Nucleic Acids Res* **36**: 1037–49.

Gao X-H, Xiao S-L, Yao Q-F, Wang Y-J, Fu X-D. 2011. An updated GA signaling “relief of repression” regulatory model. *Mol Plant* **4**: 601–6.

Garfin DE. 2003. Essential Cell Biology, Volume 1: Cell Structure, A Practical Approach. In *AES Application Focus* (eds. J. Davey and M. Lord), pp. 197–268, Oxford University Press, Oxford UK.

Gazzani S, Gendall A, Lister C, Dean C. 2003. Analysis of the molecular basis of flowering time variation in Arabidopsis accessions. *Plant Physiol* **132**: 1107–1114.

Gilroy S, Suzuki N, Miller G, Choi W-G, Toyota M, Devireddy AR, Mittler R. 2014. A tidal wave of signals: calcium and ROS at the forefront of rapid systemic signaling. *Trends Plant Sci* **19**: 623–30.

Greb T, Mylne JS, Crevillen P, Geraldo N, An H, Gendall AR, Dean C. 2007. The PHD finger protein VRN5 functions in the epigenetic silencing of Arabidopsis FLC. *Curr Biol* **17**: 73–8.

Greco TM, Miteva Y, Conlon FL, Cristea IM. 2012. Complementary proteomic analysis of protein complexes. eds. S. HOPPLER and P.D. Vize. *Methods Mol Biol* **917**: 391–407.

Griffith OW, Meister A. 1979. Potent and specific inhibition of glutathione synthesis by buthionine sulfoximine (S-n-butyl homocysteine sulfoximine). *J Biol Chem* **254**: 7558–60.

Gruber AR, Martin G, Keller W, Zavolan M. 2012. Cleavage factor Im is a key regulator of 3’ UTR length. *RNA Biol* **9**: 1405–12.

Gruber AR, Martin G, Keller W, Zavolan M. 2013. Means to an end: mechanisms of alternative polyadenylation of messenger RNA precursors. *Wiley Interdiscip Rev RNA* **5**: 183–96.

Gunderson SI, Beyer K, Martin G, Keller W, Boelens WC, Mattaj LW. 1994. The human U1A snRNP protein regulates polyadenylation via a direct interaction with poly(A) polymerase. *Cell* **76**: 531–41.

Gunderson SI, Polycarpou-Schwarz M, Mattaj IW. 1998. U1 snRNP inhibits pre-mRNA polyadenylation through a direct interaction between U1 70K and poly(A) polymerase. *Mol Cell* **1**: 255–64.

Han HJ, Tokino T, Nakamura Y. 1998. CSR, a scavenger receptor-like protein with a protective role against cellular damage causedby UV irradiation and oxidative stress. *Hum Mol Genet* **7**: 1039–46.

Hartmann U, Höhmann S, Nettesheim K, Wisman E, Saedler H, Huijser P. 2000. Molecular cloning of SVP: a negative regulator of the floral transition in Arabidopsis. *Plant J* **21**: 351–60.

He Y, Doyle MR, Amasino RM. 2004. PAF1-complex-mediated histone methylation of FLOWERING LOCUS C chromatin is required for the vernalization-responsive, winter-annual habit in Arabidopsis. *Genes Dev* **18**: 2774–84.

Helliwell C a, Robertson M, Finnegan EJ, Buzas DM, Dennis ES. 2011. Vernalization-repression of Arabidopsis FLC requires promoter sequences but not antisense transcripts. *PLoS One* **6**: e21513.

Helliwell C a, Wood CC, Robertson M, James Peacock W, Dennis ES. 2006. The Arabidopsis FLC protein interacts directly in vivo with SOC1 and FT chromatin and is part of a high-molecular-weight protein complex. *Plant J* **46**: 183–92.

Henderson IR, Dean C. 2004. Control of Arabidopsis flowering: the chill before the bloom. *Development* **131**: 3829–38.

Henderson IR, Liu F, Drea S, Simpson GG, Dean C. 2005. An allelic series reveals essential roles for FY in plant development in addition to flowering-time control. *Development* **132**: 3597–607.

Heo JB, Sung S. 2011. Vernalization-mediated epigenetic silencing by a long intronic noncoding RNA. *Science* **331**: 76–9.

Herr AJ, Molnàr A, Jones A, Baulcombe DC. 2006. Defective RNA processing enhances RNA silencing and influences flowering of Arabidopsis. *Proc Natl Acad Sci U S A* **103**: 14994–5001.

Hollerer I, Grund K, Hentze MW, Kulozik AE. 2014. mRNA 3'end processing: A tale of the tail reaches the clinic. *EMBO Mol Med* **6**: 16–26.

Hornyik C, Terzi LC, Simpson GG. 2010. The spen family protein FPA controls alternative cleavage and polyadenylation of RNA. *Dev Cell* **18**: 203–13.

Huang G-T, Ma S-L, Bai L-P, Zhang L, Ma H, Jia P, Liu J, Zhong M, Guo Z-F. 2012. Signal transduction during cold, salt, and drought stresses in plants. *Mol Biol Rep* **39**: 969–87.

Huang H, Chen J, Liu H, Sun X. 2013. The nucleosome regulates the usage of polyadenylation sites in the human genome. *BMC Genomics* **14**: 912.

Hunt a G, Meeks LR, Forbes KP, Das Gupta J, Mogen BD. 2000. Nuclear and chloroplast poly(A) polymerases from plants share a novel biochemical property. *Biochem Biophys Res Commun* **272**: 174–81.

Hunt AG. 1994. Messenger RNA 3' end formation in plants. *Annu Rev Plant Physiol Plant Mol Biol* **45**: 47–60.

Hunt AG. 2008. Messenger RNA 3' end formation in plants. *Curr Top Microbiol Immunol* **326**: 151–77.

Hunt AG. 2011. RNA regulatory elements and polyadenylation in plants. *Front Plant Sci* **2**: 109.

Hunt AG. 2014. The Arabidopsis polyadenylation factor subunit CPSF30 as conceptual link between mRNA polyadenylation and cellular signaling. *Curr Opin Plant Biol* **21C**: 128–132.

Hunt AG, Xing D, Li QQ. 2012. Plant polyadenylation factors: conservation and variety in the polyadenylation complex in plants. *BMC Genomics* **13**: 641.

Hunt AG, Xu R, Addepalli B, Rao S, Forbes KP, Meeks LR, Xing D, Mo M, Zhao H, Bandyopadhyay A, et al. 2008. Arabidopsis mRNA polyadenylation machinery: comprehensive analysis of protein-protein interactions and gene expression profiling. *BMC Genomics* **9**: 220.

Ichimura K, Mizoguchi T, Yoshida R, Yuasa T, Shinozaki K. 2000. Various abiotic stresses rapidly activate Arabidopsis MAP kinases ATMPK4 and ATMPK6. *Plant J* **24**: 655–65.

Ietswaart R, Wu Z, Dean C. 2012. Flowering time control: another window to the connection between antisense RNA and chromatin. *Trends Genet* **28**: 445–53.

Jalkanen AL, Coleman SJ, Wilusz J. 2014. Determinants and implications of mRNA poly(A) tail size--does this protein make my tail look big? *Semin Cell Dev Biol* **34**: 24–32.

Jänicke A, Vancuylenberg J, Boag PR, Traven A, Beilharz TH. 2012. ePAT: a simple method to tag adenylated RNA to measure poly(A)-tail length and other 3' RACE applications. *RNA* **18**: 1289–95.

Jeon J, Kim J. 2011. FVE, an Arabidopsis homologue of the retinoblastoma-associated protein that regulates flowering time and cold response, binds to chromatin as a large multiprotein complex. *Mol Cells* **32**: 227–34.

Jiang D, Wang Y, Wang Y, He Y. 2008. Repression of FLOWERING LOCUS C and FLOWERING LOCUS T by the Arabidopsis Polycomb repressive complex 2 components. *PLoS One* **3**: e3404.

Jin JB, Hasegawa PM. 2008. Flowering time regulation by the SUMO E3 ligase SIZ1. *Plant Signal Behav* **3**: 891–2.

Johanson U, West J, Lister C, Michaels S, Amasino R, Dean C. 2000. Molecular analysis of FRIGIDA, a major determinant of natural variation in Arabidopsis flowering time. *Science* **290**: 344–7.

Jurado AR, Tan D, Jiao X, Kiledjian M, Tong L. 2014. Structure and function of pre-mRNA 5'-end capping quality control and 3'-end processing. *Biochemistry* **53**: 1882–98.

Kaiser WM. 1979. Reversible inhibition of the calvin cycle and activation of oxidative pentose phosphate cycle in isolated intact chloroplasts by hydrogen peroxide. *Planta* **145**: 377–82.

Kang Y-N, Lai D-P, Ooi HS, Shen T-T, Kou Y, Tian J, Czajkowsky DM, Shao Z, Zhao X. 2014. Genome-wide profiling of untranslated regions by paired-end ditag sequencing reveals unexpected transcriptome complexity in yeast. *Mol Genet genomics, Epub ahead print*.

Kappel C, Trost G, Czesnick H, Ramming A, Vi SL, de Moor CH, Lenhard M. Genome-wide analysis of PAPS1-dependent polyadenylation identifies novel roles for functionally specialized poly(A) polymerases in Arabidopsis thaliana. *Unpublished*.

Kashiwabara S, Zhuang T, Yamagata K, Noguchi J, Fukamizu a, Baba T. 2000. Identification of a novel isoform of poly(A) polymerase, TPAP, specifically present in the cytoplasm of spermatogenic cells. *Dev Biol* **228**: 106–15.

Kashiwabara S-I, Noguchi J, Zhuang T, Ohmura K, Honda A, Sugiura S, Miyamoto K, Takahashi S, Inoue K, Ogura A, et al. 2002. Regulation of spermatogenesis by testis-specific, cytoplasmic poly(A) polymerase TPAP. *Science* **298**: 1999–2002.

Kim D, Pertea G, Trapnell C, Pimentel H, Kelley R, Salzberg SL. 2013. TopHat2: accurate alignment of transcriptomes in the presence of insertions, deletions and gene fusions. *Genome Biol* **14**: R36.

Kinmonth-Schultz HA, Golembeski GS, Imaizumi T. 2013. Circadian clock-regulated physiological outputs: dynamic responses in nature. *Semin Cell Dev Biol* **24**: 407–13.

Kissoudis C, van de Wiel C, Visser RGF, van der Linden G. 2014. Enhancing crop resilience to combined abiotic and biotic stress through the dissection of physiological and molecular crosstalk. *Front Plant Sci* **5**: 207.

Knight H, Knight MR. 2001. Abiotic stress signalling pathways: specificity and cross-talk. *Trends Plant Sci* **6**: 262–267.

Knight H, Trewavas AJ, Knight MR. 1997. Calcium signalling in Arabidopsis thaliana responding to drought and salinity. *Plant J* **12**: 1067–1078.

Kolbe B. 2014. Validation of PAPS1-target mRNA using different poly(A)-tail assays. University of Potsdam.

Koornneef M, Alonso-Blanco C, Blankestijn-de Vries H, Hanhart CJ, Peeters AJ. 1998. Genetic interactions among late-flowering mutants of Arabidopsis. *Genetics* **148**: 885–92.

Koornneef M, Blankestijn-de Vries H, Hanhart C, Soppe W, Peeters T. 1994. The phenotype of some late-flowering mutants is enhanced by a locus on chromosome 5 that is not effective in the Landsberg erecta wild-type. *Plant J* **6**: 911–919.

Koornneef M, Hanhart CJ, van der Veen JH. 1991. A genetic and physiological analysis of late flowering mutants in Arabidopsis thaliana. *Mol Gen Genet MGG* **229**: 57–66.

Kumar GR, Glaunsinger B a. 2010. Nuclear import of cytoplasmic poly(A) binding protein restricts gene expression via hyperadenylation and nuclear retention of mRNA. *Mol Cell Biol* **30**: 4996–5008.

Kumar SV, Lucyshyn D, Jaeger KE, Alós E, Alvey E, Harberd NP, Wigge P a. 2012. Transcription factor PIF4 controls the thermosensory activation of flowering. *Nature* **484**: 242–5.

Kumar SV, Wigge P a. 2010. H2A.Z-containing nucleosomes mediate the thermosensory response in Arabidopsis. *Cell* **140**: 136–47.

Laemmli UK. 1970. Cleavage of structural proteins during the assembly of the head of bacteriophage T4. *Nature* **227**: 680–5.

Laishram RS. 2014. Poly(A) polymerase (PAP) diversity in gene expression - Star-PAP vs canonical PAP. *FEBS Lett Epub ahead print*.

Laloi C, Stachowiak M, Pers-Kamczyc E, Warzych E, Murgia I, Apel K. 2007. Cross-talk between singlet oxygen- and hydrogen peroxide-dependent signaling of stress responses in Arabidopsis thaliana. *Proc Natl Acad Sci U S A* **104**: 672–7.

Langridge J. 1957. Effect of Day-length and Gibberellic Acid on the Flowering of Arabidopsis. *Nature* **180**: 36–37.

Lawton K, Weymann K, Friedrich L, Vernooij B, Uknes S, Ryals J. 1995. Systemic acquired resistance in Arabidopsis requires salicylic acid but not ethylene. *Mol Plant Microbe Interact* **8**: 863–70.

Lee I, Aukerman MJ, Gore SL, Lohman KN, Michaels SD, Weaver LM, John MC, Feldmann KA, Amasino RM. 1994. Isolation of LUMINIDEPENDENS: a gene involved in the control of flowering time in Arabidopsis. *Plant Cell* **6**: 75–83.

Lee JH, Ryu H-S, Chung KS, Posé D, Kim S, Schmid M, Ahn JH. 2013. Regulation of temperature-responsive flowering by MADS-box transcription factor repressors. *Science* **342**: 628–32.

Lee S, Lee H-J, Jung J-H, Park C-M. 2014. The Arabidopsis thaliana RNA-binding protein FCA regulates thermotolerance by modulating the detoxification of reactive oxygen species. *New Phytol Epub ahead print*.

Lee YJ, Lee Y, Chung JH. 2000. An intronless gene encoding a poly(A) polymerase is specifically expressed in testis. *FEBS Lett* **487**: 287–92.

Li D, Liu C, Shen L, Wu Y, Chen H, Robertson M, Helliwell C a, Ito T, Meyerowitz E, Yu H. 2008. A repressor complex governs the integration of flowering signals in Arabidopsis. *Dev Cell* **15**: 110–20.

Li H, Handsaker B, Wysoker A, Fennell T, Ruan J, Homer N, Marth G, Abecasis G, Durbin R. 2009. The Sequence Alignment/Map format and SAMtools. *Bioinformatics* **25**: 2078–9.

Lim M-H, Kim J, Kim Y-S, Chung K-S, Seo Y-H, Lee I, Kim J, Hong CB, Kim H, Park C. 2004. A new Arabidopsis gene, FLK, encodes an RNA binding protein with K homology motifs and regulates flowering time via FLOWERING LOCUS C. *Plant Cell* **16**: 731–40.

Lingner J, Kellermann J, Keller W. 1991. Cloning and expression of the essential gene for poly(A) polymerase from S. cerevisiae. *Nature* **354**: 496–8.

Liu F, Marquardt S, Lister C, Swiezewski S, Dean C. 2010. Targeted 3' processing of antisense transcripts triggers Arabidopsis FLC chromatin silencing. *Science* **327**: 94–7.

Liu F, Quesada V, Crevillén P, Bäurle I, Swiezewski S, Dean C. 2007. The Arabidopsis RNA-binding protein FCA requires a lysine-specific demethylase 1 homolog to downregulate FLC. *Mol Cell* **28**: 398–407.

Loke JC, Stahlberg EA, Strenski DG, Haas BJ, Wood PC, Li QQ. 2005. Compilation of mRNA polyadenylation signals in Arabidopsis revealed a new signal element and potential secondary structures. *Plant Physiol* **138**: 1457–68.

Love M, Huber W, Anders S. 2014. Moderated estimation of fold change and dispersion for RNA-Seq data with DESeq2. *bioRxiv*.

Macknight R, Bancroft I, Page T, Lister C, Schmidt R, Love K, Westphal L, Murphy G, Sherson S, Cobbett C, et al. 1997. FCA, a Gene Controlling Flowering Time in Arabidopsis, Encodes a Protein Containing RNA-Binding Domains. *Cell* **89**: 737–745.

Macknight R, Duroux M, Laurie R, Dijkwel P, Simpson G, Dean C. 2002. Functional significance of the alternative transcript processing of the Arabidopsis floral promoter FCA. *Plant Cell* **14**: 877–88.

Manabe Y, Tinker N, Colville A, Miki B. 2007. CSR1, the sole target of imidazolinone herbicide in Arabidopsis thaliana. *Plant Cell Physiol* **48**: 1340–58.

Mandel C, Bai Y, Tong L. 2008. Protein factors in pre-mRNA 3'-end processing. *Cell Mol Life Sci* **65**: 1099–1122.

Marquardt S, Raitskin O, Wu Z, Liu F, Sun Q, Dean C. 2014. Functional consequences of splicing of the antisense transcript COOLAIR on FLC transcription. *Mol Cell* **54**: 156–65.

Martin G, Keller W. 1996. Mutational analysis of mammalian poly(A) polymerase identifies a region for primer binding and catalytic domain, homologous to the family X polymerases, and to other nucleotidyltransferases. *EMBO J* **15**: 2593–603.

Martin G, Keller W. 2007. RNA-specific ribonucleotidyl transferases. *RNA* **13**: 1834–49.

Martin G, Möglich A, Keller W, Doublié S. 2004. Biochemical and structural insights into substrate binding and catalytic mechanism of mammalian poly(A) polymerase. *J Mol Biol* **341**: 911–25.

Martínez C, Pons E, Prats G, León J. 2004. Salicylic acid regulates flowering time and links defence responses and reproductive development. *Plant J* **37**: 209–217.

Martinson HG. 2011. An active role for splicing in 3'-end formation. *Wiley Interdiscip Rev RNA* **2**: 459–70.

May MJ, Leaver CJ. 1993. Oxidative Stimulation of Glutathione Synthesis in Arabidopsis thaliana Suspension Cultures. *Plant Physiol* **103**: 621–627.

Mazzucotelli E, Mastrangelo AM, Crosatti C, Guerra D, Stanca a. M, Cattivelli L. 2008. Abiotic stress response in plants: When post-transcriptional and post-translational regulations control transcription. *Plant Sci* **174**: 420–431.

McCracken S, Fong N, Yankulov K, Ballantyne S, Pan G, Greenblatt J, Patterson SD, Wickens M, Bentley DL. 1997. The C-terminal domain of RNA polymerase II couples mRNA processing to transcription. *Nature* **385**: 357–61.

McCracken S, Longman D, Johnstone IL, Cáceres JF, Blencowe BJ. 2003. An evolutionarily conserved role for SRm160 in 3'-end processing that functions independently of exon junction complex formation. *J Biol Chem* **278**: 44153–60.

Medler S, Al Husini N, Raghunayakula S, Mukundan B, Aldea A, Ansari A. 2011. Evidence for a complex of transcription factor IIB with poly(A) polymerase and cleavage factor 1 subunits required for gene looping. *J Biol Chem* **286**: 33709–18.

Meeks LR, Addepalli B, Hunt AG. 2009. Characterization of genes encoding poly(A) polymerases in plants: evidence for duplication and functional specialization. *PLoS One* **4**: e8082.

Meijer H a, Bushell M, Hill K, Gant TW, Willis AE, Jones P, de Moor CH. 2007. A novel method for poly(A) fractionation reveals a large population of mRNAs with a short poly(A) tail in mammalian cells. *Nucleic Acids Res* **35**: e132.

Meijer HA, de Moor CH. 2011. Fractionation of mRNA based on the length of the poly(A) tail. *Methods Mol Biol* **703**: 123–35.

Meinke G, Ezeokonkwo C, Balbo P, Stafford W, Moore C, Bohm A. 2008. Structure of yeast poly(A) polymerase in complex with a peptide from Fip1, an intrinsically disordered protein. *Biochemistry* **47**: 6859–69.

Mellman DL, Gonzales ML, Song C, Barlow C a, Wang P, Kendziorski C, Anderson R a. 2008. A PtdIns4,5P2-regulated nuclear poly(A) polymerase controls expression of select mRNAs. *Nature* **451**: 1013–7.

Meyer Y, Buchanan BB, Vignols F, Reichheld J-P. 2009. Thioredoxins and glutaredoxins: unifying elements in redox biology. *Annu Rev Genet* **43**: 335–67.

Mhamdi A, Noctor G, Baker A. 2012. Plant catalases: peroxisomal redox guardians. *Arch Biochem Biophys* **525**: 181–94.

Michaels SD, Amasino RM. 1999. FLOWERING LOCUS C Encodes a Novel MADS Domain Protein That Acts as a Repressor of Flowering. *Plant Cell* **11**: 949.

Michaels SD, Amasino RM. 2001. Loss of FLOWERING LOCUS C activity eliminates the late-flowering phenotype of FRIGIDA and autonomous pathway mutations but not responsiveness to vernalization. *Plant Cell* **13**: 935–41.

Michaels SD, He Y, Scortecci KC, Amasino RM. 2003. Attenuation of FLOWERING LOCUS C activity as a mechanism for the evolution of summer-annual flowering behavior in Arabidopsis. *Proc Natl Acad Sci U S A* **100**: 10102–7.

Millevoi S, Vagner S. 2010. Molecular mechanisms of eukaryotic pre-mRNA 3' end processing regulation. *Nucleic Acids Res* **38**: 2757–74.

Miura K, Jin JB, Lee J, Yoo CY, Stirm V, Miura T, Ashworth EN, Bressan R a, Yun D-J, Hasegawa PM. 2007. SIZ1-mediated sumoylation of ICE1 controls CBF3/DREB1A expression and freezing tolerance in Arabidopsis. *Plant Cell* **19**: 1403–14.

Mockler TC, Yu X, Shalitin D, Parikh D, Michael TP, Liou J, Huang J, Smith Z, Alonso JM, Ecker JR, et al. 2004. Regulation of flowering time in Arabidopsis by K homology domain proteins. *Proc Natl Acad Sci U S A* **101**: 12759–64.

Möller-Steinbach Y, Alexandre C, Hennig L. 2010. Flowering time control. *Methods Mol Biol* **655**: 229–37.

Murgia I, Tarantino D, Vannini C, Bracale M, Carravieri S, Soave C. 2004. Arabidopsis thaliana plants overexpressing thylakoidal ascorbate peroxidase show increased resistance to Paraquat-induced photooxidative stress and to nitric oxide-induced cell death. *Plant J* **38**: 940–53.

Murthy KG, Manley JL. 1995. The 160-kD subunit of human cleavage-polyadenylation specificity factor coordinates pre-mRNA 3'-end formation. *Genes Dev* **9**: 2672–2683.

Nemeroff ME, Barabino SM, Li Y, Keller W, Krug RM. 1998. Influenza virus NS1 protein interacts with the cellular 30 kDa subunit of CPSF and inhibits 3'end formation of cellular pre-mRNAs. *Mol Cell* **1**: 991–1000.

Nishimura N, Kitahata N, Seki M, Narusaka Y, Narusaka M, Kuromori T, Asami T, Shinozaki K, Hirayama T. 2005. Analysis of ABA hypersensitive germination2 revealed the pivotal functions of PARN in stress response in Arabidopsis. *Plant J* **44**: 972–84.

Nishimura N, Yoshida T, Murayama M, Asami T, Shinozaki K, Hirayama T. 2004. Isolation and characterization of novel mutants affecting the abscisic acid sensitivity of Arabidopsis germination and seedling growth. *Plant Cell Physiol* **45**: 1485–99.

Noctor G, Foyer CH. 1998. ASCORBATE AND GLUTATHIONE: Keeping Active Oxygen Under Control. *Annu Rev Plant Physiol Plant Mol Biol* **49**: 249–279.

Noh B, Lee S-H, Kim H-J, Yi G, Shin E-A, Lee M, Jung K-J, Doyle MR, Amasino RM, Noh Y-S. 2004. Divergent roles of a pair of homologous jumonji/zinc-finger-class transcription factor proteins in the regulation of Arabidopsis flowering time. *Plant Cell* **16**: 2601–13.

Novoa I, Gallego J, Ferreira PG, Mendez R. 2010. Mitotic cell-cycle progression is regulated by CPEB1 and CPEB4-dependent translational control. *Nat Cell Biol* **12**: 447–56.

Owttrim GW. 2006. RNA helicases and abiotic stress. *Nucleic Acids Res* **34**: 3220–30.

Page T, Macknight R, Yang CH, Dean C. 1999. Genetic interactions of the Arabidopsis flowering time gene FCA, with genes regulating floral initiation. *Plant J* **17**: 231–9.

Park-Sarge O-K, Sarge KD. 2009. Detection of sumoylated proteins. *Methods Mol Biol* **464**: 255–65.

Pazhouhandeh M, Molinier J, Berr A, Genschik P. 2011. MSI4/FVE interacts with CUL4-DDB1 and a PRC2-like complex to control epigenetic regulation of flowering time in Arabidopsis. *Proc Natl Acad Sci U S A* **108**: 3430–5.

Perochon A, Aldon D, Galaud J-P, Ranty B. 2011. Calmodulin and calmodulin-like proteins in plant calcium signaling. *Biochimie* **93**: 2048–53.

Poethig RS. 2003. Phase change and the regulation of developmental timing in plants. *Science* **301**: 334–6.

Poethig RS. 2013. Vegetative phase change and shoot maturation in plants. *Curr Top Dev Biol* **105**: 125–52.

Posé D, Verhage L, Ott F, Yant L, Mathieu J, Angenent GC, Immink RGH, Schmid M. 2013. Temperature-dependent regulation of flowering by antagonistic FLM variants. *Nature* **503**: 414–7.

Posé D, Yant L, Schmid M. 2012. The end of innocence: flowering networks explode in complexity. *Curr Opin Plant Biol* **15**: 45–50.

Preiss T, Muckenthaler M, Hentze MW. 1998. Poly(A)-tail-promoted translation in yeast: implications for translational control. *RNA* **4**: 1321–31.

Preker PJ, Lingner J, Minvielle-Sebastia L, Keller W. 1995. The FIP1 gene encodes a component of a yeast pre-mRNA polyadenylation factor that directly interacts with poly(A) polymerase. *Cell* **81**: 379–89.

Proudfoot N. 2004. New perspectives on connecting messenger RNA 3' end formation to transcription. *Curr Opin Cell Biol* **16**: 272–8.

Proudfoot NJ. 2011. Ending the message: poly(A) signals then and now. *Genes Dev* **25**: 1770–82.

Proudfoot NJ. 1989. How RNA polymerase II terminates transcription in higher eukaryotes. *Trends Biochem Sci* **14**: 105–10.

Quesada V, Dean C, Simpson GG. 2005. Regulated RNA processing in the control of Arabidopsis flowering. *Int J Dev Biol* **49**: 773–80.

Quesada V, Macknight R, Dean C, Simpson GG. 2003. Autoregulation of FCA pre-mRNA processing controls Arabidopsis flowering time. *EMBO J* **22**: 3142–52.

Raabe T, Murthy KG, Manley JL. 1994. Poly(A) polymerase contains multiple functional domains. *Mol Cell Biol* **14**: 2946–57.

Rallapalli G, Kemen EM, Robert-Seilaniantz A, Segonzac C, Etherington GJ, Sohn KH, MacLean D, Jones JDG. 2014. EXPRSS: an Illumina based high-throughput expression-profiling method to reveal transcriptional dynamics. *BMC Genomics* **15**: 341.

Ramakers C, Ruijter JM, Deprez RHL, Moorman AFM. 2003. Assumption-free analysis of quantitative real-time polymerase chain reaction (PCR) data. *Neurosci Lett* **339**: 62–6.

Ramm S. 2013. Untersuchungen zur Kontrolle des Wachstums von Pflanzenorganen am Beispiel von Arabidopsis thaliana. University of Potsdam.

Ramming A. 2014. The Role of Poly(A) Polymerase PAPS1 in Pollen Development and Growth. University of Potsdam.

Rao S, Dinkins RD, Hunt AG. 2009. Distinctive interactions of the Arabidopsis homolog of the 30 kD subunit of the cleavage and polyadenylation specificity factor (AtCPSF30) with other polyadenylation factor subunits. *BMC Cell Biol* **10**: 51.

Rataj K, Simpson GG. 2014. Message ends: RNA 3' processing and flowering time control. *J Exp Bot* **65**: 353–63.

Ratcliffe OJ, Kumimoto RW, Wong BJ, Riechmann JL. 2003. Analysis of the Arabidopsis MADS AFFECTING FLOWERING gene family: MAF2 prevents vernalization by short periods of cold. *Plant Cell* **15**: 1159–69.

Rausch T, Wachter A. 2005. Sulfur metabolism: a versatile platform for launching defence operations. *Trends Plant Sci* **10**: 503–9.

Reina-Pinto JJ, Voisin D, Teodor R, Yephremov A. 2010. Probing differentially expressed genes against a microarray database for in silico suppressor/enhancer and inhibitor/activator screens. *Plant J* **61**: 166–75.

Rentel MC, Knight MR. 2004. Oxidative stress-induced calcium signaling in Arabidopsis. *Plant Physiol* **135**: 1471–9.

Rinn JL, Kertesz M, Wang JK, Squazzo SL, Xu X, Brugmann SA, Goodnough H, Helms JA, Farnham PJ, Chang HY. 2007. NIH Public Access. **129**: 1311–1323.

Rizhsky L, Hallak-Herr E, Van Breusegem F, Rachmilevitch S, Barr JE, Rodermel S, Inzé D, Mittler R. 2002. Double antisense plants lacking ascorbate peroxidase and catalase are less sensitive to oxidative stress than single antisense plants lacking ascorbate peroxidase or catalase. *Plant J* **32**: 329–342.

Rosloski SM, Singh A, Jali SS, Balasubramanian S, Weigel D, Grbic V. 2013. Functional analysis of splice variant expression of MADS AFFECTING FLOWERING 2 of Arabidopsis thaliana. *Plant Mol Biol* **81**: 57–69.

Rothnie HM. 1996. Plant mRNA 3'-end formation. *Plant Mol Biol* **32**: 43–61.

Rothnie HM, Reid J, Hohn T. 1994. The contribution of AAUAAA and the upstream element UUUGUA to the efficiency of mRNA 3'-end formation in plants. *EMBO J* **13**: 2200–10.

Rowley MJ, Böhmdorfer G, Wierzbicki AT. 2013. Analysis of long non-coding RNAs produced by a specialized RNA polymerase in Arabidopsis thaliana. *Methods* **63**: 160–9.

Ruijter JM, Ramakers C, Hoogaars WMH, Karlen Y, Bakker O, van den Hoff MJB, Moorman AFM. 2009. Amplification efficiency: linking baseline and bias in the analysis of quantitative PCR data. *Nucleic Acids Res* **37**: e45.

Ryan K, Calvo O, Manley JL. 2004. Evidence that polyadenylation factor CPSF-73 is the mRNA 3' processing endonuclease. *RNA* **10**: 565–573.

Ryan K, Murthy KGK, Kaneko S, Manley JL. 2002. Requirements of the RNA polymerase II C-terminal domain for reconstituting pre-mRNA 3' cleavage. *Mol Cell Biol* **22**: 1684–92.

Sandalio LM, Rodríguez-Serrano M, Romero-Puertas MC, del Río LA. 2013. Role of peroxisomes as a source of reactive oxygen species (ROS) signaling molecules. ed. L.A. Del Río. *Subcell Biochem* **69**: 231–55.

Schmid M, Davison TS, Henz SR, Pape UJ, Demar M, Vingron M, Schölkopf B, Weigel D, Lohmann JU. 2005. A gene expression map of Arabidopsis thaliana development. *Nat Genet* **37**: 501–6.

Schmidt M-J, Norbury CJ. 2010. Polyadenylation and beyond: emerging roles for noncanonical poly(A) polymerases. *Wiley Interdiscip Rev RNA* **1**: 142–51.

Schmieder R, Lim YW, Edwards R. 2012. Identification and removal of ribosomal RNA sequences from metatranscriptomes. *Bioinformatics* **28**: 433–5.

Scortecci K, Michaels SD, Amasino RM. 2003. Genetic interactions between FLM and other flowering-time genes in Arabidopsis thaliana. *Plant Mol Biol* **52**: 915–22.

Shen L, Thong Z, Gong X, Shen Q, Gan Y, Yu H. 2014. The putative PRC1 RING-finger protein AtRING1A regulates flowering through repressing MADS AFFECTING FLOWERING genes in Arabidopsis. *Development* **141**: 1303–12.

Shen Y, Venu RC, Nobuta K, Wu X, Notibala V, Demirci C, Meyers BC, Wang G-L, Ji G, Li QQ. 2011. Transcriptome dynamics through alternative polyadenylation in developmental and environmental responses in plants revealed by deep sequencing. *Genome Res* **21**: 1478–86.

Sherstnev A, Duc C, Cole C, Zacharaki V, Hornyik C, Ozsolak F, Milos PM, Barton GJ, Simpson GG. 2012. Direct sequencing of Arabidopsis thaliana RNA reveals patterns of cleavage and polyadenylation. *Nat Struct Mol Biol* **19**: 845–52.

Shigeoka S, Maruta T. 2014. Cellular redox regulation, signaling, and stress response in plants. *Biosci Biotechnol Biochem* **78**: 1457–70.

Shimazu T, Horinouchi S, Yoshida M. 2007. Multiple histone deacetylases and the CREB-binding protein regulate pre-mRNA 3'-end processing. *J Biol Chem* **282**: 4470–8.

Silverman IM, Li F, Gregory BD. 2013. Genomic era analyses of RNA secondary structure and RNA-binding proteins reveal their significance to post-transcriptional regulation in plants. *Plant Sci* **205-206**: 55–62.

Simpson GG, Dean C. 2002. Arabidopsis, the Rosetta stone of flowering time? *Science* **296**: 285–9.

Simpson GG, Dijkwel PP, Quesada V, Henderson I, Dean C. 2003. FY is an RNA 3' end-processing factor that interacts with FCA to control the Arabidopsis floral transition. *Cell* **113**: 777–87.

Smyth G. 2005. Limma: linear models for microarray data. In *Bioinformatics and computational biology solutions using R and Bioconductor* (eds. R. Gentleman, V. Carey, S. Dudoit, R. Irizarry, and W. Huber), pp. 397–420, Springer, New York.

Sonmez C, Dean C. 2012. Transcription beyond borders has downstream consequences. *RNA Biol* **9**: 143–7.

Spanudakis E, Jackson S. 2014. The role of microRNAs in the control of flowering time. *J Exp Bot* **65**: 365–80.

Srikanth A, Schmid M. 2011. Regulation of flowering time: all roads lead to Rome. *Cell Mol Life Sci* **68**: 2013–37.

Staiger D, Brown JWS. 2013. Alternative splicing at the intersection of biological timing, development, and stress responses. *Plant Cell* **25**: 3640–56.

Stief A, Brzezinka K, Lämke J, Bäurle I. 2014. Epigenetic responses to heat stress at different time scales and the involvement of short RNAs. *Plant Signal Behav Epub ahead print*.

Stoilov P, Rafalska I, Stamm S. 2002. YTH: a new domain in nuclear proteins. *Trends Biochem Sci* **27**: 495–7.

Sun Q, Csorba T, Skourti-Stathaki K, Proudfoot NJ, Dean C. 2013. R-loop stabilization represses antisense transcription at the Arabidopsis FLC locus. *Science* **340**: 619–21.

Sun T-P, Gubler F. 2004. Molecular mechanism of gibberellin signaling in plants. *Annu Rev Plant Biol* **55**: 197–223.

Sung S, Amasino RM. 2004. Vernalization in Arabidopsis thaliana is mediated by the PHD finger protein VIN3. *Nature* **427**: 159–64.

Swiezewski S, Crevillen P, Liu F, Ecker JR, Jerzmanowski A, Dean C. 2007. Small RNA-mediated chromatin silencing directed to the 3' region of the Arabidopsis gene encoding the developmental regulator, FLC. *Proc Natl Acad Sci U S A* **104**: 3633–8.

Swiezewski S, Liu F, Magusin A, Dean C. 2009. Cold-induced silencing by long antisense transcripts of an Arabidopsis Polycomb target. *Nature* **462**: 799–802.

Takagaki Y, Manley JL. 1997. RNA recognition by the human polyadenylation factor CstF. *Mol Cell Biol* **17**: 3907–14.

Takagaki Y, Seipelt RL, Peterson ML, Manley JL. 1996. The polyadenylation factor CstF-64 regulates alternative processing of IgM heavy chain pre-mRNA during B cell differentiation. *Cell* **87**: 941–52.

Tarun SZ, Sachs a B. 1996. Association of the yeast poly(A) tail binding protein with translation initiation factor eIF-4G. *EMBO J* **15**: 7168–77.

Theocharis A, Clément C, Barka EA. 2012. Physiological and molecular changes in plants grown at low temperatures. *Planta* **235**: 1091–105.

Thimm O, Bläsing O, Gibon Y, Nagel A, Meyer S, Krüger P, Selbig J, Müller LA, Rhee SY, Stitt M. 2004. MAPMAN: a user-driven tool to display genomics data sets onto diagrams of metabolic pathways and other biological processes. *Plant J* **37**: 914–39.

Thomas H. 2013. Senescence, ageing and death of the whole plant. *New Phytol* **197**: 696–711.

Thomas PE, Wu X, Liu M, Gaffney B, Ji G, Li QQ, Hunt AG. 2012. Genome-wide control of polyadenylation site choice by CPSF30 in Arabidopsis. *Plant Cell* **24**: 4376–88.

Thuresson a C, Aström J, Aström a, Grönvik KO, Virtanen a. 1994. Multiple forms of poly(A) polymerases in human cells. *Proc Natl Acad Sci U S A* **91**: 979–83.

Tian B, Manley JL. 2013. Alternative cleavage and polyadenylation: the long and short of it. *Trends Biochem Sci* **38**: 312–20.

Tikhonov M, Georgiev P, Maksimenko O. 2013. Competition within Introns: Splicing Wins over Polyadenylation via a General Mechanism. *Acta Naturae* **5**: 52–61.

Tör M, Gordon P, Cuzick A, Eulgem T, Sinapidou E, Mert-Türk F, Can C, Dangl JL, Holub EB. 2002. Arabidopsis SGT1b is required for defense signaling conferred by several downy mildew resistance genes. *Plant Cell* **14**: 993–1003.

Trapet P, Kulik A, Lamotte O, Jeandroz S, Bourque S, Nicolas-Francès V, Rosnoblet C, Besson-Bard A, Wendehenne D. 2014. NO signaling in plant immunity: A tale of messengers. *Phytochem Epub ahead print*.

Trost G. 2014. Poly(A) Polymerase 1 (PAPS1) influences organ size and pathogen response in Arabidopsis thaliana. University of Potsdam.

Trost G, Vi SL, Czesnick H, Lange P, Holton N, Giavalisco P, Zipfel C, Kappel C, Lenhard M. 2014. Arabidopsis poly(A) polymerase PAPS1 limits founder-cell recruitment to organ primordia and suppresses the salicylic acid-independent immune response downstream of EDS1/PAD4. *Plant J* **77**: 688–99.

Tsuchiya T, Eulgem T. 2013. Mutations in EDM2 selectively affect silencing states of transposons and induce plant developmental plasticity. *Sci Rep* **3**: 1701.

Tsukaya H, Byrne ME, Horiguchi G, Sugiyama M, Van Lijsebettens M, Lenhard M. 2013. How do “housekeeping” genes control organogenesis?--Unexpected new findings on the role of housekeeping genes in cell and organ differentiation. *J Plant Res* **126**: 3–15.

Tzafrir I, Pena-Muralla R, Dickerman A, Berg M, Rogers R, Hutchens S, Sweeney TC, McElver J, Aux G, Patton D, et al. 2004. Identification of genes required for embryo development in Arabidopsis. *Plant Physiol* **135**: 1206–20.

Uhler JP, Hertel C, Svejstrup JQ. 2007. A role for noncoding transcription in activation of the yeast PHO5 gene. *Proc Natl Acad Sci U S A* **104**: 8011–6.

Ulitsky I, Shkumatava A, Jan CH, Subtelny AO, Koppstein D, Bell GW, Sive H, Bartel DP. 2012. Extensive alternative polyadenylation during zebrafish development. *Genome Res* **22**: 2054–66.

Van Larebeke N, Engler G, Holsters M, Van den Elsacker S, Zaenen I, Schilperoort RA, Schell J. 1974. Large plasmid in Agrobacterium tumefaciens essential for crown gall-inducing ability. *Nature* **252**: 169–70.

Veley KM, Michaels SD. 2008. Functional redundancy and new roles for genes of the autonomous floral-promotion pathway. *Plant Physiol* **147**: 682–95.

Vethantham V, Rao N, Manley JL. 2008. Sumoylation regulates multiple aspects of mammalian poly(A) polymerase function. *Genes Dev* **22**: 499–511.

Vi SL. 2013. The role of a canonical Poly(A) Polymerase in organ-identity dependent size regulation in Arabidopsis thaliana. University of Potsdam.

Vi SL, Trost G, Lange P, Czesnick H, Rao N, Lieber D, Laux T, Gray WM, Manley JL, Groth D, et al. 2013. Target specificity among canonical nuclear poly(A) polymerases in plants modulates organ growth and pathogen response. *Proc Natl Acad Sci U S A* **110**: 13994–9.

Villajuana-Bonequi M, Elrouby N, Nordström K, Griebel T, Bachmair A, Coupland G. 2014. Elevated salicylic acid levels conferred by increased expression of ISOCHORISMATE SYNTHASE 1 contribute to hyperaccumulation of SUMO1 conjugates in the Arabidopsis mutant early in short days 4. *Plant J* **79**: 206–19.

Wahle E. 1995. Poly(A) tail length control is caused by termination of processive synthesis. *J Biol Chem* **270**: 2800–8.

Wahle E, Rüegsegger U. 1999. 3'-End processing of pre-mRNA in eukaryotes. *FEMS Microbiol Rev* **23**: 277–95.

Wang ET, Sandberg R, Luo S, Khrebtukova I, Zhang L, Mayr C, Kingsmore SF, Schroth GP, Burge CB. 2008a. Alternative isoform regulation in human tissue transcriptomes. *Nature* **456**: 470–6.

Wang J-W. 2014. Regulation of flowering time by the miR156-mediated age pathway. *J Exp Bot* **65**: 4723–30.

Wang J-W, Schwab R, Czech B, Mica E, Weigel D. 2008b. Dual effects of miR156-targeted SPL genes and CYP78A5/KLUH on plastochron length and organ size in Arabidopsis thaliana. *Plant Cell* **20**: 1231–43.

Wang L, Eckmann CR, Kadyk LC, Wickens M, Kimble J. 2002. A regulatory cytoplasmic poly(A) polymerase in Caenorhabditis elegans. *Nature* **419**: 312–6.

Weill L, Belloc E, Bava F-A, Méndez R. 2012. Translational control by changes in poly(A) tail length: recycling mRNAs. *Nat Struct Mol Biol* **19**: 577–85.

Willekens H, Chamnongpol S, Davey M, Schraudner M, Langebartels C, Van Montagu M, Inzé D, Van Camp W. 1997. Catalase is a sink for H2O2 and is indispensable for stress defence in C3 plants. *EMBO J* **16**: 4806–16.

Willmann MR, Poethig RS. 2011. The effect of the floral repressor FLC on the timing and progression of vegetative phase change in Arabidopsis. *Development* **138**: 677–85.

Wilson RN, Somerville CR. 1995. Phenotypic Suppression of the Gibberellin-Insensitive Mutant (gai) of Arabidopsis. *Plant Physiol* **108**: 495–502.

Wrzaczek M, Brosché M, Kangasjärvi J. 2013. ROS signaling loops - production, perception, regulation. *Curr Opin Plant Biol* **16**: 575–82.

Wu G, Park MY, Conway SR, Wang J, Weigel D, Poethig RS. 2009. The sequential action of miR156 and miR172 regulates developmental timing in Arabidopsis. *Cell* **138**: 750–9.

Wu X, Liu M, Downie B, Liang C, Ji G, Li QQ, Hunt AG. 2011. Genome-wide landscape of polyadenylation in Arabidopsis provides evidence for extensive alternative polyadenylation. *Proc Natl Acad Sci U S A* **108**: 12533–8.

Xing D, Li QQ. 2011. Alternative polyadenylation and gene expression regulation in plants. *Wiley Interdiscip Rev RNA* **2**: 445–58.

Xing D, Wang Y, Xu R, Ye X, Yang D, Li QQ. 2013. The regulatory role of Pcf11-similar-4 (PCFS4) in Arabidopsis development by genome-wide physical interactions with target loci. *BMC Genomics* **14**: 598.

Xing D, Zhao H, Li QQ. 2008a. Arabidopsis CLP1-SIMILAR PROTEIN3, an ortholog of human polyadenylation factor CLP1, functions in gametophyte, embryo, and postembryonic development. *Plant Physiol* **148**: 2059–69.

Xing D, Zhao H, Xu R, Li QQ. 2008b. Arabidopsis PCFS4, a homologue of yeast polyadenylation factor Pcf11p, regulates FCA alternative processing and promotes flowering time. *Plant J* **54**: 899–910.

Xu R, Ye X, Quinn Li Q. 2004. AtCPSF73-II gene encoding an Arabidopsis homolog of CPSF 73 kDa subunit is critical for early embryo development. *Gene* **324**: 35–45.

Xu R, Zhao H, Dinkins RD, Cheng X, Carberry G, Li QQ. 2006. The 73 kD subunit of the cleavage and polyadenylation specificity factor (CPSF) complex affects reproductive development in Arabidopsis. *Plant Mol Biol* **61**: 799–815.

Xu Y, Gan E-S, Ito T. 2013. The AT-hook/PPC domain protein TEK negatively regulates floral repressors including MAF4 and MAF5. *Plant Signal Behav* **8**: 1–3.

Yamaguchi A, Abe M. 2012. Regulation of reproductive development by non-coding RNA in Arabidopsis: to flower or not to flower. *J Plant Res* **125**: 693–704.

Yang Q, Nausch LWM, Martin G, Keller W, Doublié S. 2014. Crystal structure of human poly(A) polymerase gamma reveals a conserved catalytic core for canonical poly(A) polymerases. *J Mol Biol* **426**: 43–50.

Yanovsky MJ, Kay SA. 2002. Molecular basis of seasonal time measurement in Arabidopsis. *Nature* **419**: 308–12.

Yao Y, Song L, Katz Y, Galili G. 2002. Cloning and characterization of Arabidopsis homologues of the animal CstF complex that regulates 3' mRNA cleavage and polyadenylation. *J Exp Bot* **53**: 2277–8.

Zhang J, Addepalli B, Yun K-Y, Hunt AG, Xu R, Rao S, Li QQ, Falcone DL. 2008. A polyadenylation factor subunit implicated in regulating oxidative signaling in Arabidopsis thaliana. *PLoS One* **3**: e2410.

Zhao J, Hyman L, Moore C. 1999. Formation of mRNA 3' ends in eukaryotes: mechanism, regulation, and interrelationships with other steps in mRNA synthesis. *Microbiol Mol Biol Rev* **63**: 405–45.

Zhao W, Manley JL. 1996. Complex alternative RNA processing generates an unexpected diversity of poly(A) polymerase isoforms. *Mol Cell Biol* **16**: 2378–86.

Zhu Z-H, Yu YP, Shi Y-K, Nelson JB, Luo J-H. 2009. CSR1 induces cell death through inactivation of CPSF3. *Oncogene* **28**: 41–51.

Zipfel C, Robatzek S, Navarro L, Oakeley EJ, Jones JDG, Felix G, Boller T. 2004. Bacterial disease resistance in Arabidopsis through flagellin perception. *Nature* **428**: 764–7.

Affidavit

I confirm that the PhD thesis entitled “Functional Specialization of *Arabidopsis* Poly(A) Polymerases in Relation to Flowering Time and Stress” is the result of my own work. I did not receive any aids or support other than stated. All sources and materials applied are listed and specified in the thesis. Furthermore I confirm that this thesis has not yet been submitted as part of another examination process, neither in identical nor in similar form.

Ich versichere hiermit, dass ich die Doktorarbeit mit dem Titel „Functional Specialization of *Arabidopsis* Poly(A) Polymerases in Relation to Flowering Time and Stress“ selbstständig und ohne unzulässige fremde Hilfe erbracht habe. Ich habe keine anderen als die angegebenen Quellen und Hilfsmittel benutzt sowie wörtliche und sinngemäße Zitate kenntlich gemacht. Die Arbeit hat in gleicher oder ähnlicher Form noch keiner Prüfungsbehörde vorgelegen.

Berlin, 20.11.2014 Hjördis Czesnick

Acknowledgements

First of all, I would like to thank Michael Lenhard for being a fantastic supervisor and for giving great scientific advice. He supported me constantly during the last three years. I am very grateful that Michael gave me the opportunity to work on my PhD in his creative and innovative lab.

I would like to thank all members of the group for the scientific discussions and for the very supportive and friendly working atmosphere. Thanks to our technicians Peggy Lange, Cindy Marona and Melanie Teltow the lab runs like clockwork. Special thanks to my office companions Christian Kappel, Adrien Sicard and Ushio Fujikura for countless discussions about science and life in general. I would like to thank Christian for the analysis of the RNA-seq data and Adrien for all the help and advice throughout the years. I thank Anahid Powell for being a very honest and critical scientist and for being a great friend. I would also like to thank Son Vi, who started the project, for sharing his great enthusiasm and optimism and Holger Breuninger for making the start in the new lab much easier for me. Thanks to my PhD student fellows Gerda Trost, Moritz Jöst, Anna Stief and Claudia Sas for sharing experiences and for our great after-lab hours. I thank Cuong Huu Nguyen and Jo Hepworth for always making me look forward to the train rides to Golm. Lastly, special thanks go to all students who were working on the project with me and who became very good friends over the years: Patrizia Thoma, Jill Kant, Moriz Halbmeier, Lisa Bartholomäus, Sascha Ramm, Anna Ramming and Ben Kolbe. It was a great pleasure to work in such an international and open-minded lab.

I would also like to thank Isabel Bäurle and her whole lab for great scientific discussions and for the support during the thermotolerance assays. Moreover, I thank Joost van Dongen and Francesco Licausi for scientific advice and for the support during the oxygen stress experiments.

I am very grateful that I had the opportunity to discuss my results with many excellent scientists at several national and international plant science conferences. Every time, I returned with many new ideas and a lot of motivation and that certainly advanced the project. Also, I very much enjoyed discussing my work with the many scientists that had been invited to visit the genetics group at the university.

Lastly, I thank my partner, my family and my friends for their constant love and support and for their confidence.